

# **Activation of C<sub>1</sub> compounds by iron and mackinawite under prebiotic conditions**

## **Dissertation**

zur Erlangung des akademischen Grades doctor rerum naturalium

(Dr. rer. nat.)

vorgelegt dem Rat der Chemisch-Geowissenschaftlichen Fakultät der  
Friedrich-Schiller-Universität Jena

von M.Sc. Mario Grosch

geboren am 09.05.1989 in Bad Brückenau

**Gutachter:**

1. Prof. Dr. Wolfgang Weigand

2. Prof. Dr. Christian Robl

Tag der Verteidigung: 18.02.2022

## **Selbständigkeitserklärung**

Ich erkläre, dass ich die vorliegende Arbeit selbständig und unter Verwendung der angegebenen Hilfsmittel, persönlichen Mitteilungen und Quellen angefertigt habe.

Ort, Datum

Unterschrift der Verfasserin/des Verfassers

## Abstract

The role of iron sulfide minerals for the terrestrial origin of life has been discussed over several decades, but until now not fully resolved. Mackinawite is the first iron sulfide formed naturally by precipitation and believed to be the precursor for every other known iron sulfide phase. Here, mackinawite was found to be selectively formed from the reaction of a wettened mixture of iron and sulfur powders during 24 h at room temperature. The mackinawite from the elements showed a similar high reactivity towards oxidation by air like the precipitated one but formed larger conglomerates of particles with lower surface areas. These conglomerates could be deactivated by introducing small amounts of air developing a passivating layer that protected the core from further oxidation. The structure and composition of the deactivated mackinawite was analyzed by powder X-ray diffraction (PXRD), scanning electron microscopy (SEM), high resolution transmission electron microscopy (TEM) and Mössbauer spectroscopy.

When the mackinawite from the elements was let in contact with different C<sub>1</sub> substrates (CO<sub>2</sub>, CO, KCN, KSCN, KOCN, CS<sub>2</sub>, CH<sub>3</sub>SH, [Fe(CN)<sub>6</sub>]<sup>3-/4-</sup> and [Fe(CN)<sub>5</sub>(NO)]<sup>2-</sup>) a range of reaction products (CS<sub>2</sub>, COS, C<sub>1</sub> to C<sub>5</sub> hydrocarbons, C<sub>1</sub> to C<sub>4</sub> thiols and oxygenated species) were formed at 25 ° and 80 °C in the presence of various acids (HCl, H<sub>2</sub>SO<sub>4</sub> and H<sub>3</sub>PO<sub>4</sub>). In experiments where KCN was directly reacted with the mixture of iron and sulfur powders at pH 9 and only later acidified, additionally cyclic sulfur compounds were formed. The reaction products were clearly identified by comparing their fragmentation pattern to the ones listed in the NIST 14 library or by their characteristic mass shift in reactions where isotopically enriched substrates were used instead. Based on the product array, a novel reduction mechanism could be formulated where the iron atom does not mediate the C fixation, but by the sulfide end-groups located especially around the low index (011) and (111) sites of the mackinawite particles. To support this assumption, the reduction of KCN was further investigated by DFT calculations on an all ferrous [Fe<sub>4</sub>S<sub>4</sub>](SR)<sub>4</sub> cluster. The reaction energy to establish a bond between the Fe and the C atom was found to be endotherm in all investigated cases, whereas the nucleophilic attack of a deprotonated sulfide end-group was found to be exothermic by -75.5 kcal mol<sup>-1</sup>. The subsequent reduction of the carbon residue into CH<sub>4</sub> and CH<sub>3</sub>SH proceeds in an overall exothermic manner if electrons and protons are available, which

is in accordance with the experimental observations. Similar mechanisms could furthermore be formulated for the reduction of other substrates used during the thesis. The electrons were found to be delivered from oxidation of  $\text{Fe}^{2+}$  ions, whereas greigite ( $(\text{Fe}^{+2}\text{Fe}^{+3}_2)\text{S}_4$ ) was formed.

The reaction conditions are plausible for prebiotic scenarios and could therefore resemble key steps in the early chemical evolution. The selective reaction between iron and sulfur is known for many decades but has never been recognized as a synthetic route towards mackinawite. This reaction, however, has the potential to change our current perspective on prebiotic processes as the already established chemistry of iron sulfides can now additionally be discussed for environments, other than undersea hydrothermal systems. It would provide a plausible route for the formation of mackinawite on land, where  $\text{H}_2\text{O}$  was only present periodically. There, iron was steadily supplied in form of meteorites and sulfur was formed by the photochemical reaction between  $\text{H}_2\text{S}$  and  $\text{SO}_2$ , released to the early atmosphere by large volcanic eruptions. The transfer of the already established mackinawite chemistry towards on-land scenarios, where dry-wet cycles can occur, enables reactions that otherwise would not be possible in the omnipresence of  $\text{H}_2\text{O}$ . Furthermore, this location allows the mackinawite to interact with the primordial atmosphere, which was a source for various substrates like  $\text{CO}$ ,  $\text{CO}_2$  and  $\text{HCN}$ . Substances like  $\text{CH}_3\text{CHO}$  and the cyclic organosulfur compounds are interesting precursors for biologically relevant molecules like DNA, RNA, or organometallic complexes like [FeFe]-hydrogenases.

## Zusammenfassung

Die terrestrische Entstehung des Lebens ist die Folge eines komplexen Netzwerks an chemischen Reaktionen, ausgehend von einfachen oxidierten Verbindungen wie Kohlenstoffdioxid ( $\text{CO}_2$ ) und Wasser ( $\text{H}_2\text{O}$ ). Welche Rolle Minerale, wie Eisensulfide, in diesem Vorgang spielten, ist bis heute nicht gänzlich aufgeklärt. Mackinawit ist die erste Eisensulfidphase, die während der Fällung von  $\text{Fe}^{2+}$  und  $\text{S}^{2-}$  Ionen gebildet wird. Daher wird angenommen, dass Mackinawit als Ausgangsstoff für alle anderen Eisensulfidphasen fungiert. Im Rahmen dieser Arbeit konnte ein ungewöhnlicher Syntheseweg für Mackinawit etabliert werden, der zwar seit Jahrhunderten bekannt ist, bislang allerdings nicht als relevante Syntheseroute in Betracht gezogen wurde, wobei eine mit Wasser befeuchtete Mischung aus Eisen- und Schwefelpulver innerhalb 24 Stunden bei Raumtemperatur selektiv Mackinawit bildet. Das aus den Elementen hergestellte Mackinawit besitzt eine ähnlich hohe Reaktivität gegenüber Luftsauerstoff wie solches, das durch Fällung von  $\text{Fe}^{2+}$  und  $\text{S}^{2-}$  Ionen gewonnen wurde. Im Gegensatz dazu führt jedoch die Reaktion zwischen den Elementen zur Bildung größeren Konglomeraten mit einer geringeren reaktiven Oberfläche. Das kontrollierte Einleiten kleiner Mengen an Luftsauerstoff führte zur Ausbildung einer passivierenden Schicht und daher zu einer Deaktivierung der Partikel. Die chemische Zusammensetzung der deaktivierten Konglomerate konnte im Anschluss mithilfe der Pulverdiffraktometrie (PXRD), Rasterelektronenmikroskopie (SEM), Hochauflösender Transmissionselektronenmikroskopie (TEM) und Mößbauer Spektroskopie untersucht werden.

Wenn Mackinawit aus den Elementen mit verschiedenen  $\text{C}_1$  Substraten ( $\text{CO}_2$ ,  $\text{CO}$ ,  $\text{KCN}$ ,  $\text{KSCN}$ ,  $\text{KOCN}$ ,  $\text{CS}_2$ ,  $\text{CH}_3\text{SH}$ ,  $[\text{Fe}(\text{CN})_6]^{3-/4-}$  und  $[\text{Fe}(\text{CN})_5(\text{NO})]^{2-}$ ) bei Temperaturen zwischen  $25^\circ$  und  $80^\circ\text{C}$ , in Anwesenheit verschiedener Säuren ( $\text{HCl}$ ,  $\text{H}_2\text{SO}_4$  und  $\text{H}_3\text{PO}_4$ ), zur Reaktion gebracht wurde, konnte eine Vielzahl an Reaktionsprodukten wie  $\text{CS}_2$ ,  $\text{COS}$ ,  $\text{C}_1$  bis  $\text{C}_5$  Kohlenwasserstoffe,  $\text{C}_1$  bis  $\text{C}_4$  Thiole und oxygenierte Verbindungen in der Gasphase der Proben nachgewiesen werden. Zusätzlich dazu konnte eine Reihe zyklischer Schwefelverbindungen erhalten werden, wenn  $\text{KCN}$  mit Mackinawit zunächst bei  $\text{pH } 9$  reagiert und diesem Gemisch erst kurz vor der GCMS Analyse der darüber befindlichen Gasphase eine Säure zugesetzt wurde. Das in der Gasphase enthaltene Produktgemisch wurde gaschromatographisch aufgetrennt und basierend auf ihrem

Massenspektrum identifiziert. Dabei wurden entweder die erhaltenen Fragmentierungsmuster, mit denen in der NIST 14 Bibliothek verglichen oder die zu erwartende Massenverschiebung beobachtet, wenn isotopenmarkierte Substrate eingesetzt wurden. Basierend auf diesen Ergebnissen konnte ein neuartiger Reduktionsmechanismus formuliert werden, welcher im Gegensatz zu früheren Annahmen nicht die Wechselwirkung zwischen Substrat und den Eisenatomen, sondern vielmehr die Interaktion mit den deprotonierten Sulfid Gruppen an der Partikeloberfläche beschreibt. Um diese Annahme zu unterstützen, wurden DFT-Rechnungen mithilfe eines vollständig reduzierten  $[\text{Fe}_4\text{S}_4](\text{SR})_4$  Clusters als Modell durchgeführt. Die Reaktionsenergie für die initiale Anbindung eines HCN-Moleküls an die Sulfid-Oberflächengruppe ist exotherm ( $-75.5 \text{ kcal mol}^{-1}$ ). In Übereinstimmung mit den experimentellen Ergebnissen verläuft die anschließende Reduktion zu  $\text{CH}_4$  und  $\text{CH}_3\text{SH}$  ebenfalls insgesamt exotherm, solange entsprechende Protonen und Elektronen vorhanden sind. Basierend auf diesem Modell konnten vergleichbare Reaktionsmechanismen für die weiteren genutzten Substrate ( $\text{SCN}^-$ ,  $\text{OCN}^-$  und  $\text{CS}_2$ ) formuliert werden. Die Elektronen werden dabei von den  $\text{Fe}^{2+}$  Ionen des Mackinawits geliefert, was zur Bildung von Greigit ( $(\text{Fe}^{+2}\text{Fe}^{+3}_2)\text{S}_4$ ) führt.

Da die hier gewählten Reaktionsbedingungen präbiotisch relevant sind, könnten die beobachteten Reaktionen als Schlüsselschritte während der frühen chemischen Evolution angenommen werden. Die Reaktion zwischen Eisen- und Schwefelpulver eröffnet jedoch bislang wenig diskutierte Szenarien, in denen die bekannte präbiotische Chemie der Eisensulfide auch unter trockeneren Bedingungen, fern von Unterseevulkanen ablaufen könnte. Eisen könnte dabei vor allem durch Meteoriten eingetragen worden sein, während der Schwefel vor allem durch die photochemische Komproportionierungsreaktion zwischen  $\text{SO}_2$  und  $\text{H}_2\text{S}$  gebildet wurde. Beide Gase wurden der Atmosphäre stetig durch enorme vulkanische Eruptionen zugeführt. Die Verlagerung der Mackinawit-Chemie von hydrothermalen Quellen auf das Land führt dazu, dass im Fall alternierender Trocken- und Feuchtphasen Reaktionen ablaufen konnten, die ausschließlich unter Wasser nicht möglich gewesen wären. So können Moleküle wie  $\text{CO}$ ,  $\text{CO}_2$  und  $\text{HCN}$ , welche vorrangige Bestandteile in einer primordialen Atmosphäre waren, direkt an der Grenzfläche Gas-/Festphase reagieren. Substanzen

wie Acetaldehyd ( $\text{CH}_3\text{CHO}$ ) und die zyklischen Schwefelverbindungen, die sich unter den oben beschriebenen Bedingungen bildeten, sind wichtige Ausgangsstoffe für biologisch relevante Moleküle wie DNA, RNA, oder metallorganische Komplexe wie [FeFe]-Hydrogenasen.



## Acknowledgements

I am deeply grateful to have received the opportunity to work on a research topic that is concerned with one of the biggest questions in human history, of how life emerged on earth. I personally was fascinated by the idea of solving this puzzle ever since I first was confronted with this topic. Shortly after I started my PhD, I soon had to realize that this question is one of a much more complex nature than I previously could imagine. However, during the vast number of hours that I spent to classify the experimental findings, I was frequently confronted with new problems to solve and could steadily advance as a scientist. Therefore, I am very thankful to Prof. Dr. Weigand and Prof. Dr. Robl who gave me the chance to work on this topic and always supported my ideas. Additionally, I want to thank all members of the Weigand group for their steady support over the last years.

During my PhD thesis I had the chance to work in close cooperation with my good friend Robert Bolney who only shortly before started his study on tochilinite. He hugely contributed to this work by closely investigating the structure and composition of the mackinawite from the elements. Due to his experimental and analytical efforts it was able for us to resolve previous inconsistencies on this topic and get a deeper understanding of the matter. His main contributions include:

- SEM/TEM, PXRD and elemental analysis of the mackinawite samples.
- Experimental evidence and theoretical completion of the reaction mechanism.
- Kinetic investigations and the establishment of the method for deactivation.

Furthermore, his way of thinking and problem solving strongly influenced my perspective on the topic of carbon fixation and prebiotic chemistry, in general. Thank you very much for the great time and hopefully see you in future projects, whether professionally or personally.

Thanks to Prof. Weigand and his engagement in establishing the still ongoing collaboration with the group of Prof. Dr. Ribbe and Prof. Dr. Hu at the University of California, Irvine (UCI), I was able to learn about the basics of the gas chromatography coupled mass spectrometry (GCMS) and able to gather the first experimental evidence

of reduced compounds. The collaboration with the UCI was later continued to support the assumptions on the reduction of HCN by the mackinawite surface groups. I therefore want to thank Dr. Martin T. Stiebritz for his efforts on performing DFT calculations and the productive discussions. I further want to thank the whole Ribbe and Hu lab for taking me in as one of their own and their great support during my stay there. A special thanks goes out to Jasper Liedtke and Megan Newcomb who took care of me from the point when I first entered UCI. I am deeply grateful to the Deutscher Akademischer Austauschdienst (DAAD) for the three-month scholarship that made the stay at the UCI possible. Another collaboration was established with the group of Prof. Dr. Trapp from the Ludwig Maximilian University of Munich (LMU). During my stay at their laboratory, I was allowed to use their GCMS setup to investigate some of my samples. I want to thank the whole group for their hospitality and support. I specially want to thank Alexander Siegle, who taught me a lot about the GCMS method, Sophia Peters for the interesting discussions in Munich, but also during her stay at our laboratory, and Prof. Dr. Trapp for his invitation to the Science of Early Life conference at Kloster Seon.

I further want to acknowledge all others who have provided measurements, experimental data, or their expertise. I thank Antje Wermann and Steffi Ebbinghaus, who did the PXRD measurements. I want to thank Mario Winkler from the group of Prof. Dr. van Slageren from the University of Stuttgart. He recorded the Mössbauer Spectra of the mackinawite samples and helped interpreting the collected data. SEM images and EDX data was collected by Steffi Stumpf, TEM images taken by Stephanie Höppener. The UV/Vis data of the green solution was provided by Maria Sittig. I further want to thank the NMR division for their fast and competent work and especially Bärbel Rambach for her patience during our method development. Furthermore, I want to thank Susanne Spangenberg and Sarah Tippner for all the many small, but nevertheless troublesome, things, they have taken care of for me. I further want to thank my students, Eric Jückstock, Hannah Busch, Frerk Wehmeyer and Yihan fLiu for their contributions to this work.

Finally, I want to thank my friends and family for their steady support despite all the ups and downs I encountered during this thesis. I am very thankful for all of you.

# Contents

<b>Selbständigkeitserklärung .....</b>	<b>III</b>
<b>Abstract .....</b>	<b>IV</b>
<b>Zusammenfassung .....</b>	<b>VI</b>
<b>Acknowledgements.....</b>	<b>IX</b>
<b>List of Publications .....</b>	<b>XIV</b>
<b>List of Abbreviations .....</b>	<b>XV</b>
<b>List of Figures .....</b>	<b>XVII</b>
<b>List of Tables .....</b>	<b>XXIII</b>
<b>Chapter 1. Introduction .....</b>	<b>1</b>
1.1 The origin of life .....	1
1.2 Mackinawite .....	10
1.3 Carbon fixation .....	14
1.4 Goal of the thesis .....	19
<b>Chapter 2. Materials and Methods .....</b>	<b>20</b>
2.1 Materials .....	20
2.2 Methods.....	20
<b>Chapter 3. Mackinawite from iron and sulfur .....</b>	<b>32</b>
3.1 Introduction.....	32
3.2 Results and Discussion .....	33
3.3 Summary .....	48
<b>Chapter 4. Reduction of cyanides .....</b>	<b>50</b>
4.1 Introduction.....	50

4.2 Results and Discussion .....	51
4.3 Summary .....	98
<b>Chapter 5. Reduction of carbon sulfur compounds .....</b>	<b>101</b>
5.1 Introduction .....	101
5.2 Results and Discussion .....	102
5.3 Summary .....	110
<b>Chapter 6. Reduction of hexacyanoferrates .....</b>	<b>111</b>
6.1 Introduction .....	111
6.2 Results and Discussion .....	112
6.3 Summary .....	117
<b>Chapter 7. Adsorption and reduction of carbon oxides .....</b>	<b>118</b>
7.1 Introduction .....	118
7.2 Results and Discussion .....	119
7.3 Summary .....	129
<b>Chapter 8. Consequences for prebiotic models .....</b>	<b>131</b>
8.1 Introduction .....	131
8.2 Mackinawite from iron and sulfur .....	133
8.3 The reduction of C <sub>1</sub> substrates .....	136
8.4 The prebiotic habitat.....	139
<b>Chapter 9. Summary and Outlook.....</b>	<b>141</b>
9.1 Summary .....	141
9.2 Outlook .....	144
<b>Chapter 10. Experimental section .....</b>	<b>145</b>

10.1 Methods.....	145
10.2 Metal sulfide synthesis .....	146
10.3 Qualitative analyses .....	150
10.4 Reduction experiments.....	151
<b>Literature.....</b>	<b>170</b>

## List of Publications

1. R. Bolney<sup>+</sup>, **M. Grosch<sup>+</sup>**, M. Winkler, J. van Slageren, W. Weigand, C. Robl, Mackinawite formation from elemental iron and sulfur. *RSC Adv.* **11**, 32464–32475 (2021). (+Equal contribution from the authors)

## List of Abbreviations

---

Archean	4 Gy to 2.5 Gy ago
DFT	Density functional theory
DMC	Dimethyl chloride
DNA	Deoxyribonucleic acid
DTP	2,4-Dithiapentane
Fc	Ferrocene
FYSP	Faint young sun paradox
GCMS	Gas chromatography - mass spectrometry
GOE	Great oxidation event
Gy	Giga years ( $10^9$ years)
Hadean	4.56 Gy to 4 Gy ago
MCS <sub>DP</sub>	Deprotonated mono coordinated surface group
MCS <sub>P</sub>	Protonated mono coordinated surface group
MFE	Moon forming event
My	Mega years ( $10^6$ years)
NIST 14	National Institute of Standards and Technology - Mass spectral library

---

---

NMR	Nuclear magnetic resonance
PTV	Programmable Temperature Vaporizing
PXRD	Powder X-ray diffraction
RNA	Ribonucleic acid
r.t.	Room temperature
Siderophile	Metal loving
SIM	Single ion mass
SHE	Standard Hydrogen Electrode
TIC	Total ion count

---



## List of Figures

<b>Figure 1</b> Increasing trend in the number of publications on the topic of prebiotic chemistry extracted from the Web of science database since 1974 using the keyword "prebiotic chemistry". .....	4
<b>Figure 2</b> Mackinawite structure alongside the a-axis (left) and the c-axis (right). yellow: sulfur; brown: iron; orange: tetrahedra. ....	10
<b>Figure 3</b> Comparison between the transfer methods. Both experimental series (black: HST-01; green: HST-02) showed that the extraction by a transfer line leads to higher levels in CH <sub>3</sub> SH.....	26
<b>Figure 4</b> Collected PXRD pattern from the reaction of iron and sulfur in acetone/water (10:1) (SP-FeS-04) and in water (SP-FeS-06) at r.t. after 5 d. ....	34
<b>Figure 5</b> Sequence of images extracted from a 9-h long video where the reaction between iron and sulfur was monitored in a 1 M NaCl solution.....	36
<b>Figure 6</b> SEM (left) and TEM (right) images of deactivated mackinawite produced from the between iron and sulfur at r.t. in a 0.01 M NaCl solution for 12 h. ....	37
<b>Figure 7 Left:</b> Collected PXRD pattern from the products from the reaction between iron and sulfur after different times. Mackinawite (Mak) started to form only after an initial induction period around 24 h. <b>Right:</b> Plot of the sulfur content of a reaction containing iron and sulfur in pure H <sub>2</sub> O over time. ....	39
<b>Figure 8</b> Mössbauer spectra of deactivated mackinawite from the reaction between iron and sulfur in a 0.01 M NaCl after 24 h. The spectrum was measured by M. Winkler....	41
<b>Figure 9</b> SEM image of mackinawite that was in contact with air for several weeks. The surface smoothed as a passivating layer of amorphous iron oxides is formed.....	42
<b>Figure 10</b> PXRD pattern of the product from the reaction of nickel and sulfur in pure H <sub>2</sub> O after 3 d at 80 °C; S = Sulfur, Hw = Heazlewoodite. ....	46
<b>Figure 11</b> Series of PXRD pattern collected from samples containing different mixtures of iron and nickel after 7 d at 80 °C in H <sub>2</sub> O.....	47

<b>Figure 12</b> Gas chromatogram (TIC) of GP-01-01 (a), GP-01-02 (b), GP-01-03 (c) and GP-01-04 (d). The full list of detected compounds is given in Table A 2. ....	53
<b>Figure 13</b> Compared TIC areas of the samples GP-01-01 to GP-01-04. ....	54
<b>Figure 14</b> Proposed reaction mechanism for the reduction of HCN by the iron surface. ....	56
<b>Figure 15</b> Proposed fate of the residue formed at BP <sub>3</sub> to explain the formation of the different C <sub>4</sub> isomers. ....	58
<b>Figure 16</b> Gas chromatogram of GP-03-01 and GP-03-02. ....	59
<b>Figure 17</b> Formation of CH <sub>3</sub> SH and CS <sub>2</sub> over a period of 96 h, together with their calculated ratio. ....	60
<b>Figure 18</b> Mass patterns retrieved from the reaction between the iron sulfur mixture with K <sup>12</sup> CN (black) and Na <sup>13</sup> CN (green). ....	61
<b>Figure 19</b> UV/Vis spectra of the filtrated green solution (solid line) together with the one of pure H <sub>2</sub> O (dashed line). Values in parentheses relate to the ones given by Taylor and Shoemith. ....	63
<b>Figure 20</b> Collected <sup>1</sup> H-NMR spectra (D <sub>2</sub> O, 400 MHz) of the aqueous phase from the reaction between the iron sulfur mixture and KCN at pH 9. ....	64
<b>Figure 21</b> <sup>1</sup> H-NMR spectra (D <sub>2</sub> O, 400 MHz) of the reaction between iron, sulfur and KCN in H <sub>2</sub> O and D <sub>2</sub> O at pH 4 and 9. The H <sub>2</sub> O signal was removed for clarity. ....	65
<b>Figure 22</b> CV diagrams of an aqueous solution derived from the reaction between iron, sulfur and KCN at 80 °C at different scan rates ( <b>top</b> ) and after the subsequent addition of acid ( <b>bottom</b> ), in the presence of 1 M [ <i>n</i> -Bu <sub>4</sub> N][PF <sub>6</sub> ]. The arrow indicates the scan direction. The potential E is referenced to the Fc <sup>+</sup> /Fc couple. ....	66
<b>Figure 23</b> Gas chromatogram (TIC) of GP-05-02. ....	69
<b>Figure 24</b> Gas chromatogram (TIC) collected from the cyclohexane extract of the aqueous phase of GP-06. ....	70

<b>Figure 25</b> Proposed mechanism for the formation of cyclic species from the reaction between iron, sulfur and KCN at 80 °C. *The standard potentials for the oxidation of iron were measured against SHE. <sup>[92]</sup> .....	71
<b>Figure 26</b> Gas chromatograms (TIC) collected from the gas phases of GP-07-01 (black, r.t.) and GP-07-02 (green, 80 °C).....	72
<b>Figure 27</b> Course of the CH <sub>3</sub> SH concentration in the headspace of samples heated for different reaction times (GP-10). Calibrated with CAL-MT-5.....	73
<b>Figure 28</b> Comparison of the mass patterns of the CH <sub>4</sub> signals gathered from the reaction with K <sup>12</sup> CN (black) and Na <sup>13</sup> CN (green).....	74
<b>Figure 29</b> Gas chromatogram (TIC) of the gas phase of GP-08-01 after the first (black) and second (green) release of reduced compounds. The gas phase was extracted using a transfer line and therefore emptied through the first extraction. ....	75
<b>Figure 30</b> Calculated areas (SIM) of CH <sub>4</sub> , H <sub>2</sub> S, CH <sub>3</sub> SH and CS <sub>2</sub> when different initial amounts of acid were added. The half-filled symbols account for the first (top filled) and second (bottom filled) extraction. Fully filled symbols illustrate the total amount after first and second extraction. ....	76
<b>Figure 31</b> Gas chromatogram obtained from GP-09-03 (black, without KCN) and GP-09-06 (green, with KCN) where the mackinawite was left compressed on the bottom of the sample vials. ....	77
<b>Figure 32</b> Collected mass patterns for the oxygenated species. All compounds showed the expected mass shift when Na <sup>13</sup> CN (green pattern) was used.....	77
<b>Figure 33</b> PXRD pattern collected from the solid reaction product from the reaction between mackinawite and KCN at pH 3; Sulfur = S, Mackinawite = Mak, Greigite = G, Prussian blue = PB. ....	79
<b>Figure 34</b> Mössbauer spectrum of the solid reaction product from the reaction between mackinawite and KCN at pH 3. Green: First doublet ( <i>D</i> <sub>1</sub> ); Orange: Second doublet ( <i>D</i> <sub>2</sub> ), Blue: First sextet ( <i>St</i> <sub>1</sub> ), Red: Second sextet ( <i>St</i> <sub>2</sub> ). The spectrum was measured by M. Winkler.....	80

<b>Figure 35</b> Comparison of some products formed from the reduction of KOCN and KSCN by iron powder at pH 3 and pH 6. ....	82
<b>Figure 36</b> Product distribution from the reduction of KOCN and KSCN by the iron sulfur mixture at pH 3. ....	83
<b>Figure 37</b> Gas chromatogram (TIC) from the reduction of KOCN and KSCN by mackinawite at pH 3. ....	84
<b>Figure 39</b> Collected mass patterns of the reaction products from the reduction of $\text{KS}^{13}\text{CN}$ (solid lines) and $\text{KO}^{13}\text{CN}$ (opaque lines) by mackinawite at pH 3. ....	85
<b>Figure 39</b> Collected mass patterns of the $\text{CH}_4$ signal from the reduction of $\text{KO}^{13}\text{CN}$ and $\text{KS}^{13}\text{CN}$ . Only the reduction of KSCN led to a $m/z = 17$ signal. ....	85
<b>Figure 40</b> Time dependent formation of $\text{CH}_3\text{SH}$ (squares) and $\text{COS}$ (circles) from KSCN (black) and KOCN over a total time frame of 188 h. ....	86
<b>Figure 41</b> Collected PXRD pattern (SP-FeS-09) of the solid residue from the reduction of KSCN by mackinawite at pH 3. Most of the reflexes could be assigned to greigite (G) and mackinawite (Mak) and an unknown compound (?). ....	87
<b>Figure 42</b> Comparison of the calculated areas from the TIC for the respective reaction products from the reduction of KSCN by mackinawite. The areas of the $\text{CH}_4$ signal were enhanced. ....	88
<b>Figure 43</b> Comparison of the structures of mackinawite alongside the a and c axis (a), and the $[\text{Fe}_4\text{S}_4](\text{SH})_4$ model complex (b). ....	89
<b>Figure 44</b> Proposed mechanism for the reduction of HCN by the mackinawite surface groups. The reaction energies (grey, in $\text{kcal mol}^{-1}$ ) were calculated by DFT on a modified $[\text{Fe}_4\text{S}_4]$ model complex. Green: Direct reduction pathway, starting at 1*, leading to the formation of $\text{CH}_3\text{SH}$ and $\text{CH}_4$ . Blue: Thionation pathway, leading to additional branching points for $\text{CH}_3\text{SH}$ formation. Orange: Pathway for C – C bond formation and subsequent production of $\text{CH}_3\text{CHO}$ and $\text{C}_1$ to $\text{C}_4$ thiols. The calculations were performed by M. T. Stiebritz, and computational details are given in 2.2.10. ....	90

<b>Figure 45</b> Proposed mechanism for the reduction of HSCN by the mackinawite surface groups. ....	92
<b>Figure 46</b> Proposed mechanism for the reduction of HOCN by the mackinawite surface groups. ....	93
<b>Figure 47</b> <sup>1</sup> H-NMR spectra (D <sub>2</sub> O, 400 MHz) of aqueous solution acquired from samples were KCN and KSCN were either reacted with iron or mackinawite. The signal at 4.7 ppm corresponds to H <sub>2</sub> O. The spectra gathered from the reaction of KCN were measured with H <sub>2</sub> O suppression to elevate the resolution. ....	96
<b>Figure 48</b> Adapted reduction mechanism for N <sub>2</sub> and NO <sub>3</sub> <sup>-</sup> supported by the mackinawite surface groups. The reduction of [H <sub>2</sub> NO <sub>3</sub> ] <sup>+</sup> is highlighted in green, the one of N <sub>2</sub> in blue. ....	97
<b>Figure 49</b> Comparison of the CS <sub>2</sub> concentration in the gas phase of mackinawite samples that were either heated (80 °C) at pH 3 (GP-17) or pH 6 (GP-18). ....	102
<b>Figure 50</b> Comparison of the product formation from samples that were charged with the CS <sub>2</sub> /EtOH mixture instead of pure CS <sub>2</sub> . (left). ....	103
<b>Figure 51</b> PXRD pattern (SP-FeS-10) collected from the solid residue of the reaction between mackinawite and CS <sub>2</sub> ; Mak* = “swollen” Mackinawite, S = Sulfur, ? = unknown. ....	104
<b>Figure 52</b> Proposed reduction mechanism involving the MCS <sub>DP</sub> of mackinawite. The reaction energies were calculated by DFT on a [Fe <sub>4</sub> S <sub>4</sub> ] model cluster. The reaction energies (grey) are given in kcal mol <sup>-1</sup> . The calculations were performed by M. T. Stiebritz. ....	106
<b>Figure 53</b> Gas chromatogram (TIC) collected from the gas phase of GP-20 after the sample was first left 2 d at r.t. and then heated to 80 °C for 3 d. ....	107
<b>Figure 54</b> PXRD pattern (SP-FeS-11) collected from the solid product after the reaction between mackinawite and CH <sub>3</sub> SNa after 3 d at 80 °C; Mak = mackinawite, G = greigite. ....	109

<b>Figure 55</b> Proposed mechanism for the reduction of CH <sub>3</sub> SH by the mackinawite surface groups. ....	110
<b>Figure 56</b> Gas chromatograms (TIC) collected from the gas phases of GP-23-02 (black), GP-24-02 (green) and GP-25-02 (blue) after 6 d at 80 °C (pH 2). ....	113
<b>Figure 57</b> TIC areas of N <sub>2</sub> O, CH <sub>4</sub> and longer hydrocarbons from GP-25-01 (1 day), GP-22-02 (3 days) and GP-25-02 (6 days). ....	114
<b>Figure 58</b> Time dependent formation of CH <sub>3</sub> SH from [Fe(CN) <sub>6</sub> ] <sup>4-</sup> , [Fe(CN) <sub>6</sub> ] <sup>3-</sup> and [Fe(CN) <sub>5</sub> (NO)] <sup>2-</sup> supported by mackinawite (80 °C, pH 3). Calibrated by CAL-MT-5. ...	115
<b>Figure 59</b> Concentration of the remaining CO <sub>2</sub> in the gas phase of mackinawite samples under dry (AD-02-01) and wet (AD-02-02) conditions with the respective dry (AD-02-03) and wet (AD-02-04) blanks. ....	120
<b>Figure 60</b> Course of the CO <sub>2</sub> concentration after subsequent injection of 100 µL ( <b>left</b> ) or 250 µL ( <b>right</b> ) CO <sub>2</sub> to samples either containing mackinawite from iron and sulfur (AD-03-01 and AD-04-03) or from precipitation (AD-03-02 and AD-04-02). Sample AD-04-01 contained mackinawite from the elements that was left in contact with air. ....	121
<b>Figure 61</b> SEM images of a mackinawite sample that was stored under 100 % CO <sub>2</sub> atmosphere for several weeks (SP-FeS-12). The surface significantly underwent chemical changes as highly defined cubic crystals formed. ....	122
<b>Figure 62</b> Gas chromatogram (TIC) collected from the gas phase of GP-09-01 and GP-09-03 after 2 d at 80 °C. ....	125
<b>Figure 63</b> Comparison of the amount in CH <sub>4</sub> , CH <sub>3</sub> SH and H <sub>2</sub> S during the subsequent gas phase extractions. Between each extraction 1 mL of a 1 M H <sub>2</sub> SO <sub>4</sub> was added. ....	126
<b>Figure 64</b> Mass patterns of the CH <sub>4</sub> signals from GP-09-01 and GP-09-02 recorded after the first (E1), second (E2) and third (E3) extraction. ....	127
<b>Figure 65</b> Proposed mechanism for the reduction of H <sub>2</sub> CO <sub>3</sub> by the mackinawite surface groups. ....	129

## List of Tables

<b>Table 1</b> Reduction systems used during the thesis.....	23
<b>Table 2</b> List of columns used during the thesis. <b>Abbr.:</b> Thickness ( <b>d</b> ), Length ( <b>l</b> ), Diameter ( <b>∅</b> ), Maximum working temperature ( <b>T<sub>max</sub></b> ).....	29
<b>Table 3</b> Retention times of gaseous compounds on the respective column used.....	29
<b>Table 4</b> Mössbauer parameters for mackinawite produced by different synthetic routes and the ones for the mackinawite from the reaction between iron and sulfur.....	40
<b>Table 5</b> Data in the literature on the d-spacing value of mackinawite produced by different synthetic routes together with the ones of the mackinawite from the reaction between iron and sulfur. ....	44
<b>Table 6</b> Relative abundancies of CH <sub>3</sub> CHO and CH <sub>3</sub> SH after subsequent gas phase extraction and acidification at 80 °C and after boiling. Calibrated with CAL-MT-2. <b>E2</b> = Second Extraction, <b>E3</b> = Third Extraction.....	78
<b>Table 7</b> Diffraction peaks collected from the solid product of SP-FeS-10, compared with the ones of SP-FeS-03. ....	105
<b>Table 8</b> Summarized relative abundances of the reaction products. The concentration of CS <sub>2</sub> was calculated from CAL-CD. ....	108
<b>Table 9</b> Comparison between AD-02-01 and AD-04-03. The amount of adsorbed CO <sub>2</sub> ( <b>n<sub>ad,calc.</sub></b> ) is estimated by subtraction the CO <sub>2</sub> concentration of the mackinawite containing samples from ones where no mackinawite was present (blank).....	121
<b>Table 10</b> Composition of the samples for SP-NiFeS-01 to SP-NiFeS-11. ....	148
<b>Table 11</b> Composition of the samples used for SP-NiFeS-12 to SP-NiFeS-21. ....	149
<b>Table 12</b> Parameters and observations for samples of LP-01. ....	151
<b>Table 13</b> Parameters and observations for the samples of LP-02.....	152
<b>Table 14</b> Composition of the samples of LP-05. ....	153
<b>Table 15</b> Composition of the samples of GP-01.....	154

<b>Table 16</b> Composition of the samples of GP-03.....	155
<b>Table 17</b> Composition of the samples of GP-04.....	155
<b>Table 18</b> Composition of the samples of GP-05.....	156
<b>Table 19</b> Composition of the samples of GP-06.....	157
<b>Table 20</b> Composition of the samples of GP-08.....	158
<b>Table 21</b> Composition of the samples of GP-11.....	159
<b>Table 22</b> Composition of the samples of GP-19.....	161
<b>Table 23</b> Composition of the samples GP-32, GP-33, GP-34, GP-35, GP-36, and GP-37. .....	163
<b>Table 24</b> Composition of the samples of GP-09.....	165
<b>Table 25</b> List of substrates for the kinetic investigations. ....	165



## Chapter 1. Introduction

The terrestrial origin of life is a one-of-a-kind event in earth's history, which until now could not be repeated under laboratory conditions.<sup>[1]</sup> While the earliest theories on this topic assumed more simplified, and straightforward approaches based on chance (1.1.1), we today know, that this singularity appeared due to a chemical evolution, starting from small and oxidized substrates like carbon dioxide (CO<sub>2</sub>).<sup>[2-5]</sup> Until now, however, only a few chemical compounds are known to support carbon fixation from CO<sub>2</sub> or other C<sub>1</sub> substrates like hydrogen cyanide (HCN). More recent theories on the origin of life therefore focused more on finding suitable and prebiotically plausible ways to resolve this problem.<sup>[6-13]</sup> Therein, iron sulfides earned a lot of attention due to their rather simple formation by precipitation at hydrothermal vents.<sup>[14-16]</sup> Mackinawite, the first iron sulfide phase formed by this process, is a layered iron sulfide with the formula Fe<sup>2+</sup>S<sup>2-</sup>. Its role as primordial energy source is still highly debated<sup>[17-19]</sup> even though it could experimentally be shown to support nitrogen fixation from nitrate (NO<sub>3</sub><sup>-</sup>).<sup>[20]</sup> This chapter gives an overview on the current standpoint of prebiotic chemistry and a more detailed view on iron sulfides and their role in this field of research.

### 1.1 The origin of life

#### 1.1.1 A brief history

For a long time in the history of humankind, life was thought to arise from non-living matter, merely by chance. Concepts of such a spontaneous origin were first explained by Aristotle in his book *On the Generation of Animals*.<sup>[21]</sup> The missing knowledge on basic biological processes did not let anyone doubt this approach as such events were common to observe. The idea on the spontaneous generation of life through lived many centuries in history but was lastly dismissed by L. Pasteur while he was conducting his research on fermentation. During the experiments he found that grapes that once were pasteurized, did not ferment anymore to produce wine. With that he assumed, that also the previously presented examples of spontaneous generation were fundamentally

flawed as, like in his experiments, the organic material was probably introduced in form of contaminations.<sup>[22]</sup> He therefore stated:

*Never will the doctrine of spontaneous generation recover from the mortal blow of this simple experiment. There is no known circumstance in which it can be confirmed that microscopic beings came into the world without germs, without parents similar to themselves. **Louis Pasteur, 1864***

The falsification of the spontaneous generation of life opened the door for new theories. It took only a few years after L. Pasteur's discovery for other scientist to assume a generation of "living" matter from purely inorganic substrates. The complexity of this hypothesis, however, was already acknowledged by C. Darwin, who called it rubbish to think about something like that.<sup>[23]</sup> Only a few years later, after E. Haeckel introduced the term prebiotic broth, C. Darwin seemingly changed his mind and wrote in a private letter:

*It is often said that all the conditions for the first production of a living organism are now present, which could ever have been present. But if (and oh! what a big if!) we could conceive in some warm little pond, with all sorts of ammonia and phosphoric salts, light, heat, electricity, etc. present, that a protein compound was formed, ready to undergo still more complex changes, at the present day such matter would be instantly devoured or absorbed, which would not have been the case before living creatures were formed. **Charles Darwin, 1868***

This first attempt to describe the formation of life was further developed first by A. I. Oparin and later by J. B. S. Haldane during the 1920s. Both were able to give a chemical description on the conditions during the first phases after the formation of the earth.<sup>[24,25]</sup> They almost simultaneously concluded that oxygen (O<sub>2</sub>) could not have been present in the primitive atmosphere and favored CO<sub>2</sub> as major atmospheric component.<sup>[26]</sup> Though, their approaches were quite different, both proposed ways to establish C – C bond formation from C<sub>1</sub> substrates. A. I. Oparin assumed that most of the initial carbon present on earth reacted to form metal carbides that upon cooling down released acetylene which would undergo polymerization under certain catalytic conditions. J. B. S. Haldane further suggested, that more complex organic compounds

would be formed, when aqueous solutions, containing CO<sub>2</sub> and ammonia (NH<sub>3</sub>), are irradiated with “chemically active ultraviolet rays”. In addition to these concepts J. D. Bernal added the possibility of clays providing active surfaces where organic material could concentrate and therefore undergo polymerization or condensation reactions.<sup>[27]</sup>

The first experimental evidence for the formation of biologically relevant molecules from purely inorganic precursors was observed during the spark discharge experiment conducted by H. C. Urey and S. L. Miller in 1953.<sup>[28]</sup> Their apparatus was used to circulate a mixture of methane (CH<sub>4</sub>), NH<sub>3</sub>, water (H<sub>2</sub>O) and hydrogen gas (H<sub>2</sub>) by heating a H<sub>2</sub>O reservoir in presence of an electrical discharge. After several days, an array of organic compounds formed and accumulated in the aqueous phase. HCN and different aldehydes were detected and proposed to act as intermediates during the formation of some of the observed products. Once formed, aldehydes, NH<sub>3</sub> and HCN can react in form of the Strecker synthesis to yield amino and hydroxy nitriles, which finally hydrolyze into β-alanine and succinic acid.<sup>[29]</sup> More recent investigations on samples derived from this experiment provided an even broader range of products, including urea, cyanoacetylene, carboxylic acids and amines.<sup>[30]</sup>

The term “chemical evolution” was first used by J. D. Bernal in 1949 and further defined by M. Calvin as a period in earth’s history, after the planet formed and before biological evolution started.<sup>[31]</sup> M. Calvin further stated that this period in earth’s history did not appeared with strict start and end points, but was more likely present already during earth’s formation and proceeded after the first life has emerged. He and his coworkers further experimentally followed the ideas of J. B. S. Haldane, who suggested the formation of “fairly complex compounds” after irradiating an aqueous solution containing CO<sub>2</sub> and NH<sub>3</sub>. They assumed, that when a solution of formic acid or formaldehyde is irradiated in presence of a nitrogen compound, it is possible for more complex molecules like amino acids or heterocyclic compounds can emerge. They further provided evidence for the formation of C<sub>4</sub> compounds from C<sub>2</sub> precursors, after using high-energy radiation.

In a later study, J. Oró and coworkers reported the formation amino and hydroxy acids from the reaction between formaldehyde and hydroxylamine hydrochloride in aqueous

solution already at temperatures below 100 °C.<sup>[32]</sup> Like during the experiments performed by H. C. Urey and S. L. Miller, HCN was assumed to be formed as intermediate. In a later study J. Oró therefore investigated the reaction of ammonium cyanide in aqueous solution and reported the formation of adenine already after 24 h at 90 °C.<sup>[33]</sup> Only shortly after his finding, J. Oró was able to resolve the formation mechanism which is based on the nucleophilic attack of both the cyanide ion, as well as NH<sub>3</sub> molecule, towards a HCN molecule. These reactions lead to the intermediate formation of 4-aminoimidazole-5-carboxamide and formamide, respectively, which in a next step can react to form adenine and NH<sub>3</sub>.<sup>[34]</sup>

The breakthrough experiments by S. L. Miller and J. Oró marked the starting point for modern theories on the emergence of life. The term prebiotic chemistry was established by R. Lohrmann and L. E. Orgel in 1974<sup>[35]</sup> and led to a steadily increasing number of publications on this topic during the following decades (Figure 1). The answer on the question of how life emerged on earth is as old as of humankind itself. In contrast to other events of this scale we until now only have understood a few aspects of the huge network leading to the formation of the first life forms able to replicate and evolve. It is

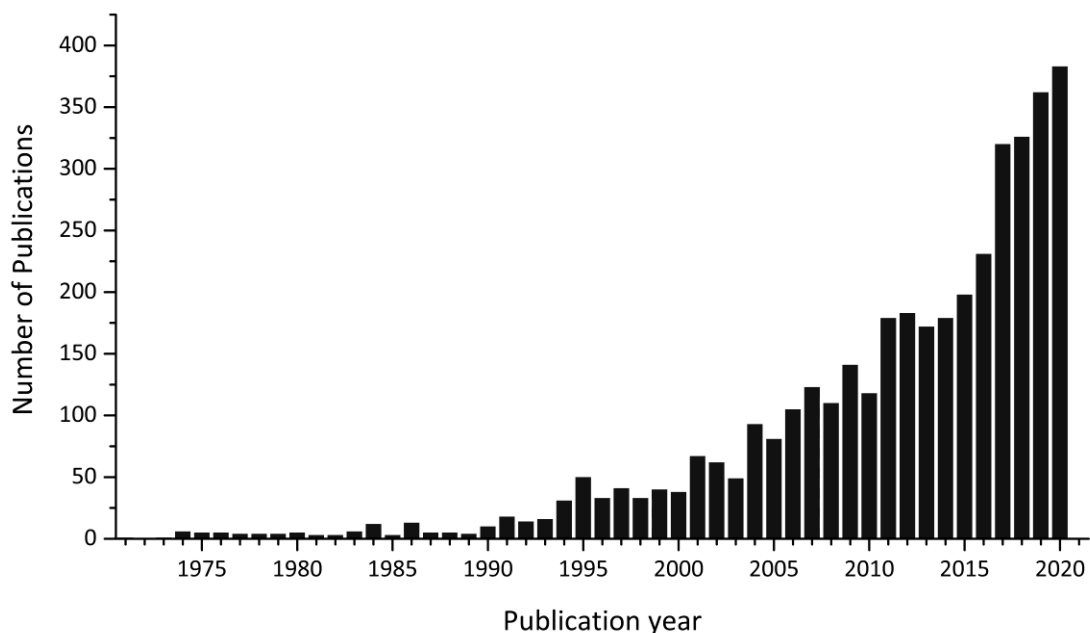


**Figure 1** Increasing trend in the number of publications on the topic of prebiotic chemistry extracted from the Web of science database since 1974 using the keyword "prebiotic chemistry".

therefore inevitable to further search for prebiotically relevant reactions and scenarios under which such an extensive chemical evolution can take place.

### **1.1.2 Theories on the origin of life**

In the decades after the first experimental evidence for the formation of organic compounds from purely inorganic precursors several theories on the origin of life were proposed. Most of the more established theories are thereby strictly divided by the question if either replication or metabolism appeared first. The groundwork for the route towards a replicating system like RNA was laid out early by the works of Miller and Oro. This idea would, however, only provide a part for the solution to this problem as especially the prebiotic relevance of inevitable precursors like HCN is still under debate. Furthermore, processes like condensation or polymerization are highly dependent on conditions of high concentrations to proceed efficiently. The idea that minerals can support such processes was already formulated by Bernal in 1949.<sup>[27]</sup> He stated that the anionic surface of finely distributed clay particles would lead to the adsorption of organic molecules and therefore concentrate the monomers. Recently, Hatton et al. provided evidence for a similar ability of mackinawite to bind nucleic acids in aqueous solution.<sup>[36]</sup> It therefore seems essential to consider the full range in prebiotically relevant reactions established until now to get a better understanding of the interconnectivity between these previously established theories. In the following section a short overview on a selection of theories on the origin of life is given.

#### **1.1.2.1 Pond theory**

The basic idea for this theory was first formulated by Darwin in a private letter to his friend Hooker. He there stated that simple inorganic precursors like  $\text{NH}_3$  and phosphorous salts would lead to the formation of more complex molecules when energy was introduced. For a long time afterwards, this idea was handled as the most anticipated scientific theory on the origin of life. The experiments conducted by Calvin and Miller furthermore supported the scenario that life emerged on the earth's early surface, where sunlight, lightning and high-energy radiation are plenty available.

With more knowledge on the formation of planetary systems and the primordial environment in general, this theory faced resistance.<sup>[37]</sup> It became clear, that the inner planets of the solar system suffered from a long-lasting bombardment and that the conditions of the earth's young surface were rather harsh, especially during the early phases after its formation. Furthermore, the previously anticipated, reduced, atmosphere was more than less disproven as a more oxidized, CO<sub>2</sub> rich, primitive atmosphere became more plausible.

The idea of an origin of life on the earth's surface did however not fully disappear as it still provides some advantages when compared to other scenarios, e.g., hydrothermal vents (1.1.2.3 and 1.1.2.4). When located at the surface of the earth, such ponds would provide wet-dry cycles whereas water would only be present periodically. This is still seen as a key step in polymerizing monomers into macro molecular structures like peptides, proteins or RNA.<sup>[38,39]</sup> Furthermore, substrates like HCN, which tend to hydrolyze into formic acid and NH<sub>3</sub> in aqueous solution, would only be accessible for e.g. adenine formation.

### **1.1.2.2 RNA world theory**

The prebiotic formation of adenine set the starting point for one of the most prominent theories on the origin of life. The RNA world theory strongly follows the approach of "replication first", which is considered to have preceded metabolism.<sup>[40]</sup> This idea was first mentioned by Gilbert who recognized that RNA possesses both, informational and catalytic properties.<sup>[41]</sup> This finding led to the general assumption that self-replicating molecules could have formed from nutrient rich aqueous solutions and started to evolve into more complex structures like DNA.<sup>[42]</sup>

The synthesis of RNA components under prebiotic conditions was extensively studied by several groups. The synthetic formation of nucleosides from deoxyribose and ribose with different bases was first reported by Orgel et al. in 1967.<sup>[43]</sup> Only shortly after that they further provided evidence of the formation of the nucleotide uridine-5-phosphate from uridine and inorganic phosphate in aqueous solution.<sup>[44]</sup> Until now further synthetic routes towards nucleoside were established by Carell et al.<sup>[45]</sup> and Sutherland et al.<sup>[46]</sup>

The RNA molecule is structurally much more complex than the reaction products from carbon fixation and, therefore, became relevant to both, store information and perform catalytic tasks as soon as more defined environments like cells were established. The route towards such a molecular allrounder seems inevitable when the origin of life is discussed. The theory, however, lacks in reasonable ways to abiotically produce necessary basic chemical components to realize the synthesis of amino acids, peptides, or higher molecular species. It therefore partly relies on the transport of pre-produced organic compounds by the LHB or comparable events to the earth during the first million years.<sup>[47,48]</sup> The term pre-produced, thereby, means that the compounds were either initially formed on the young earth and transported into space through large scale impacts where they could undergo another set of reactions or be fully produced on meteorites or comets. In scope of this thesis the RNA world theory is considered a crucial step in the origin of life but can only explain a few steps in a much greater chemoautotrophic network of reactions.

#### **1.1.2.3 The Iron Sulfur World theory**

The iron sulfur world theory (ISWT) was formulated by G. Wächtershäuser in 1988 and further developed in the following years.<sup>[49–51]</sup> Until then the origin of life was widely believed to have proceeded by a heterotrophic process, most likely following the approach of the RNA world theory. An autotrophic mechanism would be much more efficient way to produce reduced compounds, but also dependent on an appropriate energy source. Wächtershäuser introduced the idea that ferrous sulfide can react with hydrogen sulfide (H<sub>2</sub>S) or HS<sup>-</sup> to form pyrite and H<sub>2</sub> and thereby provided a plausible solution for this problem.<sup>[50,52]</sup>



$$\Delta G^0 = -38.6 \text{ kJ mol}^{-1}, \text{ pH} = 6.5$$

In addition, he postulated that the mostly anionic products from carbon fixation would remain bound in their nascent state to the positively charged surface of the pyrite particles. In contrast to other surface mediated models of condensation or polymerization on e.g. clay surfaces, the chemoautotrophic metabolism proposed by

Wächtershäuser is faced with the problem of desorption, rather than adsorption.<sup>[49]</sup> Elongated chains would only occur if a nascent species is able to survive long enough before becoming desorbed and released into solution.

In theory, this idea would provide a reasonable pathway towards the first steps of a long-lasting chemical evolution from oxidized substrates like CO<sub>2</sub>. It gained even greater popularity after the prebiotic scenario was changed from surface near shallow waters towards undersea hydrothermal vents.<sup>[10,53]</sup> Though, the earth's earliest atmosphere was probably oxidized, reduced volcanic gases like H<sub>2</sub>S and H<sub>2</sub> could have been exhausted early on as soon as the water entered the mantle in deeper depths.<sup>[54]</sup> In areas, where the concentration in dissolved metal ions is high, metal sulfides precipitate at the phase interface in form of black clouds, which led to the term "black smokers".<sup>[55,56]</sup>

The location at the bottom of the ocean thereby offers multiple benefits for a first chemoautotrophic organism to have evolved. In contrast to the earth's surface much more stable conditions can be established over long periods, even during the LHB. At such site a first organism probably fed on CO<sub>2</sub> and carbon monoxide (CO), and thereby produced methanethiol (CH<sub>3</sub>SH), which subsequently is carbonylated into thioacetic acid and further hydrolyzed into acetic acid (HAc).<sup>[10]</sup> A reasonable fate for the products is given by C. de Duve in his thioester world.<sup>[57,58]</sup> He proposed that thiols and carboxylic acids served as energy source for the origin of life. Latter are further assumed to participate in the formation of peptides and served as a feedstock for the first metabolic cycles like the acetyl-coenzyme A (CoA) pathway or the citric acid cycle.

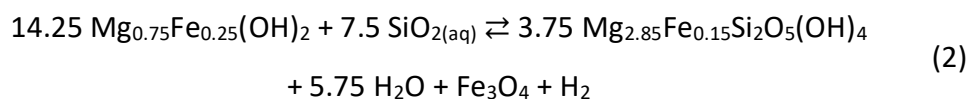
#### **1.1.2.4 Last common universal ancestor**

The theory of universal common ancestry (UCA) was already proposed by Darwin over 150 years ago and still resembles a central pillar of modern evolutionary theory.<sup>[59,60]</sup> For a long time cellular life was divided into eukaryotes and prokaryotes under the assumption that the first arose from latter. This view changed with the introduction of Archaea by Woese et al. in 1977. Based on their findings they assumed that cellular life has to be divided into three domains which all originated from a simpler last common universal ancestor (LUCA).<sup>[61–65]</sup>



Like in the case of the ISWT the introduction of hydrothermal vents as primordially relevant locations led to the assumption that LUCA first emerged in the depths of the early ocean. In contrast to the ISWT, however, Russell et al. considered the precipitated iron sulfides as a potential source of electrons due to their conductive property and the readiness of iron to switch its valence charge.<sup>[66,67]</sup> Though, the standard electrode potential for the oxidation of Fe<sup>2+</sup> is high, this process can be supported by the conductive bulk material, only allowing redox reactions at the surface of the particles. The loss of electrons in the interior leads to a reduced ionic radius of the iron and promotes diffusion processes which consequently enable the reactions into greigite or smythite.<sup>[68]</sup>

Russell et al. further proposed that the reduced, sulfide containing, alkaline exhalations would readily lead to the formation of iron sulfide membranes where they interfaced with the more acidic Hadean Ocean, which most likely was rich in iron.<sup>[14,67,69]</sup> The iron sulfide membrane is assumed to have acted as a semipermeable boundary, after the spheres were inflated with exhalations, rich in other substrates like CO<sub>2</sub>, H<sub>2</sub>S and H<sub>2</sub>, provided by the vent system. In contrast to the ISWT, where H<sub>2</sub> is mainly produced by the reaction between iron sulfides and H<sub>2</sub>S, they suggested the serpentinization reaction as a more suitable source for H<sub>2</sub>.<sup>[70]</sup>



The “Lost City” hydrothermal site, in contrast to black smokers, are white in color due to massive carbonate precipitates and exhale, as predicted by Russell et al., more alkaline aqueous solutions with a pH of 9.0 – 9.8.<sup>[71]</sup> The vents were found to be driven by the exothermic serpentinization reaction between sea water and mantle rocks, whereas the exhalations become mainly reduced and are rich in H<sub>2</sub> and CH<sub>4</sub>.<sup>[72]</sup> Based on this finding Martin et al. proposed that LUCA was not a free-living cell, but remained bound to the porous structure of the chimneys.<sup>[73]</sup> They assumed that the secure environment allowed first metabolic cycles to appear inside the compartments whereas the iron nickel sulfide layer would secure the intermediates from dissolution into the

ocean. Though, this scenario seems reasonable, no experimental evidence for such a system was provided until now.

## 1.2 Mackinawite

The generic term iron sulfide can be used to describe a wide range of chemical species in form of solid minerals or molecular complexes. Known minerals include mackinawite (FeS), pyrrhotite ( $\text{Fe}_{1-x}\text{S}$ ), troilite ( $\text{Fe}_{1-x}\text{S}$ ), greigite ( $\text{Fe}_3\text{S}_4$ ), smythite ( $\text{Fe}_3\text{S}_4$ ), pyrite ( $\text{FeS}_2$ ), marcasite ( $\text{FeS}_2$ ) and tochilinite ( $\text{Fe}_{1-e}\text{S}^*x(\text{Mg,Al,Fe})(\text{OH})_2$ ). Mackinawite is the first iron sulfide formed naturally by precipitation and is known to undergo reactions into other iron sulfides upon aging or when being heated. Due to its high tendency to undergo oxidation it today only occurs naturally under strictly anoxic conditions e.g., at undersea ridges.

### 1.2.1 Properties

Mackinawite crystallizes with tetragonal symmetry in the space group  $P4/nmm$  providing cell parameters of  $a = 3.67 \text{ \AA}$  and  $c = 5.03 \text{ \AA}$ .<sup>[74]</sup> The sulfide ions form a distorted cubic closed packed lattice with iron ions occupying one-half of the tetrahedral sites. The iron atoms in mackinawite form square sheets with a Fe to Fe distance of  $2.5967 \text{ \AA}$ , which is very close to the one observed in  $\alpha$ -iron.<sup>[74]</sup> In contrast to cubic iron, mackinawite has a layered structure as filled and empty layers alternate. The interlayer

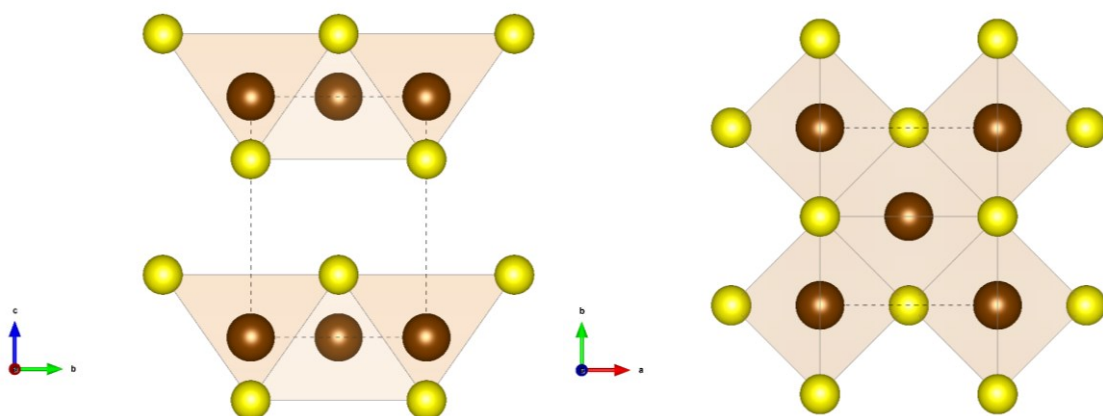
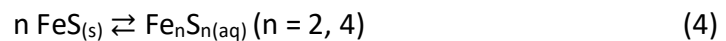


**Figure 2** Mackinawite structure alongside the a-axis (left) and the c-axis (right). yellow: sulfur; brown: iron; orange: tetrahedra.

attractions are mainly caused by van der Waals forces and the resulting interlayer spacing is nonpolar in natural mackinawite.

The Fe/S ratio in mackinawite is close to one but can vary depending on the used synthetic method. When mackinawite is produced by precipitation, both an insufficiencies in iron<sup>[75,76]</sup> but also in sulfur<sup>[77]</sup> were reported. Lennie et al. were able to produce large mackinawite crystals from the reaction of  $\alpha$ -iron (iron wire) in aqueous sulfide solution and reported a Fe/S ratio of 0.99.<sup>[74]</sup> This could later be supported by Rickard et al. who produced mackinawite by precipitation with a ratio of one. <sup>[78]</sup> They further concluded that the previous inconsistencies were mainly caused by inclusions in form of salts or other metal ions but could also follow from the formation of sulfur during the acidic dissolution.



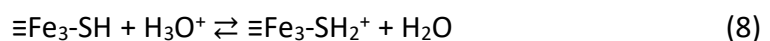
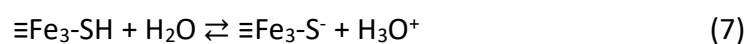
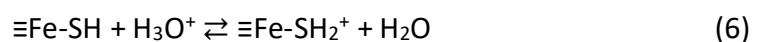
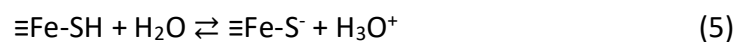
The solubility of mackinawite in aqueous systems is the sum of a pH dependent and a pH independent dissolution process.<sup>[79]</sup> The pH dependent one can partly be described by reaction 3. This process does not proceed selectively and additionally leads to the formation of black rhombic sulfur.<sup>[78]</sup> The pH independent dissolution involves the formation of aqueous iron sulfide clusters ( $\text{Fe}_n\text{S}_{n(aq)}$ ) at  $\text{pH} > 7$  (reaction 4) and has already been suggested to control the dissolution in alkaline solutions.<sup>[80]</sup>

### 1.2.2 Adsorption

The capability of mackinawite to adsorb heavy metals from aqueous solution has been studied extensively. The removal of toxic metal ions like  $\text{Cd}^{2+}$ ,  $\text{Hg}^{2+}$  or  $\text{Pb}^{2+}$  is crucial for the development of methods for wastewater treatment.<sup>[81–86]</sup> This process can either proceed through the adsorption of the heavy metals by the mackinawite surface or by incorporating the metals inside the mackinawite structure, preventing them to be released into the solution afterwards.

The surface chemistry of mackinawite is strongly influenced by the existence of functional groups. Guevremont et al. studied the behavior of mackinawite in aqueous solution and reported that the iron ions on the surface act as Lewis acids and are either coordinated by sulfide or hydroxide groups.<sup>[87,88]</sup> The hydrogen sulfide groups are more acidic than the hydroxide groups and therefore are readily deprotonated under basic conditions. The hydroxide groups, however, are only protonated under more acidic conditions. The point of zero charge ( $\text{pH}_{\text{pzc}}$ ) marks the pH at which protonated and deprotonated surface groups are similar. For pyrite, pyrrhotite, greigite, natural mackinawite and other transition metal sulfides a  $\text{pH}_{\text{pzc}} = 3$  was determined.<sup>[89]</sup> More recent investigations on synthetic mackinawite provided a much higher  $\text{pH}_{\text{pzc}} = 7.5$ .<sup>[80,81,90]</sup> The exact reason for this inconsistency is still up for debate. Wolthers et al. suggested that the  $\text{pH}_{\text{pzc}}$  can vary depending on the degree of surface oxidation, but also be influenced by undiscovered reactions like the intercalation of protons or hydroxide ions.<sup>[80]</sup>

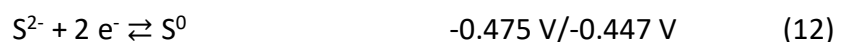
The rather high  $\text{pH}_{\text{pzc}}$  of synthetic mackinawite allows its application as surface active material, even under neutral aqueous conditions. At pH 7 most of the sulfide groups are deprotonated and offer a nucleophilic binding site for positively charged metals or organic compounds. Wolthers et al. were thereby able to formulate a surface complexation model to explain the unusual behavior observed during titration experiments. They concluded that the that multiple distinctly acidic sites must exist to explain their observations. Based on the structure of mackinawite they assumed that the surface chemistry is mainly dominated by a strongly acidic mono-coordinated sites,  $\equiv\text{Fe-SH}$ , and a weakly acidic tri-coordinated sites,  $\equiv\text{Fe}_3\text{-SH}$ .<sup>[80]</sup> The relevant surface protonation reaction can be summarized as:



The adsorption of organic molecules has only been studied throughout a few studies but shows promising results. Hatton et al. provided experimental evidence for the adsorption of different organic polymers, as well as nucleic acids, nucleosides and nucleotides onto different transition metal sulfides like copper, iron and zinc sulfides.<sup>[36]</sup> In a recent study Picard et al. reported that organic compounds can remain preserved on the surface of metastable iron sulfide minerals under anoxic conditions and therefore promote long-term carbon sequestration.<sup>[91]</sup> These findings are further supported by DFT calculations regarding the adsorption of methylamine and cysteine by the mackinawite surface. Dzade et al. thereby showed that both molecules strongly interact with surface sites of lower stability and only weakly with the most abundant and most stable (001) site.<sup>[92,93]</sup>

### 1.2.3 Redox activity

Mackinawite only contains Fe<sup>2+</sup> and S<sup>2-</sup> and therefore is classified as the highest reduced iron sulfide mineral among the known ones. Other minerals like greigite or pyrite either contain Fe<sup>3+</sup> or S<sup>-</sup> ions and were already shown to be produced from mackinawite upon oxidation or aging. The standard redox potential for the oxidation of Fe<sup>2+</sup> to Fe<sup>3+</sup> is given with 0.771 V (SHE). This value is high when compared to other oxidation processes involving iron. The oxidation of elemental iron into Fe<sup>2+</sup> or Fe<sup>3+</sup> is thereby much smaller with -0.44 V and -0.04 V.<sup>[94]</sup> The dissolution of iron in alkaline media by OH<sup>-</sup> shows the lowest standard potential with -0.89 V.<sup>[94]</sup>



The standard potential of S<sup>0</sup>/S<sup>2-</sup> is pH dependent and cannot be determined exactly as a variety of polysulfides are formed in aqueous solution. However, Berner was able to

provide a standard potential of  $-0.447\text{ V}$  for the reversible dissolution of sulfur into  $\text{S}^{2-}$ .<sup>[95]</sup> A similar value of  $-0.447\text{ V}$  is further given by Bard and coworkers.<sup>[96]</sup>

## 1.3 Carbon fixation

### 1.3.1 General information

The possibility of a changing climate, following from the ongoing industrialization, was already proposed in the middle of the 19<sup>th</sup> century. The conclusion that higher atmospheric concentration in  $\text{CO}_2$  could have an influence on global temperatures was first made by E. Foote in 1856 and was presented at the Annual Meeting of the American Association for the Advancement of Science (AAAS) in New York.<sup>[97]</sup> Nearly simultaneously this discovery was made in Europe by J. Tyndall, who exhaustingly tried to experimentally support the ideas of DeSaussure, Hopkins, Pouillet and Fourier regarding the differential passage of solar and terrestrial radiation through the atmosphere.<sup>[98,99]</sup> This apprehension was later confirmed since the composition of the atmosphere was steadily monitored by the Mauna Loa Volcanic Observatory starting from 1959.<sup>[100,101]</sup> At that point the concentration in  $\text{CO}_2$  was found to already have reached 315 ppm. The composition of the atmosphere during previous periods of earth's history was estimated on the data gathered from air trapped in the Vostok ice core, Antarctica. Based on the gathered data the atmospheric level in  $\text{CO}_2$  frequently fluctuated, but never exceeded 300 ppm over a time frame of nearly 1 My from present.<sup>[102]</sup>

With the beginning of the 21<sup>st</sup> century global  $\text{CO}_2$  emissions started to further increase, whereas natural carbon sinks like forests and swamps became scarce.<sup>[103–105]</sup> By today, global temperatures increased by approx.  $1.02\text{ }^\circ\text{C}$ , when compared to the average recorded between 1951 and 1980.<sup>[106,107]</sup> In 2019 the global concentration in  $\text{CO}_2$  peaked at 410 ppm, the highest level during the last 0.8 My in earth's history. During the 1960s the yearly increase in  $\text{CO}_2$  was  $\sim 0.6\text{ ppm}$ . This rate, however, significantly increased to 2.5 ppm from 2018 to 2019.<sup>[108]</sup> Consequently, the ambitions to establish applicable methods to remove  $\text{CO}_2$  from the atmosphere were investigated. The option of artificial carbon capture and storage (CCS) was first popularized by the Intergovernmental Panel

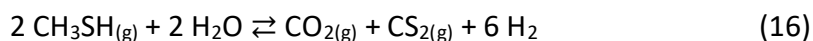
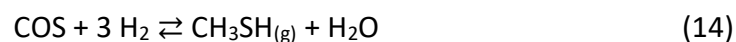
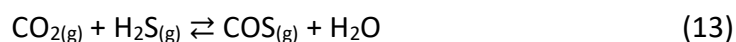
for Climate Change (IPCC) in their Special Report from 2005.<sup>[109]</sup> As this idea was acknowledged by the expert community dealing with international climate policy a lot of effort was put in finding appropriate solutions for this problem.<sup>[110]</sup>

One of the first extensive reviews on the state of the art of carbon capture was given by Mac Dowell et al. in 2010.<sup>[111]</sup> Therein they discussed three different methods that were in imminent deployment. The amine-based CO<sub>2</sub> capture, where a CO<sub>2</sub> rich gas stream is contacted with an aqueous amine solution to reversibly form water-soluble salts; The solid looping technology, where e.g. calcium oxide (CaO) and CO<sub>2</sub>, in analogy to the amine-based CO<sub>2</sub> capture, are reversibly reacted to form calcium carbonate (CaCO<sub>3</sub>); The oxyfuel combustion process, where a mixture of nearly pure O<sub>2</sub> and CO<sub>2</sub> are combusted to give flue gas, a mixture of CO<sub>2</sub> and H<sub>2</sub>O.<sup>[111]</sup> In the following years new promising materials for CCS, like ionic liquids or metal organic frameworks (MOFs), were established. Such technologies, unfortunately, still need time to elevate from the lab- to the pilot-scale. Recently, however, a first commercial plant for the direct air capture (DAC) of CO<sub>2</sub> went online and since then sells the collected CO<sub>2</sub> e.g. to greenhouses where it enhances the growth of vegetables.<sup>[112,113]</sup>

Though, applications for captured CO<sub>2</sub> exist, it can also be further processed and used as feedstock for a cheaper and cleaner energy when compared to the conventional use of hydrocarbons.<sup>[114]</sup> The term carbon capture and utilization (CCU) thereby refers to the use of CO<sub>2</sub> above atmospheric concentrations directly or as feedstock for valuable carbon containing products.<sup>[114–116]</sup> Recently, multiple reviews on possible routes for the utilization of CO<sub>2</sub> were published.<sup>[114,117–123]</sup> Al-Mamoori et al. discussed various carbon utilization processes like desalination, enhanced gas/oil recovery (EGR/EOR), mineralization and chemical conversion.<sup>[117]</sup> They further resume that all these techniques have a bigger potential than permanently sequestering the CO<sub>2</sub> underground. Besides these conventional concepts, non-conventional ones like the enhanced weathering, forestry techniques and land management could significantly contribute to both the removal and utilization of CO<sub>2</sub>.<sup>[114,123]</sup>

### 1.3.2 Iron sulfide minerals

The carbon fixation mediated by iron sulfide minerals into prebiotically relevant compounds has been intensively discussed in the past.<sup>[19,124]</sup> In scope of the ISWT, Wächtershäuser mainly discussed the role of pyrite and considered other iron sulfides as sole precursors for its formation. Later studies, however, acknowledged the potential of iron sulfide minerals like mackinawite, pyrrhotite and greigite towards carbon fixation and thereby added more aspects to the idea of a chemoautotrophic origin of life. The first experimental evidence for CO<sub>2</sub> fixation by commercially purchased iron sulfide was presented by Heinen and Lauwers in 1996.<sup>[9]</sup> They reported the formation of pyrite and small amounts of C<sub>1</sub> to C<sub>5</sub> thiols as major reaction products when they applied their FeS/acid system to reduce CO<sub>2</sub>.<sup>[9]</sup> Though, yields were only low, this reaction still remains one of the few abiotic examples for the direct fixation of CO<sub>2</sub> under hydrothermal conditions. They assumed that the reduction proceeds by the initial formation of COS from the reaction between CO<sub>2</sub> and H<sub>2</sub>S (reaction 13), which then can react with H<sub>2</sub> as following:



Huber et al. later showed that a mixed iron-nickel sulfide can be used to support the reaction between CO and CH<sub>3</sub>SH into the activated thioester and acetic acid under hydrothermal conditions.<sup>[10,125]</sup> In general, CO was found to react more readily with iron sulfides and was in later studies investigated more extensively than CO<sub>2</sub>. Cody et al. reported that when higher temperatures and pressures are applied, pyruvic acid forms from formic acid in the presence of iron sulfide and nonyl thiol.<sup>[126]</sup> They assumed that the iron sulfide is first consumed by the formation of carbonylated iron sulfur



compounds which then can subsequently provide the reduction. In a later study they further showed that carboxylic acids can be produced under the same conditions.<sup>[127]</sup>

The reduction of CO and C<sub>2</sub>H<sub>2</sub> by NiS was previously shown to result in the formation of unsaturated fatty acids that could have played a crucial role in the formation of membranous structures in aqueous media.<sup>[128]</sup> In a later study Sobotta et al. assumed that such a system could have represented an ancestor of modern biological carbon fixation cycles.<sup>[129]</sup>

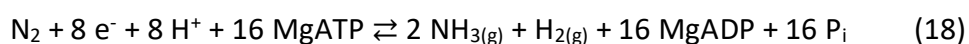
The interaction between the CO<sub>2</sub> molecule and the surface of different iron sulfides was recently studied by Dzade et al. using DFT calculations.<sup>[130–132]</sup> The CO<sub>2</sub> molecule was found to weakly interact with the most stable and most abundant (001) site but is adsorbed relatively strong on the (011) and (111) sites. At these more instable sites the CO<sub>2</sub> molecule was found to be adsorbed either retaining its linear structure or get bent and thereby lead to energetically more favorable configurations. They further found that the dissociation of CO<sub>2</sub> is energetically favored on the (111) site where it even becomes endotherm in energy at low CO<sub>2</sub> pressures and if the association process is restricted.<sup>[130]</sup>

### 1.3.3 Iron sulfur clusters

In biology, iron is an important nutrient for almost all known organisms. There, iron and iron sulfur clusters provide a variety of essential functionalities like catalysis, respiration, photosynthesis and the biochemical cycling of sulfur and nitrogen.<sup>[133]</sup> The most common iron sulfur cluster is the cubane type cluster [Fe<sub>4</sub>S<sub>4</sub>], which is involved in the electron transfer, DNA repair and small molecule sensing.<sup>[134]</sup> Despite its high reactivity with O<sub>2</sub> it is ubiquitous in biology. In almost all living systems, reducing reactions are catalyzed by enzymes like the hydrogenase (H<sub>2</sub>ase) and the nitrogenase (N<sub>2</sub>ase). The reduction thereby occurs at subsided catalytic sites which are deeply embedded inside the enzyme. For both, the H<sub>2</sub>ase and the N<sub>2</sub>ase this catalytic center was found to be based on the iron sulfur clusters, [Fe<sub>2</sub>S<sub>2</sub>] and [F<sub>8</sub>S<sub>9</sub>C], respectively.

The H<sub>2</sub>ase was first named and discovered in the 1930s by Stephenson et al. during their investigations of river mud.<sup>[135]</sup> The isolated methanogenic bacteria were thereby able to survive and grow in an inorganic medium with formate as the sole carbon source. The

formation of CH<sub>4</sub> was found to proceed stepwise by a first decomposition of formate into CO<sub>2</sub> which subsequently react with H<sub>2</sub>, produced by reaction 17.<sup>[136]</sup> Long before the molecular structure of the [FeFe] hydrogenase active site was resolved<sup>[137,138]</sup>, experimental work was done on the synthesis of similar compounds.<sup>[139]</sup> Seyfarth et al. reported that Di-μ-thiobis(tricarbonyliron) (μ-S<sub>2</sub>-[Fe<sub>2</sub>(CO)<sub>6</sub>]) can react with halide alkyls to give either alkylated or bridged diiron complexes.<sup>[140]</sup> The structural similarity to the [FeFe] hydrogenase active site led to an increased interest in modified mimics of the H<sub>2</sub>ase for industrial H<sub>2</sub> production.<sup>[141–145]</sup>



The high-resolution crystal structure of N<sub>2</sub>ase showed that the active site of the molybdenum-iron (MoFe) protein binds a complex cluster, consisting of seven iron ions, one molybdenum ion and nine sulfides, which promotes the reduction of N<sub>2</sub> into NH<sub>3</sub> (reaction 18). This cluster is referred to as the iron-molybdenum cofactor (FeMoco, M-cluster).<sup>[146]</sup> Einsle et al., however, could not give a full description of the structure as they further found a light atom in the center of the cluster which could not be identified to that point. This interstitial species could later be assigned as a carbide C<sup>4-</sup> by several working groups and provided important information to trace back the biosynthetic pathway for the designated M-cluster.<sup>[147,148]</sup> This process is initiated by two *nif*-encoded proteins (*nif* = Nitrogen fixation), NifB and NifEN, which provide the sequential formation of [Fe<sub>2</sub>S<sub>2</sub>] and [Fe<sub>4</sub>S<sub>4</sub>] clusters.<sup>[149,150]</sup> Wiig et al. showed that the carbon atom can be transferred onto a pair of [Fe<sub>4</sub>S<sub>4</sub>] clusters (designated K-cluster), which are formed at the NifB protein, by a radical SAM-dependent mechanism.<sup>[151]</sup> The methylated K-cluster can further react to give a [Fe<sub>8</sub>S<sub>9</sub>C] complex (designated L-cluster) which already contains the interstitial carbon atom.<sup>[152]</sup> In a final step the L-cluster is matured into the M-cluster upon the insertion of Mo and homocitrate by NifH before it is transported to its target location in NifDK.<sup>[149]</sup>

The Mo N<sub>2</sub>ase is the key enzyme in biological nitrogen fixation and was therefore studied extensively due to its property to reduce N<sub>2</sub> into NH<sub>3</sub>. In addition, the N<sub>2</sub>ase is also able

to reduce substrates containing either C – C, C – N and N – O double or triple bonds.<sup>[153–155]</sup> The reduction of CO<sub>2</sub> and carbonyl sulfide (COS) into CO and H<sub>2</sub>S was demonstrated with the *Azotobacter vinelandii* nitrogenase already in 1995.<sup>[156]</sup> In later studies Lee et al. provided first evidence for the reduction of CO<sub>2</sub> into alkanes and alkenes by the V-N<sub>2</sub>ase, while the Mo-N<sub>2</sub>ase was only able to support the formation of CO.<sup>[157–159]</sup> The formation of hydrocarbons from CO and CN<sup>-</sup> was shown to be supported by the isolated L-cluster, when suitable reductants like europium (II) diethylenetriaminepentaacetate (Eu(II)-DTPA) or samarium (II) iodide (SmI<sub>2</sub>) were introduced.<sup>[160]</sup>

Recently, the formation of alkanes and alkenes from CO, CO<sub>2</sub> and CN<sup>-</sup> was accomplished by a synthetic homometallic mimic of the M-cluster, the Mo-cluster.<sup>[161]</sup> This field of research hopefully will be studied even more extensively in the future as the development of methods to fixate carbon directly from the air is more urgent than ever before. The large-scale use of renewable sources thereby reassembles the most sustainable path for future generations.

#### **1.4 Goal of the thesis**

Though, the term “Origin of life” was used multiple times during the introduction, this thesis is more concerned with the processes connected to the chemical evolution of carbon substrates from highly oxidized ones like CN<sup>-</sup> or CO<sub>2</sub>. Mackinawite, due to its prebiotic plausibility, has been investigated in many studies where it could already be shown to support nitrogen fixation from gaseous dinitrogen (N<sub>2</sub>) and nitrite (NO<sub>2</sub><sup>-</sup>)/NO<sub>3</sub><sup>-</sup>, as well as desulfurization and deoxygenation of organic compounds.<sup>[162–165]</sup> Until now, no investigation on the interaction between freshly prepared mackinawite and CO<sub>2</sub> or HCN has been performed.

This thesis should therefore be used to further investigate the reductive properties of mackinawite for carbon substrate reduction. Therefore, different C<sub>1</sub> substrates including cyanides and carbonate are reacted with mackinawite in aqueous media, whereas reduction products are monitored by different analytical techniques. Similar studies on the reduction of HCN and CO<sub>2</sub> mostly report the formation of small compounds like thiols or alkanes, which accumulate in the sample gas phase and therefore should be identified, using a gas chromatography coupled mass spectrometry.

## Chapter 2. Materials and Methods

### 2.1 Materials

All salts were purchased from Sigma Aldrich and used as received, if not stated otherwise. The same applies to organic solvents like MeOH, EtOH, CS<sub>2</sub>, cyclohexane and acetone. The KCN was purchased from VWR and used as received. The labelled salts (Na<sup>13</sup>CN, KS<sup>13</sup>CN, KO<sup>13</sup>CN and Na<sub>2</sub><sup>13</sup>CO<sub>3</sub>) were purchased from Cambridge Isotope Laboratories and used as received.

The iron, nickel, cobalt, manganese, and sulfur powder were purchased from Sigma Aldrich and used as received. The purity of the metals was at least 95 %, the one of sulfur 99.998 %.

The conc. H<sub>2</sub>SO<sub>4</sub> and conc. HCl were purchased from Fischer Chemicals and the conc. H<sub>3</sub>PO<sub>4</sub> from Laborchem Apolda.

The helium (He) and CO<sub>2</sub> was purchased from Linde with a purity of 99.5 % and 95 %, respectively, and used as received.

### 2.2 Methods

#### 2.2.1 Water

The deionized H<sub>2</sub>O was placed into a 250 mL three neck round bottom flask, equipped with a gas inlet for nitrogen gas (N<sub>2</sub>). The H<sub>2</sub>O was purged with N<sub>2</sub> for at least 24 h, before being used in the experiments. When it was required, the H<sub>2</sub>O was refluxed for 15 min and let to cool down while being purged with N<sub>2</sub> to ensure the absence of any contaminations from dissolved CO<sub>2</sub>.

In presence of O<sub>2</sub>, the oxidation of mackinawite occurs already during the formation from the elements and becomes visible in form of red/orange iron(hydroxy)oxides either on top of the aqueous phase or attached to the glass walls. The N<sub>2</sub> purged H<sub>2</sub>O could be used to prepare samples that showed no sign of oxidation either optically or in the PXRD and Mössbauer spectra (4.2.2.3).

To rule out any influence of dissolved O<sub>2</sub> onto the observable properties, the H<sub>2</sub>O was degassed, using the freeze-pump-thaw method. Therefore, 20 mL of already purged H<sub>2</sub>O were placed in a closed 100 mL Schlenk flask. The Schlenk was then placed in liquid N<sub>2</sub> until the H<sub>2</sub>O froze completely. The H<sub>2</sub>O was allowed to melt after a reduced pressure was applied. With that, dissolved gas molecules accumulate in the gas phase and can be removed by again freezing the H<sub>2</sub>O and applying a reduced pressure. After three cycles, no gas bubbles emerged anymore from the melting H<sub>2</sub>O. The achieved mackinawite did not behave in a different manner than the one produced with N<sub>2</sub> purged H<sub>2</sub>O, however, oxidation products could also be observed. It seems more likely, that the O<sub>2</sub> contaminations resulted from a poor sample preparation and not from dissolved O<sub>2</sub>. The method of purging was therefore applied as standard procedure to pretreat the H<sub>2</sub>O before the experiments.

### **2.2.2 Iron powder**

The purchased iron powder was found to be contaminated with an unknown carbon source. When, however, the sole powder was acidified inside of an evacuated sample vial, mainly CH<sub>4</sub>, accompanied by smaller amounts in C<sub>2</sub> – C<sub>3</sub> alkanes and alkenes, could be detected in the headspace. The impurities probably follow from the manufacturing process, where a pre-processed magnetite slick is reduced with a mixture of coke breeze blended and ground limestone. The iron powder was therefore washed two times with a 0.1 M HCl and two times with H<sub>2</sub>O to neutralize the particles. They were then filtrated over a G4 frit, which was purged with N<sub>2</sub> to reduce a possible oxidation by O<sub>2</sub>. After partly drying the particles under a stream of N<sub>2</sub>, the slag was transferred into a Schlenk flask and fully dried under reduced pressure to give a fine powder. During this procedure, the color of the powder changed from a dark to a significantly lighter grey.

### **2.2.3 Iron sulfur mixture**

To ensure homogeneity, the processed iron and sulfur powder, together with 1 w% of NaCl, were finely grinded using a pistil and mortar. During this process, a greyish mixture is received as the sulfur was found to tightly stick to the iron particles. If once grinded together, the mixture did not separate anymore when a strong magnet was applied. It

was stored in a glass bottle for future uses and remained unchanged, even after several months.

## **2.2.4 Mackinawite synthesis**

### **2.2.4.1 From the elements**

Depending on the experiment, 1 to 100 mmol of the iron sulfur mixture were placed either in a round bottom flask, Schlenk flask or 20/25 mL sample vial. The reaction vessel was evacuated with N<sub>2</sub> by the Schlenk technique before the N<sub>2</sub> purged H<sub>2</sub>O was added through a syringe. Due to the small particle size, the iron sulfur mixture was swirled up during evacuation of the sample vials, where a thin cannula was used. Furthermore, the mixture partly tended to float upon the addition of the H<sub>2</sub>O, whereas no full conversion could be achieved. Both problems could be solved by fixating the mixture with a strong magnet at the bottom of the sample vials. Such optimal prepared samples showed full conversion after 24 h at room temperature as no magnetic material remained.

### **2.2.4.2 Precipitation**

In two separate Schlenk flasks, (NH<sub>4</sub>)<sub>2</sub>Fe(SO<sub>4</sub>)<sub>2</sub> · 6 H<sub>2</sub>O (8 g, 0.02 mol) and Na<sub>2</sub>S · 9 H<sub>2</sub>O (5 g, 0.02 mol) were diluted in 32 mL of N<sub>2</sub> purged H<sub>2</sub>O to give 0.64 M and 0.65 M solutions, respectively. First, the (NH<sub>4</sub>)<sub>2</sub>Fe(SO<sub>4</sub>)<sub>2</sub> solution (10 mL) was transferred into an evacuated 25 mL sample vial by a syringe. At room temperature 10 mL of the Na<sub>2</sub>S solution were rapidly added, whereas mackinawite formed as black precipitate. The residual aqueous phase was removed after the bulky precipitate was separated using a centrifuge.

## **2.2.5 Substrate solutions**

Depending on the necessary amount, n x 1 mmol of the respective salt (KCN, KSCN, KOCN, K<sub>2</sub>CO<sub>3</sub>, KOH, Na<sub>2</sub>S, CS<sub>2</sub> or NaSCH<sub>3</sub>) were placed into a 20 mL sample vial and evacuated with N<sub>2</sub> for three times. In the case of K<sub>3</sub>[Fe(CN)<sub>6</sub>] and K<sub>4</sub>[Fe(CN)<sub>6</sub>] n x 0.16 mmol and in the case of Na<sub>2</sub>[Fe(CN)<sub>5</sub>(NO)] n x 0.2 mmol salt were used. With a syringe,

n x 1 mL of the N<sub>2</sub> purged H<sub>2</sub>O were added to give a 1 M solution. The substrate solutions were freshly prepared before each experiment.

## 2.2.6 Reduction experiments

### 2.2.6.1 General aspects

The reduction experiments were either carried out in the 20 mL glass vials, equipped with an Al screw cap and septum, or in 25 – 60 mL crimp vials, equipped with an Al crimp cap and septum.

**Table 1** Reduction systems used during the thesis.

Label	Fe	S	Procedure
RS <sub>1</sub>	Fe <sup>0</sup>	-	<ul style="list-style-type: none"> <li>• Evacuating iron powder.</li> <li>• Adding substrate solution.</li> <li>• Heating with or without acid.</li> </ul>
RS <sub>2</sub>	Fe <sup>0</sup>	S <sup>0</sup>	<ul style="list-style-type: none"> <li>• Evacuating iron sulfur mixture together with substrate.</li> <li>• Adding H<sub>2</sub>O .</li> <li>• Heating with or without acid.</li> </ul>
RS <sub>3</sub>	Fe <sup>2+</sup>	S <sup>2-</sup>	<ul style="list-style-type: none"> <li>• Evacuating iron sulfur mixture</li> <li>• Adding H<sub>2</sub>O .</li> <li>• 24 h at r.t.</li> <li>• Adding substrate solution.</li> <li>• Heating with or without acid.</li> </ul>

Depending on the experiment, 44 – 880 mg of the iron powder or iron mixture was placed into a sample vial. After the samples were evacuated with N<sub>2</sub>, the ones containing the iron mixture were either charged with purged H<sub>2</sub>O to form mackinawite or directly combined with the substrate and H<sub>2</sub>O to investigate its influence on the mackinawite formation. An overview on the used reduction systems is given in Table 1.

The samples were evacuated with cannulas (12 cm, OD = 0.8 mm), which were mounted onto the tubing of the Schlenk line by a self-made construction. The samples were evacuated three times before further liquid components were added. The completed sample vials were then stored at 80 °C for different reaction times, if not stated otherwise. Most of the samples were heated on a heating plate, equipped with DrySyn heating blocks. When a beaker was used to imitate an oven atmosphere, the septa partly developed cracks and started to burst at temperatures over 100 °C. The open system, however, does not provide a constant gas phase temperature, but rather a gradient ranging from 80 to 75 °C.

#### **2.2.6.2 Disposal of reacted samples**

The reacted samples were fully acidified under closed conditions, using a 5 M H<sub>3</sub>PO<sub>4</sub>. Thereby the remaining mackinawite is dissolved and H<sub>2</sub>S gets formed. More oxidized iron phases were found to react with the H<sub>2</sub>S and/or HS<sup>-</sup> and S<sup>2-</sup> ions in solution. This method could be used to clean vials that were contained with oxidized iron sulfide and oxide phases. For this partly deactivated mackinawite was produced by slowly letting a fresh precipitate react with O<sub>2</sub> from the air. It was further stored in a Schlenk flask under air at – 24 °C. To clean a contaminated vial, some of the mackinawite was placed into the vial and charged with 5 M H<sub>3</sub>PO<sub>4</sub>. By shaking the vial and allowing the aqueous phase to reach the contaminated areas, most of them disappeared after the vials were left at room temperature for 30 min.

In presence of KCN, the acidification of the reaction samples led to the formation of Prussian blue, which crystallized from solution after several minutes. In experiments, where low Fe/S ratios like 1:1 were used, such samples were additionally charged with a solution of Fe<sub>2</sub>(SO<sub>4</sub>)<sub>3</sub> to quantitatively precipitate the HCN/CN<sup>-</sup> as Prussian blue. The iron



cyanide complexes were then introduced into a mixture of H<sub>2</sub>O<sub>2</sub> and KOH to react into N<sub>2</sub> and CO<sub>2</sub>.

## **2.2.7 Gas phase extraction**

### **2.2.7.1 Direct extraction**

During the first part of the thesis, the gas phase was investigated by placing the sample vials in the headspace sampler. Therein, the gas phase is extracted whereas a pressure is applied and released after an adjustable time. This method is, however, very susceptible for contaminations when samples were poorly prepared. One criterion for a well-prepared sample is, that the gas pressure should not be much higher or lower than the applied one by the headspace sampler (HS-20). When a much higher pressure is present, the applied He flow, together with some part of the sample will be pushed back into the valve. A much lower gas pressure of the sample would cause the aqueous phase to swirl up in an uncontrollable manner. To rule out the risk of such a contamination, this method was discarded with time and replaced with one of the other following two approaches.

### **2.2.7.2 Extraction using a syringe**

To reduce contaminations caused by the reaction mixture, a gas tight syringe was used to transfer 500 µL of the sample gas phase either into a clean and evacuated analysis vial when the headspace sampler was used or directly into the PTV valve of the GC. Before each extraction, the syringe was purged with N<sub>2</sub> by inserting it into a clean vial, equipped with a steady N<sub>2</sub> overpressure. This method significantly decreased the risk of contamination for the headspace sampler.

### **2.2.7.3 Extraction using a transfer line**

To achieve higher product concentrations in the analysis vial, self-made transfer lines were used to transfer a higher quantity of the sample headspace. Transfer lines were thereby produced either from a approx. 10 cm long PTFE tubing (ID = 0.5 mm, OD = 1.0 mm) equipped with two cut cannula endings (OD = 0.8 mm, fixated with Parafilm) or by

applying an angled cut to a 12 cm long cannula (OD = 0.8 mm) using a tubing plier for metal tubing. The cannula consists of chrome-nickel steel and is coated with silica. When the angled cut was carried out optimally, both ends could easily be pierce through the septa and therefore be used to connect the reaction with the analysis vial. Before each extraction, reduced pressure was applied onto the analysis vial to create a high-pressure gap between both vials.

As for the applied N<sub>2</sub>, sample vials usually contained a gas phase with at least atmospheric pressures. The back draft into the sample vial was considered only a small source of error, when compared to the one that would appear by piercing the analysis vial first. Therefore, the transfer lines were first connected with the sample vial, before the other end was immediately inserted into the analysis vial. In case of the long transfer lines, the angled cut sometimes caused parts of the septa to be stamped out during the insertion. This especially was problematic, when this side was used onto the sample vial, as the cut-out piece would immediately plug the transfer line. When used the other way

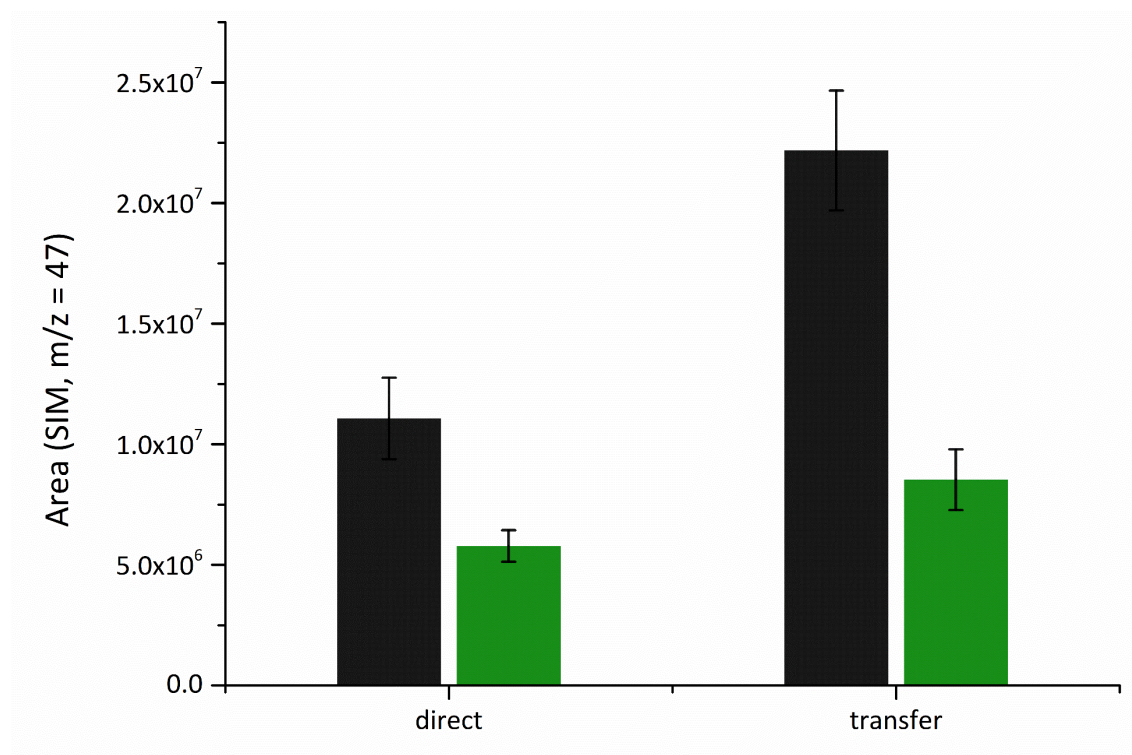


**Figure 3** Comparison between the transfer methods. Both experimental series (black: HST-01; green: HST-02) showed that the extraction by a transfer line leads to higher levels in CH<sub>3</sub>SH.

around, the cut-out piece would be blown into the analysis vial and not further cause trouble.

#### **2.2.7.4 Comparison of the methods**

The extraction method, using the transfer line, was compared to the one, where the gas phase is extracted from the sample vial by the HS-20. To avoid any contaminations, pure CH<sub>3</sub>SH samples, like the ones used during calibration, were prepared. The gas phases of samples that were directly analyzed (HST-01) showed lower levels in CH<sub>3</sub>SH than the ones that were extracted by a transfer line (HST-02). This follows from the use of a vacuumized vial as driving force which leads to bubbles emerging from the aqueous phase. In scope of the reduction experiments where a solid phase is present this can additionally lead to the removal of surface bound species. Furthermore, when the gas phase is extracted by the transfer method, the gas phase gets fully removed and the formation of previously bound or diluted species can be studied.

#### **2.2.8 Liquid phase extraction**

##### **2.2.8.1 Direct**

The aqueous phase (1 mL) of a reacted sample was extracted with a syringe and placed in a 2 mL vial. The absence of solid particles in the analysis vials was ensured by using a syringe filter with a pore size of 0.2 µm. The aqueous sample (1 µL) was then directly injected into the PTV valve of the GC.

##### **2.2.8.2 Cyclohexane**

The liquid phase of some of the samples was directly extracted with cyclohexane and investigated by using the AOS-20 liquid phase sampler (2.2.7.2). The cyclohexane was distilled once, before being injected into the sample vials using a syringe. The sample vial was then shaken by hand and left to separate for several minutes, before the organic phase was extracted with a syringe. The syringe was equipped with a 0.2 µm syringe filter before the extract was transferred into 2 mL analysis vials. The cyclohexane sample (1 µL) was then directly injected into the PTV valve of the GC

## 2.2.9 GCMS setup

### 2.2.9.1 Overview

During this thesis, reduced compounds were identified, using four different GCMS systems. The first system (**GCS-1**) is a Thermo Trace 1300 GC coupled to an ISQ-QD MS (Thermo Fisher Scientific Inc., Waltham, MA) of the Ribbe group at the UCI in Irvine, CA. System two (**GCS-2**) and three (**GCS-3**) are a Finnigan PolarisQ GCMS and a Finnigan ISQ GCMS of the Trapp group at the LMU in Munich. The last system (**GCS-4**), located in the IAAC, is a Shimadzu GCMS-QP2010 Plus, equipped with a HS-20 headspace sampler, as well as an AOC-20 liquid phase sampler. The latter system was used to analyze most of the here reported reactions and is therefore addressed as GCMS for the following chapters, if not stated otherwise.

The AOC-20 liquid phase sampler was adjusted to extract 1  $\mu\text{L}$  of the 2 mL analysis vials after rinsing the syringe with acetone for two times and with the sample solution for five times. The sample was injected into the split unit of the GC which was operated at 200 °C and a split ratio of 50.

The HS-20 sampler consists of a sample plate which transports the analysis vials into the temperature-controlled vial oven, which was operated at 100 °C. The gaseous sample is extracted whereas the vials are moved onto a syringe tip, connected to a valve. Over this valve first, a He pressure of 100 kPa is applied onto the vial, which is released after 5 min equilibration time. The gas sample is then stored in the sample line (155 °C) and leave the sampler over the transfer line (150 °C) before entering the column.

### 2.2.9.2 GC method

The column oven was typically held at 35 to 50 °C for several minutes, before the temperature was ramped up by a temperature gradient of 10 °C  $\text{min}^{-1}$  and held for another 1 to 30 min, if not stated otherwise. The long isothermal sequence at the start was thereby useful to achieve a good separation especially of  $\text{CH}_4$  from  $\text{N}_2$ ,  $\text{O}_2$  and argon (Ar) on the  $\text{CC}_1$  (2.2.8.3).

### 2.2.9.3 Columns

The different columns allowed the separation of the reaction products in varying qualities. The SH-Rtx-5 MS and SH-Rxi-624SIL MS are highly durable columns with a wide range of applications. In general, the SH-Rtx-5 MS was used to separate gaseous samples, whereas the SH-Rxi-624SIL MS was mainly used to separate liquid samples. Both they, however, showed only a poor efficiency to separate gaseous compounds with low molecular weight like N<sub>2</sub>, O<sub>2</sub>, Ar, CO<sub>2</sub> or CH<sub>4</sub>. With the RT-Q-Bond column a much better separation of CO<sub>2</sub> and CH<sub>4</sub> from the remaining compounds could be accomplished. A comparison of the retention times is given in Table 3.

**Table 2** List of columns used during the thesis. **Abbr.:** Thickness (**d**), Length (**l**), Diameter (**∅**), Maximum working temperature (**T<sub>max</sub>**).

ID	Column name	d [μm]	l [m]	∅ [mm]	T <sub>max</sub> [°C]
CC <sub>1</sub>	RT-Q-Bond	10	30	0.25	300
CC <sub>2</sub>	SH-Rtx-5MS	0.25	30	0.25	330
CC <sub>3</sub>	SH-Rxi-624SIL MS	1.8	60	0.32	320
CC <sub>4</sub>	HP-5 MS	0.25	30	0.25	325

**Table 3** Retention times of gaseous compounds on the respective column used.

ID	Linear velocity [mL min <sup>-1</sup> ]	Retention time [min]				
		N <sub>2</sub>	O <sub>2</sub>	Ar	CH <sub>4</sub>	CO <sub>2</sub>
CC <sub>1</sub>	50.4 [220520]	1.78	1.79	1.79	1.95	2.49
CC <sub>2</sub>	45.1 [260419]	1.48	1.48	1.48	1.48	1.48
CC <sub>3</sub>	38.0 [130619]	2.61	2.61	2.61	2.61	2.66

#### 2.2.9.4 CH<sub>4</sub> detection

The reaction products could be in general be well separated by using the RT-Qbond column with an applied flow rate of 104 mL min<sup>-1</sup>. The acquisition by the mass spectrometer started at 1.9 min to avoid measuring the signal for N<sub>2</sub>, O<sub>2</sub> and Ar. The first event was carried out at a mass range of  $m/z = 16 - 25$  to detect CH<sub>4</sub>. The second event (after 2.5 min) was adjusted to a mass range of  $m/z = 20 - 500$  to also detect heavier molecular species.

#### 2.2.10 Density functional theory

Density functional theory (DFT) calculations were carried out with the DFT programs in the Turbomole package, version 7.5.<sup>[166]</sup> Atomistic models of the [Fe<sub>4</sub>S<sub>4</sub>](SH)<sub>4</sub> cluster and its various reaction products, as well as the reactants considered, were built with Molden.<sup>[167]</sup> All model atoms were allowed to relax fully during structure optimizations. The reaction energies presented in Figure 4 were obtained from the electronic energies of the respective chemical species. Solvent effects were treated implicitly by the conductor-like solvent screening model<sup>[168]</sup> (COSMO) as implemented in Turbomole, assuming a dielectric constant of  $\epsilon = 80$ . Structures were optimized with the TPSS functional<sup>[169]</sup> and a def2-TZVP basis set.<sup>[170,171]</sup> Dispersion interactions were modeled by means of the DFT-D3 approach<sup>[172]</sup> as implemented in Turbomole. Computational time was reduced by exploiting the resolution-of-the-identity approximation.<sup>[173,174]</sup> Because the iron atoms in a periodic Mackinawite structure formally adopt an oxidation state of +2, the cluster models were treated in the all-ferrous state with a spin state of  $S = 4$ . This spin state is approx. 8 kcal mol<sup>-1</sup> more stable than the corresponding singlet state with the DFT methodology employed here. Unless otherwise stated, substrate reduction steps were considered to occur via coupled e<sup>-</sup>/H<sup>+</sup> transfer. Proton transfer energies were calculated by taking the deprotonation of H<sub>3</sub>O<sup>+</sup> into account. Due to the fact that Mackinawite can serve as a potent reductant via formal Fe<sup>2+</sup>/Fe<sup>3+</sup> transitions, the redox couple  $[[\text{Fe}_4\text{S}_4](\text{SH})_4]^{4-}/[[\text{Fe}_4\text{S}_4](\text{SH})_4]^{3-}$  was used herein to calculate the energetics of electron transfer steps.

### **2.2.11 Cyclic voltammetry**

Cyclic voltametric measurements were performed in a small volume three-electrode cell (glassy carbon as working electrode, diameter = 1.6 mm; platinum auxiliary electrode and Ag/Ag<sup>+</sup> in KCl/H<sub>2</sub>O as reference electrode) using a Reference 600 Potentiostat (Gamry Instruments). All experiments were carried out in N<sub>2</sub> purged H<sub>2</sub>O, using 0.1 M tetrabutylammonium hexafluorophosphate ([*n*-Bu<sub>4</sub>N][PF<sub>6</sub>]) at room temperature. Before each measurement the solution and gas phase were purged with N<sub>2</sub>, and the vitreous carbon disk was polished on a felt tissue with Al<sub>2</sub>O<sub>3</sub>. All values reported in this work are referenced to the potential of the ferrocenium ion/ferrocene (Fc<sup>+</sup>/Fc) couple.

### **2.2.12 Powder X-ray diffraction (PXRD)**

Powder X-Ray diffraction patterns were collected at two different devices, a STOE STADI P diffractometer equipped with a copper anode X-ray source and a Mythen 1K detector and a tabletop Rigaku Mini-Flex 600 equipped with a copper anode with 0.6 kW and an energy dispersive detector to minimize effects of X-ray fluorescence.

### **2.2.13 Mössbauer spectroscopy**

Mössbauer spectra were obtained on a homemade spectrometer based on a RCPTM MS-96 Mössbauer spectrometer equipped with a Ritverc Co57 in a Rh-matrix source, a YAP:Ce scintillating crystal detector, and a Janis SVT-400 helium-bath cryostat. The samples (roughly 30 mg) were filled into weighing paper that was folded to squares, and parafilm was wrapped tightly around it. The sample was inserted into an Al sample holder, which was then inserted into the Mössbauer spectrometer. Spectra were calibrated against  $\alpha$ -iron at room temperature or 80 K and fitted using the MossWinn 4.01 pro-gram.

## Chapter 3. Mackinawite from iron and sulfur

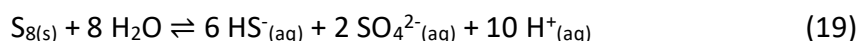
The straightforward synthesis of mackinawite from iron and sulfur was first established during the first months of this thesis. The details of the reaction between iron and sulfur, as well as the properties of the mackinawite, were resolved in the following years and has been carried out in close cooperation with my colleague R. Bolney.

### 3.1 Introduction

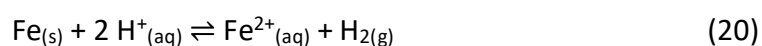
In addition to precipitation, mackinawite has been shown to be formed when an iron wire is placed into a Na<sub>2</sub>S solution. It is also known to be present during the exothermic reaction of an iron sulfur mixture which is initiated thermally. The reaction between iron and sulfur in aqueous media, however, is not present in modern textbooks, but has already been reported by Lemery in 1700. It, however, was not mentioned again until 1923 when Alsen gave a short notice on the reaction, without providing any closer description on the reaction product.

A more detailed view on the formation mechanism was reported only recently by Schmitt in 1991 and further developed by Dowling in the following year. This sulfur assisted corrosion of iron is thereby well known among corrosion scientists but was until now not widely used by chemists. It may be for this, that the first approach on synthesizing mackinawite by this route was not influenced by these previous findings, but more from the knowledge on the exothermic reaction between iron and sulfur. The formation mechanism, however, prolongs by several steps and was only clarified to a certain degree. The combined mechanism consists of the following steps:

1. Disproportionation of sulfur in water produces H<sub>2</sub>S.

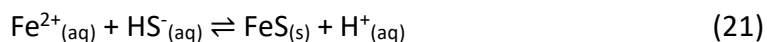


2. Dissolution of iron by the released protons.

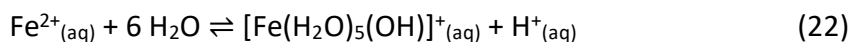




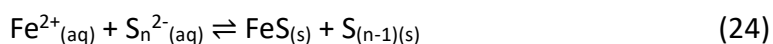
3. Formation of the first mackinawite layer.



4. Enhanced iron dissolution as re-passivation of the surface is prevented by sulfur assisted corrosion.



5. Conducting mackinawite layer leads to the reduction of sulfur molecules on the surface to form polysulfides which further can react with the iron ions to produce mackinawite.



The mechanism of the last step was, however, not fully resolved. Dowling suggested that the iron ions are transported through the developing mackinawite layer but did not provide any experimental evidence.

## 3.2 Results and Discussion

### 3.2.1 Synthesis of mackinawite

The first approaches on the synthesis of mackinawite from the elements were based on the idea of burning an iron sulfur mixture under inert conditions. After realizing, that the heated glass stick, necessary to start the reaction, was significantly cooled down by the N<sub>2</sub> stream, no further attempts of this manner were performed.

Instead, the mixture was investigated on its behavior in different organic solvents. The reaction was supposed to be accelerated through the addition of acid, as iron ions were proposed as key intermediates for the formation of iron sulfides. When a Schlenk flask containing an iron sulfur mixture was charged with toluene and further acidified with

conc. HAc, a black precipitate formed after the reaction was heated up to 60 °C (SP-FeS-01). When conc. HCl was used instead, the toluene started to heat up quickly, whereas again a black solid formed on top of the mixture (SP-FeS-02). By using EtOH, a similar course of the reaction was observed, where the black solid only appeared when the reaction vessel was heated up to 80 °C. After letting the reaction proceed at room temperature overnight, the full solid phase was dried and a PXRD pattern was collected. Though no yellow sulfur and a significant formation of black material formed, all the observed reflexes could be attributed to iron and sulfur (Figure A 1, SP-FeS-03).

When the solvent was exchanged with acetone, no reaction took place. Upon adding H<sub>2</sub>O to the reaction, more black material formed, even at room temperature. It was therefore concluded that the reaction mainly depended on the availability of H<sub>2</sub>O, rather than the absence of it. The first sample (SP-FeS-04) which did not contain any starting material was synthesized in a mixture of acetone and H<sub>2</sub>O (10:1) and was stirred without additional acid at room temperature for 5 d. After the reaction was completed, no magnetic material could be removed by the magnetic rod. The PXRD pattern of the dried reaction product only shows reflexes originating from the mackinawite, while no iron or sulfur is present anymore (Figure 4).

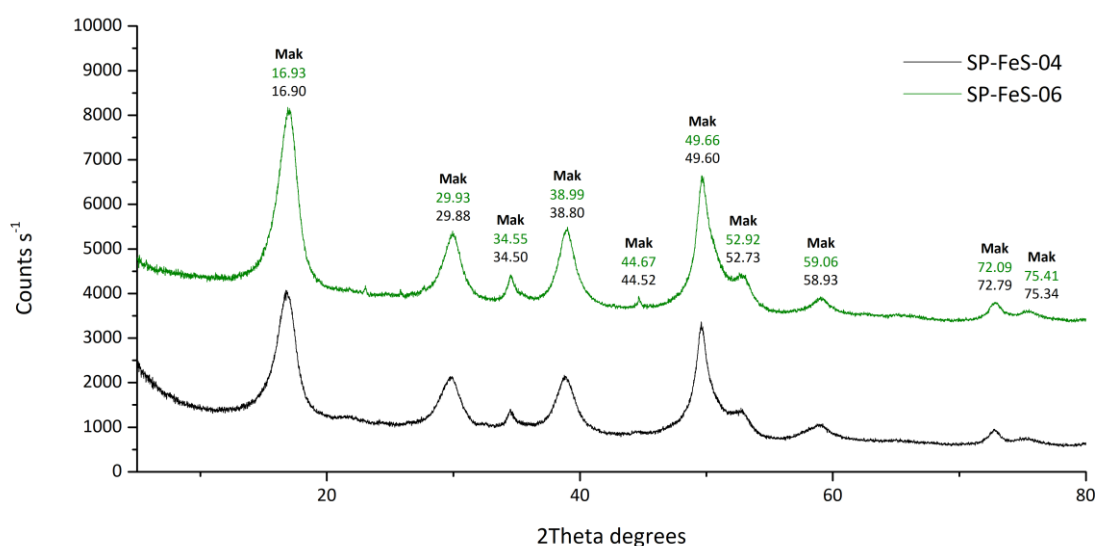


**Figure 4** Collected PXRD pattern from the reaction of iron and sulfur in acetone/water (10:1) (SP-FeS-04) and in water (SP-FeS-06) at r.t. after 5 d.

Though, the use of acetone led to a fast-drying process when the solid phase was filtrated under a stream of N<sub>2</sub>, the formed nanoparticles tend to decompose by burning when let in contact with air. The use of acetone was however seen as non-beneficial, as any further contamination with an external carbon source should be prevented in regard of the reduction experiments.

The first reaction carried out solely in H<sub>2</sub>O was performed at room temperature (pH 7) and at first did not seem to show any reactivity. When the pH of the solution was lowered by purging it with CO<sub>2</sub> it considerably darkened already after 30 min and was stirred for another 3 d (SP-FeS-05). A first PXRD pattern was collected from a sample which was taken directly from the Schlenk flask by a syringe and filtrated through a G4 frit with a N<sub>2</sub> stream applied. The observed reflexes could clearly be assigned to iron, sulfur and mackinawite (Figure A 2). Though still significant amounts of starting material were left, no other iron sulfide phase was formed under these conditions. When a magnetic rod was used to remove the remaining iron, the PXRD pattern shown in Figure A 3 could be collected. Though, the iron content was reduced, the sulfur content did not change significantly. By using degassed, O<sub>2</sub> free, H<sub>2</sub>O the reaction was found to proceed if iron and sulfur are left to react, as no sulfur reflexes were observed in the PXRD pattern collected from a sample (SP-FeS-06) that was stirred at room temperature for 5 d (Figure 5). The high selectivity and efficiency of this route further remained when the reaction was downsized, allowing us to form mackinawite (1 to 13 mmol) already inside the 20- and 25-mL glass vials.

### **3.2.2 Resolving the formation mechanism**

The missing part of the formation mechanism is the question on how the iron ions are transported to the reduced sulfur end-groups at the surface of the particle. Dowling suggested that the iron ions are transported through the formed mackinawite layers but could not provide any experimental evidence. To readdress this question an experiment was conducted whereby a chunk of recrystallized sulfur was placed onto an iron plate, supported by a sand layer inside of a three-neck round bottom flask. The level of the introduced 0.001 M NaCl solution was adjusted to the point, where only half of the sulfur

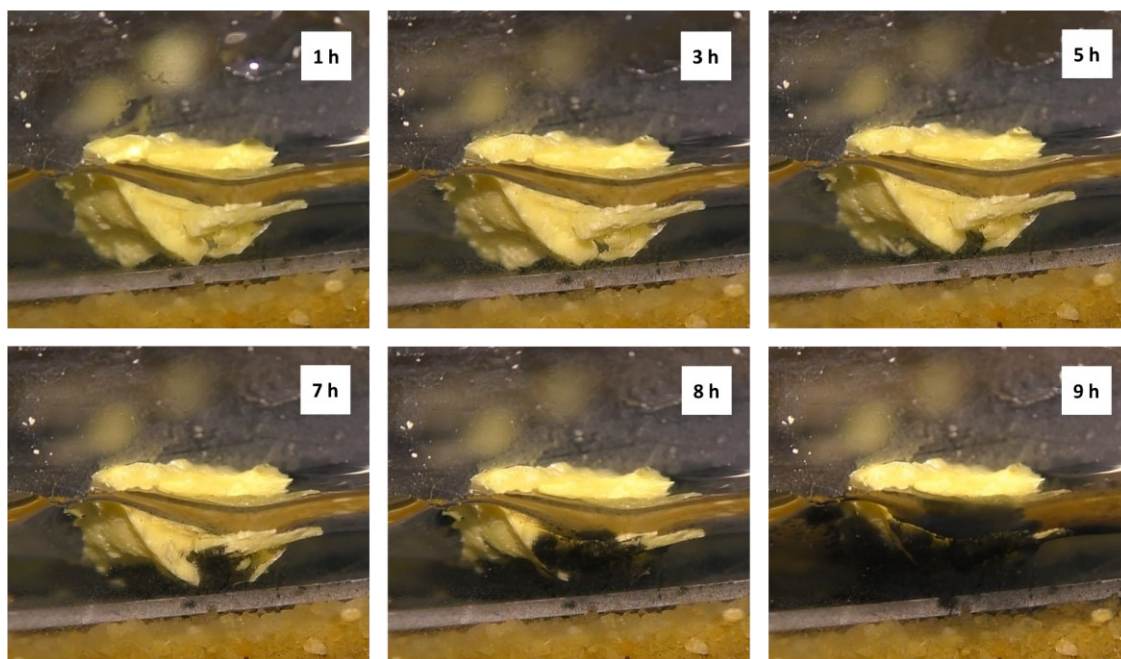


**Figure 5** Sequence of images extracted from a 9-h long video where the reaction between iron and sulfur was monitored in a 1 M NaCl solution.

crystal was covered. The progress of the reaction was observed by a video camera over 9 h. In Figure 5 sequences of the video are displayed.

The development of the black mackinawite layer can be easily followed through the high contrast given by the yellow sulfur surface. After 1 hour, no observable reaction took place, whereas after 3 h small black areas developed at the bottom of the sulfur sample. During the following hours, the sulfur assisted corrosion seemingly accelerated the process of mackinawite formation. Spreading probably from the area where iron and sulfur are closest, the mackinawite layer could be observed forming on top of the sulfur surface. In contrast to the suggestion of Dowling, we here assume the iron ions to be transported as dissolved species alongside the mackinawite layer towards the formed sulfide end-groups. During our investigations, mackinawite was only formed in the presence of  $H_2O$ . In accordance with this, again no mackinawite formation took place in this experiment at areas ranging out from the solution.

With time, the formed mackinawite particles crumbled away from the sulfur surface and were distributed in the aqueous solution, which significantly darkened over time. As both elements only show a low solubility in  $H_2O$ , the formed mackinawite particles are first distributed into solution before they undergo aging and lastly separate. This

reaction therefore represents a novel method to mobilize previously dense packed energy sources like metallic iron by supplying reactive nanoparticles to an aqueous solution.

### 3.2.3 Structure and morphology

The corresponding reflexes acquired from the PXRD pattern of both, the sample synthesized in acetone/ H<sub>2</sub>O and in H<sub>2</sub>O alone correspond to the ones reported for mackinawite in the literature. Both samples gave pattern with a high background and broadened reflexes, probably due to the low crystallinity and/or structural defects. A slight shift in the c parameter was observed when both samples are compared (Table A 1), however, in the literature much higher shifts for precipitated samples are given.

Due to the high efficiency and selectivity of the mackinawite formation from iron and sulfur, collected PXRD pattern could be further analyzed by carrying out a Rietveld refinement, with  $R_{wp} = 0.02815$ , on the PXRD pattern collected from SP-FeS-06. Based on the mackinawite crystal structure, lattice parameters of  $a = 3.6574 \pm 0.0007 \text{ \AA}$  and  $c = 5.2717 \pm 0.011 \text{ \AA}$  were obtained.<sup>[175]</sup> Due to the broadness of the reflexes, a size and strain parameter was introduced, which is in correspondence with the observed particle sizes.

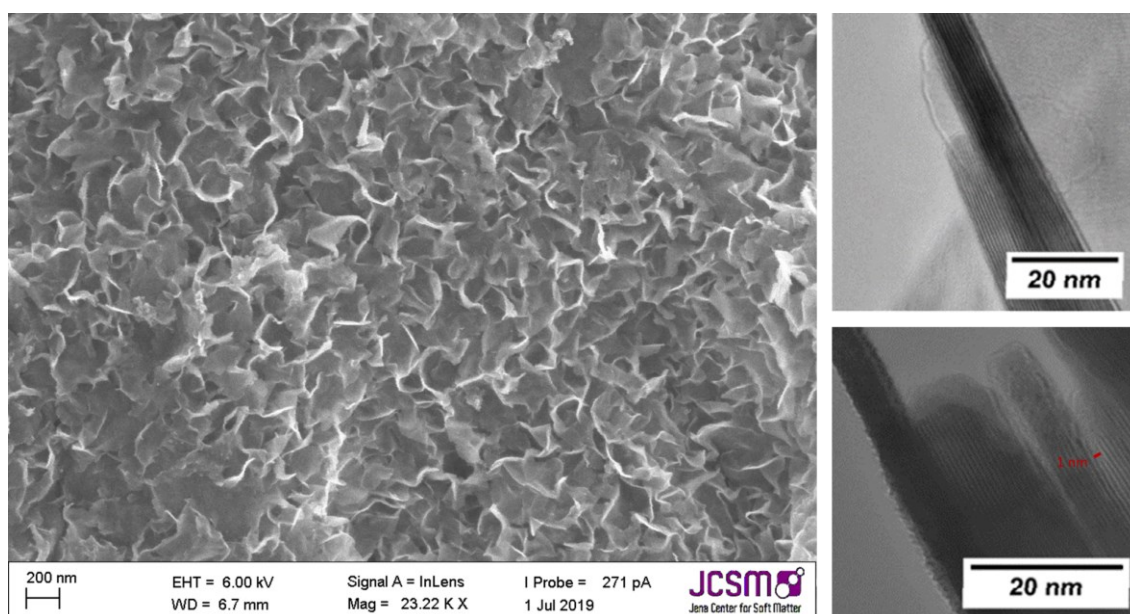


**Figure 6** SEM (left) and TEM (right) images of deactivated mackinawite produced from the between iron and sulfur at r.t. in a 0.01 M NaCl solution for 12 h.

SEM and TEM imaging showed curved platelets that form micrometer sized compartments. A SEM image of the surface of the compartments is shown in Figure 6. The sole platelets have a diameter of hundreds of nanometers, but a thickness of only 5 to 30 nm. The lattice fringes were observable through TEM imaging and gave values around 0.5 nm, which are in alignment with the c parameter of 5.27 Å.<sup>[175]</sup>

### 3.2.4 Kinetics

The collected PXRD pattern from iron sulfur mixtures at different reaction times show that the reaction only proceeds after an initial induction period. This has already been reported by several groups and is assumed to result from the slow disproportionation of sulfur to form H<sub>2</sub>S and therefore the first mackinawite layer. As soon as the mackinawite layer is formed, the sulfur assisted corrosion drastically accelerates the process. At room temperature the induction period lasted approx. 20 h, whereas the PXRD pattern after 21 h showed a significant decrease in the sulfur (222) reflex. After 24 h a broad bump formed at around 5 Å, which corresponds to the mackinawite (001) diffraction peak. With ongoing reaction time, the broad signal grew bigger, whereas the intensity of the sulfur (222) diffraction peak further decreased (Figure 7).<sup>[175]</sup> During the reaction, separated and therefore unreacted sulfur was found to accumulate at the surface of the aqueous phase. When the separation of sulfur was prevented, full conversion into mackinawite was observed.

In contrast to the long induction period, the subsequent sulfur assisted corrosion proceeded fast and started to stagnate already after 8 h. After increasing the electric conductivity of the aqueous solution by adding only small amounts of NaCl, the overall reaction rate could be significantly reduced. The full conversion into mackinawite was thereby achieved already after 12 h at room temperature and pH 7. Above pH 10.5 no reaction occurred, which may be attributed to both, a lower rate in sulfur disproportionation and a bigger passivating oxide layer preventing an efficient sulfur assisted corrosion to take place. Between pH 7 and 10, however, a heated sample containing the iron sulfur mixture and NaCl developed a dark green colored solution.

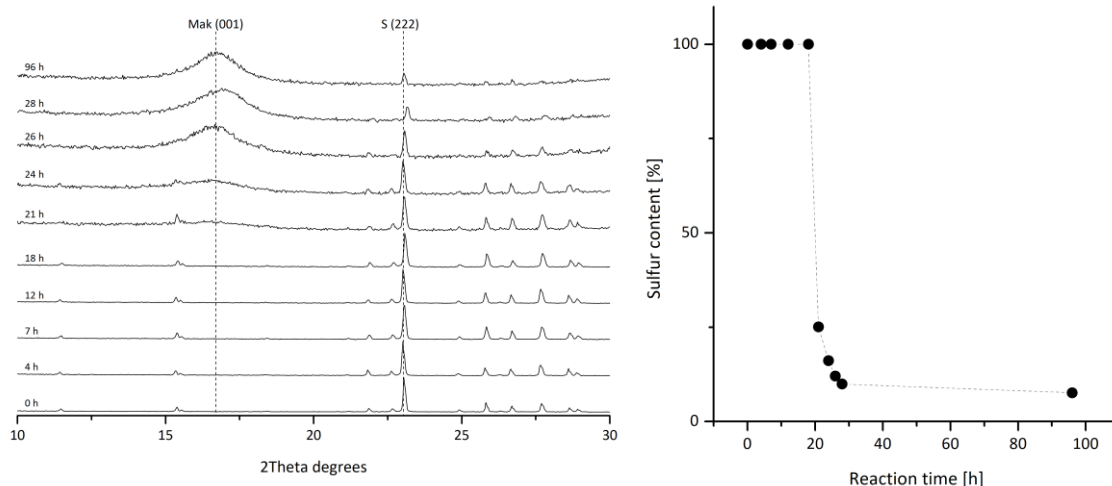


**Figure 7 Left:** Collected PXRD pattern from the products from the reaction between iron and sulfur after different times. Mackinawite (Mak) started to form only after an initial induction period around 24 h. **Right:** Plot of the sulfur content of a reaction containing iron and sulfur in pure H<sub>2</sub>O over time.

This also appeared in experiments, where KCN was added instead of KOH and is discussed in more detail in the next chapter.

### 3.2.5 Composition

The compositions of the mackinawite samples synthesized from the elements were determined with ICP-AES. The main obstacle in the acidic dissolution of mackinawite is the formation of H<sub>2</sub>S. My colleague, R. Bolney was able to establish a standard procedure, where the released H<sub>2</sub>S is oxidized to form sulfate. With this method the iron sulfur ratio of mackinawite, synthesized by this route, was determined to be Fe:S = (1.010 ± 0.004):(1.000 ± 0.003) with no starting material or other iron sulfide phases visible in the PXRD pattern. The absence of metallic iron was checked by a strong magnet, whereas only non-magnetic samples were analyzed further. The mackinawite samples acquired by filtration, however, still contained H<sub>2</sub>O that would start to condensate on the glass walls of the frit when oxidation by O<sub>2</sub> took place. When such mackinawite was heated at 80 °C at reduced pressures, the H<sub>2</sub>O could be removed, without any change in the PXRD patterns.

To gain more insight into the oxidation states of the iron atoms, a Mössbauer spectrum was collected from a deactivated mackinawite sample (SP-FeS-07) produced by the

**Table 4** Mössbauer parameters for mackinawite produced by different synthetic routes and the ones for the mackinawite from the reaction between iron and sulfur.

Reference	T [K]	d [mm s <sup>-1</sup> ]	Rel. Area [%]	Synthesis
Schröder, 2020 <sup>[176]</sup>	293	0.37	100	FeCl <sub>2</sub> /Na <sub>2</sub> S
	4	0.49		
Boursiquot, 2001 <sup>[177]</sup>	295	0.42	52	Fe/Na <sub>2</sub> S/CH <sub>3</sub> COOH
Vaughan, 1971 <sup>[178]</sup>	4	0.2	100	Fe/Na <sub>2</sub> S
This work	292	0.37	100	Fe/S
	80	0.47		

standard procedure. The spectra were measured at 293 K and 80 K over a velocity range of 4 mm s<sup>-1</sup> with reference to metallic iron (Figure 8). Both spectra could be well fitted, using a singlet with center shifts of 0.37 mm s<sup>-1</sup> and 0.47 mm s<sup>-1</sup>, respectively. Those values are in close resemblance to previously reported ones on synthetic mackinawite (Table 4). In an earlier study by Boursiquot and coworkers, mackinawite was assumed to contain a certain degree of Fe<sup>3+</sup> ions and thereby support up to 20 % without undergoing any structural change, visible in the PXRD pattern.<sup>[177,179]</sup> The obtained Mössbauer spectra could therefore be fitted using a singlet and two doublets. The singlet at 0.42 mm s<sup>-1</sup> was assigned to Fe<sup>2+</sup> ions in tetrahedral sites, whereas the doublets resulted either from the interaction with neighboring Fe<sup>3+</sup> ions or from Fe<sup>3+</sup> in tetrahedral sites.



Recently, Schröder et al. provided a Mössbauer spectra for mackinawite, precipitated from aqueous  $\text{FeCl}_2$  and  $\text{Na}_2\text{S}$  solution, which could also be well fitted with a single singlet with similar center shifts when measured at 293 K and 4 K.<sup>[176]</sup> The oxidation, observed by Boursiquot et al. was previously thought to have been induced by elemental sulfur as oxygen could be excluded.<sup>[177]</sup> Though, plenty sulfur was available during the reaction between iron and sulfur, no comparable oxidation occurred. It seems more likely that other components promote the oxidation of the mackinawite. In contrast to this work and the ones from Schröder et al. and Vaughn et al., Boursiquot et al. synthesized their mackinawite in presence of  $\text{CH}_3\text{COOH}$ .<sup>[176,177,179,180]</sup> Due to its high reactivity towards oxidized carbon substrates the  $\text{CH}_3\text{COOH}$  could have been reduced as soon as mackinawite was formed and therefore lead to high numbers of oxidized iron atoms. This would stand in strong contrast to the here applied method of passivation, where only the surface of the particles is let in contact with air. Though, the sample from

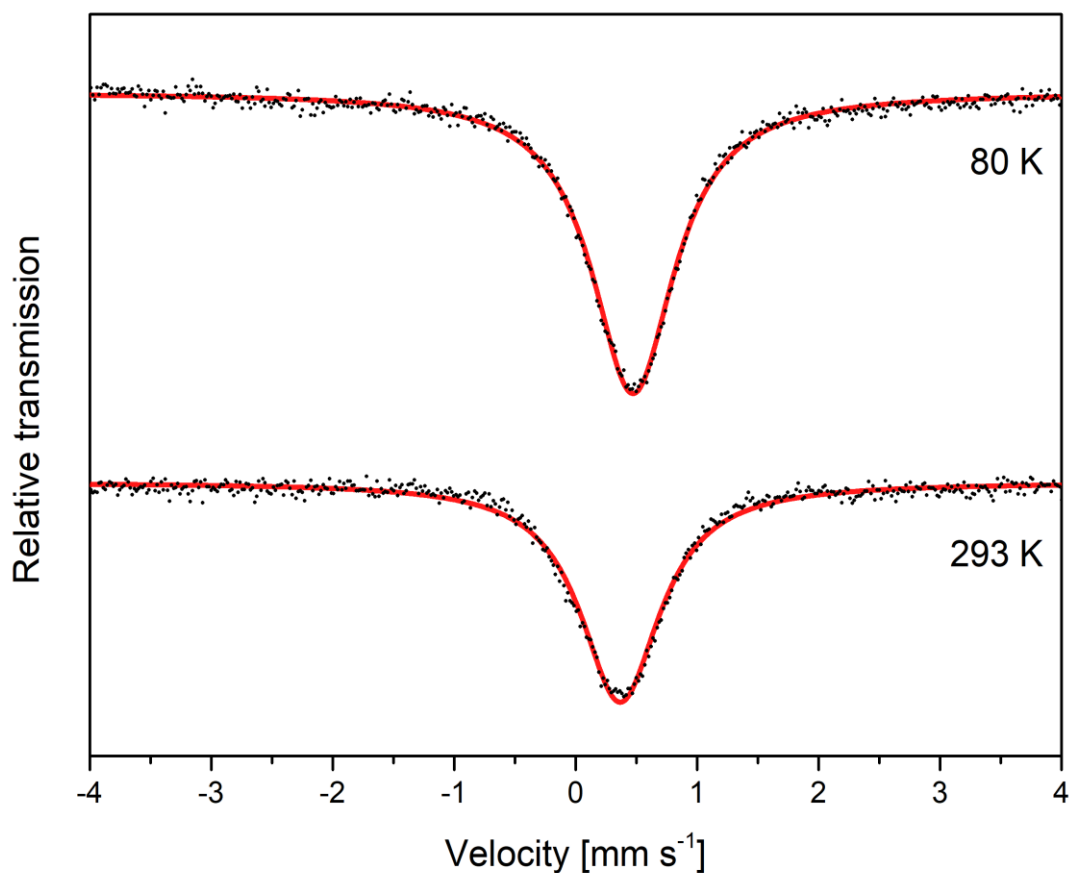


**Figure 8** Mössbauer spectra of deactivated mackinawite from the reaction between iron and sulfur in a 0.01 M NaCl after 24 h. The spectrum was measured by M. Winkler.

iron and sulfur was stored under air at least for 3 d before being analyzed by Mössbauer spectroscopy, almost no other signal than the one for Fe<sup>2+</sup> was observed.

### 3.2.6 Pyrophoricity

When the mackinawite was synthesized in acetone, a fine black powder could be obtained that reacted heavily in contact with air resulting in the formation of sparks around the opening of the N<sub>2</sub> purged Schlenk flask. This pyrophoric behavior is already reported for synthetic mackinawite formed by precipitation and remains an obstacle in establishing suitable applications to use this potential energy source. The mackinawite synthesized in acetone could not be isolated in any other way than the Schlenk technique. If a sample was filtrated over a frit with a N<sub>2</sub> stream applied, the fine powder was swirled up and blown into the air. When the reaction was, however, performed in H<sub>2</sub>O, the resulting filter cake remained intact, even after being washed with EtOH, acetone and Et<sub>2</sub>O. With the N<sub>2</sub> stream applied, the particles remained stuck to the

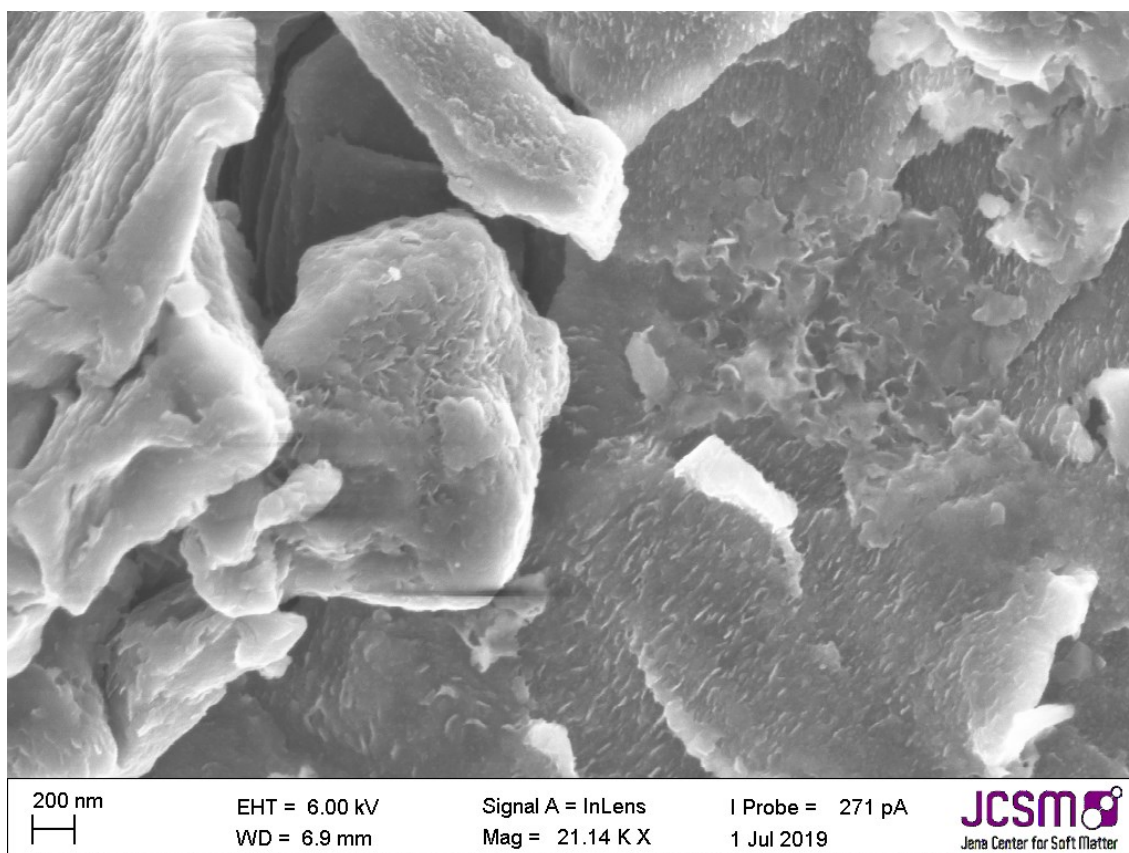


**Figure 9** SEM image of mackinawite that was in contact with air for several weeks. The surface smoothed as a passivating layer of amorphous iron oxides is formed.

bottom of the frit and could be deactivated by letting small amounts of O<sub>2</sub> enter for several times.

This procedure was used to deactivate the sample analyzed by Mössbauer spectroscopy and therefore does not lead to the formation of Fe<sup>3+</sup> ions in significant amounts. Boursiquot et al. already assumed the reaction with O<sub>2</sub> does only take place on the surface of the particles.<sup>[177]</sup> The deactivation of mackinawite apparently leads to the formation of an amorphous layer, restricting any further O<sub>2</sub> to enter the coated particle. The SEM images in Figure 9 are derived from a deactivated sample of freshly prepared mackinawite and a sample that was stored open to the air for one month.<sup>[175]</sup> The image of the deactivated sample shows the unordered surface of the mackinawite conglomerates, whereas the passivating layer is only poorly developed and thus amorphous. With time, as seen in the SEM image of the aged sample, this smooth passivating layer, consisting of greigite and iron oxides, develops further until the particles are coated only small areas exhibiting the previous, unordered, surface structure, remain.

In aqueous solution the particles only slowly transformed into greigite and magnetite, even under open conditions. Such samples still were pyrophoric after being dried. The formation of the passivating layer therefore seems to be restricted at room temperature in aqueous solution. When samples were heated open to the air the transformation into greigite occurred more rapidly and consequently more magnetic material could be collected over time inside the reaction vessel with a strong magnet, applied from the outside.

### **3.2.7 Comparison to other routes**

The lattice spacing of mackinawite has been readily discussed in previous studies and found to differ, depending on the used synthetic route and composition of the samples. Thereby two main routes were discussed, whereas mackinawite was either formed by precipitation or the reaction from iron wire with Na<sub>2</sub>S solution. Reported values for the lattice spacing range from 5 Å to 6.6 Å, a detailed overview on the previous studies is given in Table 5.

**Table 5** Data in the literature on the d-spacing value of mackinawite produced by different synthetic routes together with the ones of the mackinawite from the reaction between iron and sulfur.

Reference	Route	Fe:S	c [Å]
Berner, 1964 <sup>[181]</sup>	FeSO <sub>4</sub> /H <sub>2</sub> S (r.t.)	1.05:1	5.03
Rickard, 1969 <sup>[182]</sup>	FeSO <sub>4</sub> /Na <sub>2</sub> S (r.t.)	1:1.1	5.03
Lennie, 1995 <sup>[74]</sup>	Fe / HAc/Na <sub>2</sub> S (r.t.)	1.008:1	5.03
Mullet, 2002 <sup>[183]</sup>	Fe / HAc/Na <sub>2</sub> S (r.t.)	1:1	5.05
Wolthers, 2003 <sup>[184]</sup>	(NH <sub>4</sub> ) <sub>2</sub> Fe(SO <sub>4</sub> ) <sub>2</sub> /Na <sub>2</sub> S (r.t.)	n.d.	5.48 - 6.6
Michel, 2005 <sup>[185]</sup>	(NH <sub>4</sub> ) <sub>2</sub> Fe(SO <sub>4</sub> ) <sub>2</sub> /buffer/Na <sub>2</sub> S (r.t.)	n.d.	5.03 - 5.09
Rickard, 2006 <sup>[78]</sup>	(NH <sub>4</sub> ) <sub>2</sub> Fe(SO <sub>4</sub> ) <sub>2</sub> /Na <sub>2</sub> S (r.t.)	1:1	5.19
Ohfujii, 2006 <sup>[186]</sup>	(NH <sub>4</sub> ) <sub>2</sub> Fe(SO <sub>4</sub> ) <sub>2</sub> /Na <sub>2</sub> S (r.t.)	n.d.	5.19 (wet)
			5.08 (dried)
Jeong, 2008 <sup>[187]</sup>	FeCl <sub>2</sub> /Na <sub>2</sub> S (r.t.)	n.d.	5.20
Bourdoiseau, 2011 <sup>[188]</sup>	FeSO <sub>4</sub> /Na <sub>2</sub> S (r.t.)	n.d.	5.05
Csákberényi-Malasics, 2012 <sup>[16]</sup>	FeSO <sub>4</sub> + C <sub>2</sub> H <sub>5</sub> NS (80 °C)	n.d.	5.2 - 5.5
This work	Fe + S (r.t.)	1 : 1	5.26 - 5.29
	Fe + S (80 °C)	1 : 1	5.07 - 5.29

For precipitated mackinawite and the one produced by the reaction of iron wire in sulfide solution, typically small lattice spacings, ranging from 5.03 to 5.05 Å, are reported. In later studies, where  $(\text{NH}_4)_2\text{Fe}(\text{SO}_4)_2$ , due to its higher stability against oxidation than  $\text{FeSO}_4$ , was used more frequently, some groups reported an increase in the lattice spacing. With a refined  $c$  parameter of 5.27 Å the mackinawite formed from iron and sulfur at room temperature fits well into the reported range. This synthetic route, in contrast to the previously covered ones, can be performed completely free of any additional salt and should therefore not be comparable to earlier routes. Accordingly, a spacing of this order was until now not reported when  $\text{S}^{2-}$  was entered in form of  $\text{H}_2\text{S}$  or  $\text{Na}_2\text{S}$ . Csákberényi-Malasics et al. synthesized mackinawite from  $\text{FeSO}_4$  and thioacetamide and reported larger spacings of 5.2 Å to 5.5 Å.<sup>[16]</sup>

The structure parameters for precipitated mackinawite were reported by Lennie et al. with  $a = 3.6735$  Å and  $c = 5.0328$  Å.<sup>[74]</sup> The representative PXRD pattern shows sharp reflexes due to the high crystallinity of the samples. For the reaction between iron wire and  $\text{Na}_2\text{S}$ , similar parameters were reported by Mullet and coworkers.<sup>[183]</sup> This may be a result of the lower crystallinity of the samples formed from iron and sulfur, or a wider size distribution, due to the longer reaction times. Compared to the ones found here, the  $c$  parameter (5.27 Å), referring to the lattice spacing, is slightly decreased. Reports on the lattice spacing, however, are inconsistent as a range of 5 Å to 6 Å has been reported until now. In Table 5 most of the recorded synthetic approaches, together with the respective route, are summarized.

### 3.2.8 Synthesis of other metal sulfides

In addition to iron, nickel, manganese, and cobalt were investigated on their potential to form metal sulfides by the reaction between iron and sulfur. Following the procedure for mackinawite synthesis, the sulfur and metal powder were placed into a glass vial, evacuated, and charged with an acetone/ $\text{H}_2\text{O}$  mixture. When manganese and cobalt were used, the collected PXRD pattern did not provide any sign for metal sulfide formation, as only reflexes of the initial sulfur and metal powder were observed.

When nickel was used, the PXRD pattern of the reaction product (Figure 10) provided reflexes for nickel and sulfur, but also a third compound, which could be identified as

heazlewoodite ( $\text{Ni}_3\text{S}_2$ ). The reaction did thereby not occur at room temperature, but prolonged at 80 °C whereas the formation of a black material could be observed. Even after 3 d at higher temperatures, however, only small amounts of heazlewoodite were formed, while still big amounts of magnetic nickel remained.

Rather than synthesizing a pure nickel sulfide, iron powder was added in hope to achieve a better solubility of the nickel as it would be incorporated into the more faster developing iron sulfide structure. The collected PXRD patterns from the first experimental approaches where different ratios in iron and nickel were reacted in presence of a constant amount of sulfur at room temperature, in an acetone/ $\text{H}_2\text{O}$  mixture, are shown in Figure 11. When only iron was present, mackinawite formed. With increasing amount in nickel, the corresponding reflex appeared whereas no change in the mackinawite reflexes was observed. At an iron:nickel ration of 1:1, however, a new pair of signals appeared, corresponding with the values found for heazlewoodite. When the iron:nickel ratio was further lowered, these reflexes disappeared again and only sulfur and nickel remained.

The reaction between nickel and sulfur was found to only proceed at elevated temperatures. Therefore, the reaction between nickel, iron, and sulfur with an initial iron:nickel ration of 1:1 was studied at 80 °C either in the acetone/ $\text{H}_2\text{O}$  mixture or solely

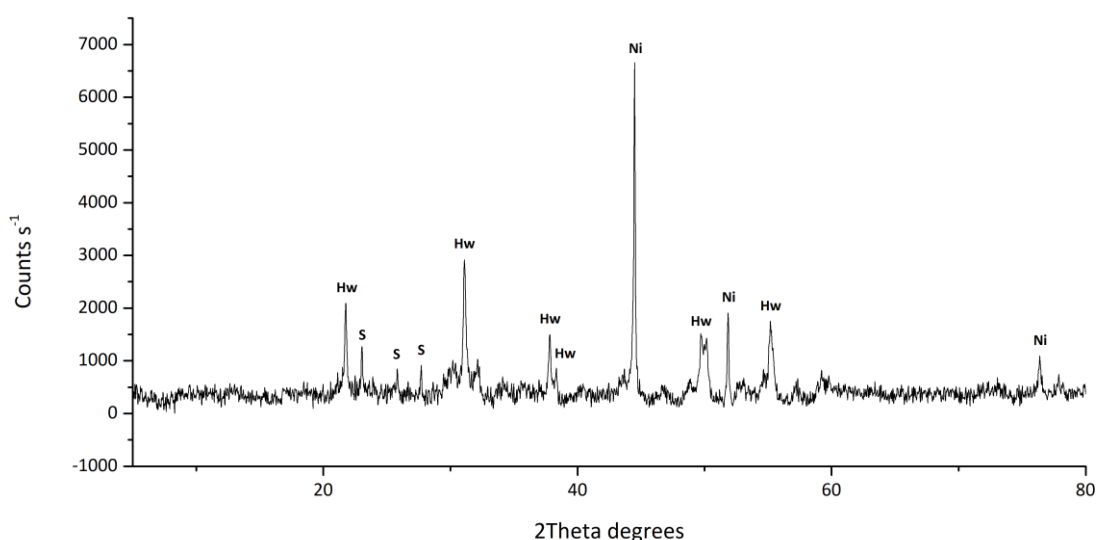


**Figure 10** PXRD pattern of the product from the reaction of nickel and sulfur in pure  $\text{H}_2\text{O}$  after 3 d at 80 °C; S = Sulfur, Hw = Heazlewoodite.

in H<sub>2</sub>O. The collected PXRD pattern of the reaction products formed in the acetone/H<sub>2</sub>O mixture are compared in Figure A 4. Both still show reflexes origin from the nickel, whereas no iron and sulfur are present anymore. Additionally, no broad signal groups, typically indicating mackinawite formation, were observed. For the product, synthesized in the acetone/H<sub>2</sub>O mixture a new group of slightly broadened signals was observed. They do not fully correspond with the literature values on heazlewoodite and were not observed during the previous experiments. When the reaction was performed in H<sub>2</sub>O, the observed diffraction peaks in the PXRD pattern of the reaction product do correspond with the ones of heazlewoodite, still significant amounts of nickel are left.

The reaction in H<sub>2</sub>O was further investigated for an array of mixtures, containing different iron:nickel ratios, at 80 °C. The collected PXRD pattern are displayed in Figure 11. When the iron:nickel ration was high (9:1), only mackinawite and nickel reflexes were observed, indicating the selective reaction between iron and sulfur. When 25 % of nickel is present, the formation of a pair of signals is observed, where one corresponds

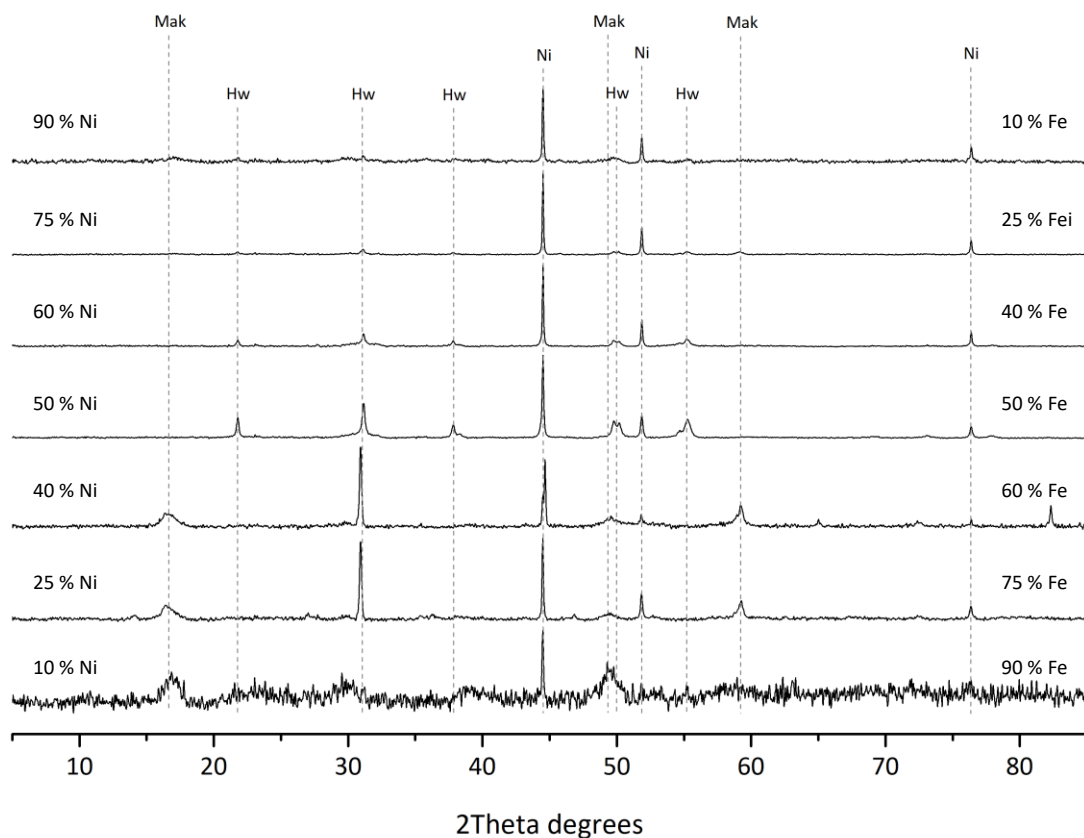


**Figure 11** Series of PXRD pattern collected from samples containing different mixtures of iron and nickel after 7 d at 80 °C in H<sub>2</sub>O.

to heazlewoodite, while the other one corresponds to mackinawite. When the ratio was set to 1:1, both signals, as well as the ones for mackinawite disappeared and only a phase corresponding to heazlewoodite formed alongside significant amounts of unreacted nickel.

### 3.3 Summary

The reaction between iron and sulfur could be shown to proceed willingly under ambient conditions while mackinawite is formed selectively. When compared to other synthetic routes like precipitation or oxidation of iron in sulfide solution, the approach of using iron and sulfur leads to the formation of mackinawite with a comparable particle structure, size, surface area and morphology. In contrast to already established routes, the reaction between iron and sulfur, however, features the following advantages:

- No use of salts like  $\text{Fe}^{2+}$  that are sensitive to oxidation.
- No use of toxic and environmental sulfur sources like  $\text{Na}_2\text{S}$  or  $\text{H}_2\text{S}$ .
- Additional reagents like salts can be introduced more precisely.
- The oxidation of the particle core can be suppressed in the absence of sulfate or acetate ions.

The reaction between iron and sulfur was found proceed when 88 mg to 8.8 g of the initial iron sulfur mixture was used and accelerated when only little amounts in sodium chloride were added. When smaller amounts in iron sulfur mixture were used, the reaction was found to only proceed partially as metallic iron remained in the vials even after heating at 80 °C. When more than 8.8 g of the mixture were reacted in the presence of sodium chloride the reaction was heating up remarkably, whereas  $\text{H}_2\text{O}$  started to condensate inside the reaction vessel. When the reaction is carried out with larger amounts of iron sulfur mixture the produced heat needs to be dissipated to avoid the  $\text{H}_2\text{O}$  from boiling and therefore limit the pressure inside the vessel.

The reaction at room temperature did not provide mackinawite when the pH of the solution was adjusted to values higher than 9. When such samples, however, were heated to 80 °C, the aqueous solution turned green while a dark green solid was formed.



Below pH 7 the reaction occurred readily under the production of H<sub>2</sub>S because of the acidic dissolution of the formed mackinawite.

The mackinawite formed by the reaction of iron and sulfur could be deactivated by continuously introducing small amounts of O<sub>2</sub> during filtration. This process takes place at the surface of the particles and does not affect the inner core. The collected Mössbauer spectra of a sample, deactivated by this method, could be well fit using a single singlet which can be attributed to Fe<sup>2+</sup> ions in tetragonal sites. No additional doublets were necessary to describe the observed spectra whereas no Fe<sup>3+</sup> are assumed to be present in tetragonal sites. This is further supported by PXRD as the collected pattern of the sample can fully be described with the data on mackinawite in the literature.

The reaction between iron and sulfur was further applicable when iron was partially exchanged with nickel. In the absence of iron, no significant reaction between nickel and sulfur was observed at room temperature. When the mixture was heated, signals corresponding to the heazlewoodite structure emerged, whereas large amounts of nickel remained even after 3 d. The PXRD pattern collected from samples containing a mixture of iron and nickel showed that heazlewoodite signals appeared most prominent when the ratio was set to 1:1. At both, lower and higher ratios, however, nickel remained present in the samples, while overall no metallic iron was observed anymore.

Mackinawite is known for its various applications due to its possibility to adsorb or intercalate ions and organic compounds, as well as its high reactivity. Latter remains a hurdle to establish suitable methods allowing us to access this range of functionalities. The particles produced by the reaction between iron and sulfur, in contrast to the ones formed by precipitation, are bigger in size but still provide broad PXRD patterns typically observed for mackinawite with low crystallinity and therefore high reactivity. In combination with the established method of deactivation, stable mackinawite nano particles can be produced that upon acidification in aqueous media would again reveal the active surface to a certain degree.

## Chapter 4. Reduction of cyanides

### 4.1 Introduction

The formation of pyrite from mackinawite and hydrogen  $H_2S$  under acidic conditions gained a lot of attention due to its possible role as energy source for prebiotic substrate reduction.<sup>[19,52,189]</sup> The formation of  $NH_3$  from  $NO_2^-$  and  $NO_3^-$  was extensively studied by several groups and has been shown to proceed with yields of up to 40 %.<sup>[20,165,190]</sup> The mackinawite supported formation of  $NH_3$  from dinitrogen ( $N_2$ ) was studied by Dörr et al. and showed much lower efficiency.<sup>[164]</sup> The reduction of  $NO_2^-$  and  $NO_3^-$  by mackinawite surprisingly bypasses the energetically more favorable formation of  $N_2$ . Until now, no mechanism explaining this observation has been proposed.

Despite the capability of mackinawite to reduce nitrogen substrates only few studies on the reduction of carbon substrates were performed. Blöchl et al. provided experimental evidence for the reduction of ethine ( $C_2H_2$ ) to ethene ( $C_2H_4$ ) and ethane ( $C_2H_6$ ) under prebiotically plausible conditions.<sup>[162]</sup> In a later study, Heinen et al. investigated the reduction of  $CO_2$  by commercially purchased iron sulfide and found a range of linear thiols to be produced under acidic conditions.<sup>[9]</sup> HCN is known to readily undergo condensation, leading to the abiotic formation of purine precursors and amino acids.<sup>[34,191–193]</sup> Furthermore, Ritson et al. recently reported the formation of simple sugars from HCN, when a photoredox system in combination with copper cyanide complexes was applied.<sup>[194,195]</sup> Though, the HCN based chemistry enables the formation of various biologically relevant molecules under prebiotic conditions, only few abiotic sources for HCN or cyanides in general are known.

Recently, Todd et al. proposed raised HCN levels due to low velocity and low angled impacts of small comets during the early and late heavy bombardment. They stated that individual impacts would lead to prebiotically significant levels in HCN that probably lasted from thousands to million years.<sup>[196]</sup> In addition to this local phenomenon, HCN can be formed due to the photochemical reaction between  $CH_4$  and  $N_2$ .<sup>[197,198]</sup> While this process would provide HCN on a global scale, abiotic sources for  $CH_4$  are likewise scarce. High prebiotic levels in  $CH_4$ , however, are debated as part of the answer for the faint

young sun paradox.<sup>[199,200]</sup> Though, earth's earliest atmosphere probably contained much higher amounts of CO<sub>2</sub><sup>[5,201]</sup>, they alone would not provide an efficient enough greenhouse effect to prevent the earth from freezing during times of lower luminosity.<sup>[202]</sup>

Until now, primordial processes based on mackinawite were mainly discussed under hydrothermal conditions.<sup>[71,203–205]</sup> The reaction between iron and sulfur provides a plausible prebiotic pathway for the formation of mackinawite on the early earth's surface and therefore opens the door for a new range of substrates to be investigated in their reaction with this highly reactive iron sulfur phase.<sup>[175]</sup>

## 4.2 Results and Discussion

### 4.2.1 General remarks

The reduction of KCN was performed with the three reduction systems **RS<sub>1</sub>**, **RS<sub>2</sub>** and **RS<sub>3</sub>** (2.2.5) at 80 °C for different reaction times. All systems led to the formation of reduced carbon species whereas the array of products relied on the used reduction system. The reduced species however only appeared in the gas phase when the aqueous solution was acidified. Therefore, the pH was adjusted either before or after the reaction, before a gas phase sample was extracted. The array of products highly depended on the presence of sulfur in form of elemental sulfur in **RS<sub>2</sub>** or in form of H<sub>2</sub>S from reaction 1 in **RS<sub>3</sub>**.

During the thesis several different acids were used to adjust the pH of the aqueous samples. The first series of samples were analyzed by the Thermo Fisher system and contained HCl. The gas phases were directly injected into the injection port of the GC system using a gas tight syringe. The gas phase of later samples analyzed by the Shimadzu systems, however, partly were extracted using the HS-20 sampler, which contains a series of metal pipes. To reduce possible damage by corrosion alternatives to HCl were evaluated. Heinen et al. reported their FeS/HCl system to further function when other mineral acids like H<sub>2</sub>SO<sub>4</sub> or HNO<sub>3</sub> were deployed.<sup>[206]</sup> Both, SO<sub>4</sub><sup>2-</sup> and NO<sub>3</sub><sup>-</sup> can potentially be reduced by mackinawite and were therefore disregarded. These problems were solved by using H<sub>3</sub>PO<sub>4</sub>, which in contrast does not produce corrosive

gases. The  $pK_s$  for the first deprotonation step of  $H_3PO_4$  is 2.14 and therefore much higher than the ones of strong acids like HCl,  $HNO_3$  or  $H_2SO_4$ . A comparison between  $H_2SO_4$  and  $H_3PO_4$  is given in section 4.2.3.

## 4.2.2 Reduction of KCN

### 4.2.2.1 Iron

The reaction between elemental iron and sulfur into mackinawite was shown to proceed highly selectively, whereas only small amounts of starting material typically remained. The presence of small amounts of elemental iron, however, cannot be completely ruled out. Therefore, samples containing the sole iron powder were prepared and reacted with KCN under different conditions. The gas phase of a sample containing iron at pH 6 (GP-01-01) did not contain any reduced species. In a sample, where the pH was adjusted to 2 (GP-01-02),  $CH_4$ ,  $C_2H_4$  and  $C_2H_6$  were detected. These impurities probably derive from contaminations on the surface of the iron particles, due to the manufacturing process (2.2.1 and 7.2.2).

When KCN was reacted with iron at pH 6 (GP-01-03), the extracted gas phase sample contained a mixture of  $CH_4$  (0.72 %),  $C_2H_4$  (17.40 %) and  $C_2H_6$  (23.10 %) as well as longer hydrocarbons like propene ( $C_3H_6$ , 13.20 %), propane ( $C_3H_8$ , 20.69 %), butene ( $C_4H_8$ , 7.41 %), butane ( $C_4H_{10}$ , 9.62 %), 1-pentene ( $C_5H_{10}$ , 3.69 %) and pentane ( $C_5H_{12}$ , 4.10 %). In the presence of acid (GP-01-04) the gas phase contained a wider range of hydrocarbons with chain lengths up to 6 carbon atoms. When the total area of reduced compounds is compared to the one recorded for GP-01-03, nearly a tenfold in products was produced. The formation of hydrocarbons (91 %) was favored in comparison to nitriles (5.6 %) and oxygenated species (3.4 %). The products were identified by comparing their fragmentation pattern to the ones provided by the NIST 14 library.

In a separate experiment the evolution of the reduced species from the mixture was further confirmed by comparing samples containing NaCN (GP-02-01) and  $Na^{13}CN$  (GP-02-02) (Figure A 13 – 27). In contrast to GP-01-04 an even wider range of products was formed, whereas chain lengths of up to 8 carbon atoms were observed. The

corresponding chromatograms of the gas phases are compared in Figure 12. The expected mass shifts were observed accordingly and are summarized in Table A 2.

Previous reports on the reduction of cyanide by nitrogenase cofactor homologs reported a more favored formation of alkenes than alkanes, as well as a higher tendency of C – C bond formation when  $\text{CN}^-$  was used instead of CO or  $\text{CO}_2$ .<sup>[207]</sup> Because of this, lower portions of methane (10 – 34 %) are typically formed in comparison to ethene (38 – 71 %).<sup>[160]</sup> The reduction of  $\text{CN}^-$  by the iron powder resulted in the formation of much smaller amounts in  $\text{CH}_4$  (1.35 %), but hydrocarbons with chain lengths up to six carbon atoms. The main products were found to be  $\text{C}_2\text{H}_2$  (13.00 %),  $\text{C}_2\text{H}_4$  (19.98 %),  $\text{C}_3\text{H}_6$  (10.97 %),  $\text{C}_3\text{H}_8$  (17.25 %),  $\text{C}_4\text{H}_{10}$  (6.16 %) and  $\text{C}_3\text{H}_8$  (7.52%), making up 74,88 % of the gas phase. The alkane/alkene ratios for the observed  $\text{C}_2$ ,  $\text{C}_3$ ,  $\text{C}_4$ ,  $\text{C}_5$  and  $\text{C}_6$  compounds was found to range from 1.1 to 2.0. Alkane formation therefore is favored, compared to alkenes.

The reduction of HCN into hydrocarbons has until now only been reported for more defined systems like the nitrogenase, its extracted and synthetic co-factors and the

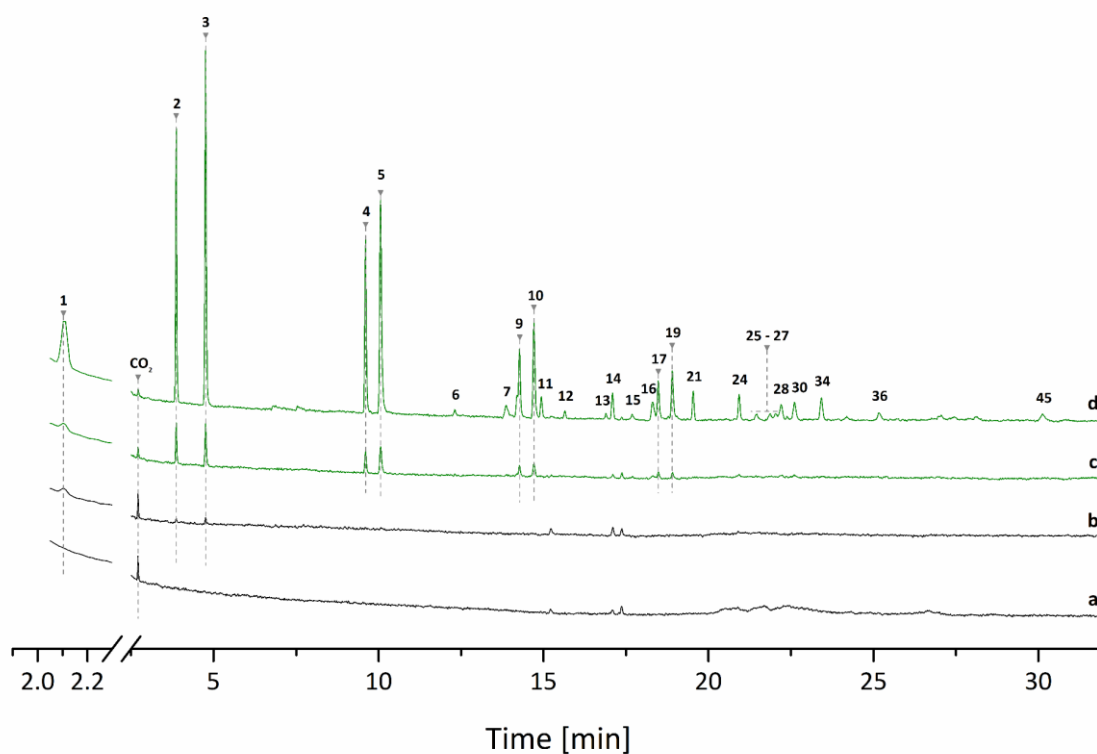
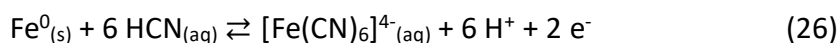
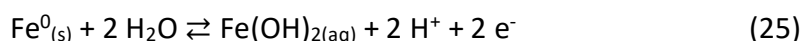


**Figure 12** Gas chromatogram (TIC) of GP-01-01 (a), GP-01-02 (b), GP-01-03 (c) and GP-01-04 (d). The full list of detected compounds is given in Table A 2.

molecular iron cyanide complex  $[\text{SiPr}_3\text{Fe}(\text{CN})]$ .<sup>[208]</sup> All reported attempts thereby needed an efficient electron source to produce reduced compounds. From the here collected data it is to assume, that the iron itself can act as efficient electron source to reduce the KCN, if protons are available.

The iron surface seemingly provides the scission of the C – N bond as non reduced species were observed from heating an aqueous HCN solution for several days. The reduction mechanism can well proceed as suggested by Rittle et al. for the molecular iron cyanide complex, where the protonation of the nitrogen atom is assumed to proceed intermediately, when the HCN is bound to the complex.<sup>[208]</sup> It is reasonable to conclude, that the reduction only takes place on the surface of the iron particles where a bonding between iron and carbon atom can be established.



Reaction 25 is known to consist of multiple steps where  $\text{OH}^-$  ions first appear as surface groups, before soluble Fe complexes are formed.<sup>[209]</sup> Though, experimental evidence is still missing, similar Fe-(CN) complexes are likely to be present during reaction (26). The first stage of this process lead to the formation of a  $\text{Fe}-(\text{CN})_{(ads)}$  unit, similar to the molecular pendant,  $[\text{SiPr}_3\text{Fe}(\text{CN})]$ .<sup>[208]</sup> Iron is an electric conductor, therefore electrons

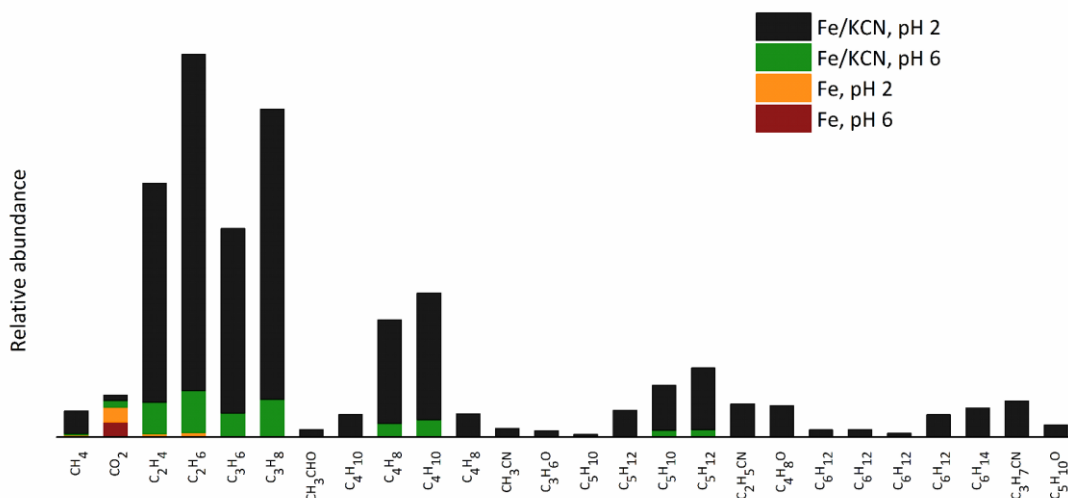
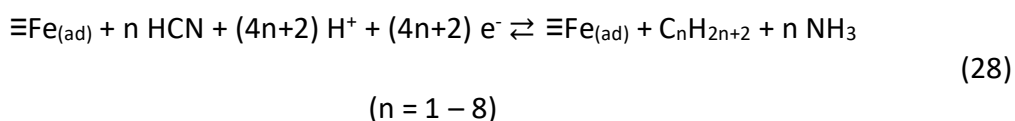
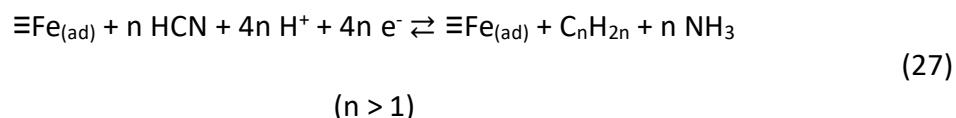


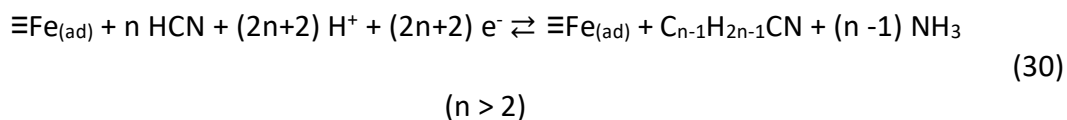
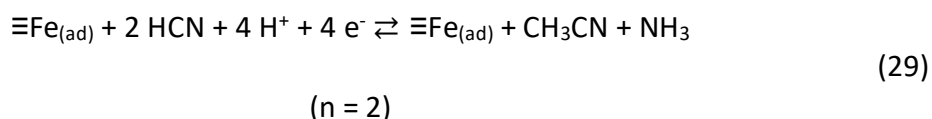
**Figure 13** Compared TIC areas of the samples GP-01-01 to GP-01-04.

are easily supplied from the bulk of the particles towards the surface atoms. For the reduction of KCN as surface bound species, the following reactions are suggested (see also Table A 3):

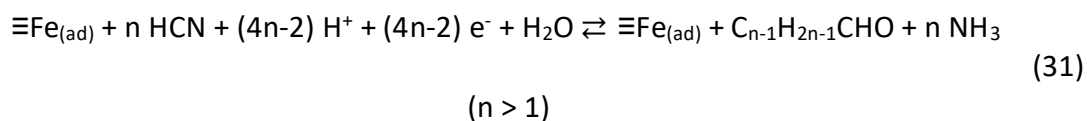
### Hydrocarbons



### Nitriles



### Aldehydes



Recently, Varma et al. reported the formation of reduced compounds containing C – C bonds from the reaction between CO<sub>2</sub> and native iron. They concluded, that the reduction takes place on top of the metal, whereas the formed intermediates and end-products remain bound to the surface during the reaction.<sup>[11]</sup> Here a similar mechanism for the reduction of HCN is proposed. Following Figure 14, the initial bonding leads to the formation of a  $\equiv\text{Fe}-(\text{CHNH})$  residue, which either is reduced and protonated or can be attacked in nucleophilic manner by a second HCN molecule. In the case of a first

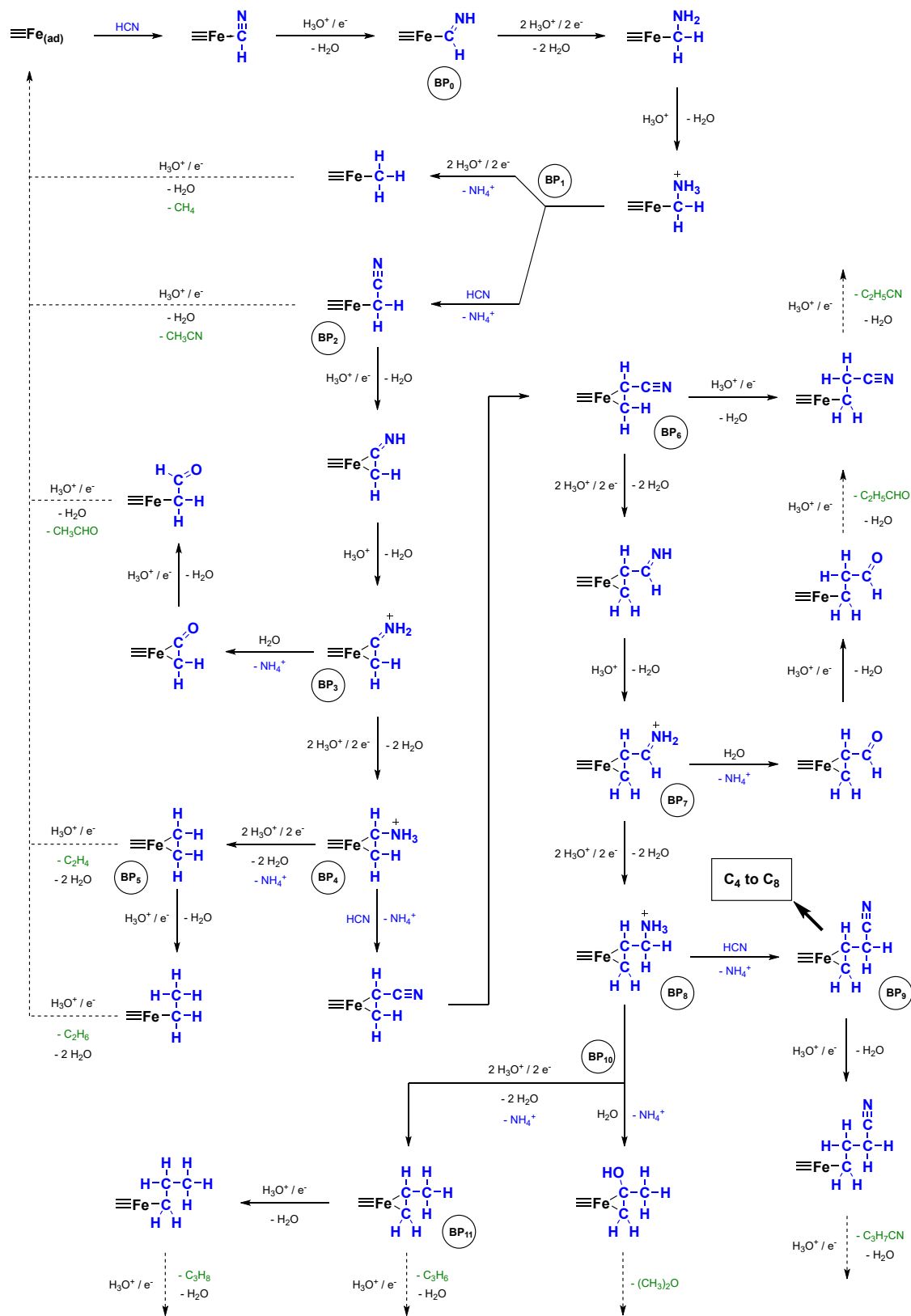


Figure 14 Proposed reaction mechanism for the reduction of HCN by the iron surface.



protonation and reduction of the primary carbon atom, the nitrogen atom leaves as  $\text{NH}_4^+$ . After a following reduction step the methyl residue can be released in form of  $\text{CH}_4$ .

The partly reduced intermediate  $\equiv\text{Fe}-(\text{CH}_2\text{NH}_3^+)$  offers a first branching point ( $\text{BP}_1$ ), where the carbon atom can further be reduced and protonated to release  $\text{NH}_3$  and  $\text{CH}_4$  or be attack by another  $\text{HCN}$  molecule in a nucleophilic manner. The nucleophile attack of the  $\text{CN}^-$  thereby supports the scission of the  $\text{C} - \text{N}$  bond like reported for  $\text{H}_2\text{S}$  during the Pt supported denitrification of amines.<sup>[210]</sup> The newly formed  $\equiv\text{Fe}-(\text{CH}_2\text{CN})$  intermediate can then either be released by reduction as the  $\text{Fe} - \text{C}$  bond is cleaved or protonation of the nitrogen atom whereas a second  $\text{Fe} - \text{C}$  bond is formed ( $\text{BP}_2$ ). A similar reaction was earlier proposed for the mechanism of  $\text{CO}$  reduction by metals in the Fischer-Tropsch reaction.<sup>[211]</sup>

The  $\equiv\text{Fe}-\eta^2-(\text{CH}_2\text{CNH}_2^+)$  residue can then either be attacked by a  $\text{H}_2\text{O}$  molecule in a nucleophilic manner, whereas  $\text{NH}_4^+$  is removed, or further reduced ( $\text{BP}_3$ ). The attack of  $\text{H}_2\text{O}$  is followed by a reduction, leading to the formation of acetaldehyde ( $\text{CH}_3\text{CHO}$ ), which clearly was identified by its mass pattern and isotopic shift. The  $\equiv\text{Fe}-\eta^2-(\text{CH}_2\text{CNH}_2^+)$  residue structurally reassembles the one formulated at  $\text{BP}_1$ . Following the previous steps, again either the direct reduction or nucleophilic attack of a  $\text{HCN}$  molecule can take place ( $\text{BP}_4$ ). When reduced, the  $\text{NH}_4^+$  again is removed, while a  $\equiv\text{Fe}-\eta^2-(\text{CH}_2\text{CH}_2)$  residue is formed ( $\text{BP}_5$ ). At this fifth branching point,  $\text{C}_2\text{H}_4$  can be directly released into the gas phase. When the second carbon atom is further reduced, appropriate formation of  $\text{C}_2\text{H}_6$  takes place.

In the case of the nucleophilic attack by  $\text{HCN}$  a second  $\text{C} - \text{C}$  bond is established. Following the fate of the residue at  $\text{BP}_2$ , either  $\text{C}_3$  nitriles, aldehydes, alkanes, or alkenes are produced. This mechanism is in good accordance with the experimental observations for shorter carbon compounds with  $n(\text{C}) \leq 3$ . With increasing chain lengths more branched compounds were produced. For butane and butene all possible isomers were identified. This can be well explained due to the  $\eta^2$ -bonding mode where both carbon atoms can be attacked by the third and fourth  $\text{CN}^-$  molecule (Figure 15). During the reduction experiments butane (7.84 %) and 1-butene (6.10 %) became the main

products among the C<sub>4</sub> compounds. They were followed by *i*-butane, 2-methyl-1-propene and 2-butene with 2.03 %, 1.83 % and 1.80 %, respectively.

If the two initially bound carbon atoms would be attached in a  $\eta^1$  – manner, e.g., perpendicular to the iron atom (Figure 14, BP<sub>2</sub>), the chain elongation mechanism would only provide the formation of 1-alkenes. The  $\eta^2$  – bound species allows a nucleophilic attack onto both carbon atoms simultaneously whereas the cleavage of the two Fe – C

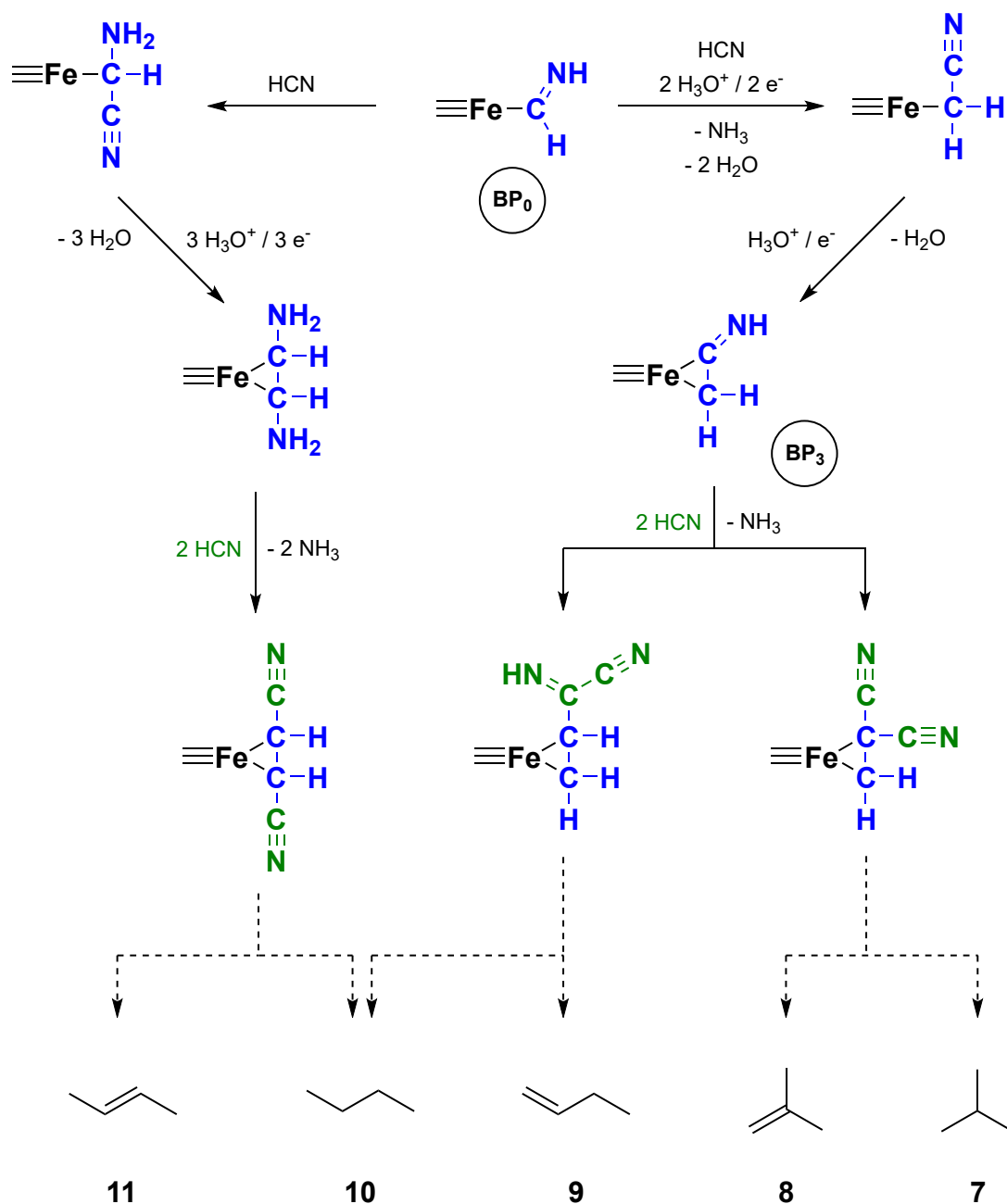


**Figure 15** Proposed fate of the residue formed at BP<sub>3</sub> to explain the formation of the different C<sub>4</sub> isomers.

bonds leaves behind a double bond. Alternatively, each carbon atom could be bound to adjacent iron atoms and lead to a similar positioning of the residue where both carbon atoms can be attacked after another or simultaneously. Both possibilities thereby align well with the experimental observations.

In case of the heteroatomic products (nitriles, ketones, and aldehydes) none containing a double bond were identified. Mechanistically this could be caused by the scission of the Fe – C bond during the nucleophilic attack of, either the HCN or H<sub>2</sub>O molecules. If, in the case of an attack by HCN, the bond between the iron and the second carbon atom is maintained, the newly added CN-residue is further reduced and C – N bond cleavage appears. In cases, where this bond undergoes scission, the second carbon atom gets protonated whereas after another reduction step the nitrile is released. The formation of aldehydes is displayed in Figure 15. The formation of ketones can follow from the attack of a HCN molecule onto the  $\equiv\text{Fe}-\eta^2-(\text{CH}_2\text{CO})$  residue formed after BP<sub>3</sub>. The second Fe – C bond is thereby only cleaved after the newly attached carbon atom is fully reduced and protonated.

#### 4.2.2.2 Iron sulfur mixture

With sulfur being present in RS<sub>2</sub> at pH 3, much less hydrocarbons and more organic sulfur compounds were formed. In Figure 16 the gas chromatograms collected from the

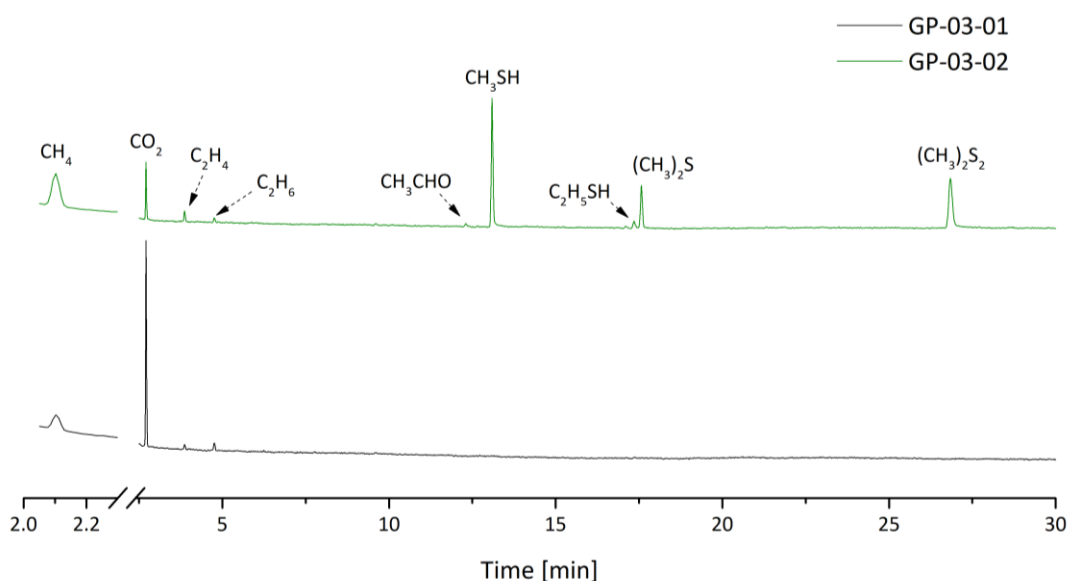


**Figure 16** Gas chromatogram of GP-03-01 and GP-03-02.

gas phases of two samples (GP-03-01 and GP-03-02), where the iron sulfur mixture and the KCN were supplied in a ratio of 10:1, are compared. At pH 6, like seen in 4.2.1.1, small amounts of CH<sub>4</sub>, C<sub>2</sub>H<sub>4</sub> and C<sub>2</sub>H<sub>6</sub> are formed. When the pH however was decreased, mainly CH<sub>4</sub> (4.16 %), CH<sub>3</sub>SH (37.84 %), (CH<sub>3</sub>)<sub>2</sub>S (12.98 %) and (CH<sub>3</sub>)<sub>2</sub>S<sub>2</sub> (29.39 %) were detected. In contrast to the iron supported reduction only low amounts in C – C products appeared. In GP-03-02 CH<sub>3</sub>CHO and C<sub>2</sub>H<sub>5</sub>SH were detected with a relative abundance of 1.10 % and 2.33 %, respectively. When the yield is calculated, 5.3 μmol (0.5 %) of CH<sub>3</sub>SH were produced in GP-03-02, while only 25.8 nmol (0.003 %) were formed in GP-03-01.

The formation of CH<sub>3</sub>SH during the reaction between the iron sulfur mixture and KCN in an equimolar ratio resulted in a wider range of products, including C<sub>1</sub> to C<sub>4</sub> thiols and CS<sub>2</sub>. This reaction was followed over a period of 96 h, whereas seven separate samples were extracted after 2 h, 4 h, 24 h, 48 h, 72 h and 96 h (GP-04). In Figure 17 the course of the reaction is illustrated. The CH<sub>3</sub>SH and CS<sub>2</sub> levels in the gas phase peaked at 48 h and declined afterwards. The same trend was observed for all reduced compounds, whereas no new products were formed in the gas phase. This observation was already made by

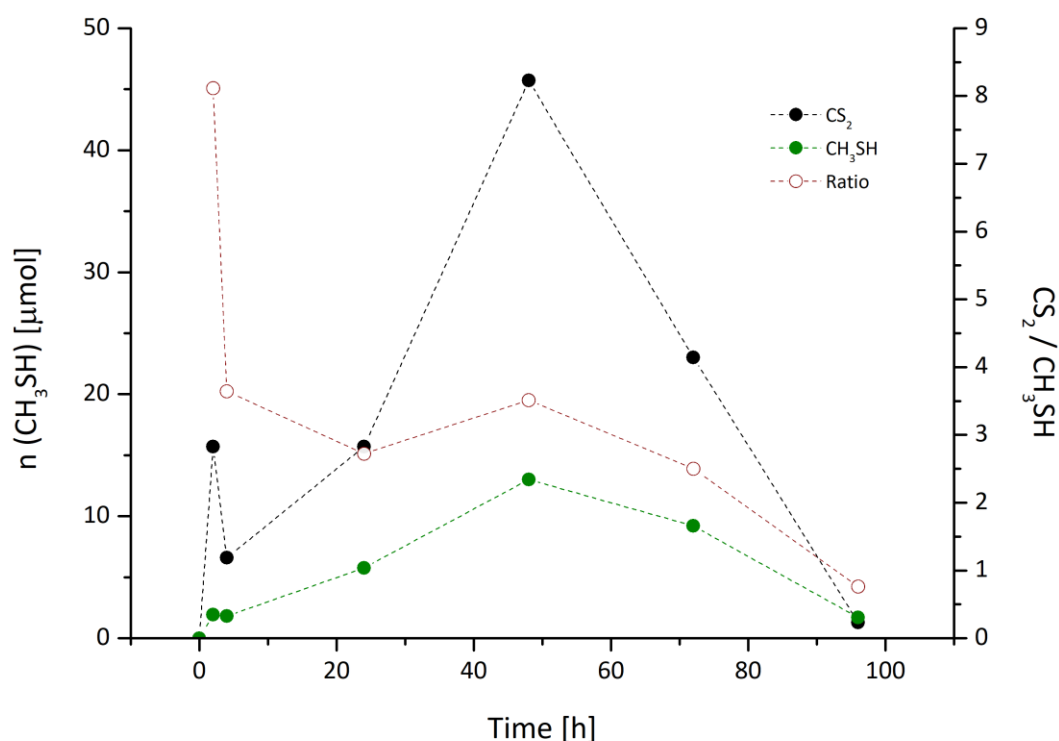


**Figure 17** Formation of CH<sub>3</sub>SH and CS<sub>2</sub> over a period of 96 h, together with their calculated ratio.

Heinen et al. who reported a similar decrease in thiol concentrations, however, only after 5 d.<sup>[9]</sup> The ration between CS<sub>2</sub> and CH<sub>3</sub>SH was found to drop significantly from around 8 to under 1 after 96 h. By applying an external calibration curve a peak CH<sub>3</sub>SH concentration of 13.01 μmol was estimated, which corresponds to a yield of 1.73 % as 0.75 mmol in KCN were initially supplied.

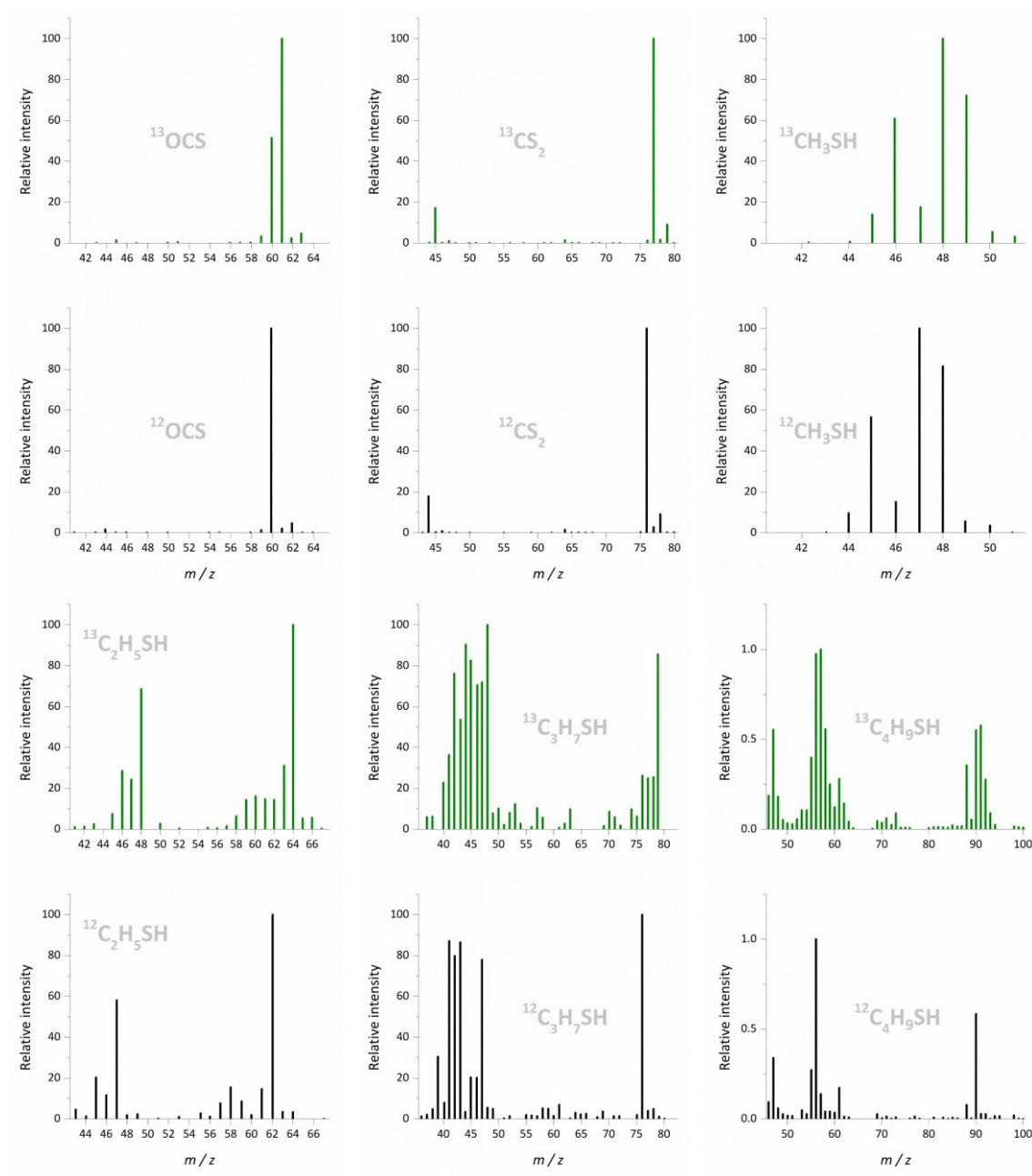


**Figure 18** Mass patterns retrieved from the reaction between the iron sulfur mixture with K<sup>12</sup>CN (black) and Na<sup>13</sup>CN (green).

The reaction products could be clearly identified by comparing the mass pattern to the ones listed in the NIST 14 library. The similarity search thereby provided values of > 90 % for all observed compounds. In addition to that the expected mass shift of +1 for COS, CS<sub>2</sub> and CH<sub>3</sub>SH, of +2 for C<sub>2</sub>H<sub>5</sub>SH, of +3 for C<sub>3</sub>H<sub>7</sub>SH, and of +4 for C<sub>4</sub>H<sub>9</sub>SH were observed when Na<sup>13</sup>CN was used instead (GP-04-07, Figure 18). In case of CS<sub>2</sub> and CH<sub>3</sub>SH the mass pattern appeared fully shifted. The mass pattern retrieved from the COS signal, however, only was partly shifted with a ratio between  $m/z$  60 : 61 of 0.5. A similar distribution was observed for the products containing a C – C bonds. The mass pattern of C<sub>2</sub>H<sub>5</sub>SH and C<sub>3</sub>H<sub>7</sub>SH both are shifted towards the expected  $m/z$  = 64 and  $m/z$  = 79, respectively, but still contained peaks that probably occur as a result from <sup>12</sup>C containing contaminations. With longer chain lengths, the influence of these contaminations significantly increased, whereby the  $m/z$  = 94 peak in the C<sub>4</sub>H<sub>9</sub>SH signal of GP-04-07 appeared only with an intensity of 2.40 %.

### **The green solution**

When the reaction between iron, sulfur and KCN was carried out in the absence of acid, the initial pH was found to range from 9 to 10. In contrast to the reaction between iron and sulfur at pH 9, where mackinawite formation is limited, full conversion was observed when KCN was present. When a sample containing each 1 mmol of iron, sulfur and KCN was charged with 3 mL H<sub>2</sub>O and heated at 80 °C, the initial colorless solution turned greenish first and further darkened during the following 24 h.

A similar color has already been reported for mixed valent iron (sulfide) hydroxides, also known as (sulfide) green rusts. Jones et al. showed that a green solution is formed, when magnetite particles were reacted with cysteamine to give a brilliant green aqueous solution.<sup>[212]</sup> Earlier observations by Taylor et al. reported a similar green color for aqueous NaFeS<sub>2</sub> solutions. They stated that the “green liquor”, an older term originating from the pulp and paper industry, is formed faster when ferric nitrate was used instead of ferrous salts.<sup>[213]</sup> In the latter case the green color furthermore only formed in the presence of air. It therefore is plausible, that the presence of Fe<sup>3+</sup> ions is inevitable for the formation. A similar observation was made for mackinawite from the elements when it was heated in the presence of KCN. Over the first 2 h of the reaction the solution

remained colorless. When it was, however, let in contact with air, the aqueous phase turned greenish as  $\text{Fe}^{2+}$  ions were oxidized.

The aqueous solution of the KCN samples fully turned green after 2 to 4 h. The reactions were carried out under nitrogen atmosphere, whereas oxidation by  $\text{O}_2$  can be ruled out. The reduction of  $\text{CN}^-$  was shown to proceed readily in the presence of iron and mackinawite (4.2.1.3) and can here likewise lead to the formation of  $\text{Fe}^{3+}$  ions. Until now only few analytical data on sulfide green rust is available. Due to the intense color Taylor et al. recorded UV/Vis spectra, giving three adsorption maxima which all can be attributed to charge transfer transitions of the iron atoms.<sup>[213]</sup> The spectra of the solution produced from the reaction between iron, sulfur and KCN is shown in Figure 19. Similar to the spectrum of  $\text{NaFeS}_2$ , three adsorption maxima were observed at 430 nm, 530 nm, and 630 nm, respectively.

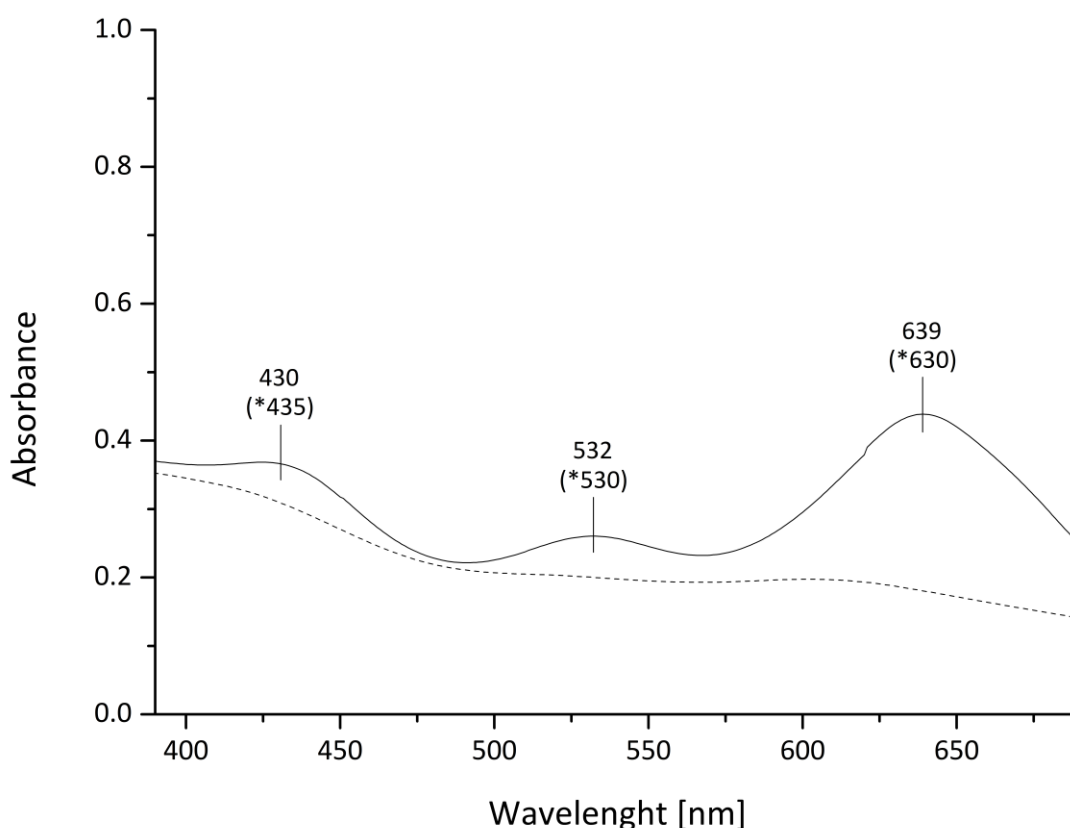


**Figure 19** UV/Vis spectra of the filtrated green solution (solid line) together with the one of pure  $\text{H}_2\text{O}$  (dashed line). Values in parentheses relate to the ones given by Taylor and Shoemith.

The green solution was further investigated by  $^1\text{H}$  NMR spectroscopy. The aqueous solution of a reacted sample was therefore extracted by a syringe and transferred in a NMR tube containing 0.05 mL of  $\text{D}_2\text{O}$ . To exclude any solid impurities, a syringe filter was applied before the content of the syringe was transferred into the NMR tube. In Figure 21 the collected  $^1\text{H}$ -NMR spectra from the reaction between iron, sulfur and KCN over time are displayed (LP-01). During this experimental series the first sample for NMR analysis was extracted as soon as the green color appeared. In total 5 singlets at 8.49 ppm, 8.11 ppm, 4.75 ppm, 3.75 ppm, 0.49 ppm and a high field shifted one at -2.20 ppm were observed. The singlets at 4.75 ppm and 3.75 ppm can be assigned to  $\text{H}_2\text{O}$  and DHO, respectively.

The  $\text{H}_2\text{O}$  signal was partly removed from the spectra to achieve a better view as product concentrations were low. When mackinawite was used instead of the iron sulfur

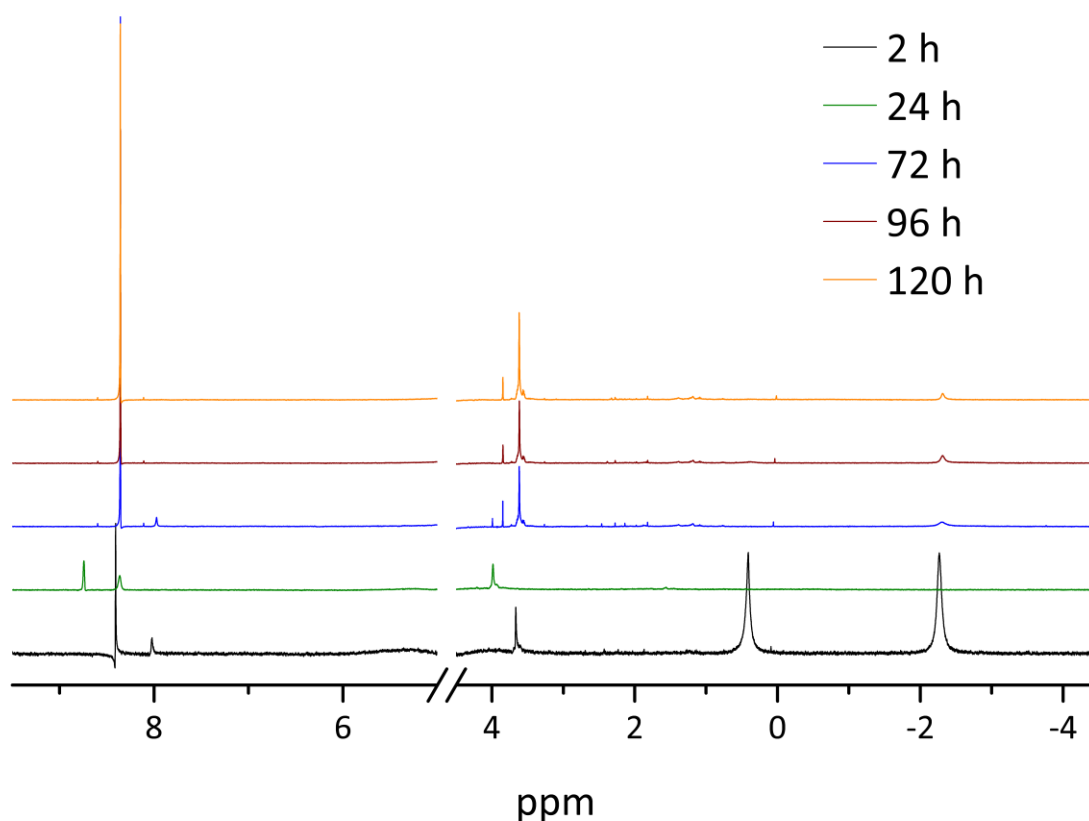


**Figure 20** Collected  $^1\text{H}$ -NMR spectra ( $\text{D}_2\text{O}$ , 400 MHz) of the aqueous phase from the reaction between the iron sulfur mixture and KCN at pH 9.



mixture, the aqueous solution turned greenish in color, but did not darken with time. Nevertheless, a faint signal, corresponding to the high field shifted proton, was detected at -2.22 ppm (LP-03, Figure A 36).

When the aqueous phase of LP-01 was investigated after different reaction times, the calculated area of the signal at -2.20 ppm peaked after 2 h. During the following days the signal remained detectable but decreased in intensity (Figure 20). It disappeared completely upon the addition of acid (Figure 21). When the initial pH was adjusted to 4, no comparable signal was observed. The peak area of the signal at 8.49 ppm was found to increase in time, but simultaneously levelled out at reaction times longer than 3 d. To examine, whether the protons derive from contaminations or from the sample itself, reactions were additionally performed in D<sub>2</sub>O (LP-02). When such samples were heated, the aqueous solution turned green like when H<sub>2</sub>O was used. When a sample was extracted the previously observed proton signals at 8.49 ppm, 8.11 ppm, 0.49 ppm and -2.20 ppm were missing (Figure 21).

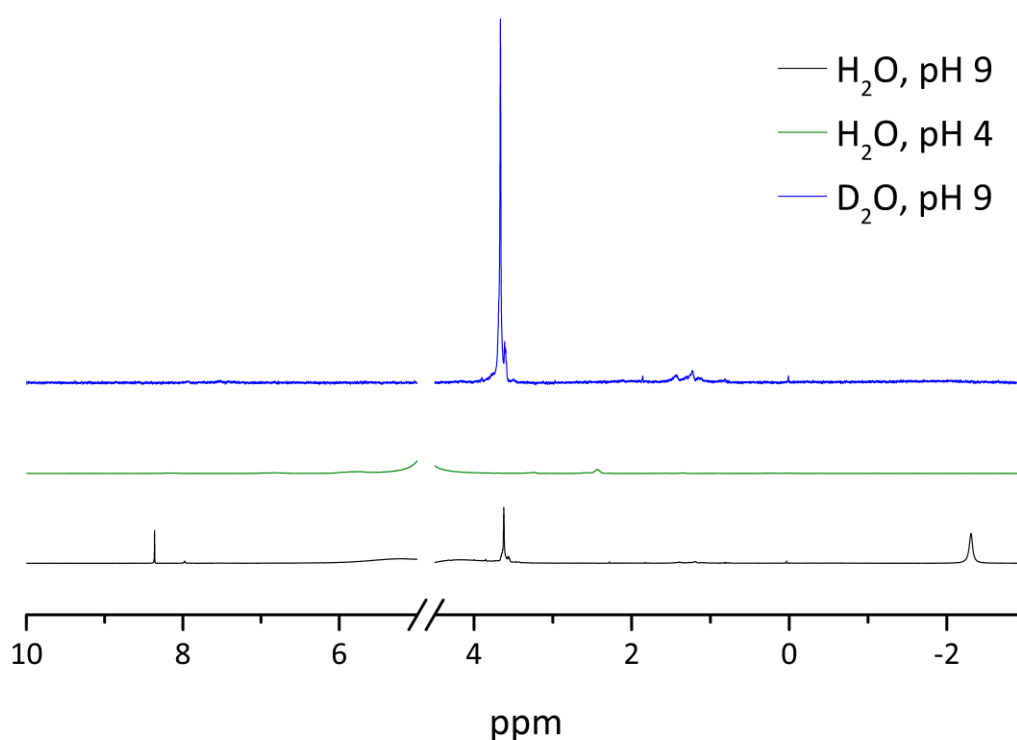


**Figure 21** <sup>1</sup>H-NMR spectra (D<sub>2</sub>O, 400 MHz) of the reaction between iron, sulfur and KCN in H<sub>2</sub>O and D<sub>2</sub>O at pH 4 and 9. The H<sub>2</sub>O signal was removed for clarity.

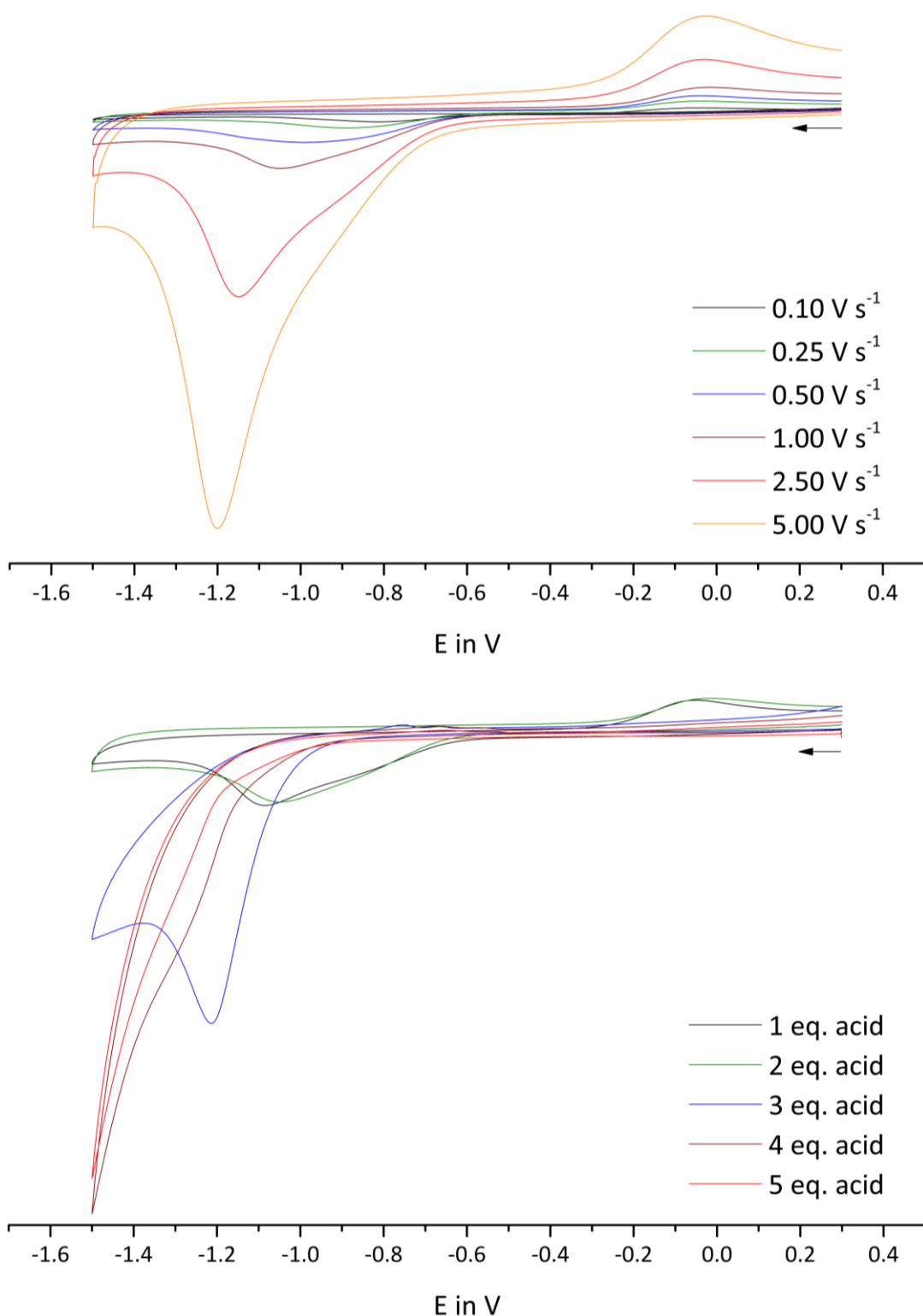


**Figure 22** CV diagrams of an aqueous solution derived from the reaction between iron, sulfur and KCN at 80 °C at different scan rates (**top**) and after the subsequent addition of acid (**bottom**), in the presence of 1 M [*n*-Bu<sub>4</sub>N][PF<sub>6</sub>]. The arrow indicates the scan direction. The potential E is referenced to the Fc<sup>+</sup>/Fc couple.

The electrochemical properties of the green solution were investigated by cyclic voltammetry. The sample was measured at pH 9 against an Ag/AgCl electrode and found to exhibit a cathodic peak potential at -1.2 V (A1) when a scan rate of 0.1 V was applied (Figure 23). After the current was reversed at -1.6 V, a corresponding anodic peak potential formed at -0.04 V (C1). When the scan rate was increased, the cathodic peak shifted towards more negative potentials while the C1 remained unchanged. The criterion for a reversible process is given by equation 1.<sup>[214]</sup> In this case the  $\Delta E$  was found to range between 0.76 V and 1.15 V and can therefore be classified as an irreversible process. This furthermore aligns well with the increasing ratio between the anodic peak current ( $I_{pa}$ ) and the cathodic peak current ( $I_{pc}$ ) with faster scan rates (Figure A 37). For a reversible or quasi-reversible process both peak currents should provide a ratio of 1, which needs to be independent from the scan rate or concentration. The anodic peak potential for the  $Fe^{2+}/Fe^{3+}$  couple was reported to appear at 0.4 V and the one for the  $[Fe(CN)_6]^{3-}/[Fe(CN)_6]^{4-}$  at 0.3 V. As no further anodic signals were observed besides A1, the here produced sample mostly contains  $Fe^{2+}$ .

$$\Delta E = E_{pa} - E_{pc} = \frac{0.057}{n} \text{ V} \quad (\text{eq 1})$$

The sample was further investigated due to its behavior upon the addition of different equivalents of HCl. After the addition of 1 equivalent of acid, a similar cyclic voltammogram compared to the one at pH 9 was collected. The first equivalent of acid probably was consumed to neutralize the solution with an initial pH of 9. Upon addition of another equivalent in HCl A1 was further shifted towards a more negative potential of -1.2 V. When the current was reversed, two newly formed peaks, C2 and C3, appeared at -0.75 V and -0.66 V, respectively, while C1 completely vanished. After the addition of 4 and 5 eq. the A1 peak was only observed in form of a faint shoulder at even higher potentials. The corresponding C2 and C3 peaks were in both cases slightly shifted towards higher potentials of -0.67 V/-0.57 V and -0.65 V/-0.54 V, respectively.

The reaction between iron, sulfur and KCN at pH > 7 did not show full conversion as especially metallic iron remained even after 5 d at 80 °C. When the aqueous phase was removed either by a rotation evaporator or under a stream of  $N_2$ , a white and yellow

solid was received. The yellow solid was insoluble in H<sub>2</sub>O and therefore assumed to be recrystallized sulfur. The white solid was soluble and gave a red colored solution upon addition of Fe<sup>3+</sup> ions. The red color thereby was assigned to the formation of Fe(SCN)<sub>3</sub>. The formation of SCN<sup>-</sup> from S<sub>8</sub> is well known to already proceed under ambient conditions. The CN<sup>-</sup> supports the ring-opening reaction where a S – S bond is broken and a CN<sup>-</sup> end-group is formed. In presence of a second CN<sup>-</sup> molecule the sulfide chain gets further cut and NCS<sup>-</sup> or NCS<sub>2</sub><sup>-</sup> are released. When the initial amount of iron was reduced, the aqueous phase did not change in color. When the iron sulfur mixture was supplied in dearth, mackinawite was formed, but again no color change was observed. Overall, no initial ratio was found where the green color formed and simultaneously all the starting material was consumed.

Once dried, the green solid remained insoluble in H<sub>2</sub>O and organic solvents like alcohols, acetone, DMC, or toluene. When the pH was lowered, the solid was dissolved under formation of H<sub>2</sub>S, identified by its typical odor. At higher pH, the solution turned faintly green, but only small amounts were dissolved, even under elevated temperatures or when ultrasound was applied. Therefore, it was not possible to produce samples of known concentrations.

### **Cyclic sulfur compounds**

When samples containing 56 mg iron, 32 mg sulfur and 65 mg KCN were heated at pH 9 for 5 d and only acidified after the reaction finished (GP-05-01, GP-05-02 and GP-05-03), a range of reduced organic compounds formed in the gas phase of the vials. A representative chromatogram is shown in Figure 23 The reaction products have been identified by GCMS head space analysis. The observed mass patterns could, however, only partly be identified by comparison to the NIST 14 database. Some of the compounds were not listed and therefore had to be identified by evaluating the fragmentation pattern and the isotopic shifts by comparing reactions containing K<sup>12</sup>CN (GP-05-02) and Na<sup>13</sup>CN (GP-05-03).

In total 17 different compounds were observed in the gas phase of GP-05-02. When Na<sup>13</sup>CN was used, the respective mass shifts of +1 for CH<sub>3</sub>SH, CS<sub>2</sub>, CH<sub>3</sub>S<sub>2</sub>H, CH<sub>2</sub>S<sub>4</sub>, CH<sub>2</sub>S<sub>5</sub> and CH<sub>2</sub>S<sub>6</sub>, of +2 for C<sub>2</sub>H<sub>6</sub>S (x2), C<sub>2</sub>H<sub>6</sub>S<sub>2</sub>, C<sub>2</sub>H<sub>4</sub>S<sub>3</sub>, C<sub>2</sub>H<sub>4</sub>S<sub>4</sub>, C<sub>2</sub>H<sub>4</sub>S<sub>5</sub>, of +3 for C<sub>3</sub>H<sub>7</sub>SH, C<sub>3</sub>H<sub>9</sub>S<sub>2</sub>,

$C_3H_6S_3$  and  $C_3H_6S_4$  were observed (Figure A 50 – 61). When the collected mass patterns of the respective signals were compared with the ones in the library, nine of them could directly be identified as methanethiol ( $CH_3SH$ , **60**), ethanethiol ( $C_2H_5SH$ , **61**), dimethylsulfide ( $C_2H_6S$ , **62**), carbon disulfide ( $CS_2$ , **63**), 1-propanethiol ( $C_3H_7SH$ , **65**), 1,2,4-trithiolane ( $C_2H_4S_3$ , **70**), 1,2,4,5-tetrathiane ( $C_2H_4S_4$ , **73**), 1,2,4,6-tetrathiepane ( $C_3H_6S_4$ , **75**) and hexathiepane ( $CH_2S_6$ , **77**). The remaining eight compounds, identified by their mass pattern and or isotopic shifts, were dihydrogen disulfide ( $H_2S_2$ , **64**), methyldisulfide ( $CH_3S_2H$ , **66**), (methylthio)methanethiol ( $C_2H_6S_2$ , **67**), 2-thia-butane-1-thiol ( $C_3H_8S_2$ , **69**), 1,2,4-trithiane ( $C_3H_6S_3$ , **71**), tetrathiolane ( $CH_2S_4$ , **72**), pentathiane ( $CH_2S_5$ , **74**) and 1,2,3,5,6-pentathiepane ( $C_2H_4S_5$ , **76**).

When the aqueous solution of GP-06 with the same composition is extracted with cyclohexane ( $C_6H_{12}$ ), furthermore (methylsulfaneyl)methanethiol ( $C_2H_6S_3$ , **78**), 2-(ethylsulfaneyl)ethane-1-thiol ( $C_3H_8S_3$ , **79**), 1,2,5-trithiepane ( $C_4H_8S_3$ , **80**), 3-ethyl-5-methyl-1,2,4-trithiolane ( $C_5H_{10}S_3$ , **81**) and 1,3,5,7-tetrathiocane ( $C_4H_8S_4$ , **82**) were identified (Figure 24). The NIST 14 library only contained the mass pattern of **82** with a similarity of 77 %. As for GP-05 the remaining compounds were identified by evaluating the mass patterns of the compounds detected in reactions containing isotopically

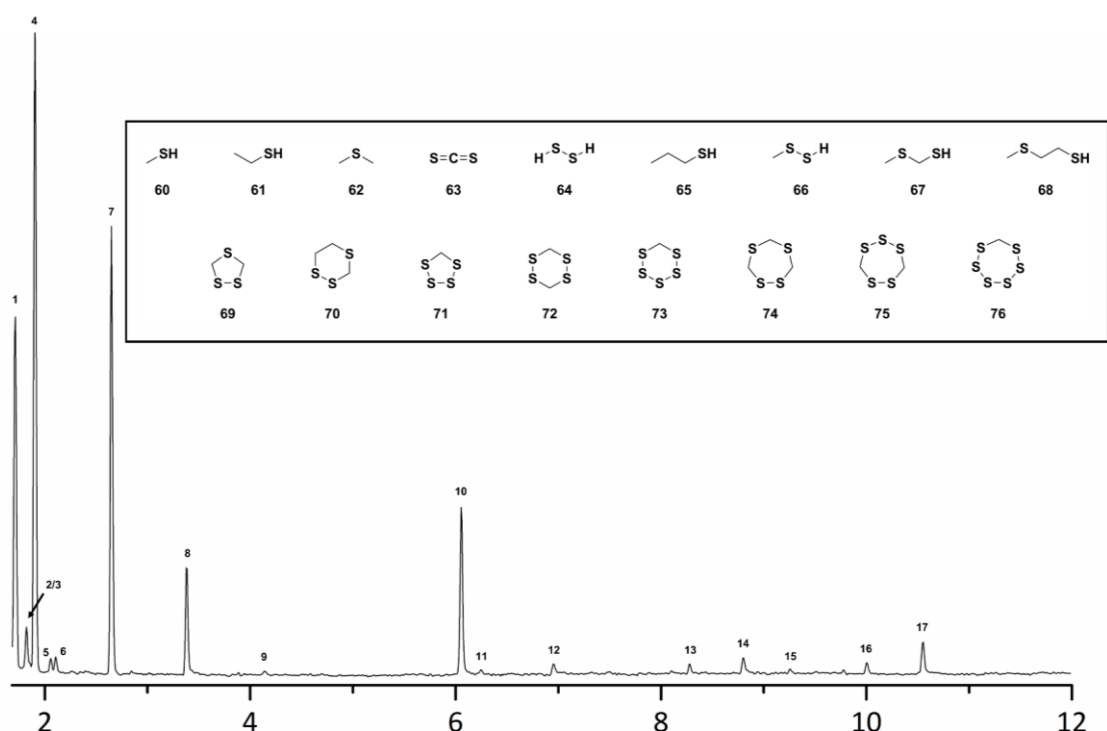


**Figure 23** Gas chromatogram (TIC) of GP-05-02.

labeled substrate and gave the expected mass shifts of +2 for C<sub>2</sub>H<sub>6</sub>S<sub>3</sub>, of +3 for C<sub>3</sub>H<sub>8</sub>S<sub>3</sub>, of +4 for C<sub>4</sub>H<sub>8</sub>S<sub>3</sub> and C<sub>4</sub>H<sub>8</sub>S<sub>4</sub>, and of +5 for C<sub>5</sub>H<sub>10</sub>S<sub>3</sub>.

The formation of hydrocarbons from CN<sup>-</sup> is known to readily proceed in the presence of nitrogenases and their extracted/synthetic cofactors. Rittle et al. were able to give a more detailed description on this process by investigating the Fe-CN complex [SiP<sup>Pr</sup><sub>3</sub>]Fe(CN) and derivatives in the presence of protons and electrons.<sup>[208]</sup> While the exact formation mechanism for CH<sub>4</sub> and NH<sub>3</sub> is still unclear, they could isolate iron complexes containing (CNH) and (CNH<sub>2</sub>) residues as intermediates of the proton coupled reduction. Based on the here observed array of products from the reaction between iron and KCN at pH 2 - 6, we assume a similar formation mechanism being enabled by the different iron surface sites. In contrast to the previously described examples on CN<sup>-</sup> reduction, however, no additional electron donor is applied.

Reaction 25 is known to consist of multiple steps where OH<sup>-</sup> ions first appear as surface groups, before soluble Fe complexes are formed.<sup>[209]</sup> Though, experimental evidence is still missing, similar Fe-(CN) complexes are likely to be present during reaction 26. The first stage of this process leads to the formation of a Fe-(CN)<sub>(ads)</sub> unit, similar to the

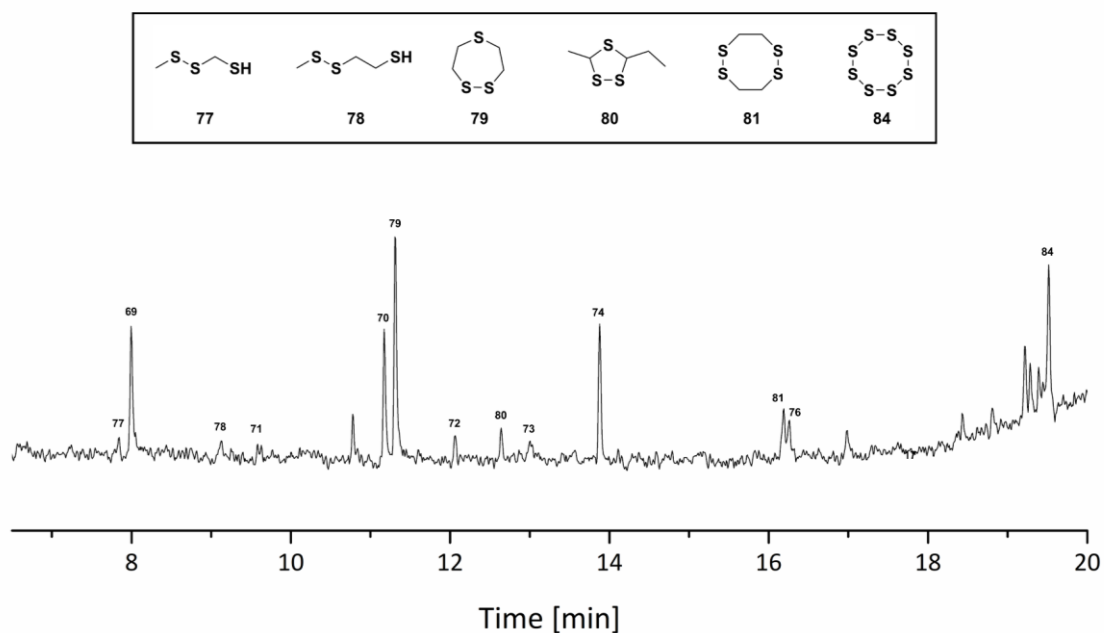
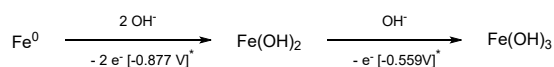


**Figure 24** Gas chromatogram (TIC) collected from the cyclohexane extract of the aqueous phase of GP-06.

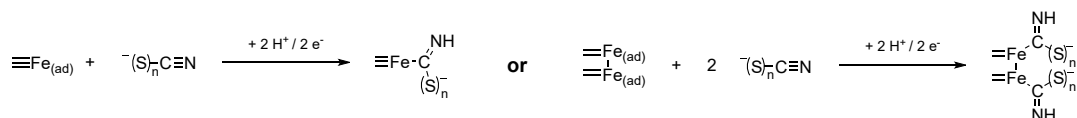
molecular pendant,  $[\text{SiP}^{\text{iPr}}_3]\text{Fe}(\text{CN})$ . As iron is an electric conductor, electrons are easily supplied by the bulk of the particles to the surface atoms where the N atom can be released as  $\text{NH}_3$ .

The aliphatic and cyclic organosulfur compounds only form when the samples were reacted at  $\text{pH} > 9$  and worked up with acid, afterwards. Under this condition the concentration in  $\text{HCN}$  is low and  $\text{CN}^-$  can first react with  $\text{S}^0$  to form polysulfides and  $\text{S}_n\text{CN}^-$  (reaction 32).<sup>[215,216]</sup> The  $\text{S}_n\text{CN}^-$  molecule, similar to the  $\text{CN}^-$ , can coordinate onto the surface iron atoms by forming a  $(\text{CNHS}_n^-)$  residue (Figure 25). In contrast to the  $\text{CN}^-$  reduction by iron, the attached polysulfide chain can undergo cyclization to form the deprotonated precursors for the cyclic  $\text{C}_1$  compounds **71**, **73** and **77**. In the case of a nucleophilic attack of an end-standing sulfide group from the adjacently bound thiocyanide residue a similar effect, leading to the more favorable scission of the primary C – N bond, can be expected.

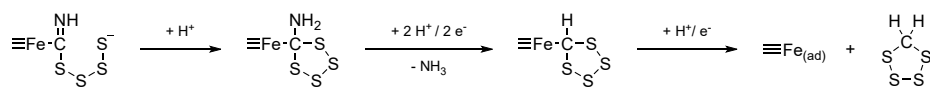
#### Electron source



#### Surface bonding



#### Tetrathiolane



#### Trithiolane

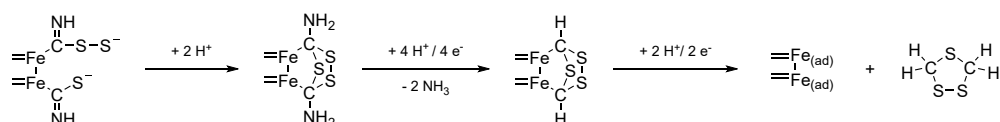
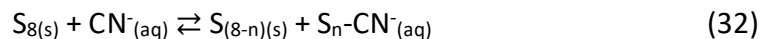


**Figure 25** Proposed mechanism for the formation of cyclic species from the reaction between iron, sulfur and KCN at 80 °C. \*The standard potentials for the oxidation of iron were measured against SHE.<sup>[92]</sup>



With shorter polysulfide chains ( $n < 4$ ), cyclization is restricted due to the elevating ring strain. The cyclic  $S_2 - S_4$  membered rings therefore most likely appear due to the reaction of two neighboring  $(CNHS_n^-)$  residue as it is displayed for **69** in Figure 25. The formation of the compounds **72** and **76** is proposed to occur similarly by the reaction of two  $S_2CN^-$  or a  $S_3CN^-$  and  $S_2CN^-$  species, respectively. Following this approach, the cyclic  $C_3$  compounds **71** and **75** are formed by the reaction of three residues attached to three different  $Fe^0$  surface atoms.

#### 4.2.2.3 Mackinawite

To investigate the reduction of KCN with mackinawite, we conducted experiments using the iron sulfide/acid system, previously reported by Heinen and coworkers.<sup>[9]</sup> In contrast to their approach, we used freshly prepared mackinawite nanoparticles, obtained by the reaction between iron and sulfur in aqueous solution. The reductive properties of mackinawite can here further be supported, as reduced organosulfur species were formed during our experiments already at room temperature.

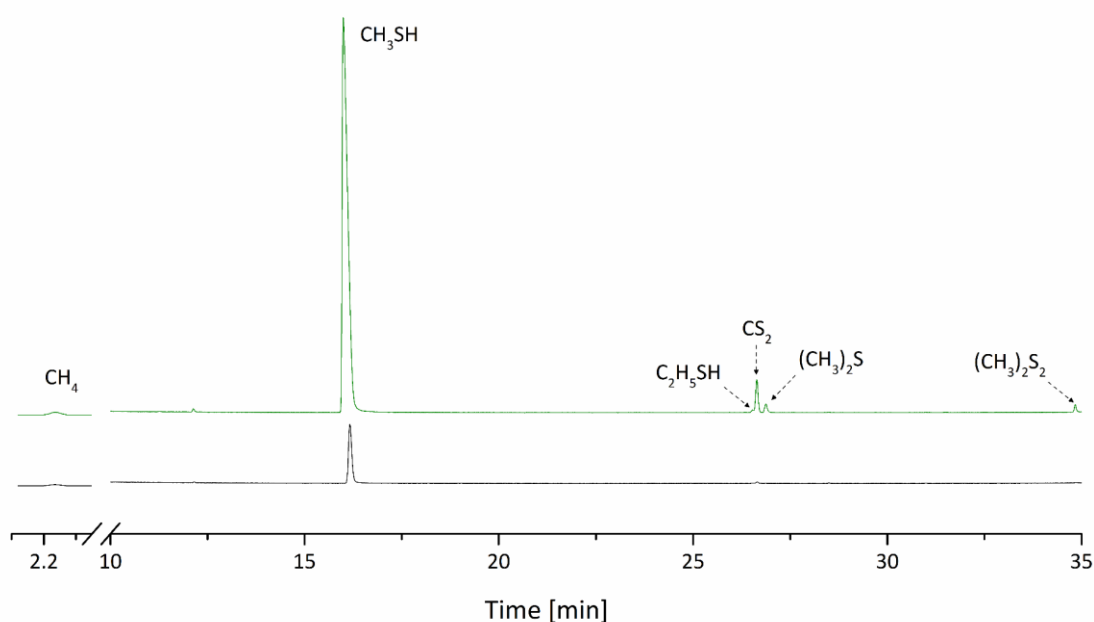
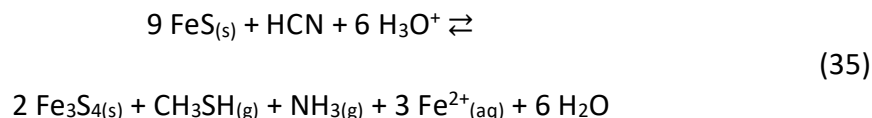
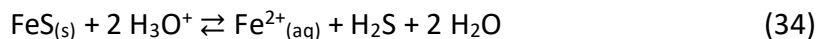


**Figure 26** Gas chromatograms (TIC) collected from the gas phases of GP-07-01 (black, r.t.) and GP-07-02 (green, 80 °C).





An excess of mackinawite selectively leads to the formation of  $\text{CH}_4$  and  $\text{CH}_3\text{SH}$ , accompanied by small amounts of  $\text{CS}_2$ , as well as traces of  $\text{C}_2\text{H}_5\text{SH}$ ,  $(\text{CH}_3)_2\text{S}$  and  $(\text{CH}_3)_2\text{S}_2$  at room temperature (GP-07-01). In Figure 26 the gas chromatogram collected from the gas phase of GP-07-01 and a sample that was heated to  $80^\circ\text{C}$  (GP-07-02), both containing 10 mmol mackinawite and 1 mmol of each, KCN and  $\text{H}_2\text{SO}_4$ , are shown. The headspace analysis gives a relative composition of 0.74 %  $\text{CH}_4$ , 97.90 %  $\text{CH}_3\text{SH}$ , 0.03 %  $\text{C}_2\text{H}_5\text{SH}$ , 1.15 %  $\text{CS}_2$ , 0.02 %  $(\text{CH}_3)_2\text{S}$  and 0.07 %  $(\text{CH}_3)_2\text{S}_2$  for GP-07-01 and one of 0.15 %  $\text{CH}_4$ , 94.50 %  $\text{CH}_3\text{SH}$ , 0.23 %  $\text{C}_2\text{H}_5\text{SH}$ , 3.44 %  $\text{CS}_2$ , 0.94 %  $(\text{CH}_3)_2\text{S}$  and 0.59 %  $(\text{CH}_3)_2\text{S}_2$  for GP-07-02. The total concentration in  $\text{CH}_3\text{SH}$  was estimated by an external calibration curve and found to increase from 0.01 mmol to 0.11 mmol and therefore gives a total yield of

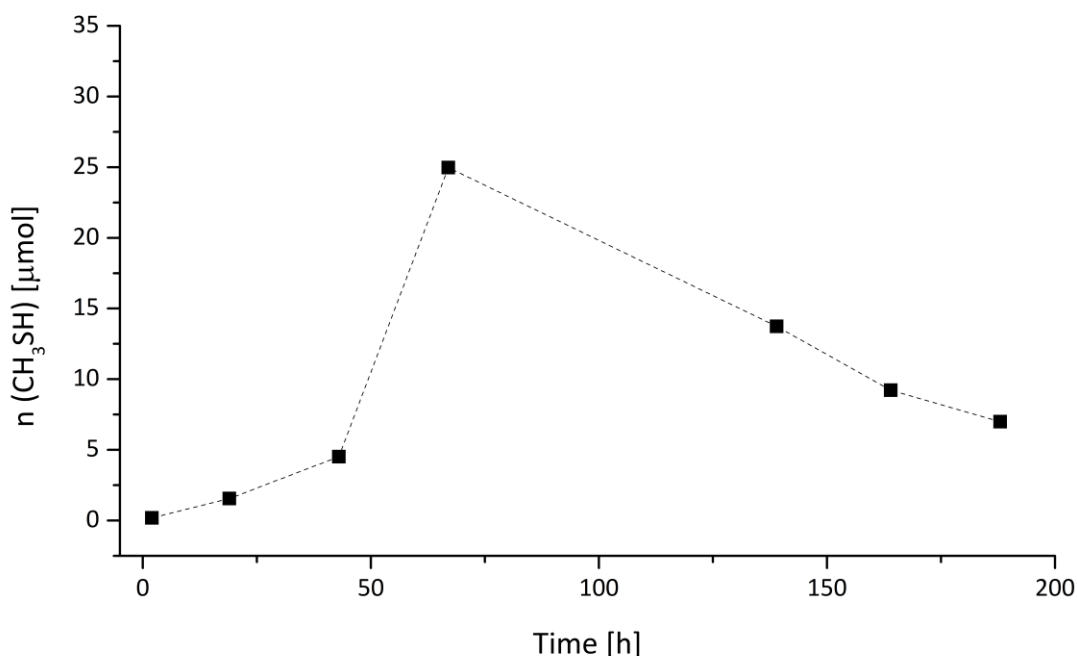


**Figure 27** Course of the  $\text{CH}_3\text{SH}$  concentration in the headspace of samples heated for different reaction times (GP-10). Calibrated with CAL-MT-5.

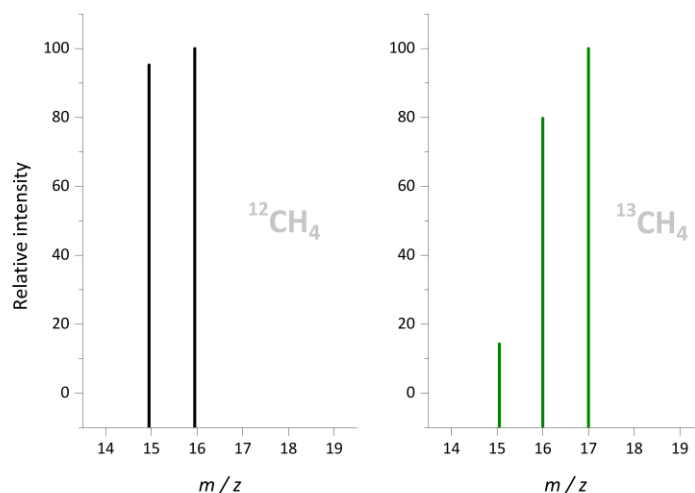


**Figure 28** Comparison of the mass patterns of the CH<sub>4</sub> signals gathered from the reaction with K<sup>12</sup>CN (black) and Na<sup>13</sup>CN (green).

~ 1 - 10 % compared to the initially introduced KCN. When the reaction was performed with Na<sup>13</sup>CN, the corresponding mass pattern of the CH<sub>4</sub> signal became fully shifted, providing a  $m/z = 17$  peak with a relative intensity of 100 %.

The rate of CH<sub>3</sub>SH formation was studied over a period of 188 h, whereas the gas phase was subsequently removed by a gas tight syringe. The course of the CH<sub>3</sub>SH concentration is shown in Figure 28. Like the one recorded for the reaction of the iron sulfur mixture, the CH<sub>3</sub>SH concentration was found to peak after 67 h and only decreased afterwards. In this sample 25.0 mmol of CH<sub>3</sub>SH were present which calculates to a yield of 2.5 %.

### **Influence of acid and secondary release**

It has already been reported by several groups, that organic compounds can be bound either to the pyrite or mackinawite surface, whereas lower concentrations in reduced species, e.g., methanethiol, are detected. The extraction method, where the transfer line is used, offers the possibility to completely remove the first gas phase. By this, the secondary release of reduced species was studied, whereas acid was again added after the gas phase was fully removed. In Figure 29 the collected gas chromatograms of the gas phase of samples containing 10 mmol mackinawite, 1 mmol KCN and 1 mmol H<sub>2</sub>SO<sub>4</sub> are displayed. The first one (black) shows the composition of the gas phase after the sample was heated at 80 °C for 5 d. The second chromatogram was collected from the same sample after a second equivalent of acid was added and the sample was only left

at 80 °C for 30 min. The sample thereby again provided a CH<sub>3</sub>SH signal even though most of the gaseous compounds should have been removed during the first extraction.

This series, in total, included five samples containing different equivalents of H<sub>2</sub>SO<sub>4</sub>. In Figure 30 the calculated areas for CH<sub>4</sub>, H<sub>2</sub>S, CH<sub>3</sub>SH and CS<sub>2</sub> are illustrated. In addition to these compounds furthermore (CH<sub>3</sub>)<sub>2</sub>S and (CH<sub>3</sub>)<sub>2</sub>S<sub>2</sub> were observed during the first extraction but were not present after the second one. In the absence of acid only small amounts of CH<sub>4</sub> were formed. As for the other three compounds the TIC area, however, significantly increased upon the addition of 0.5 mL of H<sub>2</sub>SO<sub>4</sub>. The maximum amount of CH<sub>4</sub> was present in the gas phase of the sample that contained equivalent amounts of acid and KCN, resulting in a proton:KCN ratio of 2. For CH<sub>3</sub>SH this was the case at a ratio of 1, while both CS<sub>2</sub> and H<sub>2</sub>S generally increased with more equivalents of acid. The collected gas chromatograms after the second extraction again contained reduced species, however, in lower concentrations. When the areas of the first and second extraction are summarized, the observed curve aligns well with the one of the first extraction. In contrast to CH<sub>3</sub>SH and H<sub>2</sub>S, CH<sub>4</sub> and CS<sub>2</sub> were already observed after the

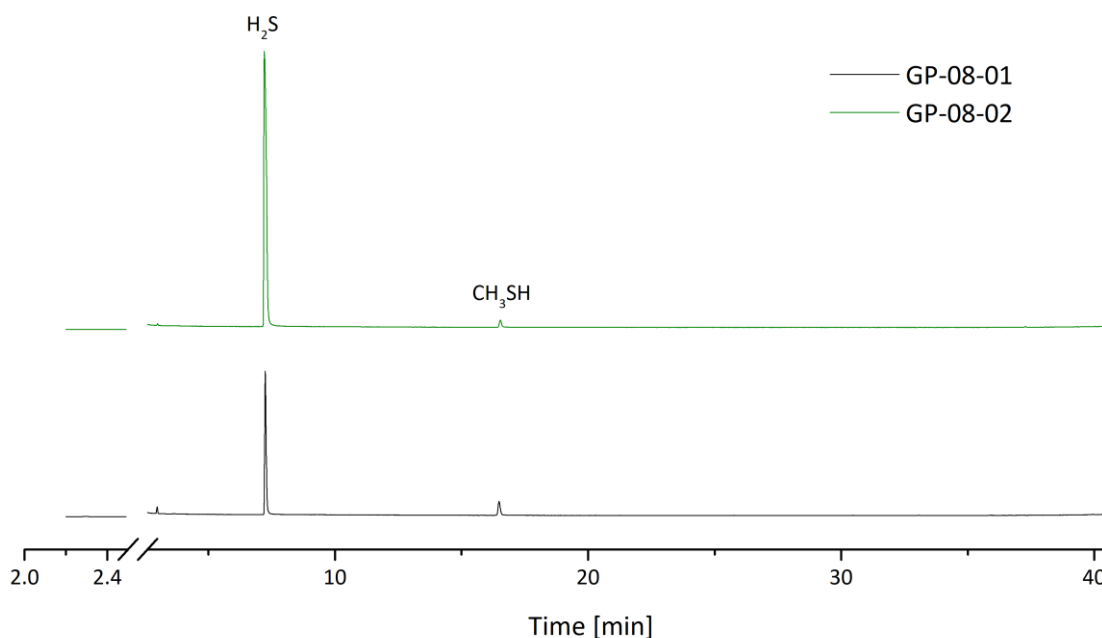


**Figure 29** Gas chromatogram (TIC) of the gas phase of GP-08-01 after the first (black) and second (green) release of reduced compounds. The gas phase was extracted using a transfer line and therefore emptied through the first extraction.

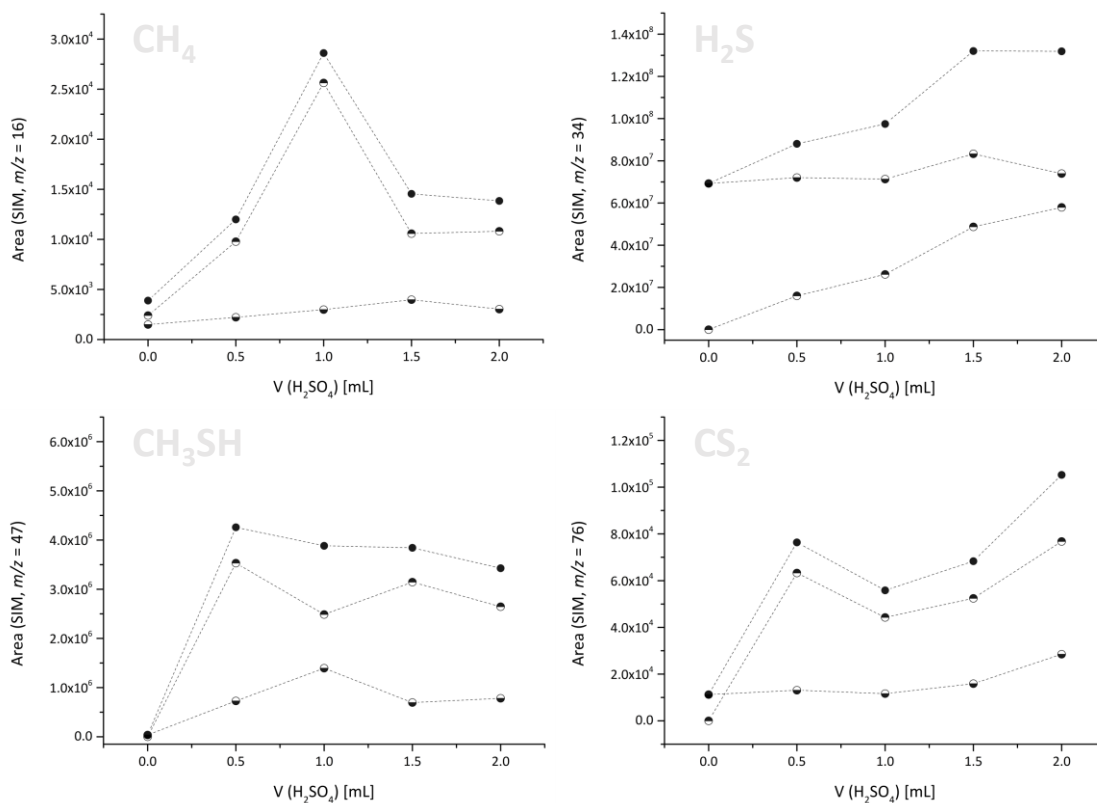


**Figure 30** Calculated areas (SIM) of CH<sub>4</sub>, H<sub>2</sub>S, CH<sub>3</sub>SH and CS<sub>2</sub> when different initial amounts of acid were added. The half-filled symbols account for the first (top filled) and second (bottom filled) extraction. Fully filled symbols illustrate the total amount after first and second extraction.

initially neutral samples were acidified before the gas phase sample was extracted for a second time.

### Limiting H<sub>2</sub>S

Following reaction 1, the protons are consumed upon the reaction with mackinawite to form H<sub>2</sub>S. This competitive reaction limits the availability of protons for the formation of the reduced compounds. The amount of H<sub>2</sub>S can be limited by simply not mixing the reactants. When samples are prepared where mackinawite remains compressed at the bottom of the vials, the same amount of acid only led to a moderate release of H<sub>2</sub>S, as the available mackinawite surface is limited. When such a sample is heated to 80 °C for 2 d, CH<sub>4</sub> (0.61 %), CH<sub>3</sub>CHO (6.31 %), CH<sub>3</sub>SH (1.25 %), C<sub>2</sub>H<sub>5</sub>OH (0.35 %), C<sub>2</sub>H<sub>5</sub>CHO (0.39 %), (CH<sub>3</sub>)<sub>2</sub>CO (0.87 %), CS<sub>2</sub> (20.06 %) and (CH<sub>3</sub>)<sub>2</sub>S<sub>2</sub> (69.18 %) are released into the sample headspace (Figure 31). The concentration in CH<sub>3</sub>SH, when compared to shaken samples,

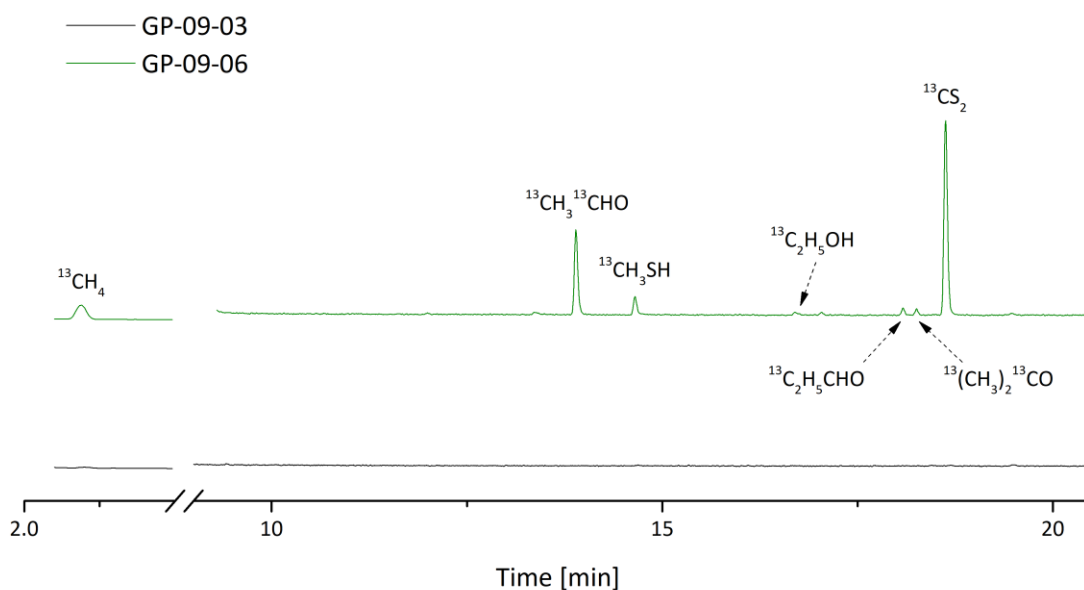


**Figure 31** Gas chromatogram obtained from GP-09-03 (black, without KCN) and GP-09-06 (green, with KCN) where the mackinawite was left compressed on the bottom of the sample vials.

was rather low. Furthermore, under such conditions no significant amounts of  $\text{C}_2 - \text{C}_4$  thiols were formed. The reaction products thereby provided the expected mass shifts of +1 for  $\text{CH}_4$ ,  $\text{CH}_3\text{SH}$  and  $\text{CS}_2$ , of +2 for  $\text{CH}_3\text{CHO}$  and  $\text{C}_2\text{H}_5\text{OH}$  and of +3 for  $\text{C}_2\text{H}_5\text{CHO}$  and  $(\text{CH}_3)_2\text{CO}$  when  $\text{Na}^{13}\text{CN}$  was used (Figure 32).

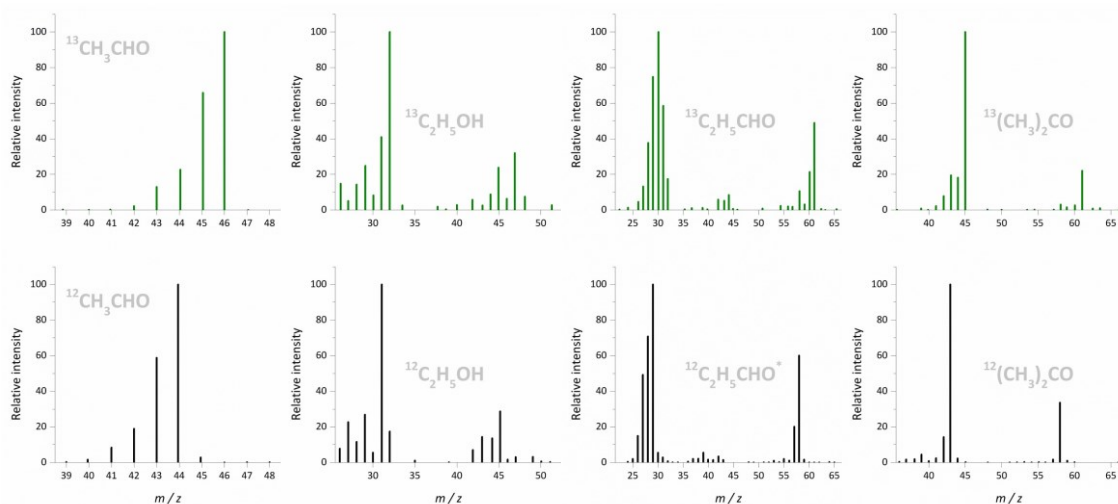


**Figure 32** Collected mass patterns for the oxygenated species. All compounds showed the expected mass shift when  $\text{Na}^{13}\text{CN}$  (green pattern) was used.

The oxygenated species were already observed in gas phases of earlier samples containing mackinawite but could not be clearly identified by their carbon shift. The limitation in H<sub>2</sub>S is hereby highly beneficial for their formation. This is reasonable as H<sub>2</sub>S is more acidic than H<sub>2</sub>O, whereas HS<sup>-</sup> would be more abundant than OH<sup>-</sup> to react with the intermediately formed carbon compounds under the applied conditions. When one of the samples (GP-09-06) was further acidified and boiled for 2 d, CH<sub>3</sub>SH became the main component in the gas phase with a relative abundance of 61.14 % while CH<sub>3</sub>CHO was only present by 0.38 % (Table 6).

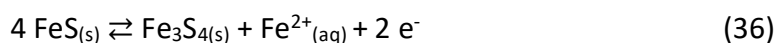
When GP-09-05 was further acidified and heated at 80 °C for the same time, a very similar gas phase composition like after the second extraction was observed. The relative abundance of CH<sub>3</sub>SH increased in respect to the one of CH<sub>3</sub>CHO. After the second extraction the CH<sub>3</sub>SH:CH<sub>3</sub>CHO ratio was found to be 0.2 after the second extraction and 0.5 after the third extraction. The subsequent addition of acid led to a more favored formation of H<sub>2</sub>S and therefore also in the product ratio.

**Table 6** Relative abundancies of CH<sub>3</sub>CHO and CH<sub>3</sub>SH after subsequent gas phase extraction and acidification at 80 °C and after boiling. Calibrated with CAL-MT-2. **E2** = Second Extraction, **E3** = Third Extraction.

ID	T [°C]	E2		E3	
		CH <sub>3</sub> CHO	CH <sub>3</sub> SH	CH <sub>3</sub> CHO	CH <sub>3</sub> SH
GP-09-03	80	-	-	-	-
GP-09-05		6.31 %	1.25 %	10.54 %	5.17 %
GP-09-04	100	-	6.02 %*	-	2.96 %*
GP-09-06		5.04 %	1.00 %	0.38 %	61.14 %

## Formation of greigite

During the reduction experiments, the mackinawite partly reacted to give greigite. Most of the previous studies reported the formation of pyrite as the major reaction product. In our experiments, however, no reflexes belonging to pyrite were observed by powder X-ray diffraction (PXRD). Greigite has recently been shown to be formed as an intermediate phase during the solid-state transformation of mackinawite into pyrite.<sup>[217,218]</sup> The formation of greigite from mackinawite itself has already been studied and was found to proceed under elevated temperatures or by contact with O<sub>2</sub> at room temperature.<sup>[188,219]</sup> Greigite is a mixed valent iron sulfide containing two Fe<sup>3+</sup> ions and one Fe<sup>2+</sup> ion per unit. Following reaction 36, the formation of greigite therefore provides 2 electrons:



In anoxic solution, mackinawite particles are known to remain stable even after weeks when the reaction is followed by PXRD.<sup>[88]</sup> Boursiquot et al. found, that the mackinawite structure can support up to 20 % in Fe<sup>3+</sup> ions, before the reaction into greigite occurs.<sup>[177]</sup> In respect to the generally low yields reported for mackinawite based carbon and nitrogen fixation reactions, such a high content in Fe<sup>3+</sup> would significantly reduce the

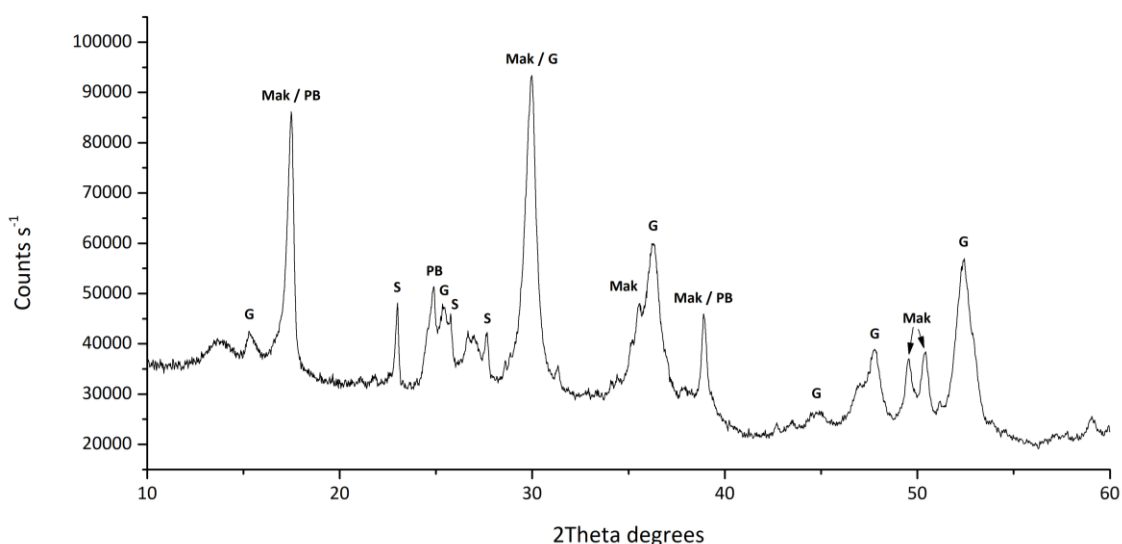


**Figure 33** PXRD pattern collected from the solid reaction product from the reaction between mackinawite and KCN at pH 3; Sulfur = S, Mackinawite = Mak, Greigite = G, Prussian blue = PB.

overall efficiency of the process. When mackinawite is precipitated from pure  $\text{FeCl}_2$  and  $\text{Na}_2\text{S}$  solutions, the Mössbauer spectrum can be well fit with a single singlet.<sup>[176]</sup> In the case of the mackinawite, formed by the here applied reaction between iron and sulfur, doublets did not appear, even after the filtrated product was deactivated by  $\text{O}_2$  from the air.

The PXRD pattern of the solid phase from the reaction of mackinawite and KCN at pH 3 (5 d at 80 °C, SP-FeS-08) is shown in Figure 33. In there, sulfur is only present in small amounts, whereas the mackinawite diffraction peaks nearly disappeared. In comparison with the literature, the remaining peaks can be identified as Prussian blue<sup>[220–222]</sup> and greigite<sup>[16,177,188,223]</sup>.

The Mössbauer spectrum of SP-FeS-08 (Figure 34) at 292 K can be well fitted using one sextet at  $St_1 = 0.58 \text{ mm s}^{-1}$  and two doublets at  $D_{1/2} = 0.35 \text{ mm s}^{-1}$ . These values, as well

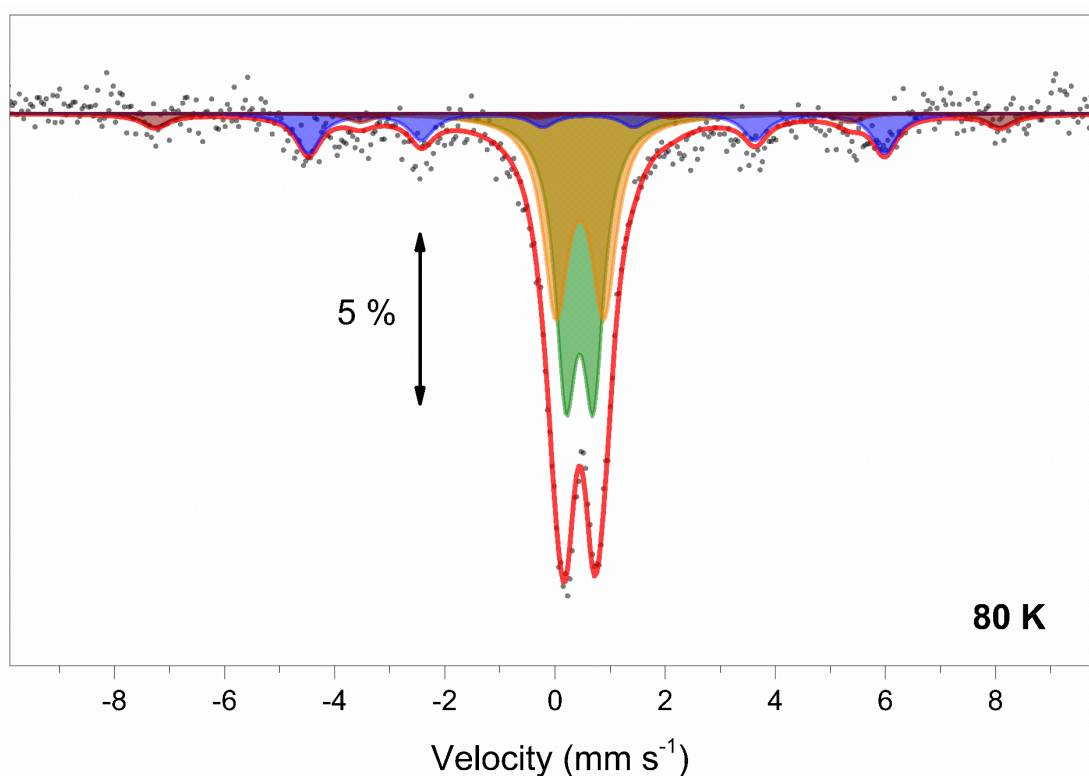


**Figure 34** Mössbauer spectrum of the solid reaction product from the reaction between mackinawite and KCN at pH 3. Green: First doublet ( $D_1$ ); Orange: Second doublet ( $D_2$ ), Blue: First sextet ( $St_1$ ), Red: Second sextet ( $St_2$ ). The spectrum was measured by M. Winkler.



as the one for the magnetic hyperfine field are comparable with the ones given by Lyubutin et al. for greigite of small particle sizes of approx. 9 nm. [224] At 80 K a second sextet at  $St_2 = 0.66 \text{ mm s}^{-1}$  appears and the remaining signals showed slightly increased isomer shifts. In contrast to pure greigite, the relative area of the doublets, compared to the sextets is slightly higher at both temperatures. The increased values can be explained due to the presence of Prussian blue giving a singlet and two doublets, but no sextet at comparable velocities. [220]

### 4.2.3 Reduction of KSCN and KOCN

#### 4.2.3.1 Iron

In the presence of iron, both potassium thiocyanate (KSCN) and potassium cyanate (KOCN) were found to be reduced into hydrocarbons at pH 2 after 3 d at 80 °C. Like during the reduction of KCN, C – C bond formation was observed, whereas C<sub>2</sub> to C<sub>5</sub> alkanes and alkenes were detected especially in the gas phase of the KOCN samples (GP-11-03, GP-11-06). The reduction of KSCN resulted in fewer hydrocarbons but provided a wider range of compounds like HCN and nitriles (GP-11-02, GP-11-05). In Figure 35 the calculated areas for the hydrocarbon evolution from KSCN and KOCN reduction is compared. The total areas gathered from EJ-PP-35/EJ-PP-39 and EJ-PP-37/EJ-PP-40 were thereby averaged.

When the reactions were carried out at pH 6, only small amounts in CH<sub>4</sub> (0.5 %) and C<sub>2</sub>H<sub>4</sub> (5.6 %) were observed GP-11-02, when compared to the areas calculated for GP-11-03 and -40. In the sample containing KOCN (GP-11-04), longer hydrocarbons with chain lengths up to 5 carbon atoms appeared. When KOCN was reacted at pH 6, again only small amounts of hydrocarbons were formed.

The products were identified by comparing their respective mass pattern to the ones available in the NIST 14 library. In all cases a high similarity of > 85 % with the library spectra was obtained. To further proof that the products are formed from the supplied substrate the reactions were additionally carried out with KS<sup>13</sup>CN and KO<sup>13</sup>CN. In the

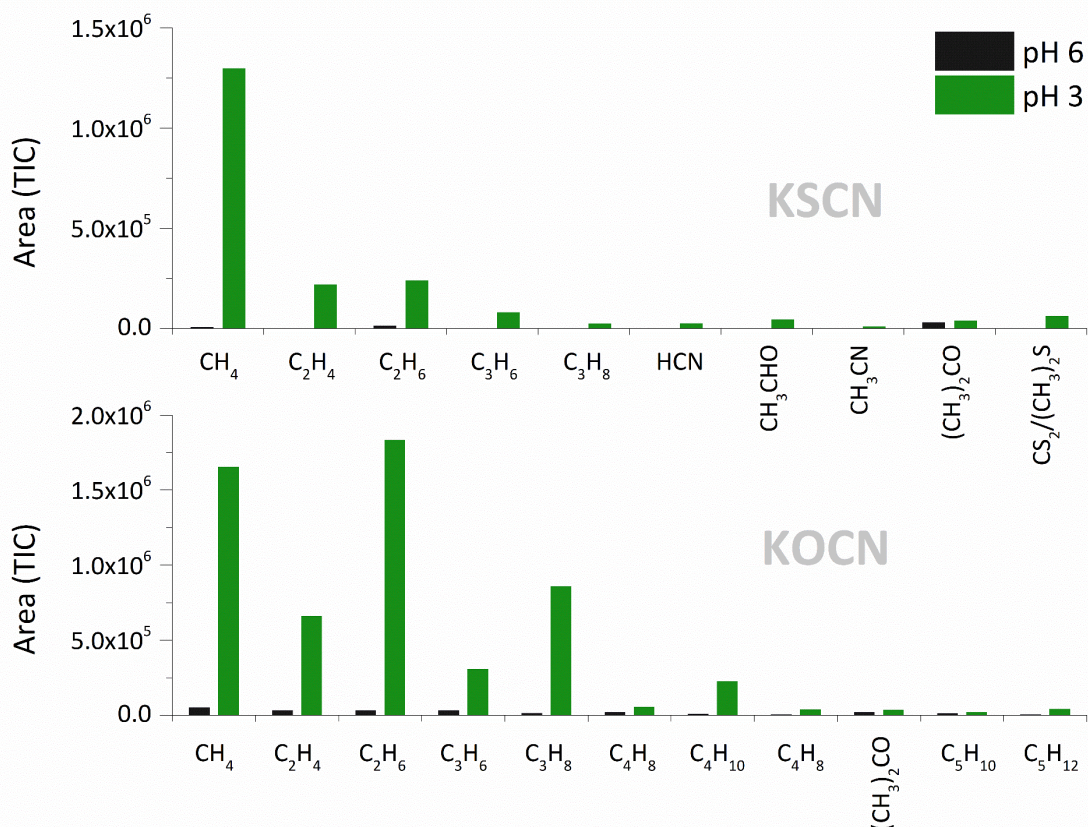


**Figure 35** Comparison of some products formed from the reduction of KOCN and KSCN by iron powder at pH 3 and pH 6.

case of  $\text{KS}^{13}\text{CN}$  (GP-11-05) all mass patterns showed the expected shift of +1 for  $\text{CH}_4$ , of +2 for  $\text{C}_2\text{H}_4$ ,  $\text{C}_2\text{H}_6$ ,  $\text{CH}_3\text{CHO}$ , acetonitrile ( $\text{CH}_3\text{CN}$ ) and  $(\text{CH}_3)_2\text{S}$ , and of +3 for  $\text{C}_3\text{H}_6$ ,  $\text{C}_3\text{H}_8$  and  $(\text{CH}_3)_2\text{CO}$ . The same was observed for the  $\text{KO}^{13}\text{CN}$  sample (GP-11-06) where the mass patterns showed the expected shift of +1 for  $\text{CH}_4$ , of +2 for  $\text{C}_2\text{H}_4$  and  $\text{C}_2\text{H}_6$ , of +3 for  $\text{C}_3\text{H}_6$ ,  $\text{C}_3\text{H}_8$  and  $(\text{CH}_3)_2\text{CO}$ , of +4 for  $\text{C}_4\text{H}_8$  and  $\text{C}_4\text{H}_{10}$ , and of +5 for  $\text{C}_5\text{H}_{10}$  and  $\text{C}_5\text{H}_{12}$ .

As reported for the reduction of KCN by iron the reduced species most likely are formed on the surface of the particles. The difference in the array of products for either KSCN or KOCN most likely follows from the high affinity between iron and sulfur. The gas phase of GP-11-05 contained HCN, which can be formed by the desulfurization of the  $\text{SCN}^-$  by the iron surface. A similar reaction was already shown to proceed in the presence of nitrogenase proteins purified from *Azotobacter vinelandii*. Seefeldt et al. further reported that the use of KOCN also leads to the formation of HCN.<sup>[225]</sup> Though, it was only observed in the gas phase of the KSCN samples, the formation of longer hydrocarbons in the KOCN samples could be a consequence of a fast consumption of

the intermediately formed HCN. The KSCN samples further contained CH<sub>3</sub>CHO and CH<sub>3</sub>CN which already were observed in the gas phase where KCN was reacted with **RS**<sub>1</sub>. This further implies that intermediately formed HCN is a key step for the formation of these products. As they furthermore are not observed during the reduction of KOCN by **RS**<sub>1</sub> an influence of sulfur cannot be ruled out.

#### 4.2.3.2 Iron sulfur mixture

In the presence of elemental sulfur both types of samples, containing either KSCN (GP-12-01) or KOCN (GP-12-02) at pH 3 lead to the formation of reduced compounds in the gas phase. At pH 7 no reaction products were observed. In the case of KSCN reduce species already appeared when samples were equipped with 0.5 mL of a 1 M H<sub>3</sub>PO<sub>4</sub>. After 5 d at 80 °C, CH<sub>4</sub>, H<sub>2</sub>S, HCN, CH<sub>3</sub>SH and CS<sub>2</sub> became detectable in the gas phase. The reduction of KOCN followed only after more acid was added to the respective

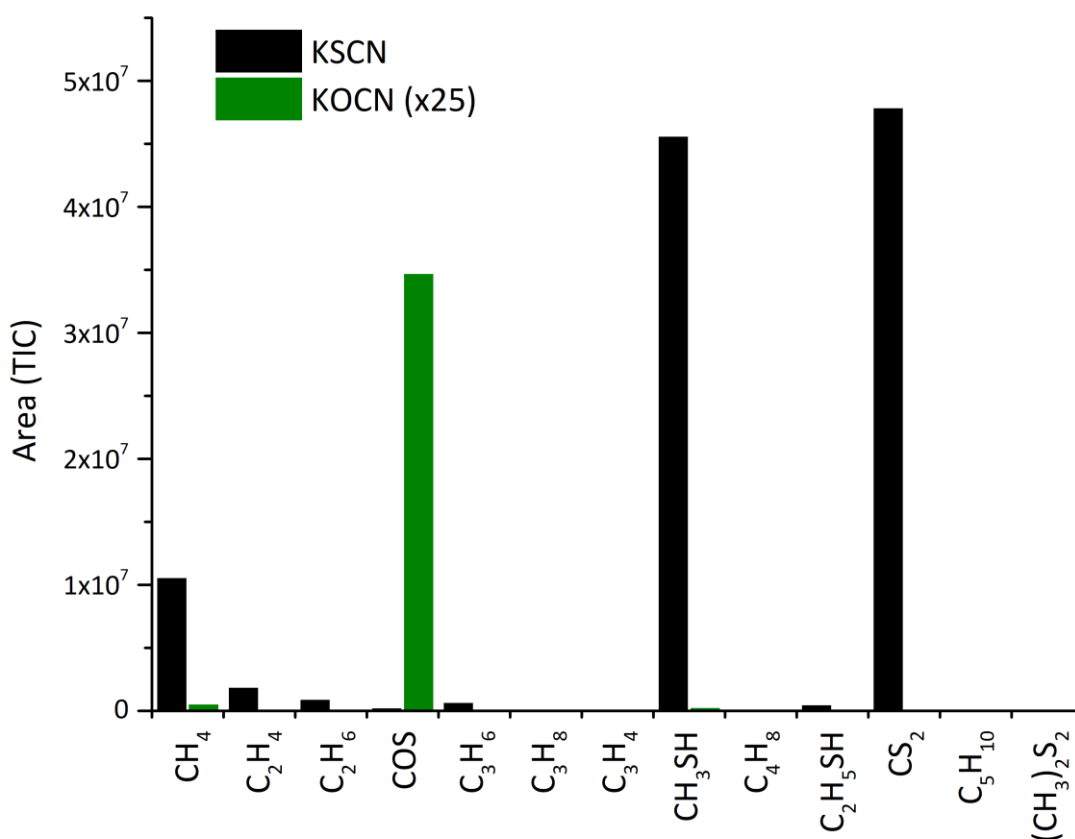


**Figure 36** Product distribution from the reduction of KOCN and KSCN by the iron sulfur mixture at pH 3.

samples. The detected levels in  $\text{CH}_3\text{SH}$ , however, remained low. In the KSCN samples the subsequent addition of acid led to increased levels in  $\text{CH}_3\text{SH}$ , but not  $\text{CH}_4$ .

In Figure 36 the calculated areas of the KSCN and KOCN samples are illustrated. When KSCN was used, a set of small hydrocarbons, including alkanes and alkenes were detected. In alignment to the reduction experiments where iron was used, the alkane/alkene ratio  $< 1$  has been determined. There, the presence of sulfur mainly led to the formation of  $\text{CH}_3\text{SH}$  and  $\text{CS}_2$ , whereas only small amounts in  $\text{C}_2\text{H}_5\text{SH}$  were detected. In the KOCN samples the sulfur was mainly transformed into COS, when the solid products like mackinawite are neglected.

#### 4.2.3.3 Mackinawite

When KSCN and KOCN were introduced as substrates, reaction products were observed in the gas phase when the samples were acidified and heated for different reaction times. In contrast to the reduction of KCN, the reaction of KSCN and KOCN more favorably led to the formation of  $\text{CS}_2$  and COS, respectively. In Figure 37 the gas chromatograms collected of the gas phase from a sample containing KSCN is compared with one containing KOCN. In addition to  $\text{CS}_2$  the KSCN sample produced  $\text{CH}_4$ , HCN and  $\text{CH}_3\text{SH}$  already after 3 d at  $80^\circ\text{C}$ . Like during the reaction with  $\text{RS}_2$ , reduced

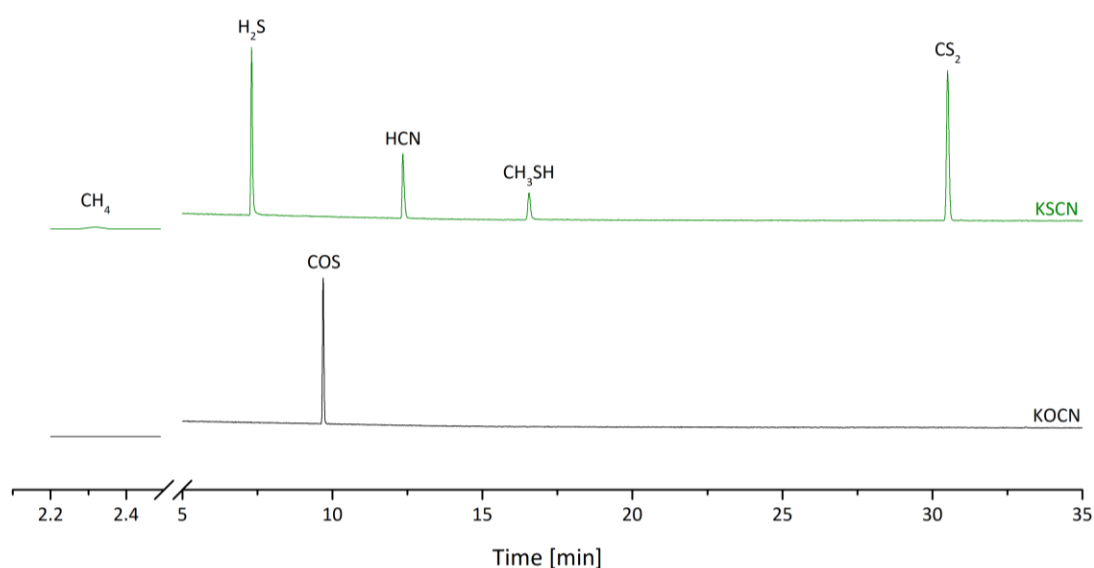


**Figure 37** Gas chromatogram (TIC) from the reduction of KOCN and KSCN by mackinawite at pH 3.

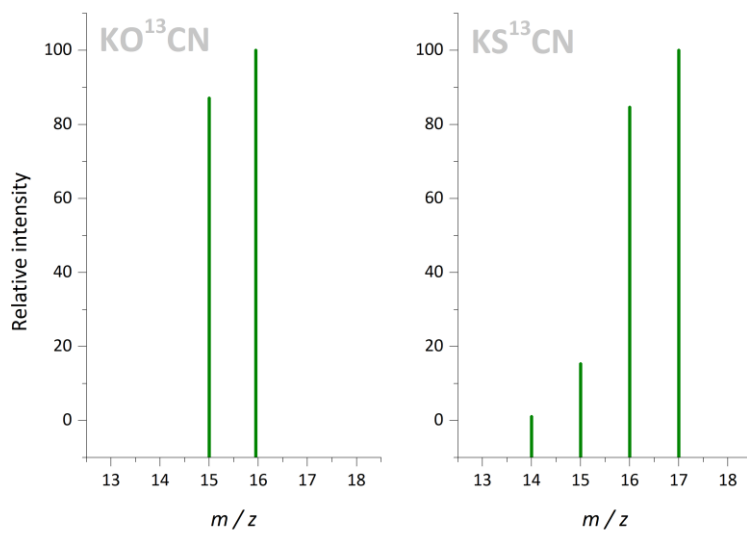


**Figure 39** Collected mass patterns of the  $\text{CH}_4$  signal from the reduction of  $\text{KO}^{13}\text{CN}$  and  $\text{KS}^{13}\text{CN}$ . Only the reduction of  $\text{KSCN}$  led to a  $m/z = 17$  signal.

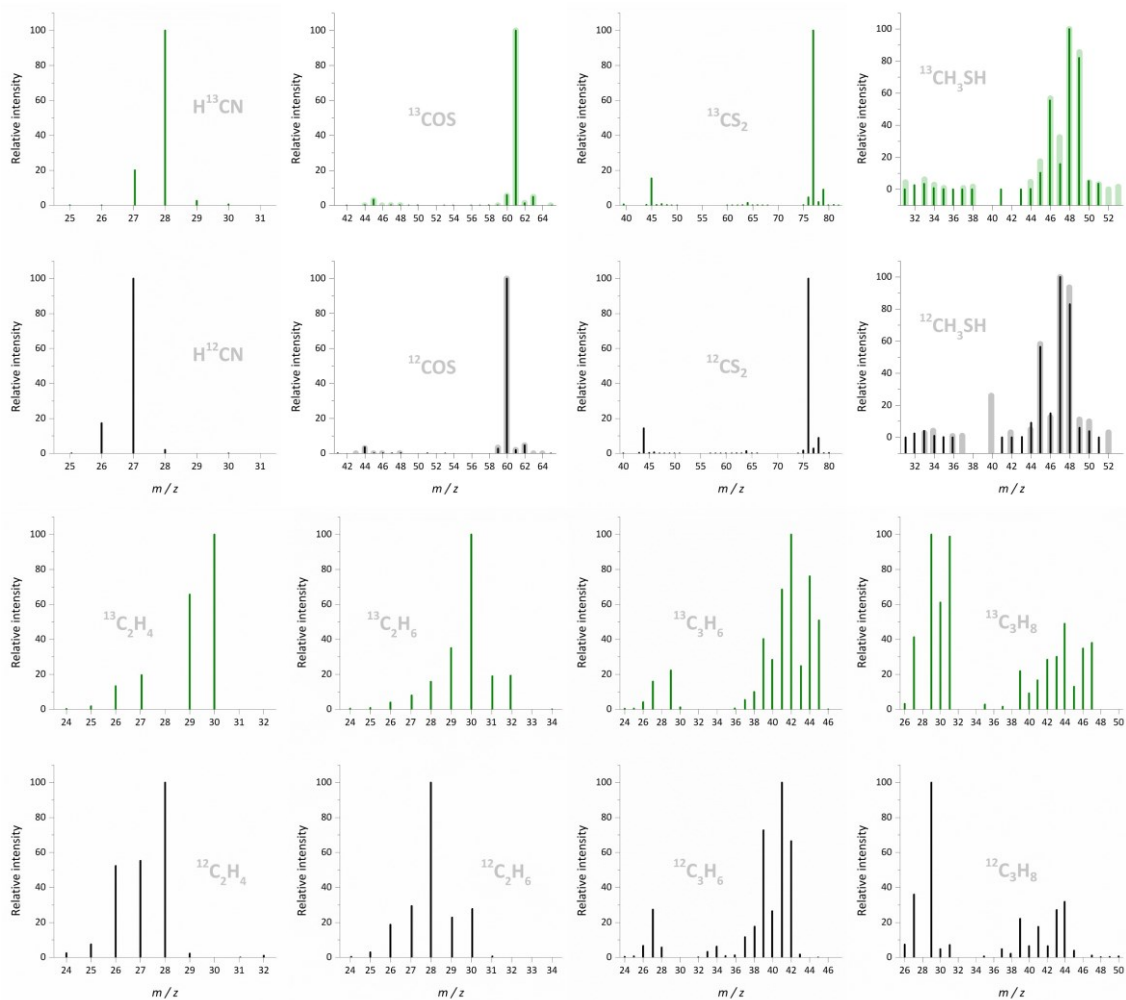


**Figure 39** Collected mass patterns of the reaction products from the reduction of  $\text{KS}^{13}\text{CN}$  (solid lines) and  $\text{KO}^{13}\text{CN}$  (opaque lines) by mackinawite at pH 3.

compounds were only formed in the KOCN samples when the pH was lowered by adding 1 mL of H<sub>3</sub>PO<sub>4</sub> (1 M).

The origin of the products from the respective substrates was confirmed in experiments where KS<sup>13</sup>CN (GP-13-01) and KO<sup>13</sup>CN (GP-13-02) were used. The gas phase of GP-13-01 showed the expected mass shift of +1 for CH<sub>4</sub> (rel. Abundance: 0.13 %), COS (0.51 %), HCN (0.05 %), CH<sub>3</sub>SH (81.68 %) and CS<sub>2</sub> (7.86 %). In GP-13-02 the gas phase contained COS (34.78 %), CH<sub>3</sub>SH (30.42 %) and CS<sub>2</sub> (19.40 %). With exception of the mass pattern of CH<sub>4</sub>, the remaining ones showed the expected shift of +1. The mass pattern of the CH<sub>4</sub> signal showed no *m/z* = 17 signal (Figure 38). Some of the CH<sub>4</sub> could thereby have been produced from carbon impurities with a lower ratio in <sup>13</sup>C. Interestingly, only the CH<sub>4</sub> signal showed a partly shifted mass pattern, whereas the mass patterns of other reaction products are not influenced and appear fully shifted (Figure 39).

In a separate experiment, both reactions were followed over a time frame of 188 h. The formation of COS from KOCN (GP-15) proceeded fast and only subsided after 2 h before starting to stagnate after 67 h (Figure 40). In the KSCN containing sample (GP-14) only

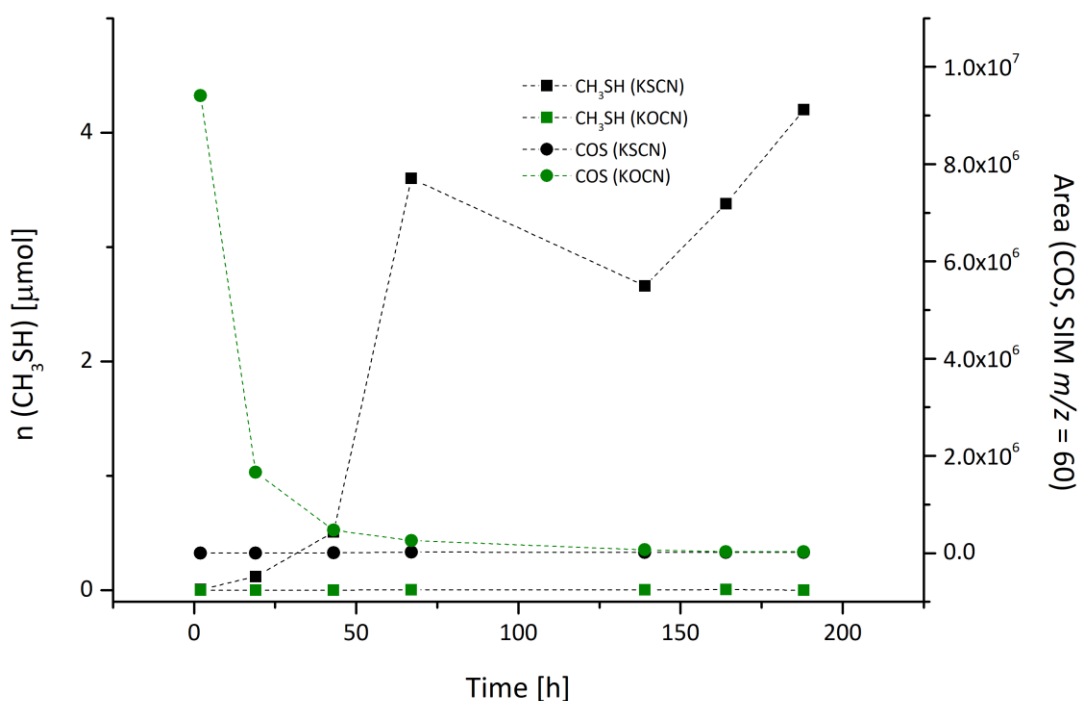


**Figure 40** Time dependent formation of CH<sub>3</sub>SH (squares) and COS (circles) from KSCN (black) and KOCN over a total time frame of 188 h.

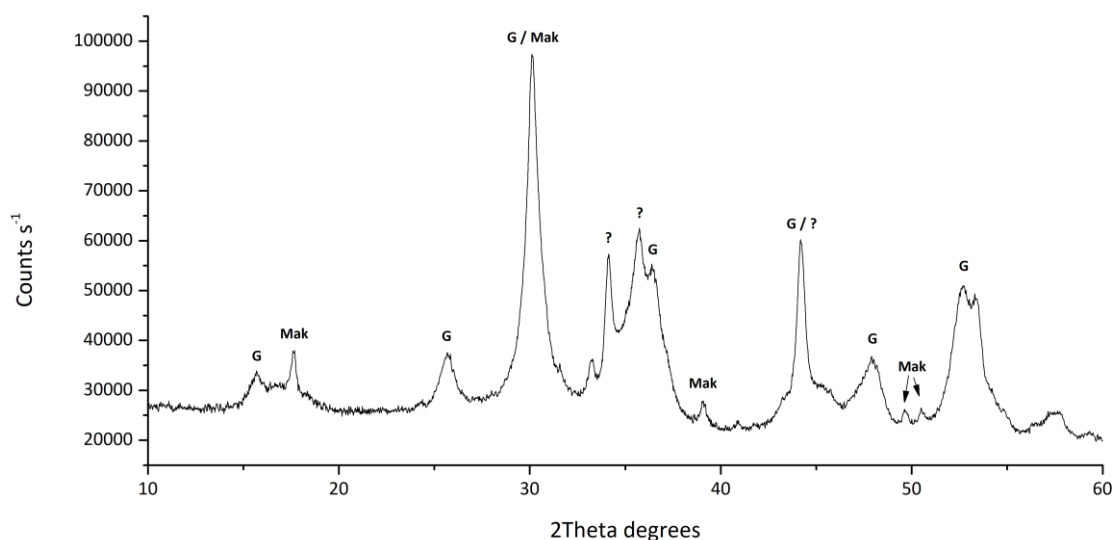


**Figure 41** Collected PXRD pattern (SP-FeS-09) of the solid residue from the reduction of KSCN by mackinawite at pH 3. Most of the reflexes could be assigned to greigite (G) and mackinawite (Mak) and an unknown compound (?).

small amounts of COS were formed, however, CH<sub>3</sub>SH was already detected after 2 h. The concentration further increased to 3.60 μmol after 67 h before first decreasing to 2.66 μmol after another 72 h, but again increasing to 4.20 μmol during the remaining reaction. The peak after 67 h is like the one observed during the reduction of KCN. The reduction of KOCN into CH<sub>3</sub>SH likewise peaked after 67 h, but only provided concentration of < 0.01 μmol.

The solid residue from the KOCN containing reaction could not be isolated as it readily reacted with air, even after being deactivated. This highly exothermic reaction led to the full oxidation of the filter cake even before the samples could be transferred outside the glass frit. The solid residue of the KSCN samples remained stable after the deactivation and could be further analyzed. The collected PXRD pattern is shown in Figure 41. The mackinawite reflexes only appear with low intensity, whereas mainly greigite reflexes were observed. A new set of signals was formed alongside the greigite but could not be further identified.

### **Influence of the acid**

The reduction of KSCN by mackinawite was shown to selectively lead to the formation of C<sub>1</sub> compounds like CH<sub>4</sub>, CH<sub>3</sub>SH and CS<sub>2</sub>. Such samples therefore provide a limited

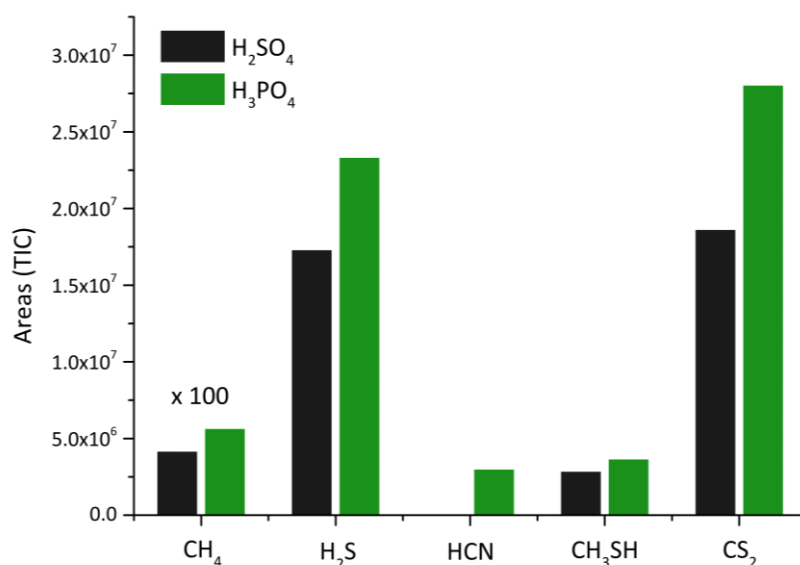


**Figure 42** Comparison of the calculated areas from the TIC for the respective reaction products from the reduction of KSCN by mackinawite. The areas of the CH<sub>4</sub> signal were enhanced.

number of processes and are well suited to investigate the influence of the used acids, H<sub>3</sub>PO<sub>4</sub> and H<sub>2</sub>SO<sub>4</sub>. HCl was not further investigated due to its corrosive properties. The calculated areas of the species present in the gas phase of the samples either containing H<sub>2</sub>SO<sub>4</sub> (GP-16-01 and GP-16-02) or H<sub>3</sub>PO<sub>4</sub> (GP-16-03 and GP-16-04), are shown in Figure 42. Both samples which contained H<sub>3</sub>PO<sub>4</sub> showed higher levels in both, the reduced species, as well as H<sub>2</sub>S and CS<sub>2</sub>.

The better efficiency of the H<sub>3</sub>PO<sub>4</sub> containing samples can be a result of more protons being available. Additionally, the formation of solid Fe<sub>3</sub>(PO<sub>4</sub>)<sub>2</sub> and FePO<sub>4</sub> can act as driving force for the full deprotonation of the H<sub>3</sub>PO<sub>4</sub>. This can be supported as the formation of a white precipitate was not observed, when H<sub>2</sub>SO<sub>4</sub> was used. The high solubility of FeSO<sub>4</sub> leads to the formation of fresh mackinawite, which in consequence would adsorb organic material and thereby limit the observable amount in the gas phase. The H<sub>2</sub>SO<sub>4</sub>, however, was only used during experiments where the subsequent release of the reduction products was investigated.

## 4.2.4 Surface supported reduction mechanism

### 4.2.4.1 KCN

Based on the surface complexation model established by Wolthers and coworkers<sup>[80]</sup> a novel reduction mechanism for the carbon fixation from HCN is presented. As discussed earlier, they assume the presence of two distinctly acidic surface groups, the strongly



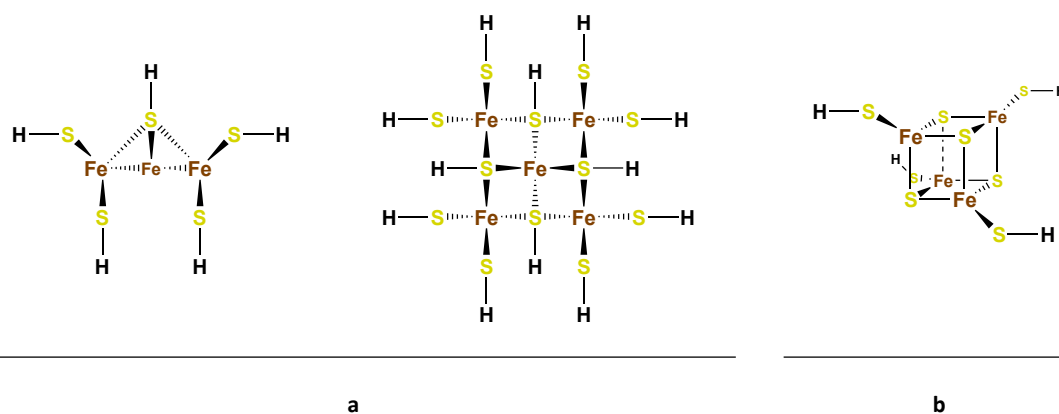
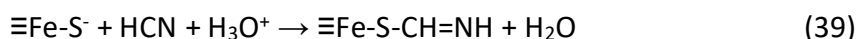
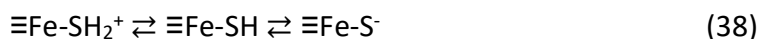


**Figure 43** Comparison of the structures of mackinawite alongside the a and c axis (a), and the  $[\text{Fe}_4\text{S}_4](\text{SH})_4$  model complex (b).

acidic mono-coordinated sites,  $\equiv\text{Fe-SH}$ , and the weakly acidic tri-coordinated sites,  $\equiv\text{Fe}_3\text{-SH}$ . The deprotonated mono-coordinated site ( $\text{MCS}_{\text{DP}}$ ) is more abundant, already before the point of zero charge of mackinawite at  $\text{pH}_{\text{PCZ}} \sim 7.5$  is reached and can therefore formally attack the HCN in a nucleophilic manner, following reaction 37.



The overall reduction proceeds due to the steady delivery of electrons by  $\text{Fe}^{2+}$  oxidation onto a surface end-group. To gain a deeper mechanistic insight into this reaction, M. T. Stiebritz calculated specific reaction energies by density functional theory (DFT) on an all ferrous  $[\text{Fe}_4\text{S}_4]$  cluster with a  $S = 4$  spin state. When equipped with thiol ligands, this model is useful for computational studies on the proposed mechanism, as the cluster solely acts as electron donor. The Fe atoms alongside the (001) and (011) sites of the mackinawite likewise provide one thiol ligand and are surrounded by three other S atoms (Figure 43).

The initial attack of a deprotonated thiol ligand is exothermic by approx.  $-75.5 \text{ kcal mol}^{-1}$  and therefore favored when compared to the bonding of the  $\text{CN}^-$  molecule onto an iron atom of the cluster, in either  $S = 4$  spin state (approx.  $+19 \text{ kcal mol}^{-1}$ ) or  $S = \frac{1}{2}$  spin state



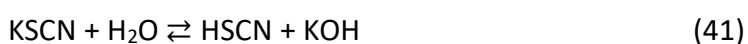
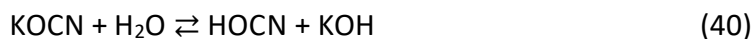
respectively. Recently, Rittle et al. reported the formation of CH<sub>4</sub> and NH<sub>3</sub> from [Si<sup>Pi</sup>Pr<sub>3</sub>]Fe(CN) and provided evidence for Fe(CNH) and Fe(CNH<sub>2</sub>) species as intermediates for the CN bond cleavage to occur.<sup>[208]</sup> The same is plausible for this case, where intermediate **1\*** undergoes protonation and reduction under release of NH<sub>3</sub> or NH<sub>4</sub><sup>+</sup> (Figure 44, steps 2-5). When the oxidation of the all-ferrous cluster into [Fe<sub>4</sub>S<sub>4</sub>]<sup>+</sup> is used as electron donor, the formation of the end-standing methyl group proceeds in an exotherm manner. Each reduction step is thereby performed under the assumption of a recovered cluster being oxidized again into [Fe<sub>4</sub>S<sub>4</sub>]<sup>+</sup>, as the reaction into greigite reassembles a steady source of electrons. At this branching point both, the ligand exchange with H<sub>2</sub>S to form CH<sub>3</sub>SH and the further formation and release of CH<sub>4</sub>, were found to be energetically favored by approx. - 3 kcal mol<sup>-1</sup> and - 61 kcal mol<sup>-1</sup>, respectively (Figure 44, step 6 + 7). In case of CH<sub>4</sub> formation an additional entropic effect makes the reaction even more exergonic.

The higher abundance in CH<sub>3</sub>SH, compared to CH<sub>4</sub> can be explained as only four electrons are needed in total, but also due to further possible branching points. In the presence of mackinawite and free protons, H<sub>2</sub>S was formed immediately and found to be present in large amounts during all experiments conducted at a pH < 7. By formulating a nucleophilic attack of H<sub>2</sub>S, NH<sub>3</sub> can be removed under subsequent reductive C – N bond cleavage (Figure 44, steps 8 + 9). After further reduction of the carbon atom, step 10 leads to the formation of a thiol residue, which either forms the end-standing methyl group by scission of the thiol ligand, or directly leads to the formation of CH<sub>3</sub>SH and the deprotonated site. A third branching point for CH<sub>3</sub>SH formation can be formulated, where an end-standing NH<sub>3</sub><sup>+</sup> group would undergo ligand exchange with H<sub>2</sub>S to form, again, the end-standing thiol group (Figure 44, step 12).

The formation of alkyl groups follows from the nucleophilic attack of a CN<sup>-</sup> molecule onto the end-standing carbon atom. In case of the model complex this reaction proceeds exothermic by - 13.8 kcal mol<sup>-1</sup> but should be limited at high H<sub>2</sub>S/HCN ratios. When the C<sub>2</sub> residue is hydrolyzed and reduced the formation of CH<sub>3</sub>CHO can be formulated. All steps were found to proceed exothermic. This is in accordance with the results from the experiments in 4.2.2.3 where CH<sub>3</sub>CHO was mainly produced from reactions where the amount of H<sub>2</sub>S was limited.

#### 4.2.4.2 KSCN and KOCN

The structural similarity of KSCN and KOCN allows both substrates to be reduced by the mackinawite surface groups, like in the case of KCN. The reaction between KOCN and mackinawite led to the selective formation of COS, while reduced species like CH<sub>3</sub>SH only appeared under more acidic conditions. The KOCN is first hydrated to give the isocyanic acid (HOCN).



Following Figure 45, the HOCN can be attacked in a nucleophilic manner by the MCS<sub>DP</sub> to give a residue that structurally reassembles an acetimid. In the next step this residue can undergo tautomerization into the amide form before it is further attacked by H<sub>2</sub>O or H<sub>2</sub>S and later release CO<sub>2</sub> or COS, respectively. When the KOCN samples were

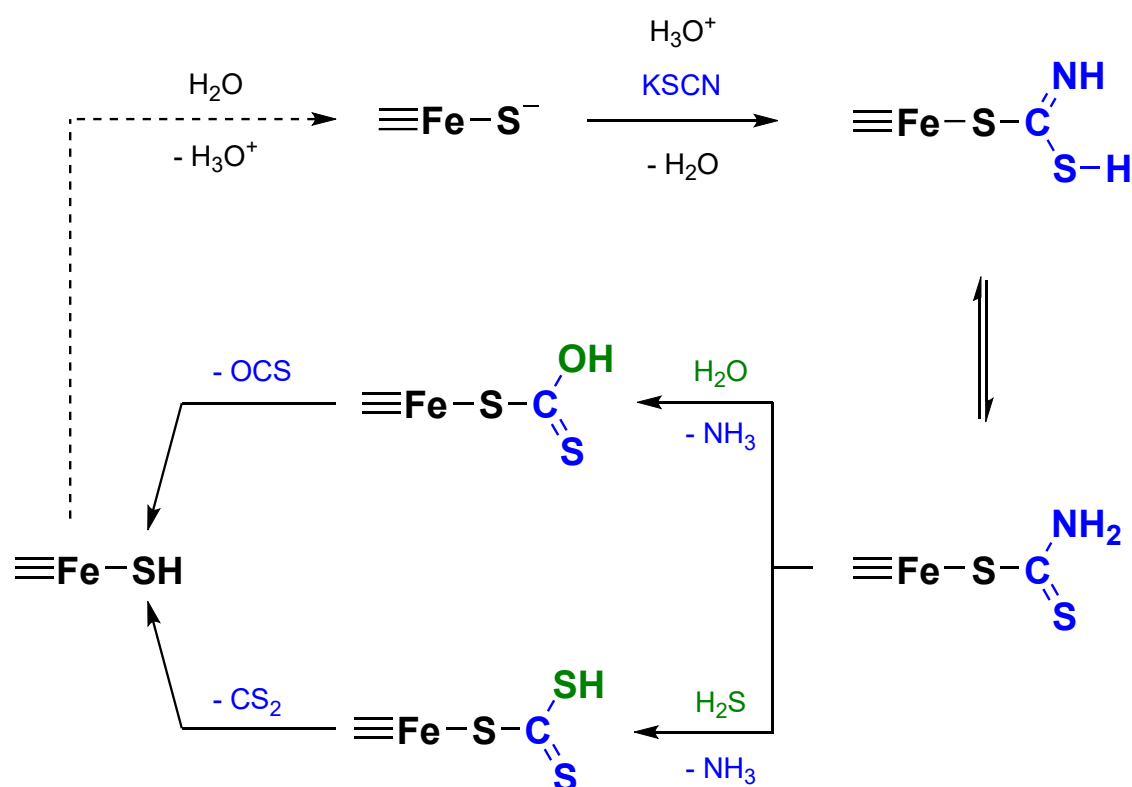


**Figure 45** Proposed mechanism for the reduction of HSCN by the mackinawite surface groups.

acidified, organic sulfur compounds like CS<sub>2</sub> and CH<sub>3</sub>SH were formed. Though, CS<sub>2</sub> could be identified due to its respective carbon shift, the observed signals remained low in intensity when compared to the one of COS. The formation of CH<sub>3</sub>SH can be achieved after the amide residue undergoes consecutive reduction and scission of the C – O bond under release of a H<sub>2</sub>O molecule. The CH<sub>3</sub>SH can then be released after being exchanged with a H<sub>2</sub>S molecule.

The reduction of KSCN mechanistically resembles the one of KOCN. The higher abundance of reduced species probably is a result of the weaker C – S bond, when compared to the one between carbon and oxygen. The release of a H<sub>2</sub>S molecule from the reduced thioamide residue in Figure 46 should therefore proceed more readily than during the reduction of KOCN. The samples containing KSCN produced only small amounts in COS when compared to CS<sub>2</sub>. In the KOCN samples the CO<sub>2</sub> levels were not followed quantitatively, whereas no conclusions regarding the ratio between CO<sub>2</sub> and COS can be made. The calculated areas of the TIC for the COS signal, however, show

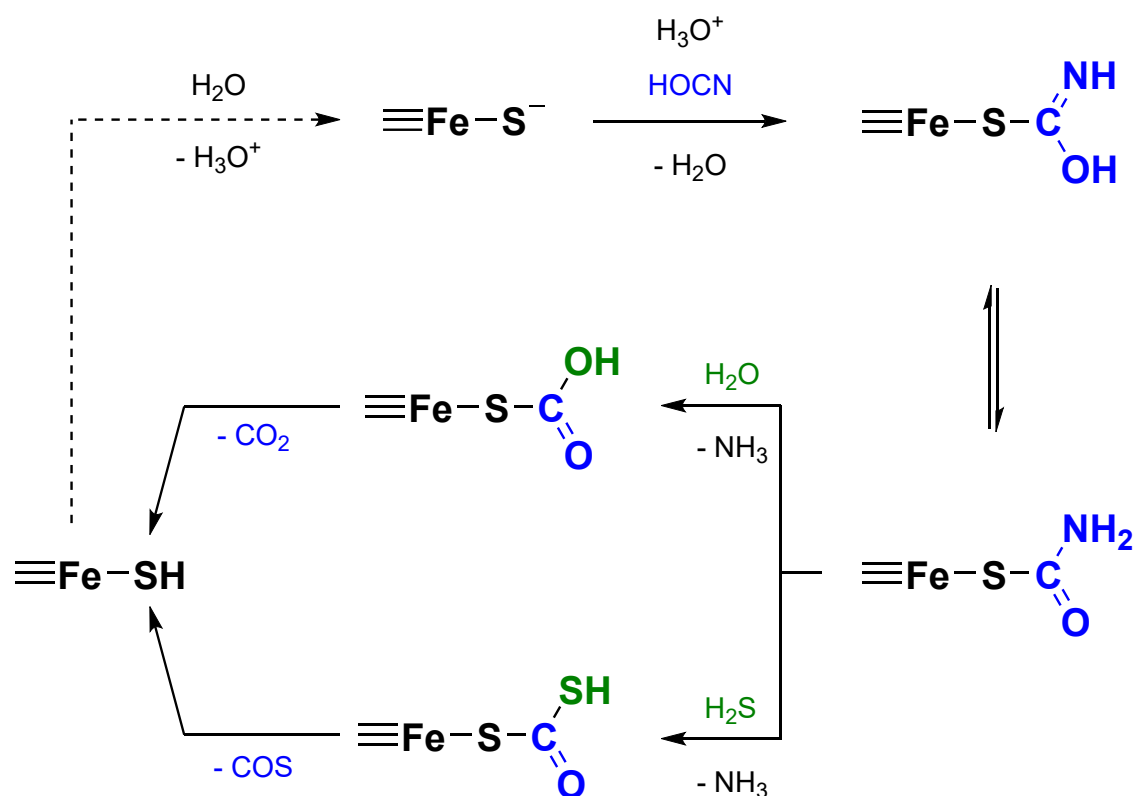


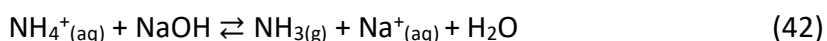
**Figure 46** Proposed mechanism for the reduction of HOCN by the mackinawite surface groups.

comparable levels to the ones observed for CS<sub>2</sub> in the KSCN samples. This at least provides evidence for the relevance of the intermediate formation of a C – S bond.

The gas phases of KSCN and KOCN samples did not contain significant amounts in C – C products. Unlike CN<sup>-</sup> both substrates only contain fully oxidized carbon atoms that are not able to attack the primary carbon atom in a similar nucleophilic manner. The KSCN samples partwise contained small amounts of HCN because of the desulfurization of HSCN by mackinawite. The highest levels in HCN were observed in GP-13-02 with a relative abundance of only 0.05 %. Though, HCN is produced it most likely directly reacts with either the MCS<sub>DP</sub> or surface bound species and therefore only appears occasionally in the gas phase of the samples.

#### 4.2.5 The fate of the nitrogen atom

In all experiments, no gaseous organic nitrogen compounds, other than nitriles, were observed. The nitrogen atom is therefore assumed to selectively undergo protonation until the C – N bond undergoes scission and NH<sub>4</sub><sup>+</sup> is released into solution. When <sup>14</sup>N-NMR spectroscopy was applied, no corresponding signal for the ammonia nitrogen was observed. When a colorimetric test (Merck) was used, again no NH<sub>4</sub><sup>+</sup> was detected. The course of the test, however, was disturbed by other components of in the filtrated aqueous phase. Even after removing Fe<sup>2+</sup> and CN<sup>-</sup> by precipitation with OH<sup>-</sup> or Fe<sup>3+</sup>, respectively, no clear result for the NH<sub>4</sub><sup>+</sup> concentration was received. Experimental proof for NH<sub>4</sub><sup>+</sup> could at last be given by the “Kreuzprobe” (QA-02). In this test the presence of NH<sub>4</sub><sup>+</sup> is proven through the release of NH<sub>3</sub> after NaOH is added to the aqueous solution. After the NaOH is added, the watch-glass is closed with another one where pH paper is fixated with a drop of H<sub>2</sub>O. The released NH<sub>3</sub> dissolved again in the H<sub>2</sub>O coating the pH strip which turned blue within seconds. A representative picture is given in Figure A 62.



The <sup>1</sup>H-NMR spectra collected from the different reduction experiments, containing mackinawite and KCN, invariably did not provide any signs for the formation of free

$\text{NH}_4^+$ . In some of the collected spectra a broadened signal in the region between 6.5 ppm and 7.5 ppm became visible. The  $^1\text{H}$ -NMR spectra of the reduction samples commonly provided a dominant singlet at 8.45 ppm. Signals of more reduced C – N compounds like  $\text{CH}_3\text{CN}$  or  $\text{CH}_3\text{NH}_2$  are typically shifted to a higher field. The structural features necessary to form a comparable singlet are further present in formic acid ( $\text{HCOOH}$ ) and formamide ( $\text{HCONH}_2$ ). Additionally, a singlet can be obtained in the case of formaldehyde, literature data however shows a much lower shift of  $>9$  ppm in acetone/ $\text{H}_2\text{O}$ .<sup>[230]</sup> The influence of  $\text{H}_2\text{S}$  was neglected as the signal was also formed at higher pH values where the pH-independent dissolution dominates.

When the aqueous solution of a sample containing equal amounts of KCN and  $\text{H}_2\text{SO}_4$  was heated at  $80\text{ }^\circ\text{C}$  for 3 d (LP-04), three distinct signals were observed in the  $^1\text{H}$ -NMR spectra (Figure A 63). The broad signal at 5.30 ppm probably is caused by HCN. The reaction further seemingly led to the release of  $\text{NH}_4^+$  as a triplet was observed in the region of 6.90 ppm to 7.18 ppm. This is in accordance with the expected formation of CO which, partly protonated, can provide a low field shifted signal at 8.21 ppm. When formic acid was investigated under the same conditions, a singlet with slightly lower shift of 8.25 ppm was obtained.

To identify the unknown compound formed during the reduction of KCN by mackinawite, further samples containing mixtures of  $\text{NH}_3$ , KCN and  $\text{HCOOH}$  were reacted at  $80\text{ }^\circ\text{C}$  for 3 d. The collected  $^1\text{H}$ -NMR spectra showed singlets between 9 ppm and 8 ppm in samples containing either KCN and  $\text{NH}_3$  (8.59 ppm), KCN and  $\text{HCOOH}$  (8.21 ppm) or  $\text{HCOOH}$  and  $\text{NH}_3$  (8.24 ppm). Both singlets in the  $\text{HCOOH}$  containing reactions are in good accordance with literature values for  $\text{HCOOH}$  and correspond to the carbon proton.<sup>[231]</sup> The slightly shifted values probably arise from differences in the pH of the samples as the  $^1\text{H}$ -NMR shift for  $\text{HCOOH}$  is pH-dependent.<sup>[232]</sup> The singlet observed during the reduction of KCN with mackinawite (8.45 ppm) is in good accordance with the one collected from the reaction between KCN and  $\text{NH}_3$  (8.59 ppm). The difference in the chemical shifts could here also arise from a different pH of the aqueous solution. The ammonolysis of HCN is well known in the literature and leads to the formation of formamidine.<sup>[34]</sup>

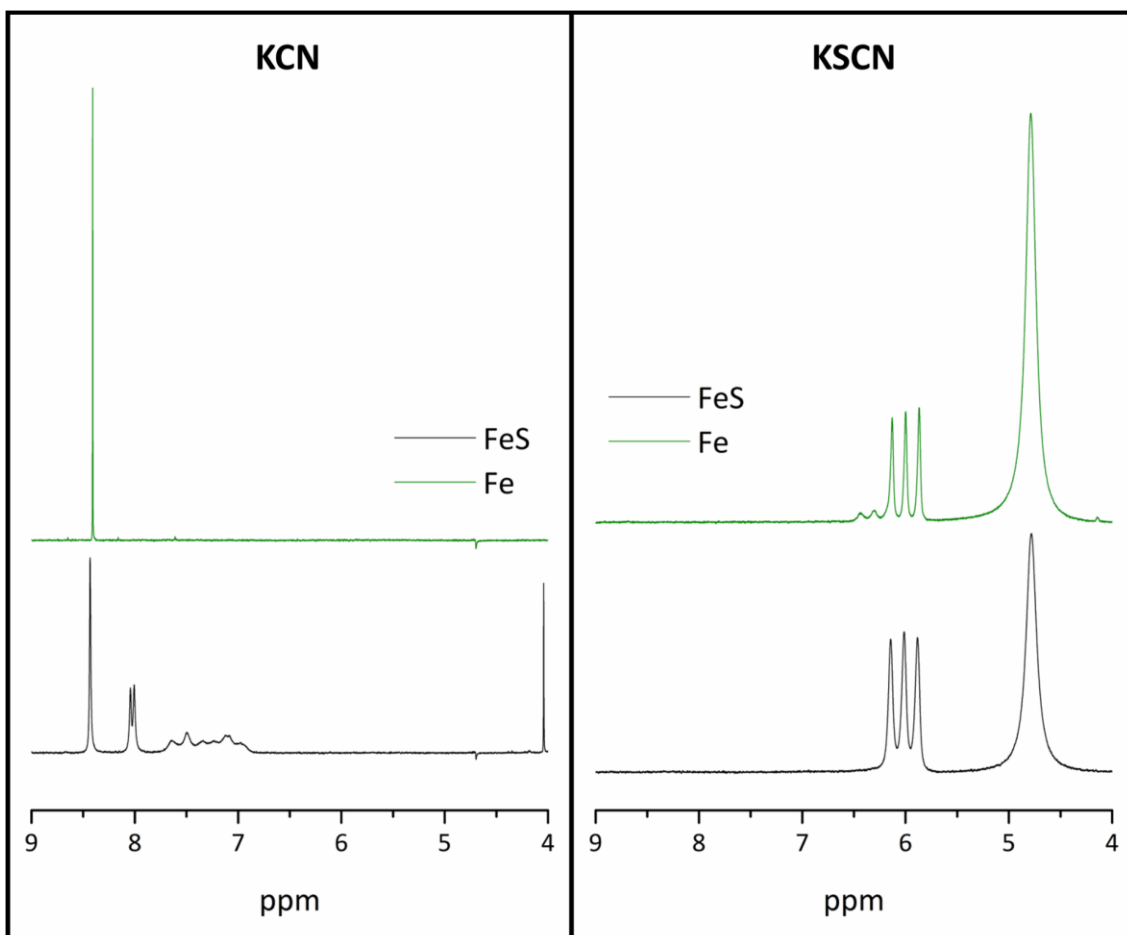
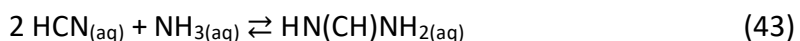


**Figure 47**  $^1\text{H}$ -NMR spectra ( $\text{D}_2\text{O}$ , 400 MHz) of aqueous solution acquired from samples were KCN and KSCN were either reacted with iron or mackinawite. The signal at 4.7 ppm corresponds to  $\text{H}_2\text{O}$ . The spectra gathered from the reaction of KCN were measured with  $\text{H}_2\text{O}$  suppression to elevate the resolution.



This reaction is independent from the applied reaction system and can act as a sink for  $\text{NH}_3$  in the presence of both iron (LP-05-01) and mackinawite (LP-05-03). When KSCN was used, both collected  $^1\text{H}$ -NMR spectra from the reaction with iron (LP-05-03) and mackinawite (LP-05-04) exhibited a triplet in the region of 5.8 – 6.3 ppm, clearly indicating the presence of  $\text{NH}_3/\text{NH}_4^+$ . As consequence of the inefficient ammonolysis of HSCN, no other signals were observed.





result from the more straightforward formation mechanism without additional branching points occurring.

The same model can be used to explain the findings on the mackinawite supported reduction of  $C_2H_2$  and  $CH_3CHO$  into  $C_2H_6$  and  $C_2H_4$ . The  $C_2H_2$  molecule displays structural similarity to HCN and can therefore react in a similar manner. The  $CH_3CHO$  on the other side can be bound over the carbonyl C atom and formally lead to the formation of an aldehyde residue, like the one displayed in our case after step 17 in Figure 44. Once bound to the  $MCS_{DP}$ , the direct proton coupled reduction can proceed as reported by Blöchl et al., whereas the necessary electrons would be donated by the mackinawite itself.<sup>[162]</sup> To validate their mechanistic considerations, they introduced various di-substituted ethyl alcohols, ethyl thiols and ethyl amines as substrates and again, observed the formation of  $C_2H_4$  as main product. This idea of desulfurization can here be further supported, as we can give evidence for  $CH_4$  formation from  $CH_3SH$  already at room temperature (5.2.2).

### 4.3 Summary

The formation of reduced compounds was accomplished by reacting KCN, KSCN or KOCN with either **RS<sub>1</sub>**, **RS<sub>2</sub>** and **RS<sub>3</sub>**. It was found that the array of products strongly depended on the type of system and substrate that was used. When iron was used KCN was found to be leading to aliphatic  $C_1 - C_8$  hydrocarbons,  $C_1 - C_6$  aldehydes and ketones and  $C_1 - C_5$  nitriles. All formed compounds were identified by comparing the collected MS patterns to those provided by the NIST 14 library. To further proof that the compounds emerged from the supplied KCN reactions with  $Na^{13}CN$  were performed and provided the expected mass shifts. Based on the range of products a reduction mechanism was proposed that is in alignment with other mechanistic proposals regarding the reduction of carbon substrates by the iron surface. A similar array of products was observed when KSCN and KOCN were reacted with the iron powder. In the case of KOCN  $C_1 - C_5$  hydrocarbons were formed, while the gas phase of the KSCN sample only contained  $C_1 - C_3$  hydrocarbons. The KSCN sample, additionally, contained HCN and organic sulfur compounds like  $CS_2$  and  $(CH_3)_2S$ .

When the iron sulfur mixture was used ( $\text{RS}_2$ ) at pH 3 the array of products changed, whereas the formation of mostly organic sulfur compounds and smaller amounts of  $\text{C}_1$  –  $\text{C}_3$  hydrocarbons were observed. In the cases of KCN and KSCN the reaction led to the formation of  $\text{CH}_3\text{SH}$  and  $\text{CS}_2$  as main products. In experiments using KOCN mostly COS and only small amounts in reduced species were formed. At pH > 7, both the reduction of KSCN and KOCN only proceeded inefficiently and, in contrast to the ones conducted at pH 3, the appearance of the reaction mixture did not change significantly. When KCN, however, was reacted in the absence of acid at pH 9 – 10 the aqueous solution turned dark green before becoming colorless again after 24 h at 80 °C. Based on the collected UV/Vis spectra the green color could arise from small iron sulfur clusters. This can further be supported as an irreversible redox peak was observed during CV experiments.

When such a sample was acidified after at least 3 d at 80 °C, aliphatic and cyclic organic sulfur compounds were detected in the gas phase. The reactions products were partly identified by comparing their mass spectra to the ones provided by the NIST 14 library. As some of the compounds were not listed, their mass patterns collected from the reaction of  $\text{K}^{12}\text{CN}$  and  $\text{Na}^{13}\text{CN}$  were compared, and their proposed structures were evaluated based on the fragmentation patterns. In contrast to the reactions at pH 3, where HCN is the dominant species, significantly higher concentrations in  $\text{CN}^-$  are present at pH 9. Additionally, under such conditions the formation of mackinawite from iron and sulfur is restricted as it depends on the acidic dissolution of iron. The  $\text{CN}^-$  can therefore readily react with the sulfur to give thiocyanates and polysulfides after an initial scission of the S – S bond. As mentioned earlier, the reaction between KSCN and iron solely led to the formation of aliphatic products, whereas no cyclic ones were observed. The formation mechanism of the cyclic products thereby most likely proceeds by the intermediate formation of  $\text{SCN}^-$  and  $\text{S}_2\text{CN}^-$ . This assumption is further supported by the fact that nearly exclusively cyclic compounds containing a disulfide bond were detected.

When mackinawite was used, nearly no hydrocarbons were formed from all three substrates. The reaction with KCN resulted in the nearly selective formation of  $\text{CH}_3\text{SH}$ , which always was accompanied by small amounts of  $\text{C}_2\text{H}_5\text{SH}$ ,  $\text{CS}_2$  and  $(\text{CH}_3)_2\text{S}$ . The reaction with KSCN in contrast led to the formation of mainly  $\text{CS}_2$  together with small

amounts of CH<sub>3</sub>SH. To get more insight into the formation mechanism of the reduced species from KCN, DFT calculations were performed with a reduced [Fe<sub>4</sub>S<sub>4</sub>](SR<sub>4</sub>) model complex. The first experiments showed that the reaction between one of the iron atoms and the HCN always gave endothermic reaction energies, which would not align with the observation that CH<sub>4</sub> and CH<sub>3</sub>SH were already formed at room temperature in the mackinawite experiment. When the HCN molecule was, however, let to be attacked by a sulfide residue of the model complex, resembling the MCS<sub>DP</sub>, the reaction became exothermic. In the case of the protonated mono coordinated surface group (MCS<sub>P</sub>) the reaction proceeded endothermic. The reduction of the newly formed residue was followed by different pathways under exothermic conditions for all products observed during the mackinawite experiments. Additionally, when the reduction of KCN by mackinawite was performed under conditions where H<sub>2</sub>S is scarce, CH<sub>3</sub>CHO became the major product, which is in alignment with the proposed mechanism. The electrons for the reaction were found to be provided by the oxidation of Fe<sup>2+</sup> in the mackinawite structure, whereas greigite was formed in all cases.

## Chapter 5. Reduction of carbon sulfur compounds

### 5.1 Introduction

The modern global sulfur budget is mainly influenced by the reduction and oxidation of oceanic sulfate. The earliest atmosphere was anoxic, whereas the earliest sulfur cycle did not contain an efficient sink for reduced atmospheric gases like H<sub>2</sub>S or sulfur particles and was therefore mostly dominated by the photolysis of SO<sub>2</sub> and H<sub>2</sub>S, as well as the dissociation of elemental sulfur.<sup>[236,237]</sup> Early Archaean microorganisms are assumed to more likely have metabolized sulfur, rather than sulfate.<sup>[238,239]</sup> This is in accordance with geological evidence from 3.49 Gy old marine sulfate deposits from Dresser Formation, Australia, which have been interpreted to host early sulfate-reducing organisms. Philippot et al. found that the metabolized sulfur probably was not produced from the surrounding sulfate as the samples show a sulfur isotopic anomaly that differs from their host environment.<sup>[240]</sup>

Like SO<sub>2</sub> and H<sub>2</sub>S, CS<sub>2</sub> has a similar prebiotic relevance as it is a component of volcanic gases. It has already been studied due to its application as solvent and sulfurization reagent for prebiotic reactions. The reaction of CS<sub>2</sub> with amines leads to the formation of dithiocarbamates.<sup>[241]</sup> These are well established chain transfer agents in polymerization reactions and known to efficiently remove metal ions from aqueous solutions by forming the respective metal complexes. Recently, it has furthermore been shown to provide the derivatization of amino acids<sup>[242]</sup> and the formation of peptide bonds.<sup>[243]</sup>

The reaction of CS<sub>2</sub> with oxalic acid under hydrothermal conditions (175 °C, pH < 0.5) was studied by Rushdi et al. who reported the formation of various linear and cyclic polysulfides and perthioesters. They proposed that the reduction follows from the decomposition of the oxalic acid into CO<sub>2</sub> and H<sub>2</sub>. Latter can then reduce the CS<sub>2</sub> to yield CH<sub>3</sub>SH and H<sub>2</sub>S, and thereby give rise to a subsequent reaction network leading to the respective species.<sup>[244]</sup> Though, such compounds are presently not part of living organisms, a similar reaction mixture was reported in hydrothermal deposits found at Guaymas Basin, California.<sup>[245]</sup>

The reduction of CS<sub>2</sub> into CO and H<sub>2</sub>S was previously found to proceed when either the extracted nitrogenase<sup>[156,246,247]</sup> or the carbon reductase<sup>[248]</sup> were used. Until now, no comparable experiments were performed with iron sulfides. A general reactivity, however, is expected as organic sulfur compounds were already found to be desulfurized and reduced in the presence of freshly precipitated mackinawite.<sup>[162]</sup> The formation of pyrite from mackinawite and H<sub>2</sub>S is a further example for this reaction.

## 5.2 Results and Discussion

### 5.2.1 Reduction of CS<sub>2</sub>

The reduction of CS<sub>2</sub> by mackinawite was first investigated in H<sub>2</sub>O. Due to its low solubility the supplied CS<sub>2</sub> floated on top of the aqueous phase. In cases where the samples were shaken, only small CS<sub>2</sub> droplets, instead of a fully separated phase were visible after 3 d at room temperature. When the gas phase of these samples was analyzed, no reduced species were observed. However, CS<sub>2</sub> levels were found to vary, depending on the pH of the solution. In Figure 49 the relative abundance in CS<sub>2</sub> for pH 3 (GP-17) and pH 6 (GP-18) are shown. In presence of acid the CS<sub>2</sub> levels in the gas phase were found to have decreased. When neutral samples were heated to 80 °C, the CS<sub>2</sub> phase again appeared after cooling down to room temperature.

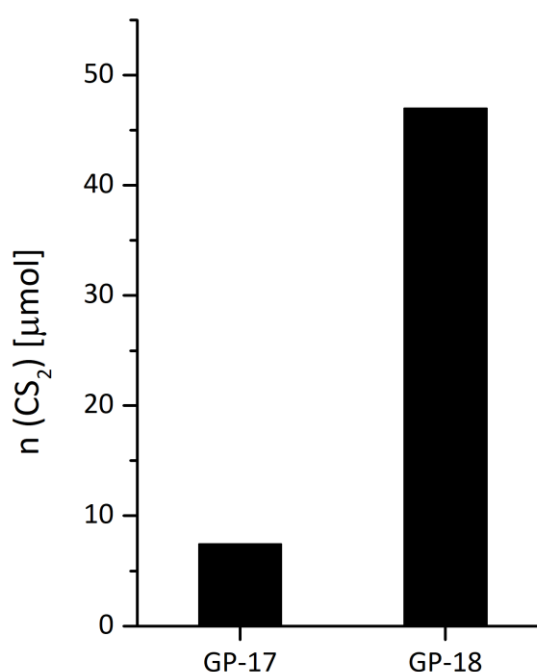


**Figure 49** Comparison of the CS<sub>2</sub> concentration in the gas phase of mackinawite samples that were either heated (80 °C) at pH 3 (GP-17) or pH 6 (GP-18).

During the reaction at elevated temperatures in H<sub>2</sub>O no reduced compounds were detected after 5 d. It was assumed that the reduction rate is restricted by the low solubility of CS<sub>2</sub> in H<sub>2</sub>O. This problem was resolved by initially dissolving the CS<sub>2</sub> in MeOH

or EtOH. When such a solution was added to the aqueous mackinawite, no separated phase was observed anymore. In samples, where only MeOH and EtOH were supplied, no reduced species occurred after heating them at 80 °C for 3 d. When CS<sub>2</sub> was present, however, CH<sub>4</sub>, CH<sub>3</sub>SH, (CH<sub>3</sub>)<sub>2</sub>S, (CH<sub>3</sub>)<sub>2</sub>S<sub>2</sub>, C<sub>2</sub>H<sub>5</sub>SCH<sub>3</sub>, C<sub>4</sub>H<sub>9</sub>SH and C<sub>4</sub>H<sub>9</sub>SCH<sub>3</sub> formed in the gas phase of the samples.

In the presence of EtOH, a similar decrease of CS<sub>2</sub> in the gas phase was observed at lower pH values. When samples (GP-19-01 to GP-19-03), which were adjusted to pH 10 by NaOH, were charged with CS<sub>2</sub> and different amounts of acid were added, no significant

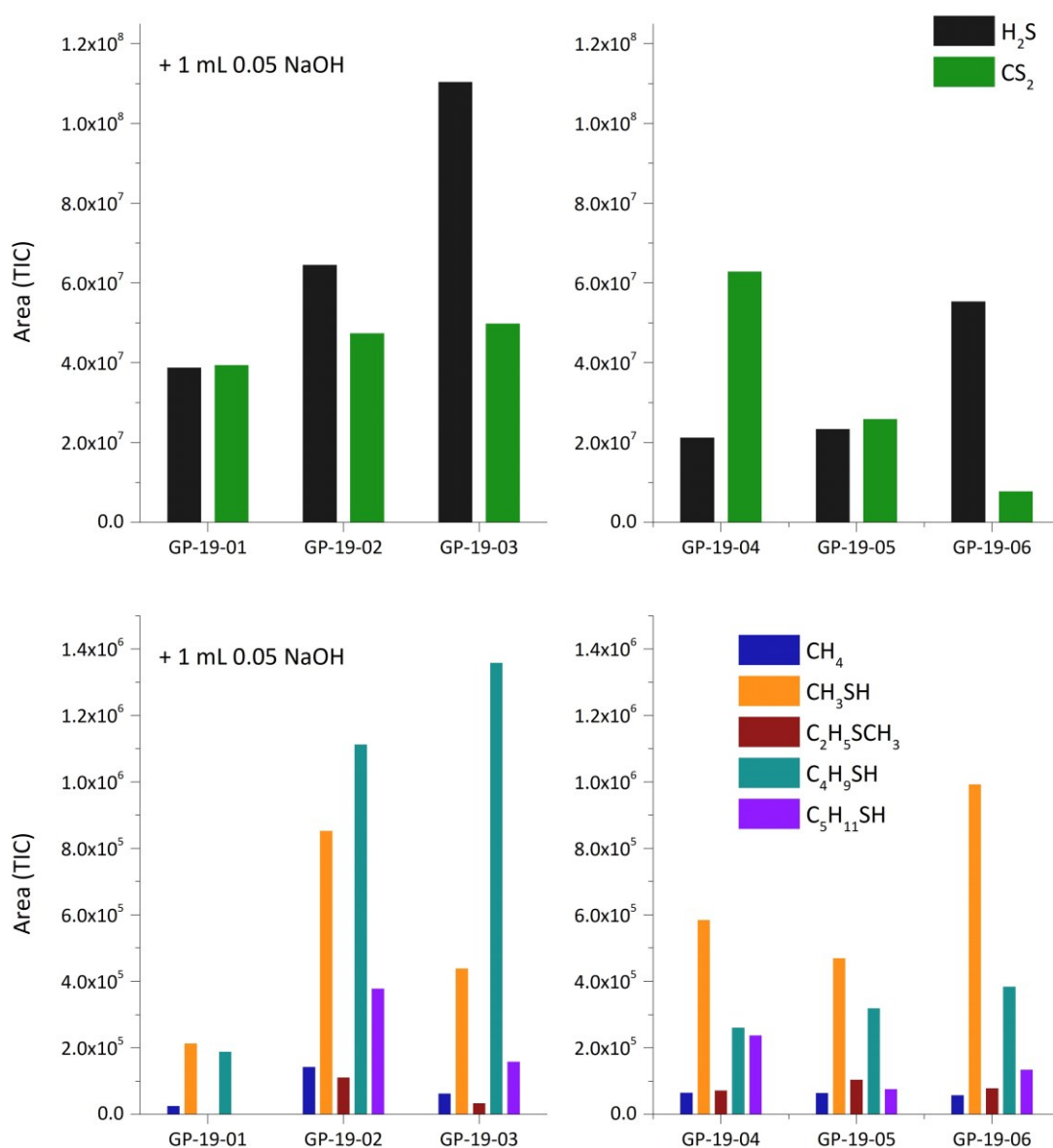


**Figure 50** Comparison of the product formation from samples that were charged with the CS<sub>2</sub>/EtOH mixture instead of pure CS<sub>2</sub>. (left).

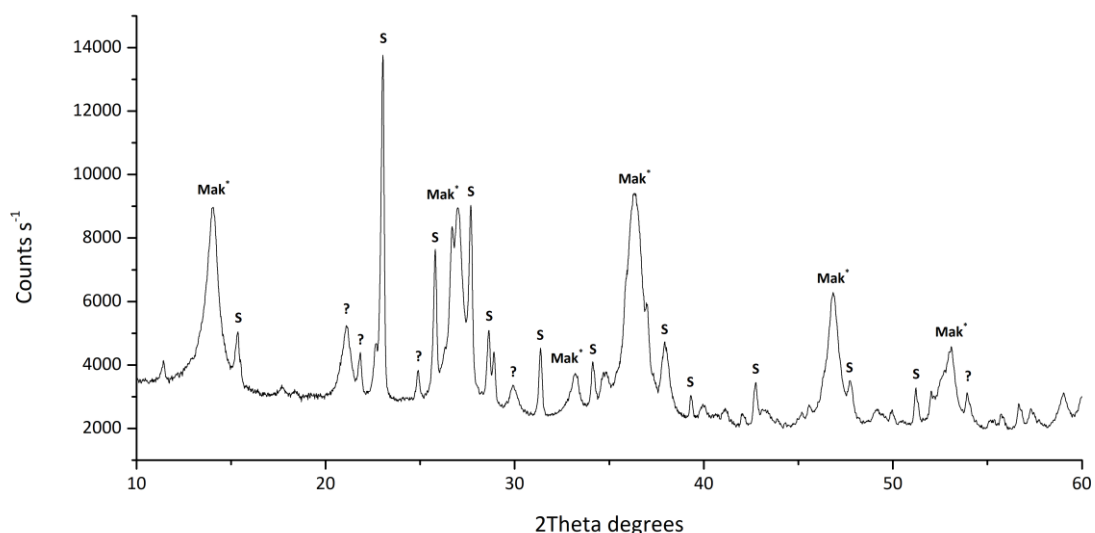


**Figure 51** PXRD pattern (SP-FeS-10) collected from the solid residue of the reaction between mackinawite and CS<sub>2</sub>; Mak\* = “swollen” Mackinawite, S = Sulfur, ? = unknown.

change in CS<sub>2</sub> gas phase concentrations was observed. In absence of any additional base (GP-19-04 to GP-19-06), however, the amount in available CS<sub>2</sub> decreased from 304.1 μmol to 37.4 μmol. The calculated areas for the CO<sub>2</sub> signal remained constant in all samples, whereas the amount in H<sub>2</sub>S increased upon further addition of acid (Figure 50). When the total areas are compared, it was found to be significantly lower in the ones with an initial pH of 6. The highest total amount in reduced species was present in GP-19-02. After the reaction was finished, only 22.9 % of the supplied CS<sub>2</sub> were present anymore. In respect of the given areas, a yield of 1.33 % in reduced species was estimated.

The collected PXRD pattern of the filtrated and deactivated solid reaction product from GP-19-03 (SP-FeS-10) is shown in Figure 51. At a first glance, the dominant diffraction peaks appear like the ones of mackinawite but are significantly shifted towards smaller 2Theta degree values. Alongside this “swollen” iron sulfide phase other diffraction peaks appeared, which could be assigned to sulfur. The sulfur reflexes do not appear shifted and showed typical angles, already discussed earlier in this work. In Table 7 the observed angles for amorphous mackinawite (SP-FeS-03) and for the solid isolated after the reaction with CS<sub>2</sub> under acidic conditions are compared.

The reaction could, like the one of HCN, proceed by the adsorption and reduction by the mackinawite surface groups. Following Figure 52, a surface bound species can be



**Table 7** Diffraction peaks collected from the solid product of SP-FeS-10, compared with the ones of SP-FeS-03.

ID	2Theta degree						
<b>SP-FeS-10</b>	14.05	27.03	31.37	36.36	46.83	47.75	53.04
<b>SP-FeS-03</b>	16.85	29.89	34.53	38.82	49.64	52.82	58.9
<b>Δ</b>	2.8	2.86	3.16	2.46	2.81	5.07	5.86

formulated if protons are available. This residue can then undergo stepwise reduction and protonation to form surface bound precursors for the observed reduced species.

The reaction energies for the reduction by the  $[\text{Fe}_4\text{S}_4]$  model complex was calculated by DFT calculations. The initial bonding process of the  $\text{CS}_2$  molecule towards the  $\text{MCS}_{\text{DP}}$  is exothermic by  $-21.7 \text{ kcal mol}^{-1}$ . The same system gave a three times larger reaction energy for the case of HCN and could therefore explain the smaller yields of approx. 1 % and 10 %, respectively. The first reduction step leads to the scission of the C – S bond and  $\text{H}_2\text{S}$  is released. The reaction energies were calculated for both, the protonated and deprotonated species  $-113.2 \text{ kcal mol}^{-1}$  and  $-158.9 \text{ kcal mol}^{-1}$ , respectively. The -CHS residue was already formulated during the reduction of HCN (Figure 44, Step 9). The reaction energies for the formation of a methyl residue from HCN are like the ones observed here, ranging between  $-113.2 \text{ kcal mol}^{-1}$  and  $-118.8 \text{ kcal mol}^{-1}$ .

The release of the reduced compounds by either ligand exchange or further reduction was described earlier. The adsorption and protonation of the  $\text{CS}_2$  molecule by the  $\text{MCS}_{\text{DP}}$ , both, are exothermic processes (Figure 52). The observation of decreased  $\text{CS}_2$  levels in the gas phase of samples at lower pH therefore aligns well with the proposed model. Once the sulfur is protonated or the carbon is reduced, the  $\text{CS}_2$  molecule cannot be released into the gas phase anymore, even when heat is applied. In samples with an initially high pH, 190  $\mu\text{mol}$  to 241  $\mu\text{mol}$  of  $\text{CS}_2$  were present, while the ones only containing acid dropped significantly with the added amount.

In some of the samples, the formation of the C – C bound species  $C_2H_5SCH_3$ ,  $C_4H_9SH$  and  $C_4H_9SCH_3$  was observed. The compounds could clearly be identified by comparing their mass pattern to the ones in the library and by their fragmentation pattern (Figure A 135). In contrast to the  $CN^-$  ion, the carbon atom in the  $CS_2$  molecule does not provide a free pair of electrons to perform a nucleophilic attack. The C – C bound compounds probably formed by a second mechanism. The reduced compounds were not clearly identified by using isotopically labelled substrate and therefore could have originated from another source. The observed areas, however, increased at lower pH values and therefore are plausible to have formed during the reaction.

In contrast to the previously discussed substrates,  $CS_2$  already contains sulfur groups, which can interact with the mackinawite surface in a different manner. In addition to the nucleophilic attack towards the  $CS_2$  molecule, an Fe – S bond can be established. When both reactions proceed at one iron atom, a steric proximity between two carbon atoms can be established. The C – C bond then would be formed upon reduction of the

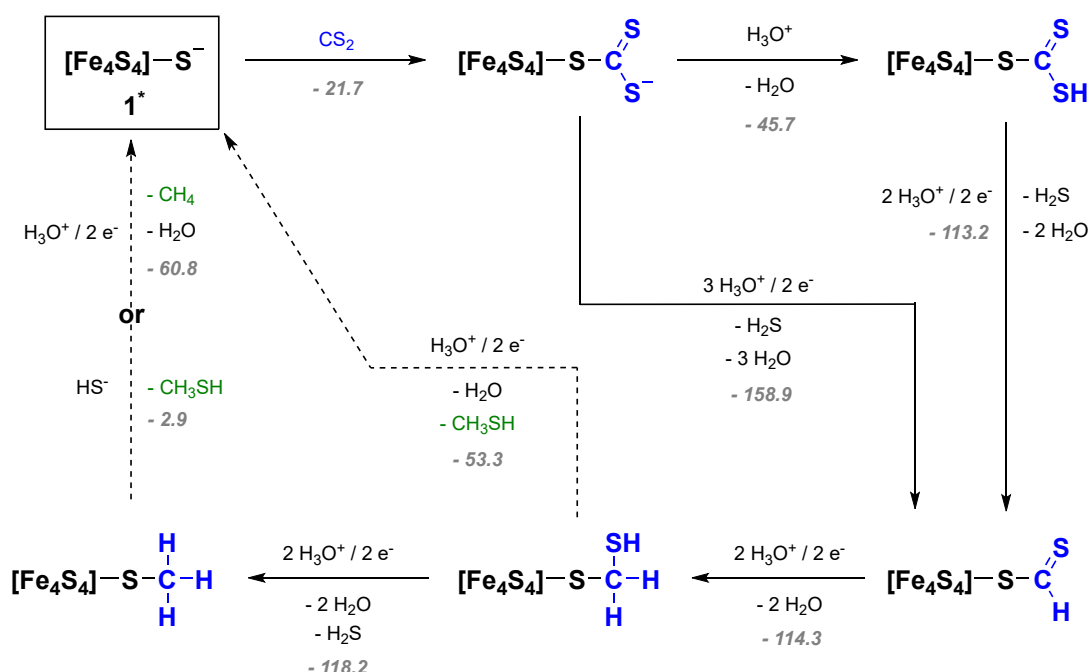


**Figure 52** Proposed reduction mechanism involving the MCS<sub>DP</sub> of mackinawite. The reaction energies were calculated by DFT on a  $[Fe_4S_4]$  model cluster. The reaction energies (grey) are given in kcal mol<sup>-1</sup>. The calculations were performed by M. T. Stiebritz.

carbon atoms by the electrons supplied from the iron, whereas various C – S bonds are broken. This approach leads to the formation of an ethyl residue, which is fixated over two sulfur atoms. The observed products, however, are sulfides with the general formula  $R^1SR^2$  ( $R^1 = CH_3$  and H;  $R^2 = C_2H_5$  and  $C_4H_8$ ). The gas phase furthermore did contain  $(CH_3)_2S$  in small amounts, when compared to the ones containing C – C bonds. The formation of methyl groups can thereby be explained by the migration of the sulfide residue into a S – C bond of an already formed methyl surface group. This process has until now not been described for sulfide surface groups, but was already assumed to appear on the iron surface during the formation of pyruvate from  $CO_2$ .<sup>[11]</sup> Besides  $(CH_3)_2S$  only compounds containing an even number of carbon atoms in  $R^2$  were formed. It is therefore plausible that the formulated ethyl group can react to form butyl groups.

### 5.2.2 Reduction of $CH_3SH$

The reaction between  $CH_3SH$  and mackinawite at pH 3 was investigated by GCMS analysis and resulted in the formation of reduced compounds. The samples were thereby reacted in  $H_2O$  and  $CH_3SH$  was produced by reaction 44 upon the addition of acid.

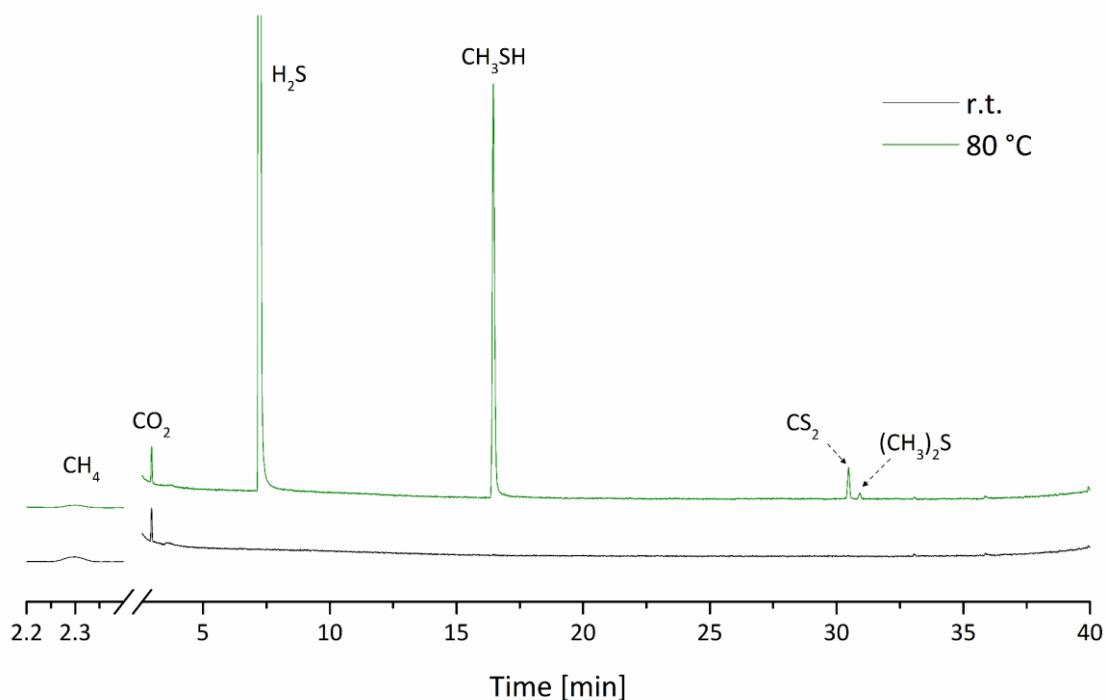
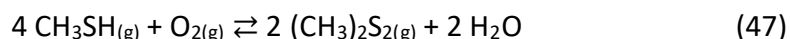
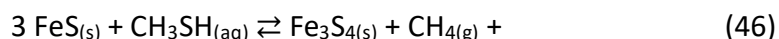
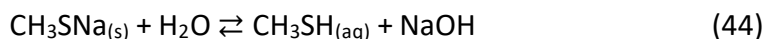


**Figure 53** Gas chromatogram (TIC) collected from the gas phase of GP-20 after the sample was first left 2 d at r.t. and then heated to 80 °C for 3 d.



In Figure 53 the gas chromatogram, obtained from samples containing mackinawite and  $\text{CH}_3\text{SNa}$  (pH 3) after 2 d at room temperature, is displayed. In comparison to the control, small amounts of  $\text{CH}_4$  were formed, while no signal corresponding to  $\text{CH}_3\text{SH}$  was observed. After the samples were left at  $80^\circ\text{C}$  for 3 d, additional signals, including the one for  $\text{CH}_3\text{SH}$ , appeared and could be identified as  $\text{H}_2\text{S}$ ,  $\text{CS}_2$  and  $(\text{CH}_3)_2\text{S}$ .

In Table 8 the relative abundances of the observed products are listed for the samples reacted at room temperature and  $80^\circ\text{C}$ . The  $\text{CH}_3\text{SNa}$  stock solution was prepared and used as the ones for the  $\text{CH}_3\text{SH}$  calibrations. In the gas phases received from the reaction of  $\text{CH}_3\text{SNa}$  with  $\text{H}_2\text{SO}_4$ ,  $\text{HCl}$  or  $\text{H}_3\text{PO}_4$  no  $\text{CH}_4$  or any other organosulfur compound other than  $\text{CH}_3\text{SH}$  or  $(\text{CH}_3)_2\text{S}_2$  were observed.

When the  $\text{CO}_2$  signals in the chromatograms of GP-20 and GP-21, before and after heating, were integrated, similar peak areas ( $\pm 3.3\%$ ) were obtained (Figure A 136). The

**Table 8** Summarized relative abundances of the reaction products. The concentration of  $\text{CS}_2$  was calculated from CAL-CD.

ID	Relative abundance						n [ $\mu\text{mol}$ ]
	$\text{CH}_4$	$\text{CO}_2$	$\text{H}_2\text{S}$	$\text{CH}_3\text{SH}$	$\text{CS}_2$	$(\text{CH}_3)_2\text{S}$	$\text{CS}_2$
r.t.	14.08	84.66	0	0	1.25	0	0.038
<b>80 °C</b>	0.04	0.52	85.43	13.27	0.54	0.12	2.94

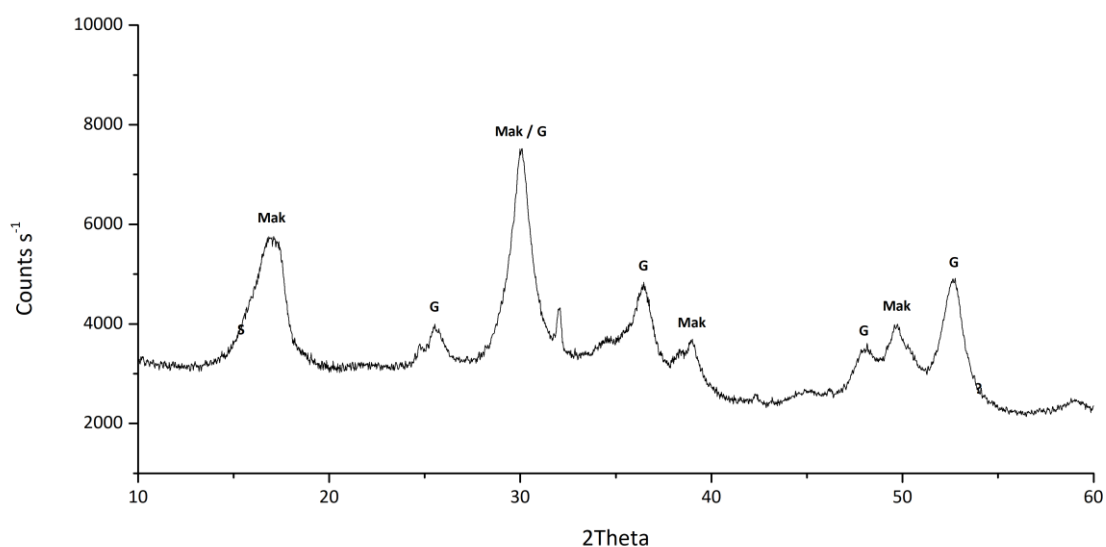


**Figure 54** PXRD pattern (SP-FeS-11) collected from the solid product after the reaction between mackinawite and  $\text{CH}_3\text{SNa}$  after 3 d at  $80^\circ\text{C}$ ; Mak = mackinawite, G = greigite.

$\text{CH}_4$  :  $\text{CO}_2$  ratio, however, significantly decreased during the reaction from 0.14 and 0.19 to 0.07, respectively. Though, GP-20-01 and GP-21-01 were extracted after the acid was added, no  $\text{H}_2\text{S}$  was observed. Upon heating, however, it became much more abundant in the gas phase with  $> 80\%$ . Likewise,  $\text{CH}_3\text{SH}$  was only observed in GP-20-02 and GP-21-02 and not released to the gas phase at lower temperatures. The approximate yield for  $\text{CS}_2$ , based on CAL-CD, was found to range from 0.002 to 0.5%.  $\text{CS}_2$  and  $(\text{CH}_3)_2\text{S}$  were only significantly produced at  $80^\circ\text{C}$ . At room temperature only minor amounts ( $< 0.1\%$ ) were formed. Sample GP-20-02 provided a maximum yield in  $\text{CS}_2$  of 0.5%.

The collected PXRD pattern from the solid reaction product is displayed in Figure 54. The sample mainly consists out of poorly crystalline mackinawite, giving broadened reflexes like the ones observed for unreacted ones. The additional reflexes could be assigned to greigite, while no other iron sulfide phase was formed. Furthermore, no significant amount in sulfur was detected. Like the previously described reactions, the electrons released by the oxidation of iron ions can be used to reduce the carbon atom.

During the reduction mechanism for HCN and  $\text{CS}_2$  (4.2.4.1 and 5.2.1), an intermediate with an end-standing methanethiol group could be formulated. The same residue follows from the nucleophilic attack of a sulfide group towards the carbon atom of  $\text{CH}_3\text{SH}$  molecule. To establish a bond between a sulfide group and the carbon atom the existing C – S bond is cleaved whereas  $\text{H}_2\text{S}$  is released into solution (Figure 55). Upon

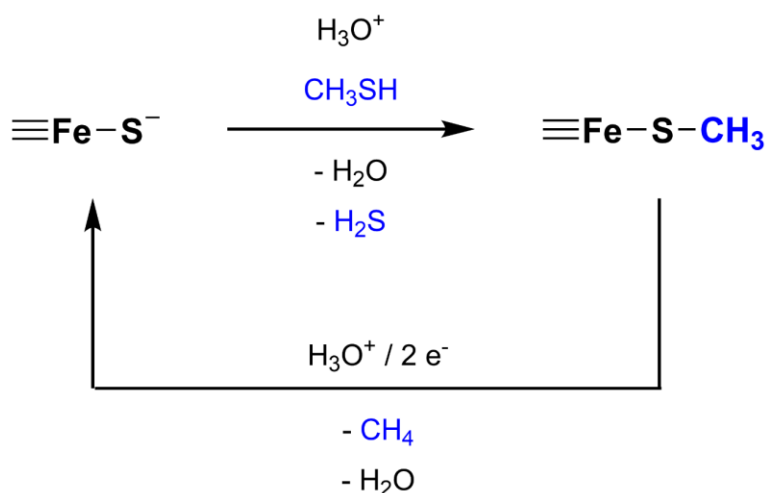


**Figure 55** Proposed mechanism for the reduction of  $\text{CH}_3\text{SH}$  by the mackinawite surface groups.

further reduction the  $\text{CH}_4$  molecule is released from the surface group under scission of the initially established C – S bond.

### 5.3 Summary

The previously suggested desulfurization of organic substrates by mackinawite could additionally be shown to proceed when  $\text{CS}_2$  and  $\text{CH}_3\text{SH}$  were used. Both substrates reacted with mackinawite and led to the formation of  $\text{CH}_4$ , in the case of  $\text{CH}_3\text{SH}$ , and to  $\text{CH}_4$ ,  $\text{CH}_3\text{SH}$ ,  $(\text{CH}_3)_2\text{S}$ ,  $(\text{CH}_3)_2\text{S}_2$ ,  $\text{C}_2\text{H}_5\text{SCH}_3$ ,  $\text{C}_4\text{H}_9\text{SH}$  and  $\text{C}_4\text{H}_9\text{SCH}_3$  in the case of  $\text{CS}_2$ . Both substrates most likely get adsorbed to the mackinawite surface when the reaction is performed at room temperature and only release the reduced compounds upon heating.

The collected PXRD of the solid residue gathered from the reactions show mackinawite and greigite, when  $\text{CH}_3\text{SH}$  was reduced, and a more complex one for the one from the  $\text{CS}_2$  reduction. In accordance with the findings from the previously described reactions, no detectable amounts of pyrite were formed, implying that the reaction mechanism follows the same pathway as discussed for KCN, KSCN and KOCN.

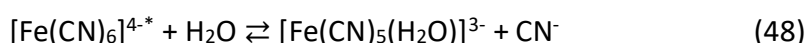
The initial bonding of the  $\text{CS}_2$  molecule was investigated by DFT calculations on the  $[\text{Fe}_4\text{S}_4]$  model complex and shown to proceed exothermic in energy. The intermediately formed residue thereby are partly identical to the ones formulated in the previous mechanisms and here also lead to the formation of  $\text{CH}_3\text{SH}$  and  $\text{CH}_4$  in an overall exothermic process.

## Chapter 6. Reduction of hexacyanoferrates

### 6.1 Introduction

Cyanides are well known for their key role in the abiotic formation of amino acids, purines, pyrimidines and further polymerized species.<sup>[29,249]</sup> While these reactions are mostly observed under laboratory conditions, natural environments, like the one of the young earth, would lead to much bigger constraints for these processes to proceed. High primordial abundances in free Fe<sup>2+</sup> and Fe<sup>3+</sup> concentrations would have led to the more favored formation of hexacyanoferrates and act as a long-term storage for cyanides.

In general, hexacyanoferrates are stable under ambient conditions, but tend to decompose by releasing hydrogen cyanide (HCN) under acidic condition at higher temperatures. This procedure was first used by Merz et al. who selectively released HCN by heating [Fe(CN)<sub>6</sub>]<sup>4-</sup> at 300 °C.<sup>[250]</sup> Since then, the use of metal cyanides as HCN sourced was further developed and showed to already proceed at temperatures under 100 °C, when an appropriate catalyst like Pt is used.<sup>[251]</sup> The release of HCN could furthermore be shown to proceed photochemically as photoaquation (reaction 48), when excitation wavelengths of 280 – 330 nm are applied.<sup>[252]</sup> Both, the thermal and photochemical, release of HCN from [Fe(CN)<sub>6</sub>]<sup>3-/4-</sup> are thereby plausible under primordial conditions.<sup>[194,253]</sup>



The [Fe(CN)<sub>6</sub>]<sup>4-</sup> molecule, besides photoaquation, can furthermore release a hydrated electron (e<sup>-</sup><sub>aq</sub>) upon irradiation with light < 313 nm. Ritson et al. already used this system to reduce HCN, in the presence of sulfite (SO<sub>3</sub><sup>2-</sup>), into simple sugars and precursors for hydroxy and amino acids. The SO<sub>3</sub><sup>2-</sup> was shown to effectively support the re-oxidation of [Fe(CN)<sub>6</sub>]<sup>3-</sup> into [Fe(CN)<sub>6</sub>]<sup>4-</sup> as it was fully consumed when supplied stoichiometrically.<sup>[194,195]</sup> The formed e<sup>-</sup><sub>aq</sub> can then be used to reduce the carbon atom of the HCN molecule under partial protonation of the nitrogen atom, like the steps suggested for the surface mediated reduction of HCN by mackinawite (4.2.4). The

formation of C – C bonds likewise follows from the nucleophilic attack of the CN<sup>-</sup> molecule onto an end-standing carbon atoms of an aldehyde or imine groups.

Both, the photoaquation and formation of a e<sup>-</sup><sub>aq</sub> are strictly limited to the presence of UV light. In the absence of light, the photoaquation reaction is reversed immediately, whereas the initially released CN<sup>-</sup> ions are again bound to form hexacyanoferrates. The release of e<sup>-</sup><sub>aq</sub> likewise stops when the light source is turned off. With the mackinawite supported reduction, a light independent release mechanism is presented. It was found that both [Fe(CN)<sub>6</sub>]<sup>3-</sup> into [Fe(CN)<sub>6</sub>]<sup>4-</sup>, as well as the [Fe(CN)<sub>5</sub>(NO)]<sup>2-</sup>, are reduced in the presence of mackinawite.

## 6.2 Results and Discussion

To test the stability of the hexacyanoferrate and nitroprusside in absence of iron or mackinawite, solutions were prepared, and the gas phase was investigated after 5 d. In samples that were reacted at pH 7 at room temperature and 80 °C no reaction products, as well as no released HCN, were observed. When the pH was lowered to 2, again no reaction occurred at room temperature. However, at 80 °C HCN was observed in the gas phase of the samples containing aqueous solutions of [Fe(CN)<sub>6</sub>]<sup>3-</sup> and [Fe(CN)<sub>6</sub>]<sup>4-</sup>. The total peak areas of the HCN signal for both substrates thereby are similar. In the gas phase of samples containing [Fe(CN)<sub>5</sub>(NO)]<sup>2-</sup> no comparable HCN signal was detected.

### 6.2.1 Iron

In the presence of iron powder, both [Fe(CN)<sub>6</sub>]<sup>3-</sup> and [Fe(CN)<sub>6</sub>]<sup>4-</sup> did not produce any reduced species at 80 °C, neither at pH 7 nor pH 2. When [Fe(CN)<sub>5</sub>(NO)]<sup>2-</sup> was used a new signal, corresponding to N<sub>2</sub>O appeared already at pH 7 (GP-22-01). At lower pH further reduced species were detected alongside increased amounts of N<sub>2</sub>O (GP-22-02). In Figure 56 the collected chromatograms from the gas phases after the reaction are displayed. The products observed in GP-22-02 could be identified as C<sub>1</sub> to C<sub>5</sub> hydrocarbons by comparing their mass pattern with the ones listed in the NIST 14 library. In Table A 5 the relative intensities of three separate samples are shown after 1, 3 and 6 d at 80 °C.



The formation of C – C bonds already proceeded after 1 day at 80 °C as C<sub>1</sub> to C<sub>5</sub> hydrocarbons were detected in the gas phase of GP-25-01. There, N<sub>2</sub>O was found to be the main product with 88 %. Among hydrocarbons, CH<sub>4</sub> was observed as major product, followed by C<sub>2</sub> and C<sub>3</sub> compounds. In the gas phase of GP-22-02, which was reacted for 3 d, a significant increase in C – C products was observed in comparison to CH<sub>4</sub>. The relative concentration in N<sub>2</sub>O was further found to decrease. In the gas phase of sample GP-25-02, again only small amounts of C – C hydrocarbons were detected, whereas a much higher CH<sub>4</sub> to N<sub>2</sub>O ratio was present.

In Figure 57 the TIC areas for N<sub>2</sub>O and hydrocarbons are compared over the different reaction times. The sample GP-25-01, which was analyzed after 1 d provides a comparably low CH<sub>4</sub>/N<sub>2</sub>O ratio of 0.06 in comparison to the ones analyzed after 3 (0.09) and 6 (0.27) d. This ratio, as well as the total amount of N<sub>2</sub>O, was found to significantly decrease with increasing reaction time. In GP-22-02, which was reacted for 3 d at 80 °C the ratio nearly reached a value of 1, whereas the levels of both N<sub>2</sub>O and CH<sub>4</sub> decreased in the gas phase.

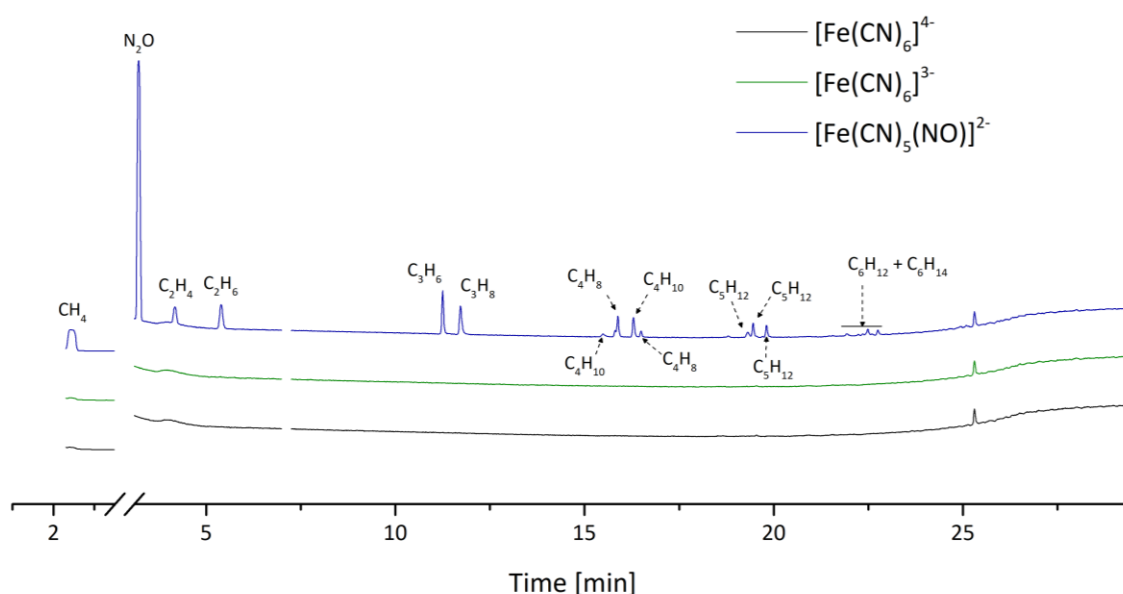


**Figure 56** Gas chromatograms (TIC) collected from the gas phases of GP-23-02 (black), GP-24-02 (green) and GP-25-02 (blue) after 6 d at 80 °C (pH 2).

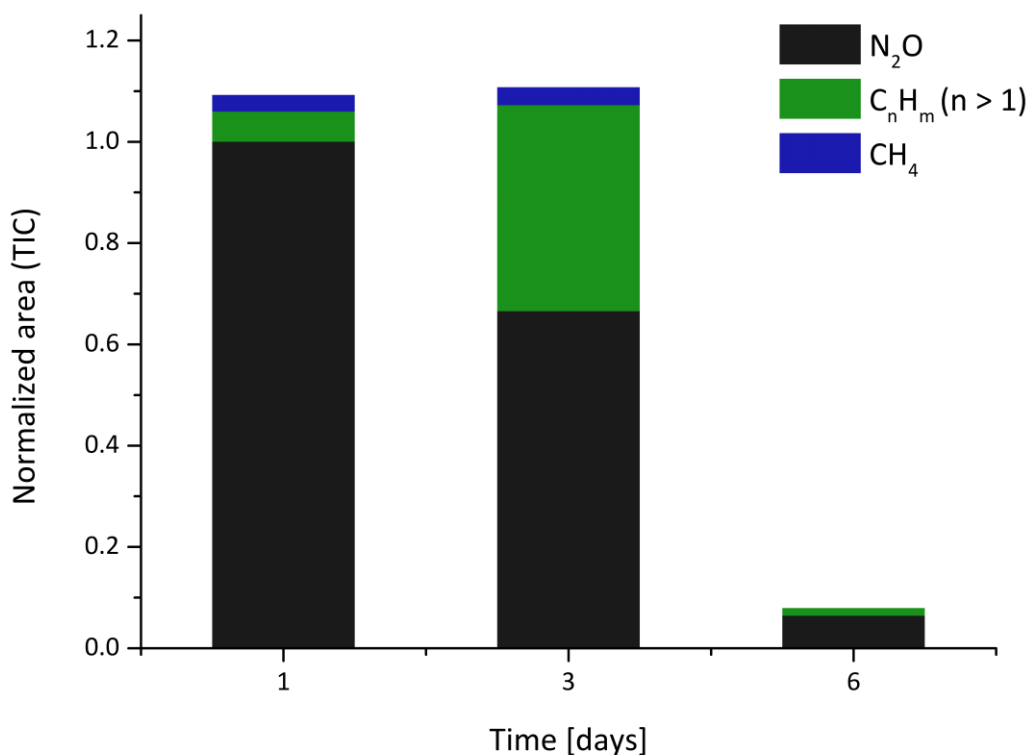


**Figure 57** TIC areas of N<sub>2</sub>O, CH<sub>4</sub> and longer hydrocarbons from GP-25-01 (1 day), GP-22-02 (3 days) and GP-25-02 (6 days).

### 6.2.2 Mackinawite

In the presence of mackinawite the array of products changed in respect to the reactions carried out with iron powder. Both, [Fe(CN)<sub>6</sub>]<sup>3-</sup> (GP-26-01) and [Fe(CN)<sub>6</sub>]<sup>4-</sup> (GP-27-01) showed no reaction in presence of iron, but led to the formation of 0.23 μmol and 0.27 μmol CH<sub>3</sub>SH, respectively, already after 1 day at 80 °C. Under the same conditions, the [Fe(CN)<sub>5</sub>(NO)]<sup>2-</sup> sample (GP-28-01) was shown to produce N<sub>2</sub>O, HCN and CS<sub>2</sub>. When the same reaction was carried out for 6 d, no reduced species were detected in the gas phase of GP-26-02 and GP-27-02. In GP-28-02, however, N<sub>2</sub>O was still detectable, but decreased by 88 % when compared to the signal after 1 day.

The formation of CH<sub>3</sub>SH from all three substrates was followed in a separate experiment over 188 h by subsequently extracting gas phase samples with a gas tight syringe. To estimate the yield of the reactions a CH<sub>3</sub>SH calibration curve was recorded by using the

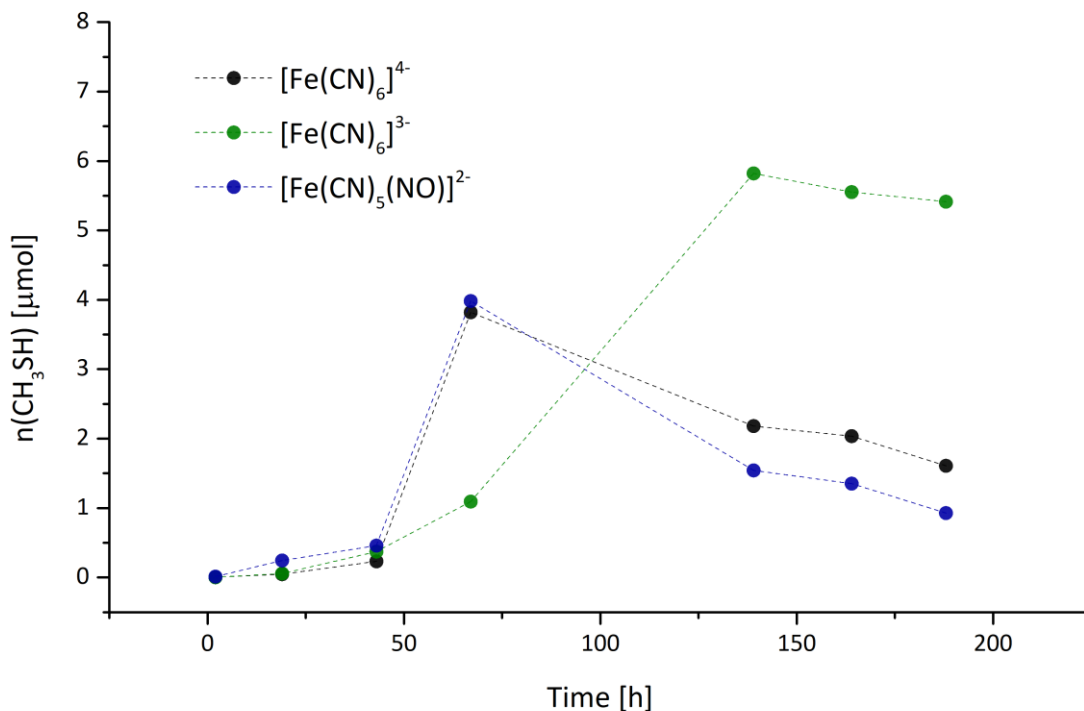


**Figure 58** Time dependent formation of CH<sub>3</sub>SH from [Fe(CN)<sub>6</sub>]<sup>4-</sup>, [Fe(CN)<sub>6</sub>]<sup>3-</sup> and [Fe(CN)<sub>5</sub>(NO)]<sup>2-</sup> supported by mackinawite (80 °C, pH 3). Calibrated by CAL-MT-5.

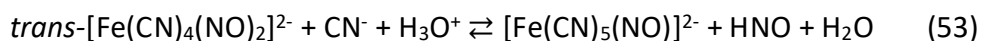
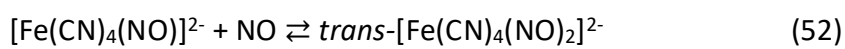
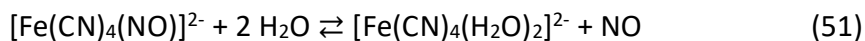
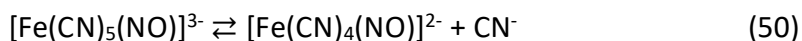
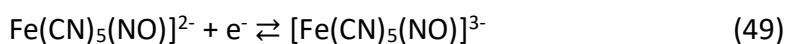
same extraction method. The summarized progress is displayed in Figure 58. The course for the samples containing [Fe(CN)<sub>6</sub>]<sup>4-</sup> (GP-29) and [Fe(CN)<sub>5</sub>(NO)]<sup>2-</sup> (GP-31) is very similar. Both first undergo an initial period, where only small amounts in CH<sub>3</sub>SH are formed. After 67 h a maximum concentration of 3.8 μmol and 3.9 μmol was recorded, respectively. Like the course during KCN reduction, the amount in CH<sub>3</sub>SH was further found only to decrease over the following days.

The course for the sample containing [Fe(CN)<sub>6</sub>]<sup>3-</sup> (GP-30) differed from the other two. The concentration in CH<sub>3</sub>SH was again found to only increase after an initial period of 2 d before a maximum of 5.8 μmol was reached. During the following days, the concentration only decreased slightly when compared to GP-29 and GP-31.

### 6.2.3 Mechanism

The reduced species observed during the experiments on metal cyanide complexes most likely were formed in analogy to the reduction of HCN. Samples containing both, [Fe(CN)<sub>6</sub>]<sup>3-</sup> and [Fe(CN)<sub>6</sub>]<sup>4-</sup> did not provide the formation of significant amounts in HCN

at pH 2 and 80°C. When  $[\text{Fe}(\text{CN})_5(\text{NO})]^{2-}$  was used, HCN was visible in the gas phase of multiple samples. The formation of hydrocarbons by **RS**<sub>1</sub> is therefore assumed to follow the mechanism formulated in 4.2.4.1. Under the same conditions the formation of N<sub>2</sub>O was observed. The N<sub>2</sub>O signal was further detected in  $[\text{Fe}(\text{CN})_5(\text{NO})]^{2-}$  samples that were reacted with **RS**<sub>3</sub>. In such, contrary to that containing iron, no significant amounts in hydrocarbons were formed. The reduction of  $[\text{Fe}(\text{CN})_5(\text{NO})]^{2-}$  leading N<sub>2</sub>O by dithionite was studied by Roncaroli et al. and described through the reactions 49 to 54.<sup>[254]</sup> In the experiments conducted in this thesis the iron powder and the mackinawite can similarly provide electrons for the initial reduction of  $[\text{Fe}(\text{CN})_5(\text{NO})]^{2-}$ .



The formation of CH<sub>3</sub>SH from all three substrates, which has been followed over time shows a similar course to the one recorded for the HCN reduction. The reduction of the iron cyanide complexes however showed decreased yields in the formation of CH<sub>3</sub>SH and therefore are assumed to undergo a primary release of an HCN molecule by reaction 50. During the control experiments conducted in the presence of iron or mackinawite, both hexacyanoferrate complexes released HCN at lower pH values. Once free, the HCN can then be reduced by the mechanism formulated in 4.2.4.1 in the case of an iron or 4.2.4.2 a mackinawite supported reaction. This can further be supported as separate experiments, where the gas phase was extracted by a transfer line. In addition to CH<sub>3</sub>SH, also other known reaction products like CH<sub>4</sub>, CH<sub>3</sub>CHO, CS<sub>2</sub> or C<sub>2</sub>H<sub>5</sub>SH were observed in the gas phase.

### 6.3 Summary

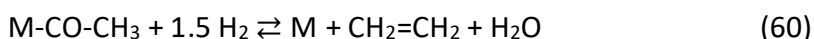
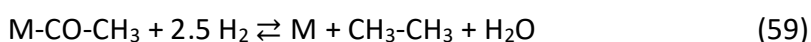
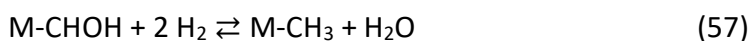
The mobilization of iron cyanide complexes by iron or mackinawite was shown to proceed readily under prebiotically relevant conditions of 80 °C in aqueous media. The reaction was found to be highly limited by the availability of free protons. At pH 7, no reduced species were formed by both systems, **RS<sub>1</sub>** and **RS<sub>3</sub>**. When the pH was lowered, both systems produced reduced species either from  $[\text{Fe}(\text{CN})_6]^{3-}$ ,  $[\text{Fe}(\text{CN})_6]^{4-}$  or  $[\text{Fe}(\text{CN})_5(\text{NO})]^{2-}$ . Iron only reacted with  $[\text{Fe}(\text{CN})_5(\text{NO})]^{2-}$  and gave an array of hydrocarbons with chain lengths up to five carbon atoms. In the presence of iron, no reduced species were detected when  $[\text{Fe}(\text{CN})_6]^{3-}$  or  $[\text{Fe}(\text{CN})_6]^{4-}$  were used.

In the presence of mackinawite all three substrates were converted into  $\text{CH}_3\text{SH}$  and small number of other compounds like  $\text{CH}_4$  and  $\text{CS}_2$ . In the case of  $[\text{Fe}(\text{CN})_5(\text{NO})]^{2-}$ ,  $\text{N}_2\text{O}$  was additionally formed from both, the reaction with iron and mackinawite. In nature a similar reaction is reported where NO is reduced to  $\text{N}_2\text{O}$  in Cytochrome c dependent nitric oxide reductase.<sup>[255]</sup> When the  $\text{CH}_3\text{SH}$  formation was followed over 188 h, a similar course as for the reduction of KCN and KSCN was observed. The highest concentration in  $\text{CH}_3\text{SH}$  with 5.82  $\mu\text{mol}$  was observed for the  $[\text{Fe}(\text{CN})_6]^{3-}$  sample after 139 h. The two other samples reached their maximum after 67 h with 3.82  $\mu\text{mol}$  in the case of  $[\text{Fe}(\text{CN})_6]^{4-}$  and 3.98  $\mu\text{mol}$  in the case of  $[\text{Fe}(\text{CN})_5(\text{NO})]^{2-}$ . The reduction of the CN-ligands probably follows from the initial release as HCN, which then can be reduced following the mechanism in 4.2.4.1.

## Chapter 7. Adsorption and reduction of carbon oxides

### 7.1 Introduction

The reduction of CO<sub>2</sub> by the Fischer-Tropsch synthesis was first established in 1925.<sup>[256]</sup> In the following years it became the most important process to produce fuels from non-petroleum sources. The reaction between CO<sub>2</sub> and H<sub>2</sub> is performed at 150 – 300 °C and pressures up to 25 bar in presence of a metal catalyst like iron or cobalt. The CO is formed by the water gas shift reaction thereby acts as the key intermediate in the formation of hydrocarbons by a stepwise growing mechanism. The reaction mechanism was readily discussed in the past and is still not fully resolved. The most established one is the direct reduction mechanism where the CO is hydrogenated and C – C bonds are formed upon insertion of a CO molecule in between the M – C bond:



In context of primordial processes, the carbon fixation from CO<sub>2</sub> is undoubtedly the most interesting and important step to explain the transition of an inorganic towards an organic world. Until now, only a few abiotic processes for the reduction of CO<sub>2</sub> are known. A more recent example for a successful reduction of CO<sub>2</sub> by mixed metal phases like awaruite (Ni<sub>3</sub>Fe) was reported by Preiner et al. who observed the formation of format, acetate, pyruvate and methanol in aqueous media at 100 °C.<sup>[257]</sup> The reaction was carried out in presence of H<sub>2</sub> and therefore follows the Fischer-Tropsch reaction. In

contrast to the ISWT the H<sub>2</sub> is thereby not produced from the iron sulfide, but rather by the serpentinization reaction (1.1.2.4).

Though, no clear evidence for the direct reduction of CO<sub>2</sub> into hydrocarbons by iron under ambient conditions were presented until now, Cvetković et al. provided evidence for the anoxic corrosion of steel by carbon contaminations. They could show that this process produces reduced compounds like CH<sub>4</sub> and C<sub>2</sub>-C<sub>4</sub> hydrocarbons, as well as oxygenated species like formate, acetate, and oxalate.<sup>[258]</sup> The formation of hydrocarbons from the reduction of trichlorethylene was thereby furthermore shown by Deng et al..<sup>[259]</sup>

## **7.2 Results and Discussion**

### **7.2.1 Adsorption of CO<sub>2</sub>**

The ability of mackinawite to bind CO<sub>2</sub> from the atmosphere was studied by monitoring the CO<sub>2</sub> concentration in the headspace of samples, using a methanizer. In a first experiment, a mackinawite sample, prepared under Ar atmosphere, was let in contact with air when being scaled (AD-01-01). A second sample (AD-01-02) was handled strictly under inert conditions to exclude any oxidation by O<sub>2</sub> from the air. Before gas phase samples were extracted the headspace of AD-01-01 was exchanged with Ar. When AD-01-01 and AD-01-02 were stored at 75 °C for 1 hour, the gas phases contained 342 ppm and 3.22 ppm CO<sub>2</sub>, respectively. The significant increase in CO<sub>2</sub> concentrations in the gas phase of the deactivated sample implies that some of the CO<sub>2</sub> from the air was adsorbed during the scaling process. Furthermore, the low levels in CO<sub>2</sub> received for AD-01-02 rule out any initial contamination of the starting material. When further 250 µL of CO<sub>2</sub> were injected into the vials, the concentration was found to increase by 156 ppm and 271 ppm for AD-01-01 and AD-01-02, respectively.

The adsorption of CO<sub>2</sub> could furthermore be shown to be insignificantly influenced in presence of H<sub>2</sub>O, only. For that the samples AD-02-01 to AD-02-04 were charged with 250 µL of CO<sub>2</sub>. After 3 mL of H<sub>2</sub>O were added to one of the control samples (AD-02-04) CO<sub>2</sub> levels of 216 ppm and 244 ppm were observed for AD-02-03 and AD-02-04,

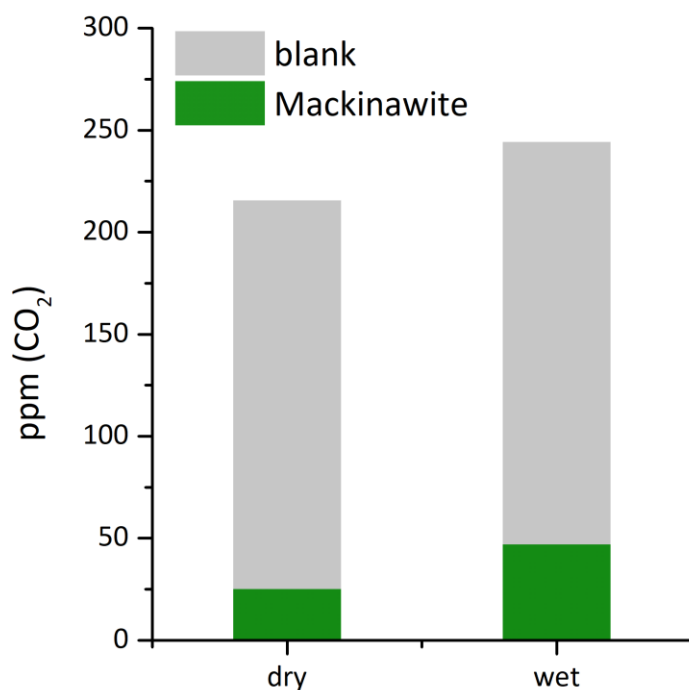


**Figure 59** Concentration of the remaining CO<sub>2</sub> in the gas phase of mackinawite samples under dry (AD-02-01) and wet (AD-02-02) conditions with the respective dry (AD-02-03) and wet (AD-02-04) blanks.

respectively. The gas phase extracted from samples containing mackinawite showed a much lower amount in CO<sub>2</sub>. In the absence of H<sub>2</sub>O, the gas phase of AD-02-01 was found to only provide 25 ppm CO<sub>2</sub>. When H<sub>2</sub>O was present (AD-02-02) the CO<sub>2</sub> level in the gas phase was found to be slightly elevated with 46 ppm (Figure 59). Both samples AD-02-02 and AD-02-04 show, that the amount of CO<sub>2</sub> in the gas phase is not significantly influenced by the presence of H<sub>2</sub>O. The slight increase in CO<sub>2</sub> levels probably is a result of the decreased gas phase volume.

In a third experiment, mackinawite prepared by precipitation (AD-03-01) was compared to the one from the reaction between iron and sulfur (AD-03-02). Therefore, two samples, together with a control, were monitored upon the subsequent addition of CO<sub>2</sub> (Figure 60, left). After 100 μL CO<sub>2</sub> were added, the control was found to contain 63 ppm of CO<sub>2</sub>, whereas the mackinawite samples only contained 3.43 ppm in the case of AD-03-01 and 13.28 ppm in the case of AD-03-02. While the CO<sub>2</sub> concentration increased in both the control and AD-03-01 upon addition of another 100 μL, the gas phase of AD-03-02 even showed a slight decrease of CO<sub>2</sub> after 300 μL were added. The mackinawite from the reaction between iron and sulfur further showed lower concentrations in CO<sub>2</sub> when compared to the other samples after supplying 300 and 400 μL but reached a CO<sub>2</sub> concentration comparable to the control and AD-03-01 after 500 μL were added.



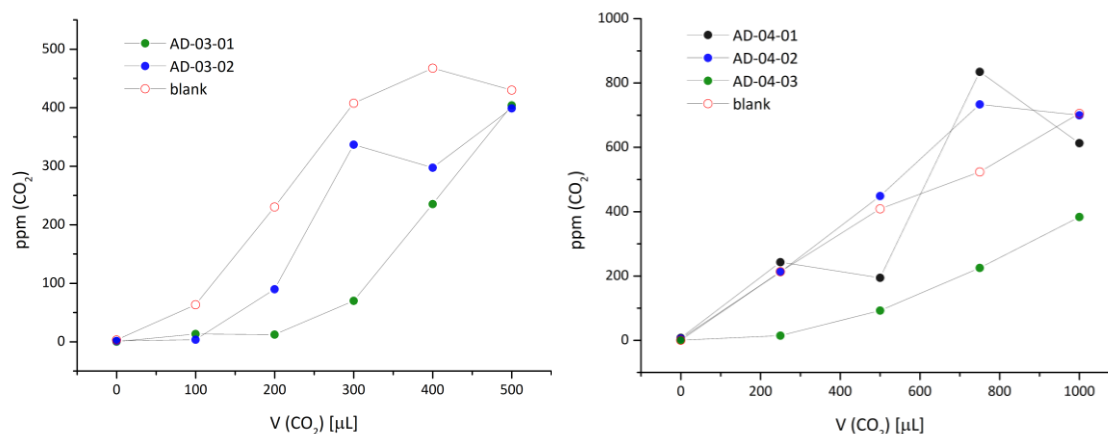


**Figure 60** Course of the CO<sub>2</sub> concentration after subsequent injection of 100 μL (**left**) or 250 μL (**right**) CO<sub>2</sub> to samples either containing mackinawite from iron and sulfur (AD-03-01 and AD-04-03) or from precipitation (AD-03-02 and AD-04-02). Sample AD-04-01 contained mackinawite from the elements that was left in contact with air.

The experiment was repeated whereas in each case 250 μL of CO<sub>2</sub> were added until a total amount of 1 mL was supplied (Figure 60, right). After adding the CO<sub>2</sub> and leaving the samples at room temperature for 1 hour, decreased CO<sub>2</sub> concentrations for AD-04-03 were observed. After the injection of the first 250 μL, the gas phase of AD-04-02 contained 212 ppm which is comparable to the control (213 ppm). As observed during the previous experiment, the gas phase of a sample containing mackinawite from the reaction between iron and sulfur (AD-04-03) showed significantly decreased level in CO<sub>2</sub> with only 14 ppm. In contrast to AD-03-01, however, a continuous increase in CO<sub>2</sub> levels was observed for all samples upon further addition of CO<sub>2</sub>.

**Table 9** Comparison between AD-02-01 and AD-04-03. The amount of adsorbed CO<sub>2</sub> ( $n_{ad,calc.}$ ) is estimated by subtraction the CO<sub>2</sub> concentration of the mackinawite containing samples from ones where no mackinawite was present (blank).

ID	V (CO <sub>2</sub> ) [μL]	n (CO <sub>2</sub> ) [μmol]		$n_{ad,calc.}$ [μmol]
		blank	mackinawite	
AD-02-01	250	11.3	1.3	10.0
AD-04-03	250	11.2	0.8	10.4

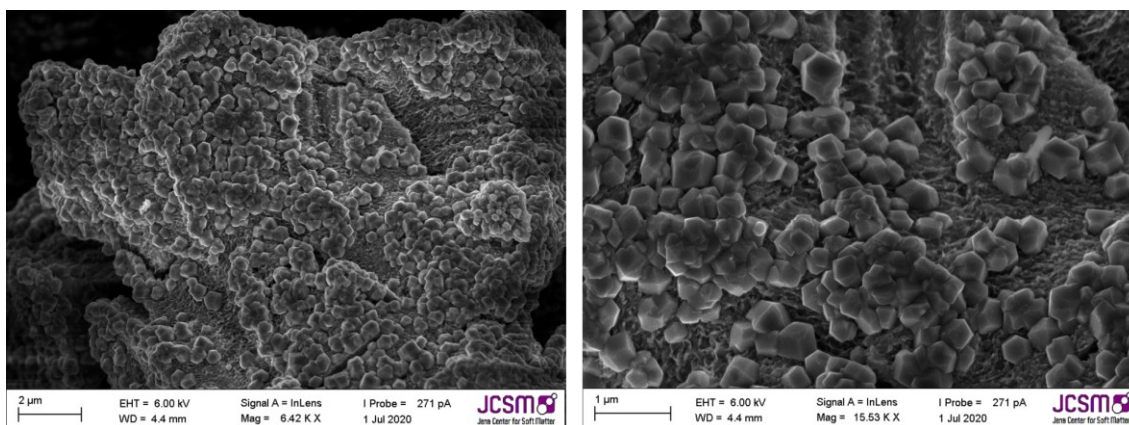


**Figure 61** SEM images of a mackinawite sample that was stored under 100 % CO<sub>2</sub> atmosphere for several weeks (SP-FeS-12). The surface significantly underwent chemical changes as highly defined cubic crystals formed.

The adsorption of CO<sub>2</sub> by mackinawite synthesized from iron and sulfur was observed when the freshly prepared samples were additionally washed with H<sub>2</sub>O and strictly handled under anoxic conditions. When O<sub>2</sub> was present during sample preparation, a significantly lowered capability to adsorb CO<sub>2</sub> results from the deactivation process, described in 3.2.6. As soon as the passivating layer is formed, the CO<sub>2</sub> molecules are not able to interact with the mackinawite surface (groups) anymore. Further evidence for this kind of reactivity can be provided from TEM images obtained from a sample that was stored under 100 % CO<sub>2</sub> atmosphere for 1 week at 80 °C. In contrast to a deactivated sample, the interaction with CO<sub>2</sub> led to the formation of a new solid phase on top of the mackinawite particles (Figure 61). The newly formed phase form well defined cubes on top of the partly deactivated mackinawite surface. Similar structures were previously reported by Lan et al. after H<sub>2</sub>S was reacted with mackinawite that was fixated on a polymer.<sup>[217]</sup> Though the surface was smoothed by the partial oxidation, the faint structure of the curved platelets is still visible. When the respective PXRD pattern was collected, the observed reflexes could be assigned to mackinawite, greigite and siderite (Figure A 176). The mackinawite signals still appear broadened, like in the PXRD pattern of the deactivated sample (SP-FeS-04), whereas the core of the particles is assumed to be still intact. The oxidation only took place at the surface until a thin passivating layer of greigite was formed. This, in consequence, would restrict any further interaction between CO<sub>2</sub> and the still reactive core of the particles.

## 7.2.2 Reduction of CO<sub>2</sub> and CO

The reduction of CO<sub>2</sub> and carbon monoxide was studied using the reduction systems **RS<sub>2</sub>** and **RS<sub>3</sub>**, both at pH 3. In both cases, H<sub>2</sub>S<sub>2</sub>, CH<sub>3</sub>SH, C<sub>2</sub>H<sub>5</sub>SH, C<sub>3</sub>H<sub>7</sub>SH, C<sub>4</sub>H<sub>9</sub>SH, <sup>t</sup>C<sub>4</sub>H<sub>9</sub>SH and (CH<sub>3</sub>)C<sub>3</sub>H<sub>6</sub>SH, were detected in the gas phase. While CS<sub>2</sub> appeared during the reduction of KCN, it was not observed after the reduction of CO<sub>2</sub> and CO. Furthermore, no significant amounts in hydrocarbons were produced. In general, **RS<sub>2</sub>** was found to lead to significantly higher amounts in reduced species under the applied conditions. The product distribution significantly changed whereas **RS<sub>2</sub>** or **RS<sub>3</sub>** was used. In the presence of mackinawite, H<sub>2</sub>S<sub>2</sub> became the main product, followed by CH<sub>3</sub>SH and other thiols in minor amounts. When the iron sulfur mixture was used, CH<sub>3</sub>SH production increased, whereby H<sub>2</sub>S<sub>2</sub> was only detected in minor amounts (Figure A 161 - 167).

The concentrations in CH<sub>3</sub>SH were calculated based on the calibration curve received from CAL-MT-1 and are given in Table A 6. The reduction of both CO (GP-32) and CO<sub>2</sub> (GP-33) by **RS<sub>2</sub>** resulted in CH<sub>3</sub>SH levels of 92.3 μmol and 122.8 μmol. When the initial CO<sub>2</sub> concentration is calculated under standard conditions, this relates to a yield of 41 % and 55 %, respectively. For the labelled samples GP-32-02 and GP-33-02 similar yields in non-labeled products were observed. When **RS<sub>3</sub>** was used, much lower amounts in CH<sub>3</sub>SH were detected. In the case of CO (GP-35), the sample containing <sup>12</sup>CO still showed a high yield with 20 %, but it was found to significantly decrease to 6 % when <sup>13</sup>CO was used. The CO<sub>2</sub> samples (GP-36) reacted with **RS<sub>3</sub>** showed comparable amounts in CH<sub>3</sub>SH.

Though, labelled substrates were used, no isotopic shifts for the products were observed. In case of the CO<sub>2</sub> experiments, the corresponding <sup>13</sup>CO<sub>2</sub> signal was detected with *m/z* = 45. Due to the low efficiency of the column to separate small gases, no corresponding signal for <sup>13</sup>CO was observed. The thiols thereby could have originated from the carbon contaminations on the iron powder. Inconsistencies in the reduction of labelled carbon substrates are known in the literature. Only recently, Sobotta et al. reported the formation of oxygenated C<sub>1</sub> to C<sub>5</sub> compounds from the reduction of CO by NiS but did only partly observe the respective carbon shifts.<sup>[129,260]</sup> A similar observation was made by Miller et al. who studied the interactions of CO<sub>2</sub> and CO with iron and iron oxide surfaces. They concluded that the clean iron surface is readily coated with a

hydroxide layer when let in contact with air.<sup>[261]</sup> On top of that a second carbon layer is formed upon the reaction with CO<sub>2</sub>. Thereby, the interaction of the surface with the labelled substrate is restricted and only reduced, non-labelled, products are detected. The property to adsorb CO<sub>2</sub> from the air does not only apply to pure metal phases but can also be observed when iron containing graphite is used. In their attempt to evaluate the influence of atmospheric CO<sub>2</sub> on samples prepared for accelerated mass spectrometry (AMS), Paul et al. reported an increased affinity of the graphitization product to react with CO<sub>2</sub> when it contained iron carbides. These are remnants of the graphitization process where the samples first are combusted into CO<sub>2</sub> before being reduced into graphite by a metal catalyst. After they removed the iron carbides by hydrogenation, no further ability to bind CO<sub>2</sub> was observed.<sup>[262]</sup>

During the experiments on the CO<sub>2</sub> and CO reduction the iron powder was not further pretreated. At this point of the thesis possible contaminations were assumed to be lost into the aqueous or gas phase as the formation of mackinawite requires the iron particles to get fully dissolved. Preexisting contaminations could however be either transported together with the iron ions onto the sulfide end groups or be adsorbed by the newly formed mackinawite surface (groups) and thereby restricted the labelled substrate to be reduced.

### **7.2.3 Reduction of CO<sub>3</sub><sup>2-</sup>**

The experiments concerned with the reduction of CO, CO<sub>2</sub> or CO<sub>3</sub><sup>2-</sup> by mackinawite showed quite inconsistent results. This matter was readily discussed over the course of this thesis as reduced carbon compounds did appear in the gas phase of samples, but for a long time no isotopic shifts were observed. As small amounts of un-labelled species appeared more than less under any applied conditions, it was seen as a necessity to show the carbon shift to support the idea of a mackinawite supported carbon fixation from carbon oxides. Experiments with D<sub>2</sub>O and acid, as they were performed by Heinen et al. did not proof the origin of the carbon source.<sup>[9,206]</sup>

The first observation of labelled CH<sub>3</sub>SH from the reaction between mackinawite and Na<sub>2</sub>CO<sub>3</sub> could be provided by my college R. Bolney.<sup>[88]</sup> He observed the formation of isotopically labelled CH<sub>3</sub>SH after heating the Na<sub>2</sub><sup>13</sup>CO<sub>3</sub> saturated mackinawite after

boiling for 3 h. In consequence of the used method,  $\text{CH}_4$  could not be observed. Furthermore, other experiments indicated, that  $\text{CH}_3\text{SH}$  and  $\text{CH}_4$  already formed, when much lower temperatures were applied. The reduction of  $\text{Na}_2^{13}\text{CO}_3$  to both  $\text{CH}_4$  and  $\text{CH}_3\text{SH}$  supported by mackinawite was finally observed for the samples GP-09-01 and GP-09-02. In contrast to standard samples, the mackinawite was here left compressed at the bottom of the vial before the excess  $\text{H}_2\text{O}$  was removed and the  $\text{Na}_2\text{CO}_3$  solution slowly introduced in a manner where the solid cake would not be destroyed. The acid (1 M, 0.5 mL) was introduced in the same manner and the samples were left in the hood overnight. After 24 h again 0.5 mL of acid were added, and the gas phase was extracted after another 24 h. In Figure 62 the normalized areas for the reduced species, together with the ones obtained from samples containing only mackinawite, are summarized. The reactions were carried out at room temperature at pH 3. The pH was adjusted by subsequently adding 0.5 mL of the 1 M  $\text{H}_2\text{SO}_4$  over 2 d. After the second portion was added, the gas phase was extracted by the method using a transfer line. Both gas phases extracted from GP-09-01 and GP-09-02 were found to already contain reduced species providing the expected isotopic shifts.

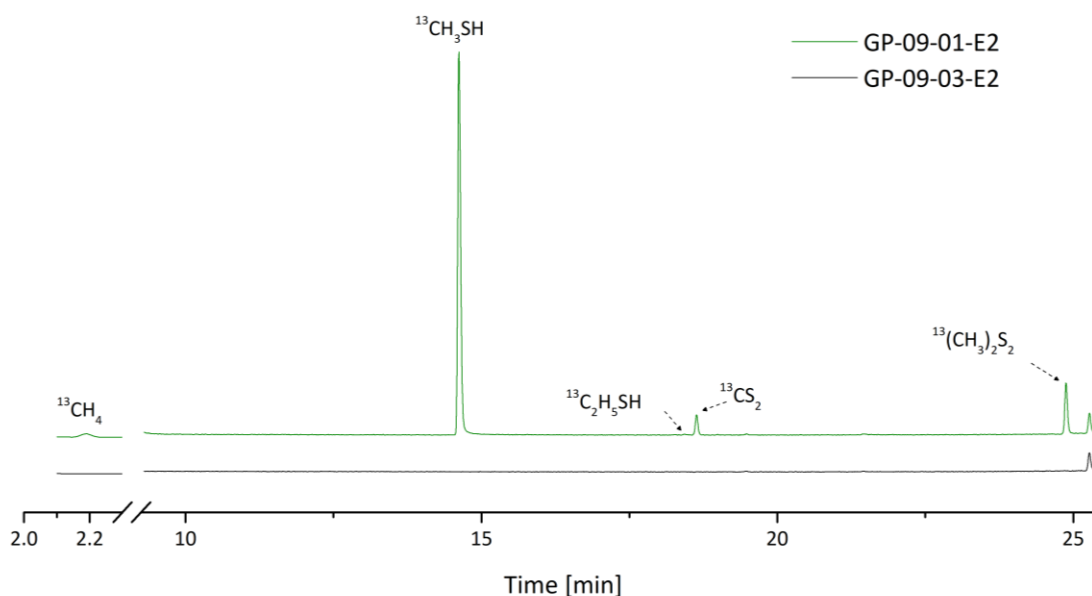


**Figure 62** Gas chromatogram (TIC) collected from the gas phase of GP-09-01 and GP-09-03 after 2 d at 80 °C.

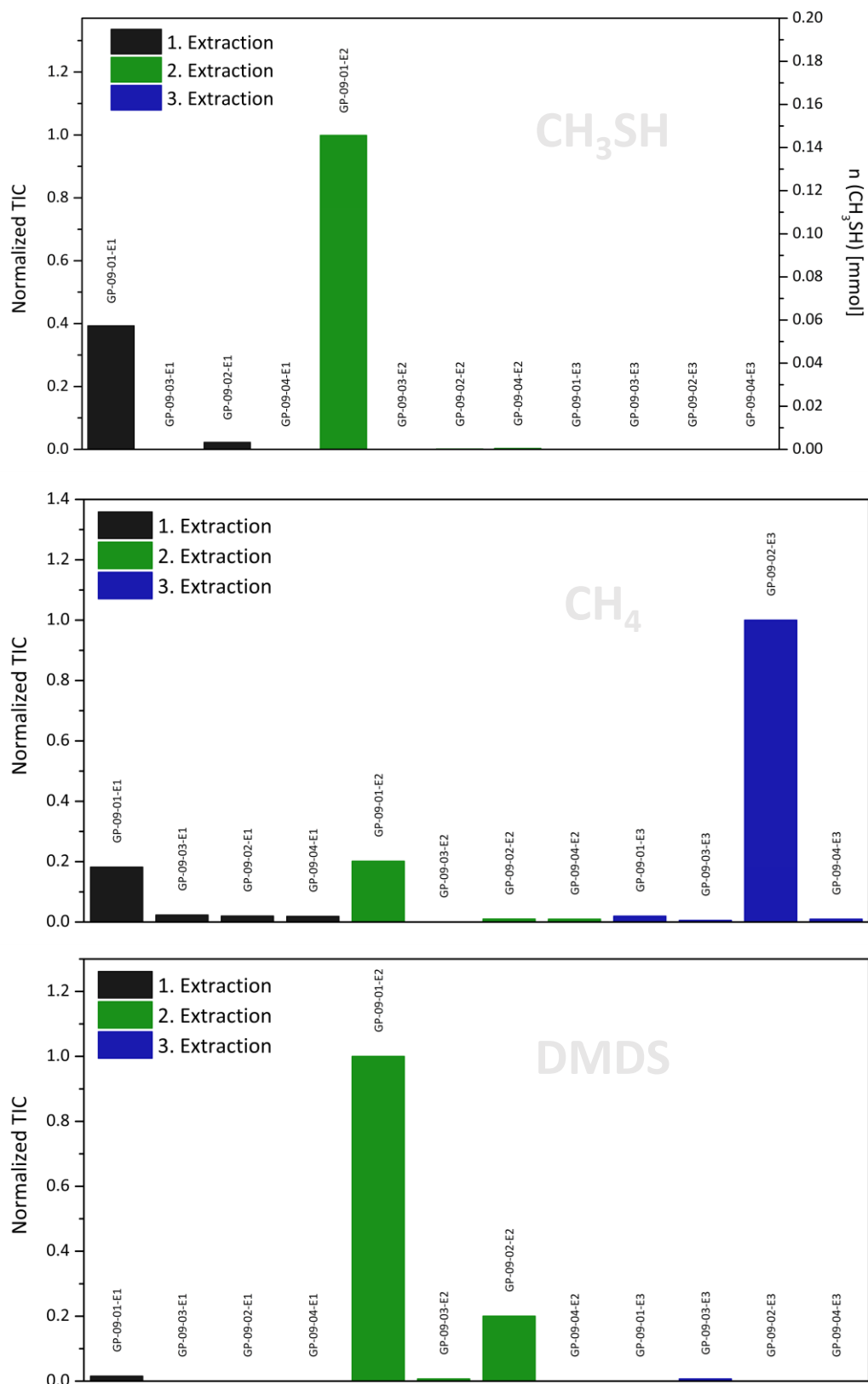


**Figure 63** Comparison of the amount in CH<sub>4</sub>, CH<sub>3</sub>SH and H<sub>2</sub>S during the subsequent gas phase extractions. Between each extraction 1 mL of a 1 M H<sub>2</sub>SO<sub>4</sub> was added.

By applying CAL-MT-2, a maximum yield of 57.35  $\mu\text{mol}$  of  $\text{CH}_3\text{SH}$  was calculated for GP-09-01, whereas the controls both provided yields  $> 0.1$  Mmol. The normalized areas derived from the TIC are displayed in Figure 63. Each sample is followed by the blank experiment. For GP-09-02 only low yields in reduced compounds were observed, however, the respective mass patterns were fully or partly shifted. After the gas phase was extracted, the samples were again charged with 1 mL of acid and heated at 80 °C or boiling for 2 d. In the gas phase of GP-09-02 (boiling) still no significant amounts in reduced compounds were formed. The gas phase of GP-09-01 (80 °C) on the other side contained 145.7  $\mu\text{mol}$  of  $\text{CH}_3\text{SH}$  and significantly increased levels in  $(\text{CH}_3)_2\text{S}_2$ . The samples were then again charged with 1 mL of acid and heated again for 1 day. Only the gas phase of GP-09-02 still contained  $\text{CH}_4$ , while no reduced species were released in the other samples. The collected mass pattern, however, was only partly shifted with a relative intensity of 19.45 % for the  $m/z = 17$  signal. After a total of three extractions GP-09-01 showed a yield in  $^{13}\text{CH}_3\text{SH}$  of 20.30 % as 1 mmol of  $\text{Na}_2^{13}\text{CO}_3$  was supplied (Table A 7). When the formation of  $(\text{CH}_3)_2\text{S}_2$  and  $\text{CH}_4$  are counted in, the total yield in reduced

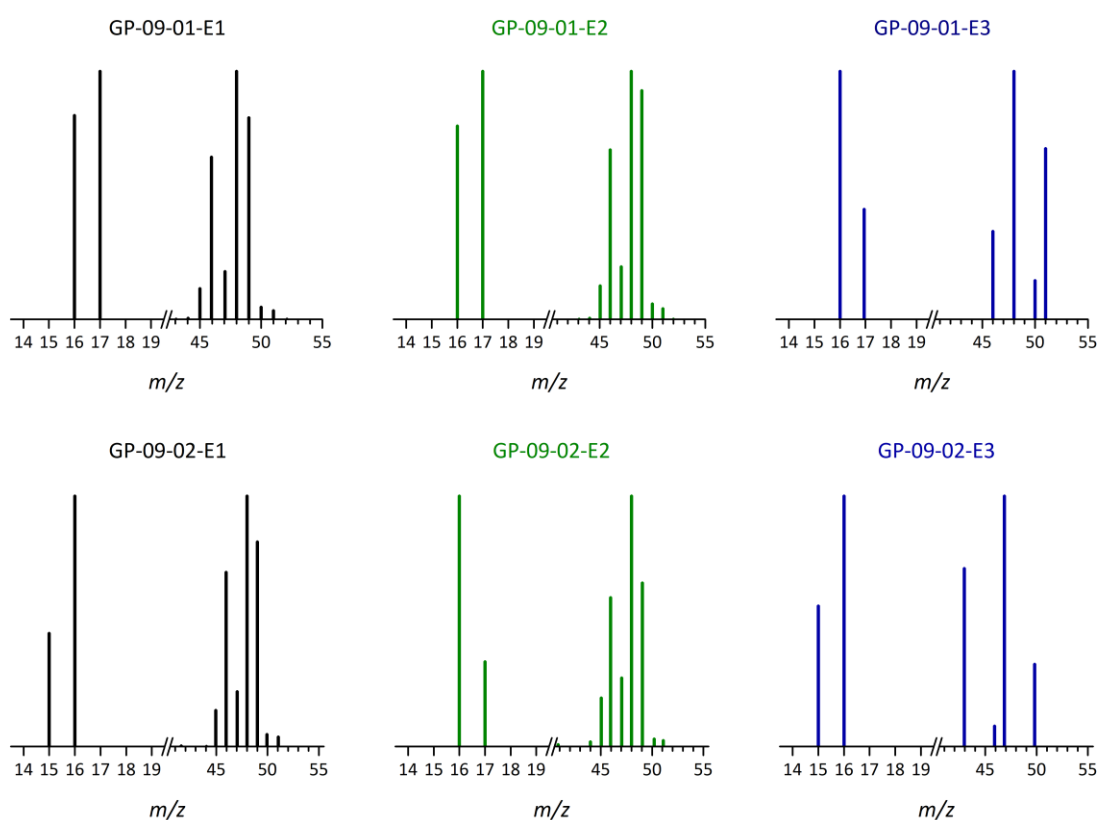


**Figure 64** Mass patterns of the  $\text{CH}_4$  signals from GP-09-01 and GP-09-02 recorded after the first (E1), second (E2) and third (E3) extraction.

species, based on the total TIC areas, correspond to 26.54 % for GP-09-01 and to 2.78 % for GP-09-02.

The CH<sub>4</sub> signal was present in all samples and can therefore, in parts, be assumed to origin from the carbon contaminations from the iron powder. In the samples GP-09-01 and GP-09-02, however a significant increase in the  $m/z = 17$  peak was observed. Following Figure 64, the  $m/z = 17$  peak in GP-09-01 appears with a relative intensity of 100 %. Though the mass peak of  $m/z = 17$  (28.03 %) is present in the chromatogram collected from the gas phase of GP-09-02, the  $m/z = 16$  peak appeared with a relative intensity of 100 %. Both samples, GP-09-01 and GP-09-02, were prepared in the same manner, but showed significant differences in the total amount formed and the observed isotopic ratio for the CH<sub>4</sub> signal. In contrast to the mass pattern of CH<sub>4</sub>, the one corresponding to the CH<sub>3</sub>SH showed the expected isotopic shifts of +1 (Figure 64). In the samples where no substrate was supplied, still a CH<sub>3</sub>SH signal was observed and probably arises from the contaminated iron powder. Accordingly, no isotopic shifts were observed.

#### 7.2.4 Reduction mechanism

The reduction of CO, CO<sub>2</sub> and CO<sub>3</sub><sup>2-</sup> can, like with the previous substrates, follow from the nucleophilic attack of the MCS<sub>DP</sub>. The procedure is summarized in Figure 65 for the CO<sub>3</sub><sup>2-</sup> molecule. If sufficient protons are available, the -C(OH)<sub>3</sub> residue can be fully protonated, whereas a H<sub>2</sub>O molecule is released. The reduction of the -COOH residue leads to one resembling an aldehyde, already formulated during the reduction of KCN (4.2.4.1). After a second reduction step a first branching point appears where either a third reduction leads to the formation of a methyl species or H<sub>2</sub>S can attack to form a methyl-thiol residue. Latter can be released as CH<sub>3</sub>SH after the last two electrons are supplied. The methyl residue can further be reduced, leading to the formation of CH<sub>4</sub>, or undergo a ligand exchange with H<sub>2</sub>S, already discussed in 4.2.4.1, and again lead to the formation of CH<sub>3</sub>SH. This mechanism is, however, not fully resolved as no intermediate species was identified until now.

Here, CS<sub>2</sub> probably also formed from the reaction of CO<sub>2</sub> with H<sub>2</sub>S by reaction 13. It could, however, simultaneous be formed at mackinawite surface sites where electrons



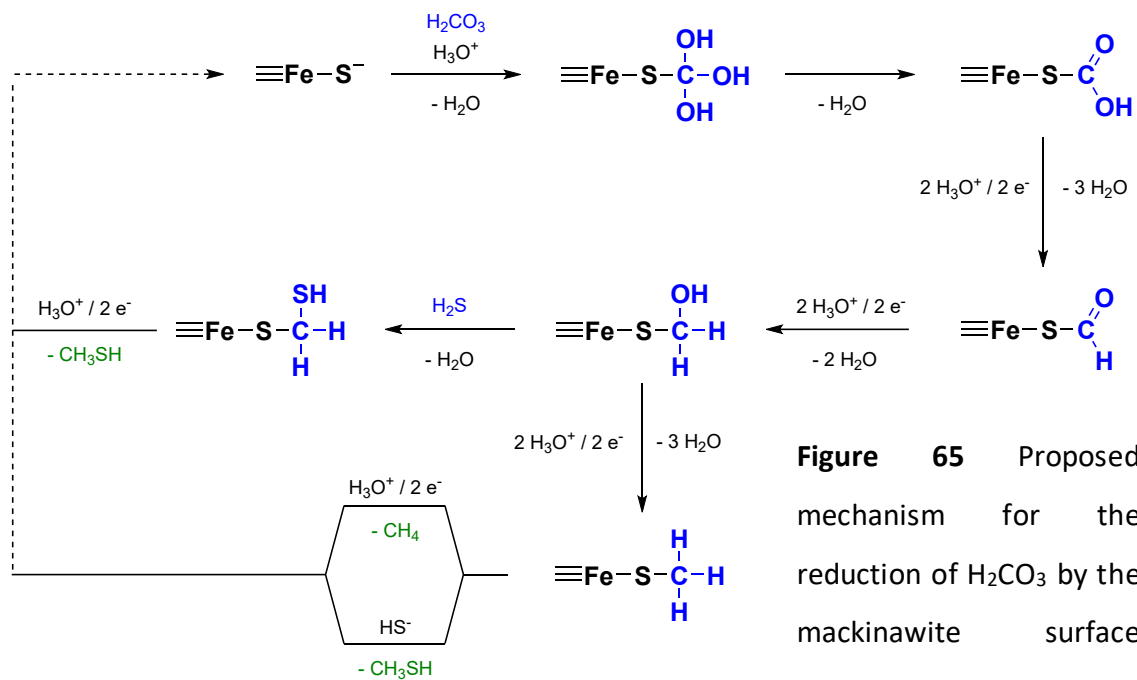


**Figure 65** Proposed mechanism for the reduction of  $\text{H}_2\text{CO}_3$  by the mackinawite surface groups.

are limited. There  $\text{H}_2\text{S}$  would promote the scission of the C – O bond in terms of a ligand exchange under the formation of C – S bonds. This reaction is independent of electrons and protons and could therefore significantly contribute to the formation of  $\text{CS}_2$  in these experiments. The  $(\text{CH}_3)_2\text{S}_2$  is most likely again formed through the oxidation of two  $\text{CH}_3\text{SH}$  molecules and does therefore not proceed on the surface of the mackinawite. This is further supported by the observation that  $(\text{CH}_3)_2\text{S}_2$  only appears in the gas phase when enough  $\text{CH}_3\text{SH}$  has been formed.

### 7.3 Summary

The adsorption of  $\text{CO}_2$  by mackinawite was studied using a methanizer and found to proceed under ambient conditions. When wet and dry mackinawite samples were supplied with a limited amount of  $\text{CO}_2$ , the total concentration in  $\text{CO}_2$  in the gas phase was significantly lower than in samples where either no mackinawite or deactivated mackinawite was used. When precipitated mackinawite was used only inconsistent results were achieved. In the first experiment a slight decrease in  $\text{CO}_2$  was observed, whereas the second experiment did not provide any evidence for  $\text{CO}_2$  adsorption for precipitated mackinawite. The one produced by the reaction of iron and sulfur possesses smaller surface areas than the ones reported for precipitated mackinawite. The size of

the particles, together with possible effects from the bulk material seemingly are influencing the absorption properties.

The reduction of CO and CO<sub>2</sub> resulted in reduced compounds in the gas phase, however, no carbon shifts were observed when labelled substrates were supplied. The exact reason for the here observed inconsistencies may also occur due to the carbon contaminations on the iron powder. During this experimental series further samples containing NaCN and Na<sup>13</sup>CN were investigated. The isotopic shifts were observed only for some of the CN<sup>-</sup> samples, even when the same iron powder was used. A fully shifted mass pattern was observed in the case of GP-04-05 and GP-34-02, but not GP-37-02. The shifts therefore only appeared when **RS**<sub>2</sub> was used to reduce KCN. It is to assume, that free CN<sup>-</sup> ions can interact with the iron surface and change places with the carbon contaminations. Through this, the CN<sup>-</sup> is reduced in presence of protons instead of the initially bound carbon and mass shifted thiols are produced. Due to the findings in 4.2, the reaction between mackinawite and CN<sup>-</sup> should also lead to the formation of CH<sub>3</sub>SH. In GP-37-02, however only small amounts of labelled CH<sub>3</sub>SH, when compared to GP-34-02, were detected.

The fully shifted mass patterns for both CH<sub>4</sub> and CH<sub>3</sub>SH could be observed in the gas phase of samples containing Na<sub>2</sub><sup>13</sup>CO<sub>3</sub>, already at room temperature. Like the mass patterns detected during the reduction of CO and CO<sub>2</sub>, however, not all appeared fully shifted. While all the CH<sub>3</sub>SH signals provided a shift of +1, unexpectedly the CH<sub>4</sub> patterns only were shifted in one of two samples. In the case of the sample with the partly shifted pattern, the relative intensity of the  $m/z = 17$  peak increased upon heating from 29.74 % to 68.89 %. In conclusion, it can be assumed that the labelled substrate must compete with the surface bound contaminations and is only let to react after those are removed. This consequently means, that the products observed during the reduction of CO and CO<sub>2</sub> most likely were formed from carbon contaminations on the iron powder. It is noteworthy that a similar array of products was reported by Heinen and Lauwers.<sup>[9,206]</sup> They did not provide any analytical data on the used iron sulfide and further were not able to show the carbon shifted products. It must be assumed, that similar carbon contaminations led to the products in their experiments.

## Chapter 8. Consequences for prebiotic models

### 8.1 Introduction

#### 8.1.1 The chemical composition of the early earth

The formation of rocky planets like ours can still be observed throughout the universe and therefore provides us with crucial information on the historical chemical composition of the earth itself. The starting conditions are highly important to trace back the chemical network which opened the way for a first living system to emerge. To understand the composition of the earth throughout its history, one must start at the point when terrestrial planets are formed. This process can still be observed in the universe today and was therefore well studied by scientists.<sup>[263]</sup>

The inner planets of our solar system are assumed to have accreted from rocky material rather rapidly ( $\sim 10^4$  years) after its formation  $\sim 4.6$  Gy ago. Iron rich olivine,  $(\text{Mg,Fe})_2\text{SiO}_4$ , is the first Mg-silicate to condense from a solar gas upon cooling and therefore vastly abundant during the formation of planetesimals ( $\sim 10$  km). Within 1 to 100 million years (My), gravitational interactions and collisions led to the formation of moon to mars sized planetary embryos and planetary bodies.<sup>[264]</sup> Core segregation is suggested to have already finished during the early periods of planetary growth as tungsten isotope anomalies found in meteorites demonstrate that their asteroidal parents segregated their cores only within a few million years.<sup>[265,266]</sup>

The main stage of planetary growth was accompanied by a steady intake of impactors from the outer solar system. Recent ruthenium (Ru) isotope studies indicate volatiles ( $\text{H}_2\text{O}$ ,  $\text{CO}_2$ ,  $\text{CH}_4$ ,  $\text{NH}_3$ ,  $\text{HCN}$ , etc.) were more likely delivered by carbonaceous chondrites during the growth period and not during a late veneer, as previously expected.<sup>[267,268]</sup> After the formation of the core was finished, mantle solidification likely started near the core and proceeded upwards.<sup>[269,270]</sup> The earth's crust is known to have nearly fully solidified until  $\sim 50$  My after its formation, before colliding with Theia, a mars-sized planetesimal, during the moon forming event (MFE).<sup>[271–273]</sup> The immense impact again

liquified the upper mantle and led to the formation of the moon and the last deep magma ocean.

The solidification of the magma ocean first led to the steady outgassing of volatiles with low solubility like CO<sub>2</sub>. The incorporated H<sub>2</sub>O is way more soluble and was only released during the late phases of the solidification process. In contrast to CO<sub>2</sub> the H<sub>2</sub>O was drastically outgassed under the formation of a first steam atmosphere. The first oceans formed at the earth's surface after the H<sub>2</sub>O started to condense. This process proceeded comparably fast and was finished after approx. 1.5 My.<sup>[274]</sup> As a consequence the H<sub>2</sub>O accumulating on the surface was able to enter the upper mantle and initiate plate tectonics.

The early surface most likely reassembled a stony landscape which was mostly oxidized due to the core mantle separation. Following from this the first volcanic gases more likely contained CO<sub>2</sub>, rather than reduced compounds. Kasting estimated that an atmosphere containing 10 bars of CO<sub>2</sub> and 1 bar of N<sub>2</sub> would provide steady surface temperatures of up to 80 °C over the first hundred million years in earth's history.<sup>[275]</sup> Due to the absence of O<sub>2</sub> consequently no ozone layer was available to shield from high energetic UV light. Therefore, the newly formed surface probably offered harsh conditions under which present life forms would not be able to survive.

It is still unclear where and when exactly the first life forms emerged on earth. The surface, however, was ruled out due to the extreme environment which furthermore suffered from a long-lasting bombardment by meteorites and comets. The size of these impactors probably ranged between 10<sup>3</sup> – 10<sup>11</sup> kg, whereas some of them would be big enough to again liquify parts of the upper mantle.<sup>[276]</sup>

### **8.1.2 Evolution of the atmosphere**

The dense steam atmosphere mainly containing H<sub>2</sub>O and CO<sub>2</sub> was much thicker than our present one. Studies suggest, that if all the carbon was present in form of CO<sub>2</sub>, surface pressures of up to 60 bar could have been reached. After the oceans formed, CO<sub>2</sub> remained the dominant atmospheric component for the following millions of years and was until now suggested to be only removed by weathering.

Throughout the Archean, earth's surface temperature remained moderate, even though the sun was 20 – 30 % fainter than today. Though the dimmer sun would not have provided high enough temperatures to keep the earth from freezing, no geological evidence for a global icing event exists. This faint young sun paradox (FYSP) was partly solved by the high concentration in H<sub>2</sub>O and CO<sub>2</sub>, providing a strong greenhouse effect. However, even when all the available carbon would have been present in form of CO<sub>2</sub>, the resulting green-house effect would not have been efficient enough. Additional green-house gases like CH<sub>4</sub> and NH<sub>3</sub> are necessary to give a plausible solution for this problem, but still lack in abiotic sources.

The terrestrial nitrogen was mostly captured by the magmatic surface environment after the MFE. It remained bound as NH<sub>4</sub><sup>+</sup> as long the upper mantle kept its reduced state. Mantel oxidation, however, occurred as a direct consequence of plate tectonics injecting oxidized fluids from the surface into the deeper layers. The necessary oxygen was probably produced by the dissociation of H<sub>2</sub>O and escape of H<sub>2</sub> into space. This process is assumed to have proceeded slowly so that reduced conditions were still available until about 2.5 – 4.0 Gy.<sup>[277]</sup>

This phase in earth's history was accompanied by another crucial change in the composition of its atmosphere. Life is assumed to have been present already before 3.5 Gy and by around 2.5 Gy, led to the evolution of green algae which were able to perform photosynthesis. The produced oxygen first led to the complete oxidation of the upper mantle before accumulating in the atmosphere. This great oxidation event (GOE) thereby marks the last significant change in earth's atmospheric composition until today.

## **8.2 Mackinawite from iron and sulfur**

### **8.2.1 Prebiotic availability of iron and sulfur**

The geological evidence from the Hadean is scarce. Therefore, the chemical composition of the early surface between earth's formation and the Archean can only be crudely estimated. After the last deep magma ocean solidified, the surface chemistry probably

was influenced by impactors delivered by a late veneer. Impactors are assumed to have struck the earth's surface regularly and partly liquified the upper mantle.

Most of the available iron on the earth's surface was probably introduced in form of iron meteorites. In contrast to stony meteorites, iron meteorites are less abundant, but more likely to have survived when passing through the dense atmosphere. Lighter meteorites would, upon entering the dense atmosphere, lose their volatiles due to the high temperatures. The leftover iron core would, upon the collision with the earth's surface either produce a large crater or shatter into smaller pieces which are distributed over the impact area.<sup>[276]</sup> Especially during the early stages after earth's formation, the intake in meteorites from the remaining dust cloud would have been high. The iron meteorites that survived the impact are furthermore relatively resistant to weathering and would only be oxidized beginning from the outer layer and create a passivating layer, whereas the core would stay intact for longer periods of time.<sup>[278]</sup>

Sulfur would have been much more abundant as soon as the first volcanic activity started. Elemental sulfur is known to be part of volcanic eruptions and can therefore accumulate around such areas. When iron rich meteorites struck near such areas, a landscape of craters filled with iron and sulfur would lead to the formation of an impact site, similar to the one described by Cockell et al<sup>[279,280]</sup>, but much richer in highly reactive metal sulfides. The earliest sulfur cycle, however, was more strongly influenced by atmospheric gas-phase reactions than today. The most abundant sulfur containing compounds exhaled by the earliest volcanoes probably were SO<sub>2</sub> and H<sub>2</sub>S. The photochemistry of both leads to the formation of elemental sulfur, sulfur particles, sulfuric acid and oceanic sulfate.<sup>[236]</sup> The elemental sulfur thereby can form aerosols that already have been assumed to be relevant for the origin of life.<sup>[238–240]</sup>

### **8.2.2 Environmental constraints**

The formation of mackinawite by the reaction between iron and sulfur has been shown to proceed highly efficiently under anoxic conditions and in the presence of water (Chapter 3). When these factors are adapted onto a global scale, a rough period for the reaction between iron and sulfur can be estimated. The earliest possible point in time for the reaction to proceed is the one, where water started to condensate from the early

steam atmosphere. If both, iron, and sulfur, were available, the sulfur assisted corrosion could have promoted the formation of iron sulfides as soon as the first oceans formed.

The upper limit for this reaction is set by the great oxidation event (GOE), approx. 2.5 Ga ago. At that point cyanobacteria developed and started to produce O<sub>2</sub> as a waste product. With higher concentrations of O<sub>2</sub> in the atmosphere the accessible iron would have gotten covered by a thick oxide layer. Even if sulfur would be able to break through and mackinawite would be formed, it would only be oxidized into other iron sulfide phases or iron(hydroxy)oxides. Since the GOE, mackinawite can only be found in anoxic environments like deep sea vent systems, where it still is produced today. The reaction between iron and sulfur probably was only available for a certain period in earth's history during the Hadean and Archean, ranging from approx. 4.4 Ga to 2.5 Ga ago.

### **8.2.3 Prebiotic relevance**

Consequently, the formation of mackinawite from iron and sulfur is a unique approach towards synthetic mackinawite under conditions plausible for the surface of the early earth (Chapter 3). The reaction was found to be very robust under a range of conditions. It proceeds in a pH range of 4 – 8 and temperatures < 100 °C. Under more acidic conditions, however, the dissolution of iron will lead to the formation of H<sub>2</sub>, whereas sulfur would not be reduced and consequently the concentration in S<sup>2-</sup> would be too small to form mackinawite. On the other hand, at pH > 8 the concentration in protons is too small to further dissolve iron to produce Fe<sup>2+</sup> ions.

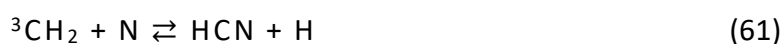
As for its various functionalities, mackinawite could have provided multiple reactions, which previously were not discussed in the context of a surface mediated process. Especially wet dry cycling of monomers would benefit from additional surface mediated concentration effects. In contrast to clays and in similarity to the RNA molecule, mackinawite inherits both structural and reducing properties.

## 8.3 The reduction of C<sub>1</sub> substrates

### 8.3.1 Abiotic CH<sub>4</sub> source

The availability of CH<sub>4</sub> on the early earth is still under debate. While earlier approaches suggested higher CH<sub>4</sub> concentrations, still only few abiotic processes for carbon fixation from CO<sub>2</sub> are known. The formation of CH<sub>4</sub> from cyanides, CS<sub>2</sub>, CH<sub>3</sub>SH and, directly from CO<sub>3</sub><sup>2-</sup> supported by mackinawite could have proceeded on the surface of the earth as long as mackinawite was available. This set of reactions would thereby act as an abiotic CH<sub>4</sub> source and could partly give a solution for the FYSP.<sup>[202]</sup>

Higher CH<sub>4</sub> concentrations in the early atmosphere were already suggested by Zahnle, who studied the photochemistry of CH<sub>4</sub> and HCN under anoxic conditions.<sup>[197]</sup> In contrast to CH<sub>4</sub>, HCN is rather long living in the atmosphere and is only partly destroyed by photodissociation or removed by rainout. The CH<sub>4</sub> molecule thereby is more reactive and known to dissociate readily by forming the electrically excited methylene radical (<sup>1</sup>CH<sub>2</sub>). In presence of nitrogen, it can react to form triplet methylene (<sup>3</sup>CH<sub>2</sub>), which can quickly react with various species. In presence of oxygen or hydroxide radicals, oligomerization into ethylene and acetylene can follow; In the presence of nitrogen atoms, the reaction leads to the formation of HCN.



The photochemical formation of HCN is highly dependent on the composition of the atmosphere. The efficiency of the reaction was found to drop significantly at low CH<sub>4</sub> mixing ratios. Mackinawite probably was produced locally in areas where iron meteorites struck the surface or where iron remained after the MFE. A consequence of the reaction between iron and sulfur is that mackinawite particles, that were formed on top of the iron surface, first crumble away before they are finely distributed into solution. The reduction of CO<sub>2</sub> or CO<sub>3</sub><sup>2-</sup> is therefore not limited to specific zones where iron was available but could have been spread by streams or rivers passing by such areas. Thereby CH<sub>4</sub> formation would not only proceed locally, but also in places which were lacking in iron and sulfur.



The experiments conducted during this thesis showed a much higher rate in CH<sub>3</sub>SH formation from reactions containing mackinawite. The rate in CH<sub>4</sub> formation from CH<sub>3</sub>SH was here found to be more efficient at lower temperatures. Under prebiotic conditions this behavior can be seen as a natural regulating system that would produce CH<sub>4</sub> in periods when the surface temperature was low. Once formed, the CH<sub>4</sub> would temporarily act as a strong greenhouse gas. In contrast to CO<sub>2</sub>, CH<sub>4</sub> only has a short lifetime as it readily reacts with hydroxide radicals, formed in the atmosphere.<sup>[197,198]</sup>

### 8.3.2 Formation of biologically relevant compounds

#### Oxygenated species

The here observed oxygenated species like aldehydes and ketones could have acted as important intermediates for biologically relevant compounds like amino acids or even DNA. Aldehydes and ketones are precursors for the formation of alanine, serine and glycine by the Strecker synthesis and therefore linked to the primordial origin of ribonucleotides.<sup>[195,281]</sup> Until now, however, only few abiotic routes leading to the formation aldehydes and ketones are known.<sup>[282]</sup> The reduction of HCN by mackinawite could be an additional prebiotic source for such oxygenated compounds.

Recently Trapp et al. showed that not only RNA, but also DNA precursors can be produced by the reaction between nucleobases and acetaldehyde. This, until then unknown process proceeds by the formation of a vinyl nucleobase, which can be reacted with D-glyceraldehyde to yield a deoxyribonucleoside.<sup>[283]</sup> The DNA molecule, due to its stability, was assumed to have evolved from the RNA molecule.<sup>[42]</sup> Until today, however, no evidence for such a transition was presented. More recent studies therefore assume an independent formation of DNA, parallel to the one of RNA.<sup>[283,284]</sup>

#### Cyclic organic sulfides

Cyclic polysulfides like 1,2,4-trithiolane and its derivatives are widely spread in nature and are, among other, the main component in e.g., Shiitake mushrooms (*Lentinus edodes*) or in stink bean (*Parkia speciosa*).<sup>[244,285,286]</sup> The thermal decomposition process thereby results in [3+2]-cycloelimination leading to the formation of reactive thiocarbonyl S-sulfides.<sup>[287]</sup> The cyclic polysulfides, as well as their decomposition products are

furthermore known to readily form diverse sulfur heterocycles via [3+2]-cycloaddition, as well as sulfur heterocyclic metal complexes like mimics of the [FeFe]-hydrogenase upon the reaction with iron carbonyls.<sup>[141,288,289]</sup>

Iron carbonyls can be formed from the reaction of iron sulfides with CO under prebiotically plausible conditions. Cody et al. showed that hydrogenase analogs are produced from a mixture containing iron sulfide, CO and a thiol at 250 °C under elevated pressures.<sup>[126]</sup> They state that such compounds would provide the prebiotic earth with crucial biochemical functionality. If iron carbonyls are available, a much wider array of such biochemically important compounds could have been produced from the reaction with the here observed cyclic disulfides.

Active sites of the hydrogenase, acetyl-CoA synthase or nitrogenase, typically containing iron and sulfur, act as catalyst for hydrogen evolution, as well as nitrogen and carbon fixation.<sup>[290]</sup> If such compounds were available during the earliest stages of the chemical evolution, primitive enzymes could have formed as soon as the first oligomeric or polymeric species like peptides or lipids emerged.

### **8.3.3 Hexacyanoferrates as HCN storage**

The fast formation of hexacyanoferrates from aqueous iron ions and  $\text{CN}^-$  is an important constraint for the availability of free HCN on the early earth. The concentrations in iron ions in the early oceans was presumably high<sup>[291]</sup> and would lead to the formation of hexacyanoferrates, as soon as HCN was delivered through comets or formed photochemically.<sup>[196,197]</sup> Hexacyanoferrates have already been discussed for their prebiotic relevance by Keefe et al. and suggested to have only been available in significant concentrations only when HCN formation rates were high and temperatures were low ( $< 0\text{ °C}$ ).<sup>[292]</sup>

In addition of the already discussed release mechanisms described earlier (6.1), the direct formation of  $\text{CH}_4$  and  $\text{CH}_3\text{SH}$  mediated by iron and mackinawite could have influenced the local hexacyanoferrate reservoirs. In contrast to other mechanisms, the direct reduction already proceeds at ambient temperatures and is independent from other environmental influences like UV radiation. The biggest advantage, however,

would be that no additional catalyst is needed to reduce the HCN once it is released from the complex.

## 8.4 The prebiotic habitat

Current prebiotic models cover a wide range of processes from the chemical evolution of small species to the formation of a first working cell. These processes are mostly constrained by the environmental conditions given through the geological habitat. After the H<sub>2</sub>O condensed from the dense steam atmosphere, the first oceans were formed, whereas two distinctly different surface environments for prebiotic processes became available: (1) Hydrothermal vents, located at the bottom of the newly formed oceans or (2) ponds and lakes located on the continents.<sup>[5,293,294]</sup> Both scenarios, where H<sub>2</sub>O is either permanently or only frequently present, bear up- and downsides for processes of the early chemical and biological evolution. The omnipresence of H<sub>2</sub>O results in highly diluted conditions whereas especially the formation of longer macromolecules would be a challenging task to complete.<sup>[295]</sup> Under more dry conditions, e.g. on the early continents high temperatures and photo radiation would steadily lead to the evaporation of H<sub>2</sub>O from small ponds or lakes.<sup>[296]</sup> The subsequent concentration process can be assumed highly beneficial for the evolution of oligomeric and polymeric species. Furthermore, due to the direct contact with the atmosphere a much greater variety in substrates would become available and hydrolysis would only occur locally.

The harsh conditions on-land, however, do not seem suitable for biological systems to survive for long periods of time.<sup>[297]</sup> The steady intake of meteorites and other cosmic impactors decreased drastically after the MFE, leading to a moderate impact rate over time with, however, multiple cataclysms.<sup>[298]</sup> Thereby, the earths primordial continent probably underwent critical changes in its geography which would be disadvantageous for an efficient biological evolution. The location at the bottom of the ocean, however, reassembles a more suitable habitat for this step, as environmental changes only occur slowly.

Both locations, on-land and at the bottom of the oceans, until now, were mainly discussed separately. The presence of mackinawite on-land, however, leads to a novel

scenario where C fixation products could have been transported towards hydrothermal fields by rivers. Mackinawite, in addition to its reductive properties, is well known to adsorb different chemical species like heavy metals or organic compounds (1.3.3). When it is produced from the elements, reactive conglomerates are removed from the reaction center if the surrounding H<sub>2</sub>O is in movement (3.2.2). On the prebiotic continents moderate to heavy rainfall and/or volcanic hot springs<sup>[299]</sup> would therefore wash away the formed mackinawite, which could then act as a sponge for small, reduced species. This loaded mackinawite would then be transported into the oceans over time where the particles would get diluted, but the reduced compounds remain attached. Such a permanent intake of mackinawite to shallow hydrothermal fields could act as a secondary chemical food source in addition to the vent exhalations. There the adsorbed compounds are probably released due to different environmental conditions like pH or temperature.

With the additional mackinawite based chemistry on-land a much wider range of prebiotically relevant compounds becomes available for already established prebiotic models. The simplicity and selectivity of the reaction between iron and sulfur, as well as the high reactivity of the produced mackinawite, are easily accessible under early earth conditions and should therefore be considered as prebiotically relevant.

## Chapter 9. Summary and Outlook

### 9.1 Summary

In this thesis a novel approach for the synthesis of mackinawite from iron and sulfur was presented. Furthermore, this nano-particular mackinawite, as well as iron, were shown to mediate the reduction of C<sub>1</sub> substrates under prebiotically plausible conditions. The investigated substrates included CN<sup>-</sup>, SCN<sup>-</sup>, OCN<sup>-</sup>, CO<sub>2</sub>, CO, CO<sub>3</sub><sup>2-</sup>, CS<sub>2</sub>, CH<sub>3</sub>SH, [Fe(CN)<sub>6</sub>]<sup>3-</sup>, [Fe(CN)<sub>6</sub>]<sup>4-</sup> and [Fe(CN)<sub>5</sub>(NO)]<sup>2-</sup>. When CN<sup>-</sup>, SCN<sup>-</sup>, OCN<sup>-</sup> and [Fe(CN)<sub>5</sub>(NO)]<sup>2-</sup> were reacted with iron, mainly hydrocarbons, accompanied by smaller amounts of oxygenated species and nitriles. The reduction of [Fe(CN)<sub>5</sub>(NO)]<sup>2-</sup> furthermore led to the formation of N<sub>2</sub>O. In the presence of sulfur, the product range changed as more organic sulfur compounds like CH<sub>3</sub>SH or CS<sub>2</sub> were formed. In the absence of iron, only small amounts of hydrocarbons, mostly with short chain lengths for two or three carbon atoms, were produced, while a more selective formation of organic sulfur compounds was observed.

In contrast to previous studies on the reduction of substrates by mackinawite no significant amounts in pyrite were formed. The PXRD pattern, due to the low crystallinity of the mackinawite formed from iron and sulfur, often showed an intensive baseline, whereas other iron sulfide phases could eventually not have been detected. Upon the reaction with KCN and KSCN the mackinawite, however, reacted to form greigite. In the case of KCN this could further be supported by Mössbauer spectroscopy. The missing formation of pyrite could hereby be a consequence of the presence of aldehydes which act as a switch during the oxidation of mackinawite. Rickard et al. provided evidence that the absence of aldehydes the S<sup>2-</sup> in mackinawite is more likely to be oxidized than the Fe<sup>2+</sup>. In the presence, however, the Fe<sup>2+</sup> gets oxidized and leads to the formation of greigite and not pyrite.<sup>[300]</sup> As CH<sub>3</sub>CHO was formed during the reduction experiments where mackinawite was reacted with KCN, it could have acted as such a switch a prevented pyrite formation. During the reduction experiments where carbon oxides were used, the formation of a thin, shiny, layer was observed. The appearance of such a layer was already reported by other groups as pyrite but could here not be further identified.

The metal or metal sulfide mediated reduction of carbon and nitrogen substrates is most widely assumed to proceed on the active surface of such materials. To explain the array of products from the here conducted experiments, especially the ones from KCN, DFT calculations were performed on a modified  $[\text{Fe}_4\text{S}_4]$  model complex. Though, the reduction is mostly assumed to proceed more efficiently when the substrate is reduced at the iron site, no investigations on the chemical activity of the mackinawite surface groups was conducted until now. The DFT calculations only provided unsatisfying results when the HCN molecule was let to interact with one of the iron atoms. When the HCN molecule was, however, let to interact with the deprotonated sulfide residue, the formation of the resulting S – C bond was found to be exothermic in energy by  $-75.5 \text{ kcal mol}^{-1}$ . The following formation of  $\text{CH}_4$ ,  $\text{CH}_3\text{SH}$  and  $\text{CH}_3\text{CHO}$  was found to proceed by an overall exothermic process and therefore is in alignment with the experimental observations that the reduction of KCN already proceeds at room temperature. Additionally, DFT calculations for the reaction of mackinawite with  $\text{CS}_2$  again was found to be exothermic by  $-21.7 \text{ kcal mol}^{-1}$  and was followed by an overall exothermic reduction into  $\text{CH}_4$  and  $\text{CH}_3\text{SH}$ .

The formation of reduced compounds from different hexacyanoferrates and nitroprusside further underlines the reductive capability of mackinawite and iron. When the substrates were reacted in the absence of any solid phase, either no reduced species or solely HCN was observed in the gas phase of the samples. The formation of e.g.,  $\text{CH}_3\text{SH}$  probably follows from the subsequent release of HCN from the complexes as the formed amounts were low, in comparison to the ones detected in the KCN samples.

The evidence for the reduction of carbon oxides was rather inconsistent, when compared to the one of KCN. The shifted mass patterns of  $\text{CH}_4$  and  $\text{CH}_3\text{SH}$  were collected from a series of samples but could, partly, not be reproduced in later experiments. This is in accordance with other studies on this matter where similar inconsistencies were reported.<sup>[128,129,260]</sup> Based on the here gathered results it appears most likely that unlabeled carbon contaminations were introduced by the iron powder and led to a lower intensity for the  $m/z = 17$  peak in the  $\text{CH}_4$  signal. However, the presence of  $\text{CH}_4$  signals with a fully shifted mass pattern provides strong evidence for this reaction to be accessible. This is further underlined as the mass pattern of  $\text{CH}_3\text{SH}$  appeared fully shifted

in most of the experiments. In addition, the mackinawite synthesized from iron and sulfur was shown to efficiently bind CO<sub>2</sub> from the gas phase of samples that were consecutively charged with CO<sub>2</sub>. This was already predicted by DFT calculations and could here be shown to proceed much less effectively when precipitated or deactivated mackinawite was used.

The here investigated reactions are highly relevant for the field of prebiotic chemistry as they provide new routes towards more reduced carbon substrates that can act as intermediates during the formation of more complex molecules like RNA or DNA. However, not only the reductive property of mackinawite, but also its formation from the elements leads to a scenario that previously has not been considered in the context of the origin of life. Due to this reaction mackinawite, and therefore a lot of processes that previously have only been assumed to be available at the bottom of the ocean are now accessible at the surface of the early earth. There, substrate concentrations would have been much higher than at hydrothermal sites, where the omnipresence of H<sub>2</sub>O would always lead to diluted conditions. Furthermore, HCN, which is considered a key molecule for the formation of the first life, is only available at the surface as it would rapidly hydrolyze into NH<sub>3</sub> and HCOOH when being dissolved in the ocean.

The direct reduction of KCN and Na<sub>2</sub>CO<sub>3</sub> would have acted as an abiotic source for CH<sub>4</sub>. Higher atmospheric concentrations in CH<sub>4</sub> were already assumed, but suitable sources were missing until now. To this point it is not clear if this reaction would have influenced the early atmospheric composition in a global scale, but the rather short reaction times of days indicate that at least elevated local levels in CH<sub>4</sub> are thinkable. Furthermore, as the reduction of CH<sub>3</sub>SH, the main product from KCN and Na<sub>2</sub>CO<sub>3</sub> reduction, was shown to also yield CH<sub>4</sub>, an overall decent rate in CH<sub>4</sub> formation under conditions available on the early surface are thinkable. The CH<sub>3</sub>SH would thereby not be diluted into the ocean and rather accumulate around the reaction center. With new mackinawite being formed and transported by streams of H<sub>2</sub>O through these areas, the CH<sub>3</sub>SH could again serve as substrate.

The cyclic organic sulfur compounds like 1,2,4-Trithiolane that were formed during the reaction between the iron sulfur mixture and KCN at pH 9 further display a class of

compounds with a high prebiotic relevance. Cyclic compounds containing disulfide bonds are interesting precursors for many organic reactions, as well as [FeFe] hydrogenase model complexes that provide the reversible oxidation of H<sub>2</sub>. Such complexes could therefore have acted as the first energy transformers for primitive organism.

## 9.2 Outlook

The formation of mackinawite from iron and sulfur has a high potential to change our view on the processes that appeared on the surface of the early earth. Until now, however, no clear claims on the abundance of iron and sulfur, as well as the effectivity of this reaction under such harsh conditions can be made. This scenario should be evaluated in future approaches.

The same goes for the effectivity of the carbon substrate reduction, which here often varied in between the experiments. The result of the experiments was influenced by several factors including pH, temperature, the amount of reducing agent, the amount of H<sub>2</sub>O, the physical composition of the solid phase and the overall redox state of the sample. To get a deeper understanding of this system all these factors must be tested separately for all substrates onto their influence.

However, the general finding, that carbon reduction can proceed by mackinawite surface groups and not by the iron itself opens the door for a new class of catalysts for CO<sub>2</sub> reduction that focus more on the surface structure, than on its reduction strength.



## Chapter 10. Experimental section

### 10.1 Methods

#### HST-01

The  $\text{CH}_3\text{SNa}$  (70 mg, 1 mmol) was placed into a 20 mL glass vial and evacuated with  $\text{N}_2$ . By adding 10 mL of  $\text{N}_2$  purged  $\text{H}_2\text{O}$  a 1 M stock solution was prepared. In a new, evacuated 20 mL vial, 1 mL of the stock solution was diluted with 9 mL  $\text{H}_2\text{O}$  to give a 0.1 M solution for the experiments. In six separate and evacuated vials 1 mL of the diluted stock solution were added and further charged with 1 mL of a 1 M  $\text{H}_3\text{PO}_4$  before heated to 80 °C for 30 min. Three of the samples were then analyzed using the HS-20 to extract the gas phase sample in presence of the aqueous phase. The gas phases other three samples were transferred into clean and vacuumized vials by a transfer line and the sampled by the HS-20.

#### HST-02

The  $\text{CH}_3\text{SNa}$  (70 mg, 1 mmol) was placed into a 20 mL glass vial and evacuated with  $\text{N}_2$ . By adding 10 mL of  $\text{N}_2$  purged  $\text{H}_2\text{O}$  a 1 M stock solution was prepared. In a new, evacuated 20 mL vial, 0.5 mL of the stock solution was diluted with 9.5 mL  $\text{H}_2\text{O}$  to give a 0.05 M solution for the experiments. In six separate and evacuated vials 1 mL of the diluted stock solution were added and further charged with 1 mL of a 1 M  $\text{H}_3\text{PO}_4$  before heated to 80 °C for 30 min. Three of the samples were then analyzed using the HS-20 to extract the gas phase sample in presence of the aqueous phase. The gas phases other three samples were transferred into clean and vacuumized vials by a transfer line and the sampled by the HS-20.

## 10.2 Metal sulfide synthesis

### SP-FeS-01

The iron (0.88 g, 0.0156 mol) and sulfur powder (0.50 g, 0.0156 mol) were brought together in a Schlenk flask, equipped with a magnetic stir bar, and mixed with a glass rod. After evacuation, approx. 20 mL of toluene and 2 mL conc. acetic acid were added. No reaction occurred at room temperature, but the black solid, as well as H<sub>2</sub>S, started to form at 60 °C. After 5 min at 80 °C, no yellow sulfur could be observed in the reaction mixture.

### SP-FeS-02

The iron (0.88 g, 0.0156 mol) and sulfur powder (0.50 g, 0.0156 mol) were brought together in a Schlenk flask, equipped with a magnetic stir bar, and mixed with a glass rod. After evacuation, approx. 20 mL of toluene and 2 mL conc. HCl were added, whereas the liquid phase started to heat up and a black solid slowly formed. The formation of H<sub>2</sub>S from sulfur was furthermore confirmed by its typical odor.

### 10.2.1 PXRD

#### SP-FeS-03

The iron (0.88 g, 0.0156 mol) and sulfur powder (0.50 g, 0.0156 mol) were brought together in a Schlenk flask, equipped with a magnetic stir bar, and mixed with a glass rod. After evacuation, approx. 20 mL of EtOH and 2 mL conc. acetic acid were added, whereas no reaction was observed. When the mixture was heated to 80 °C, the odor of H<sub>2</sub>S became recognizable and some black solid formed. The sample was then stirred over night at room temperature and investigated by PXRD after filtration over a G4 frit.

#### SP-FeS-04

The iron (0.88 g, 0.0156 mol) and sulfur powder (0.50 g, 0.0156 mol) were brought together in a Schlenk flask, equipped with a magnetic stir bar, and mixed with a glass rod. After evacuation, 20 mL of degassed acetone, together with 2 mL of H<sub>2</sub>O, were

added through a syringe. After 5 d at room temperature no magnetic iron or yellow sulfur were observed anymore. The mackinawite was washed with acetone, whereas the excess solvent was first carefully removed with a syringe, before the sample was dried under reduced vacuum to give a fine black powder which immediately burns when let in contact with air.

#### **SP-FeS-05**

The iron (0.88 g, 0.0156 mol) and sulfur powder (0.50 g, 0.0156 mol) were brought together in a Schlenk flask, equipped with a magnetic stir bar, and mixed with a glass rod. After evacuation, 20 mL of degassed H<sub>2</sub>O were added through a syringe whereas no reaction occurred after the mixture was stirred at room temperature for 30 min. A second Schlenk flask was equipped with 10 g of Na<sub>2</sub>CO<sub>3</sub> and 20 mL of H<sub>2</sub>O. By adding a 1 M HCl to the second Schlenk, CO<sub>2</sub> developed and was used to purge the reaction mixture. After another 3 d at room temperature the aqueous phase started to turn dark due to the formation of mackinawite particles.

#### **SP-FeS-06**

The iron (0.88 g, 0.0156 mol) and sulfur powder (0.50 g, 0.0156 mol) were brought together in a Schlenk flask, equipped with a magnetic stir bar, and mixed with a glass rod. After evacuation, 20 mL of degassed H<sub>2</sub>O were added through a syringe. After 5 d at room temperature no magnetic iron and only small amounts of yellow sulfur were observed anymore. The mackinawite was then filtered over a G4 frit and dried under a stream of N<sub>2</sub> until most of the H<sub>2</sub>O was removed and the powder did not stick anymore. The sample remained unreactive after small amounts of O<sub>2</sub> were introduced for several times.

#### **SP-NiS**

The nickel (0.88 g, 0.0156 mol) and sulfur powder (0.50 g, 0.0156 mol) were brought together in a Schlenk flask, equipped with a magnetic stir bar, and mixed with a glass rod. After evacuation, 20 mL of degassed H<sub>2</sub>O were added through a syringe. After 3 d at 80 °C no magnetic iron or yellow sulfur were observed anymore. The mackinawite

was washed with H<sub>2</sub>O, whereas the excess solvent was first carefully removed with a syringe, before the sample was dried under reduced vacuum to give a fine black powder.

**Table 10** Composition of the samples for SP-NiFeS-01 to SP-NiFeS-11.

Nr.	n [mmol]			m [g]		
	Fe	Ni	S	Fe	Ni	S
1	20	0	20	1.12	0	0.64
2	18	2	20	1.008	0.116	0.64
3	16	4	20	0.896	0.232	0.64
4	14	6	20	0.784	0.348	0.64
5	12	8	20	0.672	0.464	0.64
6	10	10	20	0.56	0.58	0.64
7	8	12	20	0.448	0.696	0.64
8	6	14	20	0.336	0.812	0.64
9	4	16	20	0.224	0.928	0.64
10	2	18	20	0.112	1.044	0.64
11	0	20	20	0	1.16	0.64

#### SP-NiFeS-01 to SP-NiFeS-11

Different ratios of the iron, nickel, and sulfur powder were prepared by following Table 10. The mixtures were evacuated and charged with acetone/H<sub>2</sub>O (10:1) using a syringe. The acetone (1 L), together with the H<sub>2</sub>O (0.1 L), was degassed by purging with N<sub>2</sub> for 4

h. The reactions were carried out at 80 °C for 7 d. The solid reaction product was filtrated over a G4 frit and dried under N<sub>2</sub>.

### SP-NiFeS-12 to SP-NiFeS-21

Different ratios of the iron, nickel, and sulfur powder were prepared by following Table 11. The mixtures were placed in different Schlenk flasks and evacuated with N<sub>2</sub>, before being charged with H<sub>2</sub>O, using a syringe. The reactions were carried out at 80 °C for 7 d. The solid reaction product was filtrated over a G4 frit and dried under N<sub>2</sub>.

**Table 11** Composition of the samples used for SP-NiFeS-12 to SP-NiFeS-21.

Nr.	n [mmol]			m [g]		
	Fe	Ni	S	Fe	Ni	S
22	21.1	2.4	15.6	1.18	0.14	0.5
23	17.6	5.9	15.6	0.98	0.35	0.5
24	14.0	9.4	15.6	0.79	0.55	0.5
25	11.7	11.7	15.6	0.66	0.69	0.5
26	9.4	14.0	15.6	0.52	0.82	0.5
27	5.9	17.6	15.6	0.33	1.03	0.5
28	2.4	21.1	15.6	0.13	1.24	0.5

### 10.2.2 Mössbauer spectroscopy

#### SP-FeS-07

The iron sulfur mixture (0.88 g, 10 mmol) was placed into a 25 mL vial, equipped with an Al-cap and septa. After the mixture was evacuated with N<sub>2</sub> for three times 5 mL of N<sub>2</sub>

purged H<sub>2</sub>O were added. The mackinawite formed after 24 h at room temperature, whereas no magnetic iron remained. The reaction product was then separated using a G4 frit under a steady N<sub>2</sub> stream. To remove any moisture the filter cake was further washed with EtOH, acetone and diethylether. After the washing process was finished small amounts of air were let to enter until no exothermic reaction occurred anymore. The deactivated product was then stored in a plastic vial in presence of O<sub>2</sub> until it was analyzed by Mössbauer spectroscopy.

### 10.3 Qualitative analyses

#### QA-01

In a 25 mL glass vial 0.32 g, 10 mmol of sulfur and 0.065 g, 1 mmol, KCN were mixed, evacuated with N<sub>2</sub> for three times and charged with 3 mL of purged H<sub>2</sub>O. The reaction was then left at 80 °C to proceed for 5 d, before liquid samples for qualitative analysis were extracted by a syringe. A 1 M Fe<sup>3+</sup> solution was prepared by placing 2.4 g, 10 mmol, of Fe(NO<sub>3</sub>)<sub>3</sub> into a 25 mL vial and charging with 10 mL of purged H<sub>2</sub>O after evacuating the sample. When both solutions were injected into an empty vial under N<sub>2</sub> atmosphere, the solution turned deep red, indicating the presence of Fe(SCN)<sub>3</sub>.

#### QA-02

Two clean watch glasses were placed on the workbench. In the concave part of the first watch glass a small piece of pH was fixated with a drop of deionized H<sub>2</sub>O. The second one was equipped with a decent amount (approx. 0.5 g) of NaOH. The aqueous phase of a reacted mackinawite/KCN sample was extracted by a syringe. The solid particles were removed by using a syringe filter while around 2 mL of the solution were added to the NaOH. After quickly covering the second watch glass with the first one, the pH paper started to turn blue indicating the presence of NH<sub>3</sub>.

## 10.4 Reduction experiments

### 10.4.1 NMR spectroscopy

#### LP-01

In a 100 mL Schleck flask 5 g (56.8 mmol) of the crude iron sulfur mixture together with 1 g (15.4 mmol) of KCN were evacuated for three times before 40 mL of H<sub>2</sub>O were added. The closed vessel was heated for a total of 10 d at 80 °C. Multiple samples (Table 12) were extracted with a syringe after different reaction times, whereas the collected solution was filtrated through a syringe filter before being placed (0.4 mL) in an NMR tube, which was charged with 0.05 mL of D<sub>2</sub>O and purged with a N<sub>2</sub> stream.

**Table 12** Parameters and observations for samples of LP-01.

ID	Color	Time [d]	pH
LP-01-01	green	1	10
LP-01-02	colorless	1	1
LP-01-03	green/blue	2	9
LP-01-04	colorless	3	9
LP-01-05	colorless	4	9

**Table 13** Parameters and observations for the samples of LP-02.

ID	Color	Solvent	pH
LP-02-01	green	H <sub>2</sub> O	10
LP-02-02	colorless	D <sub>2</sub> O	9
LP-02-03	colorless	H <sub>2</sub> O	4

**LP-02**

In a 100 mL Schleck flask 5 g (56.8 mmol) of the crude iron sulfur mixture together with 1 g (15.4 mmol) of KCN were evacuated for three times before 40 mL of D<sub>2</sub>O were added (Table 13). The closed vessel was heated for 16 h at 80 °C. The reaction was simultaneously performed in H<sub>2</sub>O. After 16 h samples were extracted with a syringe, whereas the collected solution was filtrated through a syringe filter before being placed (0.4 mL) in an NMR tube, which was charged with 0.05 mL of D<sub>2</sub>O and purged with a N<sub>2</sub> stream.

**LP-03**

In a 25 mL vial with Al-cap and septa 2.5 g (28.9 mmol) of the crude iron sulfur mixture, together with 0.48 g (7.5 mmol) of KCN, were evacuated and charged with 10 mL of N<sub>2</sub> purged H<sub>2</sub>O. A second sample only containing the mixture of iron and sulfur was prepared in the same manner but first let to form mackinawite before the KCN was added. Samples for NMR spectroscopy were extracted with a syringe after 24 h. The reaction solution was filtered through a syringe filter while transferring it into a NMR tube, containing 0.05 mL of D<sub>2</sub>O.

**LP-04**

In a 25 mL vial with Al-cap and septa 0.48 g (7.5 mmol) of KCN was evacuated under N<sub>2</sub> and charged with 10 mL of N<sub>2</sub> purged H<sub>2</sub>O. The sample was further charged with 2 mL



of a 1 M H<sub>2</sub>SO<sub>4</sub> and left at 80 °C for 3 d. The sample for the NMR spectroscopy was extracted with a syringe and placed into a NMR tube, containing 0.05 mL of D<sub>2</sub>O.

#### LP-05

In a 25 mL vial with Al-cap and septa 2.5 g (28.9 mmol) of the crude iron sulfur mixture together with 0.48 g (7.5 mmol) of KCN or 0.73 g (7.5 mmol) KSCN were evacuated for three times before 10 mL of H<sub>2</sub>O were added (Table 14). The reaction was further performed with mackinawite, which beforehand was let to form from the iron sulfur mixture before the substrate and 5 mL of a 1 M HCl were added. The closed vessel was heated for 3 d at 80 °C. NMR samples were extracted with a syringe, whereas the collected solution was filtrated through a syringe filter before being placed (0.4 mL) in an NMR tube, which was charged with 0.05 mL of D<sub>2</sub>O and purged with a N<sub>2</sub> stream.

**Table 14** Composition of the samples of LP-05.

ID	m [g]			
	Fe	FeS	KCN	KSCN
LP-05-01	2.5	-	0.48	-
LP-05-02	-	2.5	-	0.73
LP-05-03	-	2.5	0.48	-
LP-05-04	2.5	-	-	0.73

#### 10.4.2 GCMS analysis

##### GP-01

For each sample 1 g of crude iron powder was placed in a 20 mL glass vial, which was evacuated with N<sub>2</sub>. It was then charged with N<sub>2</sub> purged H<sub>2</sub>O, substrate solution, and acid following Table 15. The samples were then stored at 80 °C for 5 d. When the reaction

finished, the gas phase samples were extracted by applying the method using a transfer line into a clean vial. The samples were analyzed by **GCS-4**.

**Table 15** Composition of the samples of GP-01.

ID	V [mL]			
	H <sub>2</sub> O	1 M KCN	1 M H <sub>3</sub> PO <sub>4</sub>	total
GP-01-01	3	0	0	3
GP-01-02	2	0	1	3
GP-01-03	2	1	0	3
GP-01-04	1	1	1	3

### GP-02

For each sample 0.88 g (10 mmol) of the iron powder was placed in a 20 mL glass vial, which was evacuated with N<sub>2</sub> for three times and charged with 2 mL N<sub>2</sub> purged H<sub>2</sub>O, 1 mL of a 1 M KCN (GP-02-01) or 1 M Na<sup>13</sup>CN (GP-02-02) solution and 1 mL of a 1 M H<sub>3</sub>PO<sub>4</sub>. The samples were then stored at 80 °C for 5 d before gas phase samples were extracted by a transfer line into a clean vial and analyzed by **GCS-4**.

### GP-03

For both samples 1g (12.4 mmol) of the crude iron sulfur mixture was placed in a 20 mL vial which was evacuated with N<sub>2</sub> for three times and charged with N<sub>2</sub> purged H<sub>2</sub>O, substrate, and acid following Table 16. The samples were then stored at 80 °C for 5 d before gas phase samples were extracted by a transfer line into a clean vial and analyzed by **GCS-4**.

**Table 16** Composition of the samples of GP-03.

ID	V [mL]			
	H <sub>2</sub> O	1 M KCN	1 M H <sub>3</sub> PO <sub>4</sub>	total
GP-03-01	2	1	0.1	3
GP-03-02	1	1	1	3

**GP-04**

The samples were prepared inside a glovebox under Ar atmosphere. All reaction were carried out with **RS<sub>2</sub>** and either contained NaCN, Na<sup>13</sup>CN or CO<sub>2</sub> (Table 17). The iron mixture, together with the NaCN/Na<sup>13</sup>CN was scaled into the vials under air before being transferred into the glovebox. In the case of the CO<sub>2</sub> sample no salt was added to the iron sulfur mixture. All samples were charged with 1 mL of Ar purged H<sub>2</sub>O, closed with an Al-cap and septa, and moved outside the glovebox. The gas phase of GP-04-06 was cycled with CO<sub>2</sub> for 10 times, before all samples were stored at 75 °C for different reaction times. After the reaction was finished, 1 mL of a 5 M HCl was added, and the gas phase was investigated by extracting 250 µL using a gas tight syringe and analyzing the mixture by **GCS-1**. Calibrated with CAL-MT-1.

**Table 17** Composition of the samples of GP-04.

ID	n [mmol]			V [mL]	t [h]
	Fe/S	KCN	CO <sub>2</sub>	total	
GP-04-01	1.14	1	-	2	2
GP-04-02	1.14	1	-	2	4
GP-04-03	1.14	1	-	2	24

<b>GP-04-04</b>	1.14	1	-	2	48
<b>GP-04-05</b>	1.14	1	-	2	72
<b>GP-04-06</b>	1.14	1	-	2	96
<b>GP-04-07</b>	1.14	1 (Na <sup>13</sup> CN)	-	2	2

### GP-05

For each sample different amounts of the iron sulfur mixture or mackinawite together with NaCN or Na<sup>13</sup>CN were placed in a 20 mL vial which was evacuated with N<sub>2</sub> for three times and charged with 1 mL N<sub>2</sub> purged H<sub>2</sub>O. The mackinawite samples were first produced from the reaction between iron and sulfur before the substrate was added following Table 18. After 5 d at 80 °C 1 mL of a 1 M HCl was added, and the samples were analyzed with the HS-20 directly from the reaction vial and analyzed by **GCS-4**.

**Table 18** Composition of the samples of GP-05.

ID	System	n [mmol]		
		Fe-System	NaCN	Na <sup>13</sup> CN
<b>GP-05-01</b>	RS <sub>2</sub>	0.75	0.71	-
<b>GP-05-02</b>	RS <sub>2</sub>	3	2.84	-
<b>GP-05-03</b>	RS <sub>2</sub>	0.75	-	0.71
<b>GP-05-04</b>	RS <sub>3</sub>	0.75	0.71	-
<b>GP-05-05</b>	RS <sub>3</sub>	3	2.84	-

## GP-06

For each sample different amounts of the iron sulfur mixture or mackinawite together with sulfur and KCN or Na<sup>13</sup>CN were placed in a 20 mL vial which was evacuated with N<sub>2</sub> for three times and charged with 1 mL N<sub>2</sub> purged H<sub>2</sub>O. The mackinawite samples were first produced from the reaction between iron and sulfur before the substrate was added (Table 19). After 3 d at 80 °C 2 mL of a 1 M H<sub>2</sub>SO<sub>4</sub> was added, and the samples were extracted with 3 mL of distilled cyclohexane. The organic phase was extracted with a syringe and transferred into a 2 mL GC vial by using a syringe filter. For each run 1 ML of the cyclohexane samples were then injected into the split port by the AOC sampler of the GCS-4.

**Table 19** Composition of the samples of GP-06.

ID	n [mmol]				
	Fe	FeS	S	NaCN	Na <sup>13</sup> CN
GP-06-01	1	-	1	1	-
GP-06-02	1	-	2	1	-
GP-06-03	1	-	1		1
GP-06-04	1	-	2	-	1
GP-06-05	-	1	1	1	-
GP-06-06	-	1	2	1	-
GP-06-07	-	1	1		1
GP-06-08	-	1	2	-	1

### GP-07

For each sample 0.88 g (10 mmol) of the iron sulfur mixture was placed in a 20 mL glass vial and evacuated with N<sub>2</sub> for three times. After adding 1 mL of the N<sub>2</sub> purged H<sub>2</sub>O the mixture was let to form mackinawite before 1 mL of a 1 M KCN solution and 1 mL of a 1 M H<sub>2</sub>SO<sub>4</sub> were added, and the samples were heated at 80 °C for 3 d. The gas phases of the samples were then extracted by a transfer line into a clean vial. After the first gas phase extraction, again 1 mL of acid was added, and the gas phases extracted for a second time after the samples were further reacted overnight. The sample GP-07-01 was reacted at room temperature. All gas phase samples were analyzed by **GCS-4**. Calibrated with CAL-MT-4.

### GP-08

For each sample 0.88 g (10 mmol) of the iron sulfur mixture was placed in a 20 mL glass vial and evacuated with N<sub>2</sub> for three times. After adding 1 mL of the N<sub>2</sub> purged H<sub>2</sub>O the mixture was let to form mackinawite before 1 mL of a 1 M KCN solution and different amounts of acid were added, following Table 20.

**Table 20** Composition of the samples of GP-08.

ID	V (1 M KCN) [mL]	V (1 M H <sub>2</sub> SO <sub>4</sub> ) [mL]
GP-08-01	1	-
GP-08-02	1	0.5
GP-08-03	1	1
GP-08-04	1	1.5
GP-08-05	1	2
GP-08-06	-	-

The gas phases of the samples were then extracted by a transfer line into a clean vial. After the first gas phase extraction, again 1 mL of acid was added, and the gas phases extracted for a second time after the samples were left to react for another 24 h. Both gas phases were analyzed by **GCS-4**. Calibrated with CAL-MT-3

### GP-11

For each sample 1 g of crude iron powder was placed in a 20 mL glass vial and evacuated with N<sub>2</sub> for three times. After adding 1 mL of the N<sub>2</sub> purged H<sub>2</sub>O, the substrate and acid were supplied, following Table 21. After 3 d the reaction was finished, and the gas phases of the samples were then extracted by a syringe into a clean vial and analyzed by **GCS-4**.

**Table 21** Composition of the samples of GP-11.

ID	V [mL]				
	H <sub>2</sub> O	1 M H <sub>3</sub> PO <sub>4</sub>	1 M KSCN	1 M KO CN	total
GP-11-01	1	1	1	0	3
GP-11-02	2	0	1	0	3
GP-11-03*	1	1	1	0	3
GP-11-04	1	1	0	1	3
GP-11-05	2	0	0	1	3
GP-11-06*	1	1	0	1	3

\*KS<sup>13</sup>CN and KO<sup>13</sup>CN used instead of KSCN and KO CN

### **GP-12**

For each sample 1 g (12.4 mmol) of the crude iron sulfur mixture together with either 1 mmol of KSCN (GP-12-01) or KOCN (GP-12-02) were placed in a 20 mL glass vial and evacuated with N<sub>2</sub> for three times. After adding 3 mL of the N<sub>2</sub> purged H<sub>2</sub>O, the samples were further charged with 1 mL of a 1 M H<sub>3</sub>PO<sub>4</sub> and let to react for 5 d at 80 °C before the gas phase was extracted by a transfer line into a vacuumized, clean, vial and analyzed by **GCS-4**.

### **GP-13**

For each sample 0.88 g (10 mmol) of the iron sulfur mixture was placed in a 20 mL glass vial and evacuated with N<sub>2</sub> for three times. After adding 1 mL of the N<sub>2</sub> purged H<sub>2</sub>O the mixture was let to form mackinawite before either 1 mL of a 1 M KCN (GP-13-01) or a 1 M Na<sup>13</sup>CN (GP-13-02) solution together with 1 mL or a 1 M H<sub>3</sub>PO<sub>4</sub> were added. The samples were then left at 80 °C for 3 d before the gas phase was transferred into a clean vial with a gas tight syringe and analyzed by **GCS-4**.

### **GP-16**

For each sample 0.88 g (10 mmol) of the iron sulfur mixture was placed in a 20 mL glass vial and evacuated with N<sub>2</sub> for three times. After adding 1 mL of the N<sub>2</sub> purged H<sub>2</sub>O the mixture was let to form mackinawite before 1 mL of a 1 M KSCN solution together with either 1 mL of a 1 M H<sub>3</sub>PO<sub>4</sub> (GP-16-01 and GP-16-02) or a 1 M H<sub>2</sub>SO<sub>4</sub> (GP-16-03 and GP-16-04) were added. The samples were then left at 80 °C for 3 d before the gas phase was transferred into a clean vial with a gas tight syringe and analyzed by **GCS-4**.

### **GP-17/GP-18**

For each sample 0.88 g of crude iron sulfur mixture was placed in 20 mL glass vials and evacuated with N<sub>2</sub> for three times. After adding the N<sub>2</sub> purged H<sub>2</sub>O, mackinawite was formed within 24 h at room temperature. The residual H<sub>2</sub>O was removed by a syringe after the vials were centrifuged and the mackinawite was washed with 5 mL of purged H<sub>2</sub>O. After 1 mmol of CS<sub>2</sub> was directly injected into all sample vials by a syringe, two samples (GP-17) were reacted at pH 6 and two (GP-18) charged with 1 mL of a 1 M



H<sub>3</sub>PO<sub>4</sub>. When the reaction was finished after 3 d at 80 °C, the gas phase samples were taken by a gas tight syringe and analyzed by **GCS-4**.

### GP-19

For each sample 0.88 g of crude iron sulfur mixture was placed in a 20 mL glass vial and evacuated with N<sub>2</sub> for three times. After adding the N<sub>2</sub> purged H<sub>2</sub>O, mackinawite was formed within 24 h at room temperature. The residual H<sub>2</sub>O was removed by a syringe after the vials were centrifuged and the mackinawite was washed with 5 mL of purged H<sub>2</sub>O. In the absence of any residual H<sub>2</sub>O the base was added to the first 3 samples before 1 mL of a 1 M CS<sub>2</sub>/EtOH solution, H<sub>2</sub>O and acid were supplied, following Table 22. When the reaction was finished after 3 d at 80 °C, the gas phases of the samples were then extracted by a gas tight syringe into a clean vial which was equipped with reduced pressure and analyzed by **GCS-4**. Calibrated with CAL-MT-3.

**Table 22** Composition of the samples of GP-19.

ID	V [mL]			
	H <sub>2</sub> O	1 M H <sub>2</sub> SO <sub>4</sub>	0.05 M NaOH	total
GP-19-01	1.5	1	1	3.5
GP-19-02	1	1.5	1	3.5
GP-19-03	0	2.5	1	3.5
GP-19-04	3	0.5	0	3.5
GP-19-05	2.5	1	0	3.5
GP-19-06	1.5	2	0	3.5

### **GP-20 / GP-21**

For each sample 0.88 g (10 mmol) of crude iron sulfur mixture was placed in a 20 mL glass vial and evacuated with N<sub>2</sub> for three times. After adding the N<sub>2</sub> purged H<sub>2</sub>O, mackinawite was formed within 24 h at room temperature. The residual H<sub>2</sub>O was removed by a syringe after the vials were centrifuged and the mackinawite was washed with 5 mL of purged H<sub>2</sub>O. All four samples were then charged with 1 mL of a 1 M CH<sub>3</sub>SNa solution, different amounts of acid and were left at room temperature for 2 d. After the first gas phase extraction the samples were further left at 80 °C for 3 d. The gas phases were transferred into a clean vial using transfer line and analyzed by **GCS-4**.

### **GP-22**

Two samples containing 0.56 g (10 mmol) of the iron powder were evacuated, charged with 2 mL N<sub>2</sub> purged H<sub>2</sub>O and 1 mL of a 1 M Na<sub>2</sub>[Fe(CN)<sub>5</sub>(NO)] solution, before being reacted at pH 6 (GP-22-01) or pH 3 (GP-22-02) for 3 d at 80 °C. After the reaction was finished, the gas phase was extracted with a syringe and analyzed by **GCS-4**.

### **GP-23 / GP-24 / GP-25**

For each sample 0.56 g (10 mmol) of the iron powder was placed in a 20 mL glass vial and evacuated with N<sub>2</sub> for three times. After adding the N<sub>2</sub> purged H<sub>2</sub>O, either 1 mL of a 1 M K<sub>4</sub>[Fe(CN)<sub>6</sub>] (GP-23), K<sub>3</sub>[Fe(CN)<sub>6</sub>] (GP-24) or Na<sub>2</sub>[Fe(CN)<sub>5</sub>(NO)] (GP-25) were added by a syringe. After 1 mL of a 1 M was injected, they were stored with or without acid at 80 °C for 6 d. The gas phase was transferred into a clean vial with a gas tight syringe and analyzed by **GCS-4**.

### **GP-26 / GP-27 / GP-28**

For each sample 0.88 g (10 mmol) of the iron sulfur mixture was placed in a 20 mL glass vial and evacuated with N<sub>2</sub> for three times. After adding the N<sub>2</sub> purged H<sub>2</sub>O, mackinawite was formed within 24 h at room temperature. The samples were then charged with either 1 mL of a 1 M K<sub>4</sub>[Fe(CN)<sub>6</sub>] (GP-26), K<sub>3</sub>[Fe(CN)<sub>6</sub>] (GP-27) or Na<sub>2</sub>[Fe(CN)<sub>5</sub>(NO)] (GP-28) by a syringe. They were then stored with or without acid 80 °C for 6 d. The gas phase was transferred into a clean vial with a gas tight syringe and analyzed by **GCS-4**.

**Table 23** Composition of the samples GP-32, GP-33, GP-34, GP-35, GP-36, and GP-37.

ID	n [mmol]				V [mL]
	Fe/S	KCN	CO <sub>2</sub>	CO	total
GP-32-01	1.14	-	-	0.22	2
GP-32-02*	1.14	-	-	0.22	2
GP-33-01	1.14	-	0.22	-	2
GP-33-02*	1.14	-	0.22	-	2
GP-34-01	1.14	1			
GP-34-02*	1.14	1			2
ID	n [mmol]				V [mL]
	FeS	KCN	CO <sub>2</sub>	CO	total
GP-35-01	1.14	-	-	0.22	2
GP-35-02*	1.14	-	-	0.22	2
GP-36-01	1.14	-	0.22	-	2
GP-36-02*	1.14	-	0.22	-	2
GP-37-01	1.14	1			2
GP-37-02*	1.14	1			2

\*K<sup>13</sup>CN, <sup>13</sup>CO and <sup>13</sup>CO<sub>2</sub> used instead of KCN, CO and CO<sub>2</sub>.

### **GP-32 / GP-33 / GP-34 / GP-35 / GP-36 / GP-37**

The samples were prepared inside a glovebox under Ar atmosphere. In case of **RS<sub>2</sub>**, 100 mg (1.14 mmol) of the iron sulfur mixture, together with 65 mg (1 mmol) NaCN or Na<sup>13</sup>CN were placed into a 20 mL glass vial and transferred into the glovebox. 2 mL of the Ar-purged H<sub>2</sub>O was added, the vials were closed with an Al-crimp cap equipped with a poly-butyl septa and transferred outside the glovebox. The reaction started after 1 mL of a 5 M HCl was added and the samples were left at 75 °C for 3 d. When CO/<sup>13</sup>CO or CO<sub>2</sub>/<sup>13</sup>CO<sub>2</sub> were used as substrates, the iron sulfur mixture was first supplied with H<sub>2</sub>O inside the glovebox before the gas phase was removed and repeatedly charged with the respective gas (Table 23).

In case of **RS<sub>3</sub>**, the mackinawite was first allowed to be formed by adding H<sub>2</sub>O to 100 mg (1.14 mmol) of the crude iron sulfur mixture. The mackinawite was synthesized at 75 °C in absence of any additional salt. After 24 h no magnetic iron was observed when a magnet was applied from the outside of the vials. For samples containing CN<sup>-</sup>, the vials were transferred back into the glovebox where they were opened and the NaCN/Na<sup>13</sup>CN was added in form of a solid. When CO/<sup>13</sup>CO or CO<sub>2</sub>/<sup>13</sup>CO<sub>2</sub> were used, the gas phase of the vials containing the synthetic mackinawite was directly exchanged with the respective gas. Then the samples were left at 75 °C for 3 d and analyzed by **GCS-1**.

### **GP-09**

For each sample 0.88 g (10 mmol) of the iron powder was placed in a 20 mL glass vial and evacuated with N<sub>2</sub> for three times. After adding the N<sub>2</sub> purged H<sub>2</sub>O, mackinawite was formed within 24 h at room temperature. The residual H<sub>2</sub>O was removed by a syringe after the vials were centrifuged and the mackinawite was washed with 5 mL of purged H<sub>2</sub>O. In the absence of any residual H<sub>2</sub>O the substrate was added, following Table 24, in a manner, that the bulk of mackinawite was not disturbed and remained on the bottom of the vials. The same procedure was applied, when the first 0.5 mL of the acid were added. The samples were then stored at room temperature for 24 h before another 0.5 mL of acid were added. The gas phases of the samples were then extracted by a transfer line into a clean vial which was equipped with reduced pressure.

After the first gas phase extraction, another 1 mL of H<sub>2</sub>SO<sub>4</sub> was added and the samples were left at 80 °C or boiled for 48 h. The gas phase was then transferred into a clean vial with reduced pressure using a transfer line and analyzed by **GCS-4**.

**Table 24** Composition of the samples of GP-09.

ID	V [mL]				
	H <sub>2</sub> O	1 M Na <sup>13</sup> CN	1 M Na <sub>2</sub> <sup>13</sup> CO <sub>3</sub>	1 M H <sub>2</sub> SO <sub>4</sub>	total
GP-09-01	1	-	1	1	3
GP-09-02	1	-	1	1	3
GP-09-03	2	-	-	1	3
GP-09-04	2	-	-	1	3
GP-09-05	1	1	-	1	3
GP-09-06	1	1	-	1	3

**Table 25** List of substrates for the kinetic investigations.

ID	Substrate	ID	Substrate
GP-10	KCN	GP-29	K <sub>4</sub> [Fe(CN) <sub>6</sub> ]
GP-14	KSCN	GP-30	K <sub>3</sub> [Fe(CN) <sub>6</sub> ]
GP-15	KOCN	GP-31	Na <sub>2</sub> [Fe(CN) <sub>5</sub> (NO)]

### **GP-10 / GP-14 / GP-15 / GP-29 / GP-30 / GP-31**

For each sample 0.88 g (10 mmol) of the iron powder was placed in a 20 mL glass vial and evacuated with N<sub>2</sub> for three times. After adding the N<sub>2</sub> purged H<sub>2</sub>O, mackinawite was formed within 24 h at room temperature. The samples were then supplied with 1 mL of a 1 M substrate solution and 1 mL of a 1 M H<sub>3</sub>PO<sub>4</sub>, following Table 25, and stored at 80 °C. After 2 h, 19 h, 43 h, 67 h, 139 h, 164 h and 188 h gas phase samples were extracted by a gas tight syringe and transferred into clean vials. With each extraction 500 mL of N<sub>2</sub> from the analysis vial were injected into the sample vial. The gas phases were analyzed by **GCS-4**. Calibrated by CAL-MT-5.

### **10.4.3 Methanizer**

#### **AD-01**

For each sample 100 mg (1.24 mmol) of the iron sulfur mixture were placed into a 20 mL glass vial and transported inside the glove box. After 5 mL of Ar purged H<sub>2</sub>O were added, the samples were transferred in the oven and let to react overnight at 75 °C. The samples were then again transferred into the glove box where the vials were opened and the mackinawite sludge was filtrated. The wet solid was left for several hours to dry completely before being transferred in clean vials. The sample AD-01-01 was thereby removed from the glove box and let in contact with air during the scaling process, whereas AD-01-02 was strictly held under inert conditions. Both gas phases were analyzed with the methanizer before and after heating them to 75 °C for 1 h. The gas phase sample was thereby extracted with a gas tight syringe and directly injected into the split port of the machine.

#### **AD-02**

Two mackinawite samples were prepared like described for AD-01. Here, however, one of them was dried (AD-02-01) whereas the aqueous phase in the other sample AD-02-02 was not removed. Two blanks were prepared under the same conditions, whereas one contained H<sub>2</sub>O (AD-02-03) and the other remained empty (AD-02-04). All samples were charged with 250 µL CO<sub>2</sub> from a vial containing a 100 % CO<sub>2</sub> gas phase. After that

the samples were mixed and left to equilibrate for at least 30 min. The gas phase was then extracted by a gas tight syringe and analyzed by the methanizer.

### **AD-03**

One mackinawite sample (AD-03-01) was prepared like described for AD-01. A second one was prepared by precipitation of 0.34 g (1.7 mmol)  $\text{FeCl}_2$  and 0.41 g (1.7 mmol)  $\text{Na}_2\text{S}$  (AD-03-02). The salts were therefore scaled under air and then transferred into the glove box. There both salts were dissolved in 10 mL of Ar purged  $\text{H}_2\text{O}$  before the solutions were unified whereas the black solid quickly precipitated. The mackinawite was separated by filtration and left to dry inside the glove box. Both, the mackinawite from precipitation and from the reaction of iron and sulfur, were placed into clean vials, closed with an Al-cap and septa, and consecutively charged with 100  $\mu\text{L}$  of  $\text{CO}_2$  from a vial containing a 100 %  $\text{CO}_2$  gas phase. After each injection the samples were let to equilibrate for at least 30 min before gas phase samples were extracted with a gas tight syringe and analyzed by the methanizer.

### **AD-04**

The procedure for the samples AD-04-03 (precipitated mackinawite) and AD-04-02 (iron sulfur mixture) follows the one described for AD-03 with the exception that each sample was charged with 250  $\mu\text{L}$   $\text{CO}_2$ . The sample AD-04-01 contained mackinawite formed from iron and sulfur, but was, contrary to AD-04-03, allowed to get in contact with air.

## **10.4.4 PXRD / Mössbauer spectroscopy**

### **SP-FeS-08**

In a 25 mL vial 0.88 g (10 mmol) of the iron sulfur mixture were evacuated and charged with 3 mL of  $\text{N}_2$  purged  $\text{H}_2\text{O}$ . After the mixture fully turned into mackinawite 1 mL of a 1 M KCN and 1 mL of a 1 M  $\text{H}_2\text{SO}_4$  were added, and the reaction left at 80 °C for 5 d. The solid residue was separated by a G4 frit, whereas a steady stream of  $\text{N}_2$  was applied. After introducing little amounts of air for three times the product did not show any pyrophoric behavior and was further analyzed by PXRD and Mössbauer spectroscopy.

**SP-FeS-09**

After the reaction finished (GP-13) the solid residue was filtrated using a G4 frit while steadily applying a N<sub>2</sub> stream to prevent the sample from burning. After the sample was deactivated, it was stored in a plastic vial and later analyzed by PXRD.

**SP-FeS-10**

After the reaction finished (GP-17) the solid residue was filtrated using a G4 frit while steadily applying a N<sub>2</sub> stream to prevent the sample from burning. After the sample was deactivated, it was stored in a plastic vial and later analyzed by PXRD.

**SP-FeS-11**

After the reaction finished (GP-18) the solid residue was filtrated using a G4 frit while steadily applying a N<sub>2</sub> stream to prevent the sample from burning. After the sample was deactivated, it was stored in a plastic vial and later analyzed by PXRD.



## **Appendix**

Further experimental data and supplementary material can be found on the CD in the back cover of this thesis.

## Literature

- [1] J. Trefil, H. J. Morowitz, E. Smith, *Am. Sci.* **2009**, *97*, 206.
- [2] J. F. Kasting, *Science* **1993**, *259*, 920–926.
- [3] J. F. Kasting, J. L. Siefert, *Science* **2002**, *296*, 1066–1068.
- [4] G. Wächtershäuser, *J. Mol. Evol.* **2016**, *82*, 75–80.
- [5] H. Lammer, A. L. Zerkle, S. Gebauer, N. Tosi, L. Noack, M. Scherf, E. Pilat-Lohinger, M. Güdel, J. L. Grenfell, M. Godolt, A. Nikolaou, *Astron. Astrophys. Rev.* **2018**, *26*, 1–66.
- [6] G. Fuchs, *Annu. Rev. Microbiol.* **2011**, *65*, 631–658.
- [7] I. A. Shkrob, T. W. Marin, H. He, P. Zapol, *J. Phys. Chem. C* **2012**, *116*, 9450–9460.
- [8] N. Kitadai, R. Nakamura, M. Yamamoto, S. Okada, W. Takahagi, Y. Nakano, Y. Takahashi, K. Takai, Y. Oono, *Commun. Chem.* **2021**, *4*, 1–9.
- [9] W. Heinen, A. M. Lauwers, *Orig. Life Evol. Biosph.* **1996**, *26*, 131–150.
- [10] C. Huber, G. Wächtershäuser, *Science* **1997**, *276*, 245–247.
- [11] S. J. Varma, K. B. Muchowska, P. Chatelain, J. Moran, *Nat. Ecol. Evol.* **2018**, *2*, 1019–1024.
- [12] A. J. Kamphuis, F. Picchioni, P. P. Pescarmona, *Green Chem.* **2019**, *21*, 406–448.
- [13] M. Preiner, J. C. Xavier, F. L. Sousa, V. Zimorski, A. Neubeck, S. Q. Lang, H. Chris Greenwell, K. Kleinermanns, H. Tüysüz, T. M. McCollom, N. G. Holm, W. F. Martin, *Life* **2018**, *8*, 1–22.
- [14] L. M. White, R. Bhartia, G. D. Stucky, I. Kanik, M. J. Russell, *Earth Planet. Sci. Lett.* **2015**, *430*, 105–114.
- [15] J. W. Morse, F. J. Millero, J. C. Cornwell, D. Rickard, *Earth Sci. Rev.* **1987**, *24*, 1–42.
- [16] D. Csákberényi-Malasics, J. D. Rodriguez-Blanco, V. K. Kis, A. Rečnik, L. G. Benning, M. Pósfai, *Chem. Geol.* **2012**, *294–295*, 249–258.

- [17] W. Borgeson, N. A. Matlin, G. Wächtershäuser, A. Lazcano, J. L. Bada, *Science* **2002**, *298*, 747–749.
- [18] J. L. Bada, A. Lazcano, *Science* **2002**, *296*, 1982–1983.
- [19] A. D. Keefe, S. L. Miller, G. McDonald, J. Bada, *Proc. Natl. Acad. Sci. U. S. A.* **1995**, *92*, 11904–11906.
- [20] D. P. Summers, N. Lerner, *Orig. Life Evol. Biosph.* **1998**, *28*, 1–11.
- [21] A. Platt, *Work. Aristotle Transl. into English* **1912**, *5*, 1–40.
- [22] B. L. Ligon, *Semin. Pediatr. Infect. Dis.* **2002**, *13*, 134–141.
- [23] S. Tirard, *Orig. Life Evol. Biosph.* **2010**, *40*, 215–220.
- [24] J. B. S. Haldane, *Ration. Annu.* **1929**, *148*, 3–10.
- [25] A. I. Oparin, J. D. (Bernal), *Orig. life* **1924**.
- [26] S. Tirard, *J. Genet.* **2017**, *96*, 735–739.
- [27] J. D. Bernal, *Proc. Phys. Soc. Sect. B* **1949**, *62*, 597–618.
- [28] S. L. Miller, *Science* **1953**, *117*, 528–529.
- [29] S. L. Miller, H. C. Urey, *Science* **1959**, *130*, 245–251.
- [30] J. L. Bada, *Chem. Soc. Rev.* **2013**, *42*, 2186–2196.
- [31] M. Calvin, *Chem. Evol. Orig. Life* **1956**, *44*, 248–263.
- [32] J. Oró, A. Kimball, R. Fritz, F. Master, *Arch. Biochem. Biophys.* **1959**, *85*, 115–130.
- [33] J. Oró, *Biochem. Biophys. Res. Commun.* **1960**, *2*, 407–412.
- [34] J. Oró, *Nature* **1961**, 1193–1194.
- [35] L. E. Orgel, R. Lohrmann, *Acc. Chem. Res.* **1974**, *7*, 368–377.
- [36] B. Hatton, D. Rickard, *Orig. Life Evol. Biosph.* **2008**, *38*, 257–270.
- [37] M. Waldrop, *Science* **1990**, *250*, 1078–1080.
- [38] C. B. Mast, S. Schink, U. Gerland, D. Braun, *Proc. Natl. Acad. Sci. U. S. A.* **2013**, *110*,

8030–8035.

- [39] M. Morasch, D. Braun, C. B. Mast, *Angew. Chemie* **2016**, *128*, 6788–6791.
- [40] A. Pross, *Orig. Life Evol. Biosph.* **2004**, *34*, 307–321.
- [41] W. Gilbert, *Nature* **1986**, *319*, 618.
- [42] A. Lazcano, R. Guerrero, L. Margulis, J. Oró, *J. Mol. Evol.* **1988**, *27*, 283–290.
- [43] C. Reid, L. E. Orgel, C. Ponnampereuma, *Nature* **1967**, *216*, 936.
- [44] R. Lohrmann, L. E. Orgel, *Science* **1968**, *161*, 64–66.
- [45] S. Becker, I. Thoma, A. Deutsch, T. Gehrke, P. Mayer, H. Zipse, T. Carell, *Orig. life* **2016**, *352*, 833–836.
- [46] J. Xu, N. J. Green, C. Gibard, R. Krishnamurthy, J. D. Sutherland, *Nat. Chem.* **2019**, *11*, 457–462.
- [47] C. Meinert, I. Myrgorodska, P. De Marcellus, T. Buhse, L. Nahon, S. V. Hoffmann, L. Le Sergeant D’Hendecourt, U. J. Meierhenrich, *Science* **2016**, *352*, 208–212.
- [48] C. Meinert, J. J. Filippi, P. De Marcellus, L. Le Sergeant D’Hendecourt, U. J. Meierhenrich, *Chempluschem* **2012**, *77*, 186–191.
- [49] G. Wächtershäuser, *Microbiol. Rev.* **1988**, *52*, 452–484.
- [50] G. Wächtershäuser, *Orig. Life Evol. Biosph.* **1990**, 173–176.
- [51] G. Wächtershäuser, *Prog. Biophys. Mol. Biol.* **1992**, *58*, 85–201.
- [52] E. Drobner, H. Huber, G. Wächtershäuser, D. Rose, K. O. Stetter, *Nature* **1990**, *346*, 742–744.
- [53] M. Keller, E. Blöchl, G. Wächtershäuser, K. O. Stetter, *Lett. to Nat.* **1994**, *368*, 836–838.
- [54] J. R. Cann, M. R. Strens, *Nature* **1982**, *298*, 147–149.
- [55] F. N. Spiess, K. C. Macdonald, T. Atwater, R. Ballard, A. Carranza, D. Cordoba, C. Cox, V. M. Diaz, G. J. Francheteau, J. Guerrero, J. Hawkins, R. Haymon, R. Hessler,

- T. Juteau, M. Kastner, R. Larson, B. Luyendyk, J. D. Macdougall, S. Miller, W. Normark, J. Orcutt, C. Rai, *Science* **1980**, *207*, 1421–1433.
- [56] R. M. Haymon, *Nature* **1983**, *301*, 695–698.
- [57] C. de Duve, *Nature* **1988**, *336*, 209–210.
- [58] C. de Duve, *Mol. Orig. life* **1998**, 219–236.
- [59] C. Darwin, *On the Origin of Species by Means of Natural Selection: Or the Preservation of the Favoured Races in the Struggle for Life.*, **1859**.
- [60] D. L. Theobald, *Nature* **2010**, *465*, 219–222.
- [61] C. R. Woese, G. E. Fox, *J. Mol. Evol.* **1977**, *10*, 1–6.
- [62] C. R. Woese, *J. Mol. Evol.* **1979**, *13*, 95–101.
- [63] C. R. Woese, O. Kandler, M. L. Wheelis, *Proc. Natl. Acad. Sci. U. S. A.* **1990**, *87*, 4576–4579.
- [64] P. Forterre, *Curr. Opin. Genet. Dev.* **1997**, *7*, 764–770.
- [65] P. Forterre, V. Da Cunha, M. Gaïa, *eLS* **2018**, 1–7.
- [66] M. J. Russell, R. M. Daniel, A. J. Hall, J. A. Sherringham, *J. Mol. Evol.* **1994**, *39*, 231–243.
- [67] M. J. Russell, A. J. Hall, *J. Geol. Soc. London.* **1997**, *154*, 377–402.
- [68] R. E. Krupp, *Eur. J. Mineral.* **1994**, *6*, 265–278.
- [69] M. J. Russell, A. J. Hall, D. Turner, *Terra Nov.* **1989**, *1*, 238–241.
- [70] M. J. Russell, A. J. Hall, W. Martin, *Geobiology* **2010**, *8*, 355–371.
- [71] W. Martin, J. Baross, D. Kelley, M. J. Russell, *Nat. Rev. Microbiol.* **2008**, *6*, 805–814.
- [72] D. S. Kelley, J. A. Karson, D. K. Blackman, G. L. Früh-Green, D. A. Butterfield, M. D. Lilley, E. J. Olson, M. O. Schrenk, K. K. Roe, G. T. Lebon, P. Rivizzigno, *Nature* **2001**, *412*, 145–149.

- [73] M. C. Weiss, M. Preiner, J. C. Xavier, V. Zimorski, W. F. Martin, *PLoS Genet.* **2018**, *14*, 1–19.
- [74] A. R. Lennie, S. A. T. Redfern, P. F. Schofield, D. J. Vaughan, *Mineral. Mag.* **1995**, *59*, 677–683.
- [75] D. T. Rickard, *Stock. Contrib. Geol.* **1969**, *20*, 65–95.
- [76] R. A. Berner, *Science* **1962**, *137*, 669–670.
- [77] R. E. Sweeney, I. R. Kaplan, *Econ. Geol.* **1973**, *68*, 618–634.
- [78] D. Rickard, A. Griffith, A. Oldroyd, I. B. Butler, E. Lopez-Capel, D. A. C. Manning, D. C. Apperley, *Chem. Geol.* **2006**, *235*, 286–298.
- [79] D. Rickard, *Geochim. Cosmochim. Acta* **2006**, *70*, 5779–5789.
- [80] M. Wolthers, L. Charlet, P. R. van Der Linde, D. Rickard, C. H. van Der Weijden, *Geochim. Cosmochim. Acta* **2005**, *69*, 3469–3481.
- [81] N. K. Niazi, E. D. Burton, *Environ. Pollut.* **2016**, *218*, 111–117.
- [82] Y. Yang, Y. Xie, X. Li, *J. Environ. Biol.* **2015**, *36*, 393–398.
- [83] H. Y. Jeong, B. Klaue, J. D. Blum, K. F. Hayes, *Environ. Sci. Technol.* **2007**, *41*, 7699–7705.
- [84] D. S. Han, M. Orillano, A. Khodary, Y. Duan, B. Batchelor, A. Abdel-Wahab, *Water Res.* **2014**, *53*, 310–321.
- [85] C. A. Coles, S. R. Rao, R. N. Yong, *Environ. Sci. Technol.* **2000**, *34*, 996–1000.
- [86] M. Park, J. Park, J. Kang, Y. S. Han, H. Y. Jeong, *J. Hazard. Mater.* **2018**, *360*, 17–23.
- [87] J. Guevremont, D. R. Strongin, M. A. A. Schoonen, J. Bebie, in *Abstr. Pap. Am. Chem. Soc.*, **1997**, pp. 140-GEOC.
- [88] R. Bolney, Synthesis of mackinawite and tochilinite analogues and investigations on carbon fixation in a prebiotic context, **2021**.
- [89] A. M. Widler, T. M. Seward, *Geochim. Cosmochim. Acta* **2002**, *66*, 383–402.

- [90] M. Wolthers, L. Charlet, C. H. van Der Weijden, P. R. van der Linde, D. Rickard, *Geochim. Cosmochim. Acta* **2005**, *69*, 3483–3492.
- [91] A. Picard, A. Gartman, J. Cosmidis, M. Obst, C. Vidoudez, D. R. Clarke, P. R. Girguis, *Chem. Geol.* **2019**, *530*, 1–13.
- [92] N. Y. Dzade, A. Roldan, N. H. De Leeuw, *J. Chem. Phys.* **2013**, *139*, 124708.
- [93] N. Y. Dzade, A. Roldan, N. H. de Leeuw, *Phys. Chem. Chem. Phys.* **2016**, *18*, 32007–32020.
- [94] P. W. Atkins, *Physical Chemistry*, VCH, **1985**.
- [95] R. A. Berner, *Geochim. Cosmochim. Acta* **1963**, *27*, 563–575.
- [96] A. Bard, *Standard Potentials in Aqueous Solution*, Routledge, **2017**.
- [97] E. Foote, *Am. J. Sci. Arts* **1856**, *22*, 382–382.
- [98] M. Hulme, *Weather* **2009**, *64*, 121–123.
- [99] C. S. M. Pouillet, *Comptes rendus l'Académie des Sci.* **1838**, *7*, 24–65.
- [100] R. B. Bacastow, C. Keeling, T. P. Whorf, *J. Geophys. Res. Atmos.* **1985**, *90*, 10529–10540.
- [101] K. W. Thoning, P. P. Tans, W. D. Komhyr, *J. Geophys. Res. Atmos.* **1989**, *94*, 8549–8565.
- [102] D. Lüthi, M. Le Floch, B. Bereiter, T. Blunier, J. M. Barnola, U. Siegenthaler, D. Raynaud, J. Jouzel, H. Fischer, K. Kawamura, T. F. Stocker, *Nature* **2008**, *453*, 379–382.
- [103] M. Fernandez-Martinez, J. Sardans, F. Chevallier, P. Ciais, M. Obersteiner, S. Vicca, J. G. Candell, A. Bastos, P. Friedlingstein, S. Sitch, S. L. Piao, I. A. Janssens, J. Penuelas, *Nat. Clim. Chang.* **2013**, *9*, 73–79.
- [104] T. A. M. Pugh, M. Lindeskog, B. Smith, B. Poulter, A. Arneeth, V. Haverd, L. Calle, *Proc. Natl. Acad. Sci. U. S. A.* **2019**, *116*, 4382–4387.
- [105] A. M. Thomson, K. V. Calvin, L. P. Chini, G. Hurtt, J. A. Edmonds, B. Bond-Lamberty,

- S. Frohking, M. A. Wise, A. C. Janetos, *Proc. Natl. Acad. Sci. U. S. A.* **2010**, *107*, 19633–19638.
- [106] H. Shaftel, S. Callery, R. Jackson, D. Bailey, “Global temperature,” can be found under <https://climate.nasa.gov/vital-signs/global-temperature/>, **2021**.
- [107] J. Hansen, M. Sato, R. Ruedy, K. Lo, D. W. Lea, M. Medina-Elizade, *Proc. Natl. Acad. Sci. U. S. A.* **2006**, *103*, 14288–14293.
- [108] R. Lindsey, “Climate Change: Atmospheric Carbon Dioxide,” can be found under <https://www.climate.gov/news-features/understanding-climate/climate-change-atmospheric-carbon-dioxide> (last accessed 07/11/2021), **2020**.
- [109] IPCC, *Special Report on Carbon Dioxide Capture and Storage In: Metz B, Davidson O, de Coninck HC, Loos M, Meyer LJ (Eds) Prepared by Working Group III of the Intergovernmental Panel on Climate Change*, **2005**.
- [110] J. R. Meadowcroft, O. Langhelle, *Caching the Carbon*, Edward Elgar Publishing, **2009**.
- [111] N. MacDowell, N. Florin, A. Buchard, J. Hallett, A. Galindo, G. Jackson, C. S. Adjiman, C. K. Williams, N. Shah, P. Fennell, *Energy Environ. Sci.* **2010**, *3*, 1645–1669.
- [112] Climeworks, “Climeworks unveils the world’s first commercial direct air capture plant,” can be found under <https://climeworks.com/news/today-climeworks-is-unveiling-its-proudest-achievement> (last accessed 07/11/2021), **2017**.
- [113] F. Swain, “Cooling the planet by filtering excess carbon dioxide out of the air on an industrial scale would require a new, massive global industry – what would it need to work?,” can be found under <https://www.bbc.com/future/article/20210310-the-trillion-dollar-plan-to-capture-co2> (last accessed 07/11/2021), **2021**.
- [114] C. Hepburn, E. Adlen, J. Beddington, E. A. Carter, S. Fuss, N. Mac Dowell, J. C. Minx, P. Smith, C. K. Williams, *Nature* **2019**, *575*, 87–97.
- [115] O. S. Bushuyev, P. De Luna, C. T. Dinh, L. Tao, G. Saur, J. van de Lagemaat, S. O.



- Kelley, E. H. Sargent, *Joule* **2018**, *2*, 825–832.
- [116] M. Najera, R. Solunke, T. Gardner, G. Vesper, *Chem. Eng. Res. Des.* **2011**, *89*, 1533–1543.
- [117] A. Al-Mamoori, A. Krishnamurthy, A. A. Rownaghi, F. Rezaei, *Energy Technol.* **2017**, *5*, 834–849.
- [118] A. Kätelhön, R. Meys, S. Deutz, S. Suh, A. Bardow, *Proc. Natl. Acad. Sci. U. S. A.* **2019**, *166*, 11187–11194.
- [119] C. A. Trickett, A. Helal, B. A. Al-Maythalony, Z. H. Yamani, K. E. Cordova, O. M. Yaghi, *Nat. Rev. Mater.* **2017**, *2*, 1–16.
- [120] J. F. D. Tapia, J. Y. Lee, R. E. H. Ooi, D. C. Y. Foo, R. R. Tan, *Sustain. Prod. Consum.* **2018**, *13*, 1–15.
- [121] Z. Zhang, S. Y. Pan, H. Li, J. Cai, A. G. Olabi, E. J. Anthony, V. Manovic, *Renew. Sustain. Energy Rev.* **2020**, *125*, 109799.
- [122] D. Li, M. Kassymova, X. Cai, S. Q. Zang, H. L. Jiang, *Coord. Chem. Rev.* **2020**, *412*, 213262.
- [123] J. Singh, D. W. Dhar, *Front. Mar. Sci.* **2019**, *6*, 1–9.
- [124] G. Wächtershäuser, *Origin of Life in an Iron-Sulfur World*, Cambridge University Press, **1998**.
- [125] C. Huber, G. Wächtershäuser, *Science* **1998**, *281*, 670–672.
- [126] G. D. Cody, N. Z. Boctor, T. R. Filley, R. M. Hazen, J. H. Scott, A. Sharma, J. Yoder, *Science* **2000**, *289*, 1337–1339.
- [127] G. D. Cody, N. Z. Boctor, J. A. Brandes, T. R. Filley, R. M. Hazen, H. S. Yoder, *Geochim. Cosmochim. Acta* **2004**, *68*, 2185–2196.
- [128] C. Scheidler, J. Sobotta, W. Eisenreich, G. Wächtershäuser, C. Huber, *Sci. Rep.* **2016**, *6*, 1–7.
- [129] J. Sobotta, T. Geisberger, C. Moosmann, C. M. Scheidler, W. Eisenreich, G.

- Wächtershäuser, C. Huber, *Life* **2020**, *10*, 1–8.
- [130] N. Y. Dzade, A. Roldan, N. H. De Leeuw, *J. Chem. Phys.* **2015**, *143*, 8.
- [131] D. Santos-Carballal, A. Roldan, N. Y. Dzade, N. H. De Leeuw, *Philos. Trans. R. Soc. A Math. Phys. Eng. Sci.* **2017**, *376*, 20170065.
- [132] N. Y. Dzade, Computational study of the interactions of small molecules with the surfaces of iron-bearing minerals, **2014**.
- [133] B. J. Vaccaro, S. M. Clarkson, J. F. Holden, D. W. Lee, C. H. Wu, F. L. Poole, J. J. H. Cotelesage, M. J. Hackett, S. Mohebbi, J. Sun, H. Li, M. K. Johnson, G. N. George, M. W. W. Adams, *Nat. Commun.* **2017**, *8*, 1–9.
- [134] D. C. Johnson, D. R. Dean, A. D. Smith, M. K. Johnson, *Annu. Rev. Biochem.* **2005**, *74*, 247–281.
- [135] M. Stephenson, L. H. Stickland, *Biochem. J.* **1932**, *26*, 712–724.
- [136] R. K. Thauer, *Microbiology* **1998**, *144*, 2377–2406.
- [137] O. D. Dailey, N. T. Prevost, G. D. Strahan, *JAOCs, J. Am. Oil Chem. Soc.* **2008**, *85*, 647–653.
- [138] Y. Nicolet, C. Piras, P. Legrand, C. E. Hatchikian, J. C. Fontecilla-Camps, *Structure* **1999**, *7*, 13–23.
- [139] H. Reihlen, A. Gruhl, G. von Hessling, *J Liebigs Ann Chem* **1929**, *472*, 268–287.
- [140] D. Seyferth, G. B. Womack, M. K. Gallagher, M. Cowie, B. W. Hames, J. P. Fackler, A. M. Mazany, *Organometallics* **1987**, *6*, 283–294.
- [141] J. Windhager, M. Rudolph, S. Bräutigam, H. Görls, W. Weigand, *Eur. J. Inorg. Chem.* **2007**, 2748–2760.
- [142] T. R. Simmons, G. Berggren, M. Bacchi, M. Fontecave, V. Artero, *Coord. Chem. Rev.* **2014**, *270–271*, 127–150.
- [143] A. Q. Daraosheh, H. Görls, M. El-Khateeb, G. Mloston, W. Weigand, *Eur. J. Inorg. Chem.* **2011**, *2*, 349–355.

- [144] J. C. Fontecilla-Camps, A. Volbeda, C. Cavazza, Y. Nicolet, *Chem. Rev.* **2007**, *107*, 4273–4303.
- [145] H. Abul-Futouh, W. Imhof, W. Weigand, L. R. Almazahreh, *Inorganics* **2019**, *7*, 1–11.
- [146] O. Einsle, T. Akif, S. L. A. Andrade, B. Schmid, M. Yoshida, J. B. Howard, D. C. Rees, *Science* **2002**, *297*, 1696–1700.
- [147] K. M. Lancaster, M. Roemelt, P. Ettenhuber, Y. Hu, M. W. Ribbe, F. Neese, U. Bergmann, S. DeBeer, *Science* **2011**, *334*, 974–977.
- [148] T. Spatzal, M. Aksoyoglu, L. Zhang, S. L. A. Andrade, E. Schleicher, S. Weber, D. C. Rees, O. Einsle, *Science* **2011**, *334*, 940.
- [149] Y. Hu, M. W. Ribbe, *Angew. Chemie - Int. Ed.* **2016**, *55*, 8216–8226.
- [150] R. M. Allen, R. Chatterjee, M. S. Madden, P. W. Ludden, V. K. Shah, *Crit. Rev. Biotechnol.* **1994**, *14*, 225–249.
- [151] J. A. Wiig, Y. Hu, C. C. Lee, M. W. Ribbe, *Science* **2012**, *337*, 1672–1676.
- [152] J. A. Wiig, Y. Hu, M. W. Ribbe, *Nat. Commun.* **2015**, *6*, 1–6.
- [153] J. F. Rubinson, B. K. Burgess, J. L. Corbin, M. J. Dilworth, *Biochemistry* **1985**, *24*, 273–283.
- [154] B. K. Burgess, D. J. Lowe, *Chem. Rev.* **1996**, *96*, 2983–3011.
- [155] C. E. McKenna, A. M. Simeonov, H. Eran, M. Bravo-Leerabhandh, *Biochemistry* **1996**, *35*, 4502–4514.
- [156] L. C. Seefeldt, S. A. Ensign, M. E. Rasche, *Biochemistry* **1995**, *34*, 5382–5389.
- [157] C. C. Lee, Y. Hu, M. W. Ribbe, *Science* **2010**, *329*, 642.
- [158] J. G. Rebelein, Y. Hu, M. W. Ribbe, *Angew. Chemie - Int. Ed.* **2014**, *53*, 11543–11546.
- [159] C. C. Lee, Y. Hu, M. W. Ribbe, *Angew. Chemie - Int. Ed.* **2012**, *51*, 1947–1949.
- [160] C. C. Lee, Y. Hu, M. W. Ribbe, *MBio* **2015**, *6*, 1–6.

- [161] N. S. Sickerman, K. Tanifuji, C. C. Lee, Y. Ohki, K. Tatsumi, M. W. Ribbe, Y. Hu, *J. Am. Chem. Soc.* **2017**, *139*, 603–606.
- [162] E. Blöchl, M. Keller, G. Wächtershäuser, K. O. Stetter, *Proc. Natl. Acad. Sci. U. S. A.* **1992**, *89*, 8117–8120.
- [163] A. Smirnov, D. Hausner, R. Laffers, D. R. Strongin, M. A. A. Schoonen, *Geochem. Trans.* **2008**, *9*, 1–21.
- [164] M. Dörr, J. Käßbohrer, R. Grunert, G. Kreisel, W. A. Brand, R. A. Werner, H. Geilmann, C. Apfel, C. Robl, W. Weigand, *Angew. Chemie - Int. Ed.* **2003**, *42*, 1540–1543.
- [165] D. P. Summers, *Orig. Life Evol. Biosph.* **2005**, *35*, 299–312.
- [166] R. Ahlrichs, M. Bär, M. Häser, H. Horn, C. Kölmel, *Chem. Phys. Lett.* **1989**, *162*, 165–169.
- [167] S. G. Molden, *J Comput Aided Mol Des* **2000**, *14*, 123–134.
- [168] A. Klamt, G. Schüürmann, *J. Chem. Soc. Perkin Trans. 2* **1993**, 799–805.
- [169] J. Tao, J. P. Perdew, V. N. Staroverov, G. E. Scuseria, *Phys. Rev. Lett.* **2003**, *91*, 146401.
- [170] A. Schäfer, C. Huber, R. Ahlrichs, *J. Chem. Phys.* **1994**, *100*, 5829–5835.
- [171] F. Weigend, R. Ahlrichs, *Phys. Chem. Chem. Phys.* **2005**, *7*, 3297–3305.
- [172] S. Grimme, J. Antony, S. Ehrlich, H. Krieg, *J. Chem. Phys.* **2010**, *132*, 154104.
- [173] K. Eichkorn, F. Weigend, O. Treutler, R. Ahlrichs, *Theor. Chem. Acc.* **1997**, *97*, 119–124.
- [174] F. Weigend, *Phys. Chem. Chem. Phys.* **2006**, *8*, 1057–1065.
- [175] R. Bolney, M. Grosch, M. Winkler, J. van Slageren, W. Weigand, C. Robl, *RSC Adv.* **2021**, *11*, 32464–32475.
- [176] C. Schröder, M. Wan, I. B. Butler, A. Tait, S. Peiffer, C. A. McCammon, *Minerals* **2020**, *10*, 1090.

- [177] S. Boursiquot, M. Mullet, M. Abdelmoula, J. M. Génin, J. J. Ehrhardt, *Phys. Chem. Miner.* **2001**, *28*, 600–611.
- [178] D. J. Vaughan, M. S. Ridout, *J. Inorg. Nucl. Chem.* **1971**, *33*, 741–746.
- [179] M. Mullet, S. Boursiquot, M. Abdelmoula, J. M. Génin, J. J. Ehrhardt, *Geochim. Cosmochim. Acta* **2002**, *66*, 829–836.
- [180] I. T. Sines, D. D. Vaughn, R. Misra, E. J. Popczun, R. E. Schaak, *J. Solid State Chem.* **2012**, *196*, 17–20.
- [181] Robert A. Berner, *J. Geol.* **1964**, *72*, 293–306.
- [182] D. Rickard, *Stock. Contrib. to Geol.* **1969**, *20*, 67–95.
- [183] M. Mullet, S. Boursiquot, M. Abdelmoula, J.-M. Génin, J.-J. Ehrhardt, *Geochim. Cosmochim. Acta* **2002**, *66*, 829–836.
- [184] M. Wolthers, S. J. Van Der Gaast, D. Rickard, *Am. Mineral.* **2003**, *88*, 2007–2015.
- [185] F. M. Michel, S. M. Antao, P. J. Chupas, P. L. Lee, J. B. Parise, M. A. A. Schoonen, *Chem. Mater.* **2005**, *17*, 6246–6255.
- [186] H. Ohfujii, D. Rickard, *Earth Planet. Sci. Lett.* **2006**, *241*, 227–233.
- [187] H. Y. Jeong, J. H. Lee, K. F. Hayes, *Geochim. Cosmochim. Acta* **2008**, *72*, 493–505.
- [188] J. A. Bourdoiseau, M. Jeannin, C. Rémazeilles, R. Sabot, P. Refait, *J. Raman Spectrosc.* **2011**, *42*, 496–504.
- [189] D. Rickard, *Geochim. Cosmochim. Acta* **1997**, *61*, 115–134.
- [190] A. D. Gordon, A. Smirnov, S. L. Shumlas, S. Singireddy, M. DeCesare, M. A. A. Schoonen, D. R. Strongin, *Orig. Life Evol. Biosph.* **2013**, *43*, 305–322.
- [191] L. E. Orgel, R. A. Sanchez, J. P. Ferris, *J. Mol. Biol.* **1967**, *30*, 223–253.
- [192] J. D. Sutherland, *Angew. Chemie - Int. Ed.* **2016**, *55*, 104–121.
- [193] E. Borquez, H. J. Cleaves, A. Lazcano, S. L. Miller, *Orig. Life Evol. Biosph.* **2005**, *35*, 79–90.

- [194] D. Ritson, J. D. Sutherland, *Nat. Chem.* **2012**, *4*, 895–899.
- [195] D. J. Ritson, J. D. Sutherland, *Angew. Chemie - Int. Ed.* **2013**, *52*, 5845–5847.
- [196] Z. R. Todd, K. I. Öberg, *Astrobiology* **2020**, *20*, 1–12.
- [197] K. J. Zahnle, *J. Geophys. Res.* **1986**, *91*, 2819–2834.
- [198] F. Tian, J. F. Kasting, K. Zahnle, *Earth Planet. Sci. Lett.* **2011**, *308*, 417–423.
- [199] C. Sagan, G. Mullen, *Science* **1972**, *177*, 52–56.
- [200] J. F. Kasting, *Chem. Life's Orig.* **1993**, 149–176.
- [201] T. Owen, R. D. Cess, V. Ramanathan, *Nature* **1979**, *277*, 640–642.
- [202] J. F. Kasting, S. Ono, *Philos. Trans. R. Soc. B Biol. Sci.* **2006**, *361*, 917–929.
- [203] N. G. Holm, *Orig. Life Evol. Biosph.* **1992**, *22*, 5–14.
- [204] M. S. Dodd, D. Papineau, T. Grenne, J. F. Slack, M. Rittner, F. Pirajno, J. O'Neil, C. T. S. Little, *Nature* **2017**, *543*, 60–64.
- [205] M. J. Russell, A. Ponce, *Life* **2020**, *10*, 1–24.
- [206] W. Heinen, A. Lauwers, *Proc. K. Ned. Akad. Van Wet.* **1997**, *100*, 11–25.
- [207] C. C. Lee, K. Tanifuji, M. Newcomb, J. Liedtke, Y. Hu, M. W. Ribbe, *ChemBioChem* **2018**, *19*, 649–653.
- [208] J. Rittle, J. C. Peters, *Angew. Chemie - Int. Ed.* **2016**, *55*, 12262–12265.
- [209] A. B. Shein, I. L. Rakityanskaya, S. F. Lomaeva, *Prot. Met.* **2007**, *43*, 54–58.
- [210] M. Cattenot, E. Peeters, C. Geantet, E. Devers, J. L. Zotin, *Catal. Letters* **2005**, *99*, 171–176.
- [211] B. H. Davis, *Fuel Process. Technol.* **2001**, *71*, 157–166.
- [212] C. J. Jones, S. Chattopadhyay, N. I. Gonzalez-Pech, C. Avendano, N. Hwang, S. S. Lee, M. Cho, A. Ozarowski, A. Prakash, J. T. Mayo, C. Yavuz, V. L. Colvin, *Chem. Mater.* **2015**, *27*, 700–707.
- [213] P. Taylor, D. W. Shoosmith, *Can. J. Chem.* **1978**, *56*, 2797–2802.

- [214] D. H. Evans, M. O'Connell, Kathleen, A. Petersen, Ralph, J. Kelley, Michael, J. *Chem. Educ.* **2011**, 71–85.
- [215] P. D. Bartlett, R. E. Davis, *J. Am. Chem. Soc.* **1958**, 80, 2513–2516.
- [216] A. J. Parker, N. Kharasch, *Chem. Rev.* **1959**, 59, 583–628.
- [217] Y. Lan, E. C. Butler, *Appl. Geochemistry* **2014**, 50, 1–6.
- [218] S. Hunger, L. G. Benning, *Geochem. Trans.* **2007**, 8, 1–20.
- [219] A. R. Lennie, S. A. T. T. Redfern, P. E. Champness, C. P. Stoddart, P. F. Schofield, D. J. Vaughan, *Am. Mineral.* **1997**, 82, 302–309.
- [220] H. Ming, N. L. K. Torad, Y. D. Chiang, K. C. W. Wu, Y. Yamauchi, *CrystEngComm* **2012**, 14, 3387–3396.
- [221] T. Arun, K. Prakash, R. Kuppusamy, R. J. Joseyphus, *J. Phys. Chem. Solids* **2013**, 74, 1761–1768.
- [222] T. Arun, K. Prakash, R. Justin Joseyphus, *J. Magn. Magn. Mater.* **2013**, 345, 100–105.
- [223] A. R. Lennie, S. A. T. Redfern, P. E. Champness, C. P. Stoddart, P. F. Schofield, D. J. Vaughan, *Am. Mineral.* **1997**, 82, 302–309.
- [224] I. S. Lyubutin, S. S. Starchikov, C. R. Lin, S. Z. Lu, M. O. Shaikh, K. O. Funtov, T. V. Dmitrieva, S. G. Ovchinnikov, I. S. Edelman, R. Ivantsov, *J. Nanoparticle Res.* **2013**, 15, 13.
- [225] M. E. Rasche, L. C. Seefeldt, *Biochemistry* **1997**, 36, 8574–8585.
- [226] R. Shabana, H. J. Meyer, S.-O. Lawesson, *Phosphorus and Sulfur* **1985**, 25, 297–305.
- [227] D. Goff, J. Fernandez, *Tetrahedron Lett.* **1999**, 40, 423–426.
- [228] D. Brillon, *Synth. Commun.* **1992**, 22, 1397–1401.
- [229] S. Goswami, A. C. Maity, N. K. Das, *J. Sulfur Chem.* **2007**, 28, 233–237.
- [230] M. Rivlin, U. Eliav, G. Navon, *J. Phys. Chem. B* **2015**, 119, 4479–4487.

- [231] S. K. Bharti, A. Bhatia, S. K. Tewari, O. P. Sidhu, R. Roy, *Magn. Reson. Chem.* **2011**, *49*, 659–667.
- [232] T. Tynkkynen, M. Tiainen, P. Soininen, R. Laatikainen, *Anal. Chim. Acta* **2009**, *648*, 105–112.
- [233] M. M. Cortese-Krott, B. O. Fernandez, M. Kelm, A. R. Butler, M. Feelisch, *Nitric Oxide - Biol. Chem.* **2015**, *46*, 14–24.
- [234] M. Schmidt, R. R. Wägerle, *Angew. Chemie* **1958**, *19*, 594–595.
- [235] M. Schmidt, R. R. Wägerle, *ZAAC - J. Inorg. Gen. Chem.* **1964**, *330*, 48–58.
- [236] M. Kumar, J. S. Francisco, *Proc. Natl. Acad. Sci. U. S. A.* **2017**, *114*, 864–869.
- [237] J. Farquhar, H. Bao, M. Thiemens, *Science* **2000**, *289*, 756–758.
- [238] K. O. Stetter, G. Gaag, *Nature* **1983**, *305*, 309–311.
- [239] K. S. Habicht, D. E. Canfield, J. Rethmeier, *Geochim. Cosmochim. Acta* **1998**, *62*, 2585–2595.
- [240] P. Philippot, M. Van Zuilen, K. Lepot, C. Thomazo, J. Farquhar, M. J. Van Kranendonk, *Science* **2008**, *319*, 1534–1538.
- [241] L. B. Sebrell, C. E. Boord, *Contrib. from Chem. Lab. op Johns Hopkins Univ.* **1923**, *45*, 2390–2399.
- [242] B. Basak, D. Bandyopadhyay, M. Patra, A. Banerji, A. Chatterjee, J. Banerji, *J. Chromatogr. Sci.* **2005**, *43*, 104–105.
- [243] L. J. Lemam, Z. Z. Huang, M. R. Ghadiri, *Astrobiology* **2015**, *15*, 709–716.
- [244] A. I. Rushdi, B. R. T. Simoneit, *Astrobiology* **2005**, *5*, 749–768.
- [245] O. E. Kawka, B. R. T. Simoneit, *Org. Geochem.* **1987**, *11*, 311–328.
- [246] M. E. Rasche, L. C. Seefeldt, *Biochemistry* **1997**, *36*, 8574–8585.
- [247] M. J. Ryle, H. I. Lee, L. C. Seefeldt, B. M. Hoffman, *Biochemistry* **2000**, *39*, 1114–1119.



- [248] S. A. Ensign, *Biochemistry* **1995**, *34*, 5372–5381.
- [249] J. Oró, A. P. Kimball, *Arch. Biochem. Biophys.* **1961**, *94*, 217–227.
- [250] V. Merz, W. Weith, *Berichte der Dtsch. Chem. Gesellschaft* **1877**, 746–765.
- [251] T. Schareina, A. Zapf, M. Beller, *Chem. Commun.* **2004**, *4*, 1388–1389.
- [252] M. Reinhard, G. Auböck, N. A. Besley, I. P. Clark, G. M. Greetham, M. W. D. Hanson-Heine, R. Horvath, T. S. Murphy, T. J. Penfold, M. Towrie, M. W. George, M. Chergui, *J. Am. Chem. Soc.* **2017**, *139*, 7335–7347.
- [253] J. Xu, D. J. Ritson, S. Ranjan, Z. R. Todd, D. D. Sasselov, J. D. Sutherland, *Chem. Commun.* **2018**, *54*, 5566–5569.
- [254] F. Roncaroli, R. Van Eldik, J. A. Olabe, *Inorg. Chem.* **2005**, *44*, 2781–2790.
- [255] M. R. A. Blomberg, *Biochemistry* **2017**, *56*, 120–131.
- [256] F. Fischer, H. Tropsch, *Brennstoff-Chemie* **1926**, *7*, 97–104.
- [257] M. Preiner, K. Igarashi, K. B. Muchowska, M. Yu, S. J. Varma, K. Kleinermanns, M. K. Nobu, Y. Kamagata, H. Tüysüz, J. Moran, W. F. Martin, *Nat. Ecol. Evol.* **2020**, *4*, 534–542.
- [258] B. Z. Cvetković, J. Rothardt, A. Büttler, D. Kunz, G. Schlotterbeck, E. Wieland, *Environ. Eng. Sci.* **2018**, *35*, 447–461.
- [259] B. Deng, T. J. Campbell, D. R. Burris, *Environ. Sci. Technol.* **1997**, *31*, 1185–1190.
- [260] J. Sobotta, M. Schmalhofer, T. M. Steiner, W. Eisenreich, G. Wächtershäuser, C. Huber, *Heliyon* **2017**, *3*, e00368.
- [261] D. J. Miller, M. C. Biesinger, N. S. McIntyre, *Surf. Interface Anal.* **2002**, *33*, 299–305.
- [262] D. Paul, H. A. Been, A. T. Aerts-Bijma, H. A. J. Meijer, *Radiocarbon* **2016**, *58*, 407–418.
- [263] J. E. Chambers, *Earth Planet. Sci. Lett.* **2004**, *223*, 241–252.
- [264] A. N. Youdin, F. H. Shu, *Astrophys. J.* **2002**, *580*, 494–505.

- [265] T. S. Kruijer, M. Touboul, M. Fischer-Gödde, K. R. Bermingham, R. J. Walker, T. Kleine, *Science* **2014**, *344*, 1150–1154.
- [266] B. M. S. Hansen, *Astrophys. J.* **2009**, *703*, 1131–1140.
- [267] T. Kleine, *Nature* **2011**, *477*, 168–169.
- [268] M. Fischer-Gödde, T. Kleine, *Nature* **2017**, *541*, 525–527.
- [269] D. Walker, J. Longhi, J. F. Hayes, *Proc. Lunar Sci. Conf. 6th* **1975**, 1103–1120.
- [270] L. T. Elkins-Tanton, *Annu. Rev. Earth Planet. Sci.* **2012**, *40*, 113–139.
- [271] A. N. Halliday, *Philos. Trans. R. Soc. A Math. Phys. Eng. Sci.* **2008**, *366*, 4163–4181.
- [272] D. Herwartz, A. Pack, B. Friedrichs, A. Bischoff, *Science* **2014**, *344*, 1146–1150.
- [273] R. Dvorak, B. Loibnegger, T. I. Maindl, *Astron. Nachrichten* **2017**, *338*, 366–374.
- [274] T. Lebrun, H. Massol, E. Chassefière, A. Davaille, E. Marcq, P. Sarda, F. Leblanc, G. Brandeis, *J. Geophys. Res. E Planets* **2013**, *118*, 1155–1176.
- [275] J. F. Kasting, *Science* **1993**, *235*, 415.
- [276] P. A. Bland, N. A. Artemieva, *Meteorit. Planet. Sci.* **2006**, *41*, 607–631.
- [277] J. F. Kasting, D. H. Egglar, S. P. Raeburn, *J Geol* **1993**, *101*, 245–257.
- [278] V. Chevrier, P. Rochette, P. E. Mathé, O. Grauby, *Geology* **2004**, *32*, 1033–1036.
- [279] C. S. Cockell, *Philos. Trans. R. Soc. B Biol. Sci.* **2006**, *361*, 1845–1855.
- [280] G. R. Osinski, C. S. Cockell, A. Pontefract, H. M. Sapers, *Astrobiology* **2020**, *20*, 1121–1149.
- [281] M. Schulte, E. Shock, *Orig. Life Evol. Biosph.* **1995**, *25*, 161–173.
- [282] M. W. Powner, J. D. Sutherland, *Philos. Trans. R. Soc. B Biol. Sci.* **2011**, *366*, 2870–2877.
- [283] J. S. Teichert, F. M. Kruse, O. Trapp, *Angew. Chemie - Int. Ed.* **2019**, *58*, 9944–9947.
- [284] J. P. Dworkin, A. Lazcano, S. L. Miller, *J. Theor. Biol.* **2003**, *222*, 127–134.

- [285] D. Liang, J. Bian, L. W. Deng, D. Huang, *J. Funct. Foods* **2017**, *35*, 197–204.
- [286] M. Dermiki, N. Phanphensophon, D. S. Mottram, L. Methven, *Food Chem.* **2013**, *141*, 77–83.
- [287] R. Huisgen, J. Rapp, *Tetrahedron* **1997**, *53*, 939–960.
- [288] R. Huisgen, G. Mlostoń, K. Polborn, F. Palacios-Gambra, *Liebigs Ann.* **1997**, *1997*, 187–192.
- [289] G. Mlostoń, J. Romański, W. Weigand, H. Heimgartner, *European J. Org. Chem.* **2019**, *2019*, 1867–1875.
- [290] U.-P. Apfel, W. Weigand, M. Horch, I. Zebger, O. Lenz, T. Fujishiro, in *Bioorganometallic Chem.*, De Gruyter, **2020**, pp. 13–136.
- [291] J. C. G. Walker, P. Brimblecombe, *Precambrian Res.* **1985**, *28*, 205–222.
- [292] A. D. Keefe, S. L. Miller, *Orig. Life Evol. Biosph.* **1996**, *26*, 111–129.
- [293] B. K. D. Pearce, R. E. Pudritz, D. A. Semenov, T. K. Henning, *Proc. Natl. Acad. Sci. U. S. A.* **2017**, *114*, 11327–11332.
- [294] S. Maruyama, K. Kurokawa, T. Ebisuzaki, Y. Sawaki, K. Suda, M. Santosh, *Geosci. Front.* **2019**, *10*, 1337–1357.
- [295] A. Omran, M. Pasek, *Life* **2020**, *10*, 1–8.
- [296] S. Becker, C. Schneider, H. Okamura, A. Crisp, T. Amatov, M. Dejmek, T. Carell, *Nat. Commun.* **2018**, *9*, 1–9.
- [297] E. G. Nisbet, N. H. Sleep, *Nature* **2001**, *409*, 1083–1091.
- [298] B. K. D. Pearce, A. S. Tupper, R. E. Pudritz, P. G. Higgs, *Astrobiology* **2018**, *18*, 343–364.
- [299] B. Damer, D. Deamer, *Astrobiology* **2020**, *20*, 429–452.
- [300] D. Rickard, I. B. Butler, A. Oldroyd, *Earth Planet. Sci. Lett.* **2001**, *189*, 85–91.